

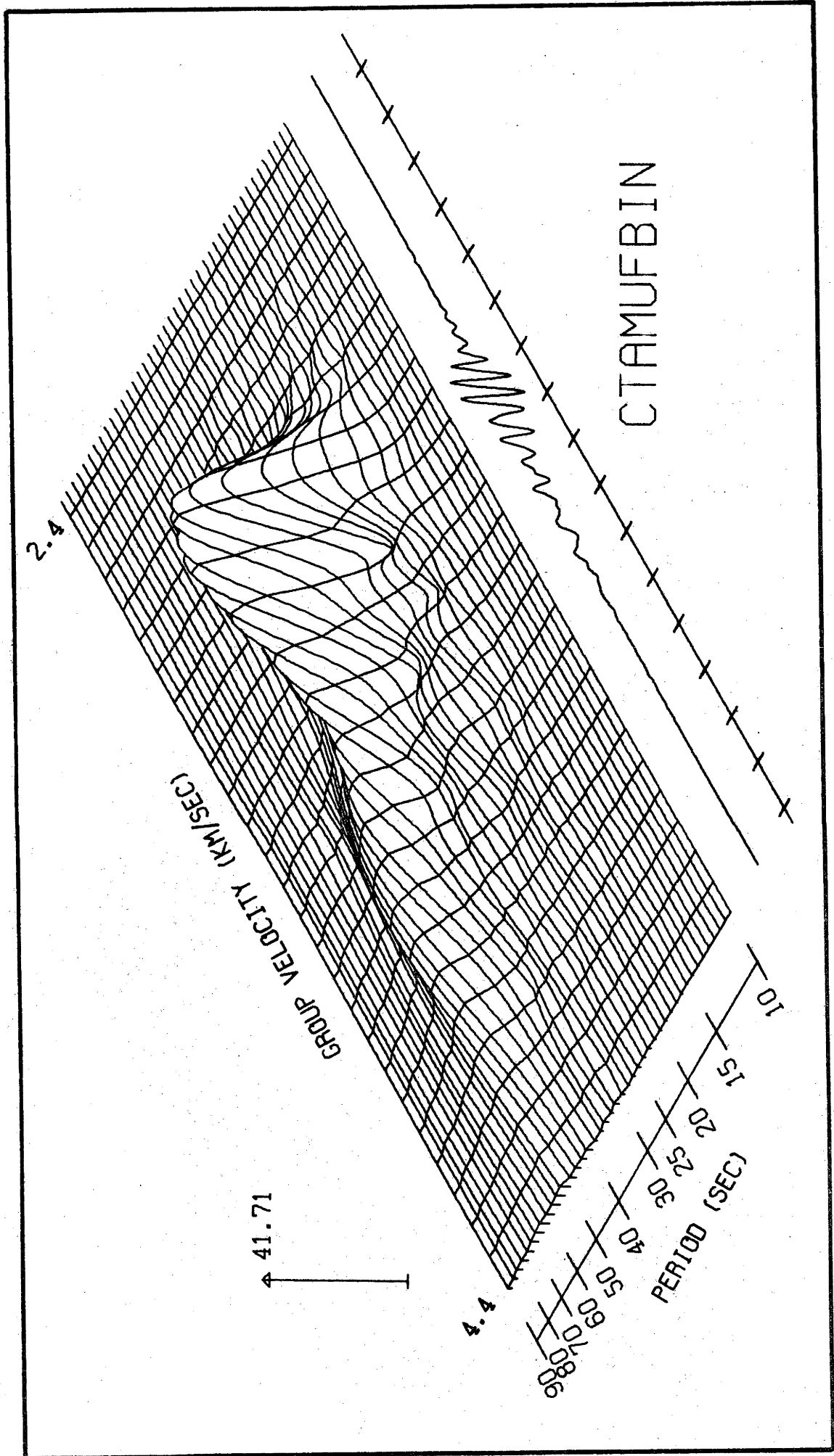
SURFACE WAVE STUDIES OF THE
AUSTRALIAN UPPER MANTLE

A thesis submitted for the
degree of
DOCTOR OF PHILOSOPHY
in the
Australian National University

by

JOHN HENRY GONCZ

May 1974



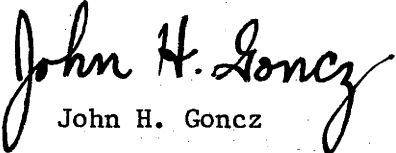
Frequency-time analysis of summed cross-correlations - group velocity.

STATEMENT

The studies described in this thesis were carried out while I was a full-time research scholar at the Australian National University, Canberra, A.C.T.

Except where mentioned in the text or in the preface, the research described in this thesis is my own.

This thesis has never been submitted to another university or similar institution.


John H. Goncz

May 1974

ABSTRACT

The analysis and inversion of Australian surface wave data indicates the presence of a well-defined low shear velocity channel in the upper mantle under eastern Australia between depths of 90 and 200 km, and the absence of a similar structure beneath the shield area of central and western Australia.

Frequency-time analysis of the sum of cross-correlations of many surface wave records made possible the determination of Rayleigh wave group velocities over the extremely wide period range 10 to 180 s. Smooth Rayleigh wave phase velocity curves have been obtained by integrating the group velocity curves. Since no other filtering is used in processing the data, these results constitute unbiased dispersion observations. Monte Carlo inversion of these data shows that accurate group velocity measurements are needed to reduce the non-uniqueness bounds of Earth models. There is an anomalous, and perhaps questionable, dip in the group velocity curve at around 110 s for some of the eastern paths. It is not apparent in western Australia. Love wave group velocity measurements are perturbed by interference between the fundamental mode and higher modes. Nevertheless, Love wave phase velocities have been measured with sufficient accuracy by averaging an ensemble of events with varying epicentral distances. Low contrast models of the crust and upper mantle which fit the Rayleigh wave observations do not fit the Love wave data. The fitting problem is more pronounced in eastern Australia. Inclusion of a thin almost-liquid layer into the models enables a better fit to both Rayleigh and Love wave fundamental mode observations. A critical comparison of the Monte Carlo models with other geophysical information from eastern, western and central Australia shows general agreement about the crust-upper mantle structure, except for body wave station anomalies, which are larger than the models indicate.

PREFACE

The Earth's upper mantle has become an increasingly active area of geophysical research, largely because more precise information about the characteristics of the low velocity zone which it contains is vital to the understanding of the mechanics of plate movements. The theory is widely accepted that material within the low velocity zone is partially melted and acts as a lubricant upon which the plates can slide, as well as providing the return path in the advective/convective cycle. Information about the low velocity zone can be obtained from body wave observations and also from geochemical information derived from laboratory experiments, but analysis of surface wave dispersion provides the most definitive information about shear wave velocities in the region, and these in turn can supply the most direct evidence of partial melting.

The presence of noise complicates the analysis and interpretation of surface wave data, by reducing the precision of velocity measurements and by restricting the range of periods that can be analysed. On the other hand, theory and experience both show that high-precision dispersion information over an extended period range is needed to delineate the structure of the upper mantle. Diverse methods for overcoming these problems have been proposed. The method of summing cross-correlations of signals from events at varying epicentral distances, which forms the basis of the present study, is in many respects analogous to techniques in seismic array processing which have resulted in an order of magnitude enhancement of body wave signals.

The project of studying the upper mantle under the Australian continent was initiated in April 1972 by Dr John Cleary's suggestion that the results of a Rayleigh wave study of this region by Thomas [1968] might be extended by the use of now available, more powerful methods of surface wave analysis.

The project has been highly computer-oriented and the author would like to acknowledge the scientists whose computer programs he has

used in the course of his investigations. The major ones are:

Dr A. Dziewonski	GROUVE (multiple filter analysis)
Dr R. Massé	TEQUILA (surface wave computation)
Mr J.A.B. Palmer	LIN36 (contouring program).

GROUVE had to be completely rewritten in order to fit on a mini-computer, and this exercise afforded a thorough understanding of its capabilities. Several other programs, such as distance and azimuth computation, have been used. Originating from various sources, these programs are now part of the library of any geophysical research establishment.

The major geophysical contributions arriving from this study are listed below. Contributions to information science are also included in the list.

1. The existence of a well-defined low shear velocity channel in the upper mantle under eastern Australia, in the depth range 90 to 200 km, has been established.
2. The upper mantle under central and western Australia does not contain a similarly well-defined low velocity channel. In this respect it is similar to shield areas found in other parts of the world. The difficulty which this observation presents to the theory of plate tectonics does not appear to be generally recognized.
3. Group velocity measurements of surface waves with periods from 10 s to 180 s have been obtained for well-defined geological regions by the combined use of sums of cross-correlations and addition of their frequency-time analysis matrices. This is a major extension of the period range usually encompassed by group velocity studies, and has made possible the advances in surface wave observation and analysis indicated below.
4. Smooth phase velocity curves have been obtained by integration of the group velocity curves. Since this process incorporates information into the phase velocity curve additional to that obtained by harmonic analysis alone, it is superior to conventional smoothing techniques.
5. Dispersion information over this extended period range overlaps with information derived from the decomposition of world-circling waves. Average world regional information was tested against specific portions

of the Earth and found to be concordant. This has not been accomplished prior to this study.

6. The Australian surface wave observations confirm the difficulty of fitting Rayleigh and Love wave data simultaneously to isotropic Earth models, especially for continental-tectonic paths. Although this problem is not solved, application of the work of others shows that special models which include anisotropic conditions or thin high-contrast layers can satisfy the data.

7. The upper mantle models derived by the present study are in harmony with other geophysical observations in Australia. They are, however, in apparent conflict with observations of P and S station anomalies from which the presence of partial melting in the upper mantle was originally inferred. This may indicate the need for more sophisticated modelling techniques in which, perhaps, the effects of lateral heterogeneity need to be explored.

8. Mode interference of Love waves has been demonstrated with real data, showing that group velocity measurements are perturbed, and consequently that the determination of phase velocities obtained by integration of group velocities is unreliable for Love waves. Nevertheless, sufficiently accurate measurements of Love wave phase velocities have been obtained by Fourier analysis of sums of cross-correlations of ensembles of signals from events at varying epicentral distances.

9. A novel, efficient, accurate computer-assisted digitizing system has been devised.

10. A major surface wave study has been implemented on a mini-computer.

11. Automated methods of handling seismic information have been developed using state-of-the-art computer programs and peripheral devices. Contour plots of frequency-time analyses of signals were found to be a form of graphic output capable of presenting large amounts of information in a manner suitable for human assimilation and evaluation. It is believed that applications for these methods could be found in other fields, for example, speech analysis and interpretation of medical information such as electro-encephalograms.

ACKNOWLEDGEMENTS

Dr R.S. Anderssen helped formulate the approach used in the Monte Carlo inversion of the data. The ANU Computer Centre's UNIVAC 1108 computer was used to perform the inversion, and it is a pleasure to acknowledge the support of the staff of the Centre.

Professor Anton L. Hales, Director of the newly-established Research School of Earth Sciences, gave the author considerable guidance and stimulation stemming from his extensive experience in geophysics.

Members of the Department of Engineering Physics, Messrs J.W. Blamey and C.W. Vance afforded many worthwhile discussions. Dr I.D.G. McLeod is especially thanked for his computing advice. He was also responsible for the superlative PDP-15 computing installation used for the major part of this study. The use of the facilities of the department, headed by Professor S. Kaneff, is gratefully acknowledged.

The friendship and interest of fellow research scholars, Dr D.W. King and Dr M.H. Worthington, was apparent in their participation in many fruitful discussions.

Dr Cleary's long association with Australian geophysics was of great assistance in the interpretation of the inversion results within that framework, and his contribution is gratefully acknowledged.

I am sincerely grateful to my supervisors, Dr K.J. Muirhead and Dr Cleary, for encouragement and guidance throughout the study.

PUBLICATIONS

The papers listed below have resulted from the work described herein. A list of the author's previous publications, not related to the present study, is included in Appendix C.

J.H. Goncz (1972). - 'Computer aided digitization of seismic traces', Proceedings of the Decus-Australia August 1972 Symposium, pp.45-46. (abstract)

J.H. Goncz (1973). - 'Digital analysis of dispersed seismic signals', presented at first seminar on Digital Signal Processing, A.N.U., December, 1973. To be published in A.N.U. Computer Centre Technical Report No. 45, 1974, 'Digital Signal Processing - Proceedings of a One-Day Seminar, Dec. 1973'.

J.H. Goncz (1974). - 'Computer aided digitization of chart records',
J. Phys. E: Sci. Instrum. 7, 20-22.

J.H. Goncz and A.L. Hales. - 'Analysis to extended periods of
Rayleigh and Love wave dispersion across Australia'
(forthcoming).

J.H. Goncz, J.R. Cleary and K.J. Muirhead. - 'Variations in upper
mantle structure beneath Australia from surface wave
observations' (forthcoming).

C O N T E N T S

PREFACE	v
CHAPTER 1. A REVIEW	1
1.1 Surface wave observations	1
1.2 Analytical methods for obtaining phase and group velocity	4
1.3 Inversion	8
1.4 The present study	10
CHAPTER 2. DATA ACQUISITION AND DIGITIZATION	14
2.1 Data selection and acquisition	14
2.2 Digitization and management of data	21
2.3 Digitizing instruments	22
2.4 Digitizing system	24
CHAPTER 3. NUMERICAL ANALYSIS OF DISPERSED SEISMIC SIGNALS	28
3.1 Introduction	28
3.2 Phase velocity and group velocity	29
3.3 The two-station method	33
3.4 Time-varying filtration (TVF)	36
3.5 Cross-correlation	40
3.6 Frequency-time analysis (FTAN)	42
CHAPTER 4. ANALYSIS OF OBSERVED DISPERSION	47
4.1 Introduction	47
4.2 The path CTA-ADE: Rayleigh waves	48
4.3 Other Australian paths: Rayleigh waves	63
4.4 Further signal averaging	73
4.5 Derivation of phase velocity curves by integrating group velocity	83
4.6 Discussion: Results at long periods	86
4.7 Love waves	89

CHAPTER 5. INVERSION	111
5.1 The working model	111
5.2 Testing procedure	114
5.3 High contrast models	122
5.4 Higher Love modes	123
5.5 Conclusions	124
CHAPTER 6. DISCUSSION OF RESULTS	127
6.1 Comparison with other surface wave studies	128
6.2 Comparison with Australian body wave studies	132
6.3 Relation to other Australian geophysical data	137
6.4 Discussion: Anisotropy	138
6.5 A suggestion for further work	140
APPENDIX A. OBSERVED DISPERSION DATA	142
APPENDIX B. MONTE CARLO MODELS	144
APPENDIX C. PRIOR PUBLICATIONS BY AUTHOR	147
APPENDIX D. EXAMPLES OF SEISMIC DATA PRESENTATION	149
REFERENCES	163

I L L U S T R A T I O N S

1.1	Knopoff's phase velocity groups	5
2.1	Two-station sketch	15
2.2	Errors caused by great circle deviation	16
2.3	World map showing epicenters	17
2.4	Axes of some recording instruments	23
2.5	Computing loop used in digitizing seismograms	25
2.6	Digitizing with a Calcomp plotter (photo)	26
3.1	Phase velocity curves ADE-MUN	35
3.2	Group arrival event 3 at ADE:- (FTAN, TVF)	37
3.3	Group arrival event 3 at MUN:- (FTAN, TVF)	38
3.4	Group velocity FTAN plot of event 3	45
3.5	Flow chart of group velocity-FTAN-procedure	46
4.1	Group arrival event 7	49
4.2	Group arrival event 9	50
4.3	Group arrival event 12	51
4.4	Group arrival event 19	52
4.5	Group arrival event 21	53
4.6	Group arrival event 136	54
4.7	Phase velocity CTA-ADE (TVF)	55
4.8	Group velocity events 7, 9	57
4.9	Group velocity events 12, 19	58
4.10	Group velocity events 21, 136	59
4.11	Group velocity, sum of cross-correlations, CTA-ADE	60
4.12	Phase velocity CTA-ADE, comparison	61
--	Vector addition of signals and noise	63
4.13	Group velocity ADE-MUN, CTA-MUN:- (FTAN plot)	64
4.14	Group velocity CTA-TAU, ADE-TAU:- (FTAN plot)	65
4.15	Group velocity ADE-RIV, CTA-RIV:- (FTAN plot)	66
4.16	Group velocity RIV-MUN, RIV-TAU:- (FTAN plot)	67
4.17	Phase velocity for 9 paths, common scale	68
4.18	Phase velocity for 9 paths, displaced scale	69
4.19	Map Australia, boundary of shield region	70

4.20	Thomas's results for CTA-MUN, CTA-ADE	72
4.21	Knopoff, shield phase velocity curves	74
4.22	Knopoff, 'aseismic platform' phase velocity curves	75
4.23	FTAN plot ridge crests, all nine paths	76
4.24	'WA2' sum of FTAN matrices, Rayleigh wave	77
4.25a	'EA1' sum of FTAN matrices, Rayleigh wave	78
4.25b	'EA2' sum of FTAN matrices, Rayleigh wave	79
4.26	'Total' Australia sum of all FTAN matrices, Rayleigh wave	80
4.27	Rayleigh wave group velocity on linear period axis	81
4.28a	'WA2' family of phase velocity curves	85
4.28b	'EA2' family of phase velocity curves	86
4.29	Rayleigh wave phase velocity curves for Australia	87
4.30	Love wave group arrival, event 9	92
4.31	Love wave group arrival, event 21	93
4.32	Love wave group arrival, event 136	94
4.33	Love wave group velocity, events 9, 21	95
4.34	Love wave group velocity, event 136	96
4.35	Love wave group velocity, path RIV-MUN	97
4.36	Love wave group velocity, paths CTA-MUN, ADE-MUN	98
4.37	Love wave group velocity, paths RIV-ADE, RIV-TAU	99
4.38	Love wave group velocity, paths CTA-TAU, CTA-ADE	100
4.39	Love wave group velocity, paths CTA-RIV, ADE-TAU	101
4.40	'West' Australia Love wave group velocity:- (FTAN plot)	102
4.41	'East' Australia Love wave group velocity:- (FTAN plot)	103
4.42	'Total' Australia Love wave group velocity:- (FTAN plot)	104
4.43	Love wave group velocity in Australia	105
4.44a	Love wave phase velocities for 9 paths, common scale	106
4.44b	Love wave phase velocities for 9 paths, displaces axes	107
4.45	Love wave phase velocities, integrated group velocity curves	108
4.46	'East' family of Love wave phase velocity curves	109
4.47	Partial derivatives from Bloch's model	110
5.1	'East' Monte Carlo models	116
5.2	Observed and calculated dispersion (Rayleigh, 'East')	117
5.3	Observed and calculated dispersion (Love, 'East')	118
5.4	'West' Monte Carlo models	119
5.5	Observed and calculated dispersion (Rayleigh, 'West')	120
5.6	Observed and calculated dispersion (Love, 'West')	121

6.1	Models from Knopoff [1972]	128
6.2	Comparison with shield models	130
6.3	Comparison with tectonic models	131
6.4	More 'East' Monte Carlo models	136

T A B L E S

2.1	Earthquakes used in this study	18
2.2	Characteristics of recording instruments	23
4.1	Event data for CTA-ADE path	48
5.1	Density and compressional velocity for inversion study	114

CHAPTER 1

A REVIEW

Lateral variation in the upper mantle beneath Australia has been suggested by heat flow studies and body wave information (discussed in detail in Chapter 6). The velocity and density structure of the Earth's upper mantle can be investigated by analysing the dispersion of surface waves that traverse a region and by inverting this information to find possible Earth models, the calculated dispersion of which matches the observed dispersion. Much progress has been made during the past decade in reducing the effect of noise always present in the observed data and in understanding what kind of information is needed to constrain possible Earth models in the inverse problem.

This dissertation studies the surface wave dispersion across the Australian continent and presents Earth models derived by inverting the information so obtained.

It will be shown that prior to this study the knowledge of surface wave dispersion across Australia was quite limited, and thus the first part of the study is *acquisition of data*. Secondly, the *analysis of dispersion* is complicated by noise which limits the accuracy obtainable and the period range over which measurements can be made. Thirdly, the ultimate goal of *inversion* is to be able to make definitive statements consistent with the observed data about the structure of the Earth in the regions concerned. This first chapter presents a review of major developments according to these three topics, and discusses their relevance to the thesis.

1.1 SURFACE WAVE OBSERVATIONS

The amplitudes of surface waves generated by earthquakes or explosions are functions of the source and the transmission properties of the Earth between the epicenter and the recording station. Geometrical spreading on the surface of the Earth, temporal spreading by propagation

through a dispersive medium, and attenuation, reduce the wave amplitude as distance from the source increases.

It is convenient to consider surface wave observations in three categories:

- (1) single observations from a source direct to recording station, which can be called 'direct observations',
- (2) observations of the same wave train at two stations lying on a great circle with the location of the epicenter — the 'two-station method'—and
- (3) multiple observations at the same station of a wave train whose amplitude is large enough for it to be detected after several world-circling traverses.

Direct observations and two-station observations are useful in studying the dispersion of limited, well-defined portions of the Earth. Multiple observations of world-circling waves contain information only about the average properties of the Earth over the great circle path defined by the locations of the epicenter and the recording station. The prevalent method of recording a full day's data as a helical trace on a revolving drum tends to make direct observation of large earthquakes impossible. When a large amount of energy is released at the source the galvanometer trace is either driven off-scale or so seriously overwritten that the seismogram is indecipherable.

Low attenuation of the longer period mantle-sensing waves permits observation of multiple circumferential traverses a long time after the earthquake, in some cases for days after. In other words, direct observations are characterized by relatively high geographical resolution and low long period energy content; multiple observations are characterized by high long period energy, little short period energy and poor geographical resolution.

Free oscillations of the Earth can be interpreted as standing waves created by interference of travelling waves propagating in opposite directions. Duality between wavelengths and the eigenmodes of vibration of the Earth is concisely expressed by the relation

$$\lambda = \frac{2\pi a}{(N + \frac{1}{2})} \quad (1.1)$$

[Brune, Nafe and Alsop, 1961] where N , an integer, is the order number of the eigenmode, λ is the wave length and a is the radius of the Earth. The factor $\frac{1}{2}$ is a consequence of the $\pi/4$ phase shift undergone by the wave at each antipodal passage. Studies of circumferential traverses and free oscillations by Toksöz and Ben-Menahem [1963], and more recently by Gupta and Santó [1973], Dziewonski [1970b] and Kanamori [1970], have provided accurate measurements of phase velocities for both Love and Rayleigh waves at very long periods. With improvements in data acquisition and analytical methods, regional differences in the path comprising a circumferential traverse are discernible. Toksöz and Anderson [1966] first divided the Earth into oceanic, mountain-tectonic, and shield areas on the basis of regional differences detected by surface wave observations.

Studies of free oscillations and circumferential traverses of waves from great earthquakes yield averaged surface wave information in the period range from the gravest mode of vibration (3227 s) to periods as short as 150 s. On the other hand, direct surface wave observations cover the period range from less than 10 s to somewhat over 100 s, depending on the instrumentation and the method of analysis used. They provide a means of studying lateral inhomogeneity in the upper mantle over a geographically well-defined sector of the Earth. The period range from 100 to 200 s, in which group velocity is inversely dispersed, is poorly covered by either method. One of the aims of this thesis has been to develop methods of analysis that would extend the period range of phase velocities derived from direct observations in order to overlap with the phase velocity information obtained from multiple traverse observations.

The results of many surface wave studies of direct observations carried out since 1963 (when the world-wide seismic network became operational), are summarized by Knopoff [1972], who groups the data into five geophysical regions, and also by Brune [1969], who uses seven crustal groups. The shape and magnitude of the Rayleigh wave phase velocity curve plotted against period is used to discriminate the types. The nomenclature of these two authors differs, as does their number of types of crust-mantle structures. Their groupings are listed below, spaced to show the correspondence between their terminologies.

<u>Knopoff</u>	<u>Brune</u>
Shield	Shield
Aseismic	Mid-continent
	Basin and range
Mountainous	Alpine
	Great island arc
Oceanic	Deep ocean
Rift	Shallow water mid-ocean ridge

Knopoff cites over 50 studies of direct observations that yield phase velocities to periods longer than 60 s; he does not summarize the more numerous studies of dispersion at shorter periods. Fig. 1.1, reproduced from Knopoff, shows the Rayleigh wave spans for his five groupings. Inversion of typical phase velocity curves from each of the five groups established markedly different shear velocity profiles in the upper mantle. The low velocity channel is absent, or nearly so, under shield areas. In the other regions, its depth and velocity contrast with layers above and below it are not known in detail. Completely unknown is the distance over which the change in structure takes place.

1.2 ANALYTICAL METHODS FOR OBTAINING PHASE AND GROUP VELOCITY

There have been a number of recent significant advances in digital methods of obtaining surface wave dispersion information from seismograms. The treatise by Dziewonski and Hales [1972] gives a comprehensive discussion of all the methods of numerical analysis used to obtain phase and group velocities from observed seismic signals.

Prior to the introduction of the digital computer as a powerful analytical tool in the early 1960s, the peak and trough method [Brune, Nafe and Oliver, 1960] was used to analyse surface wave observations. This graphical method encounters difficulties with (a) low signal/noise ratio, (b) periods corresponding to the Airy phase, and (c) propagation conditions in which different modes arrive at the recording station at the same time. These conditions impose limitations on the period range which can be studied, and early regional dispersion studies tended to be restricted to periods considerably shorter than 60 s. This limited period range restricts the amount of velocity information which can be obtained by inversion of the data.

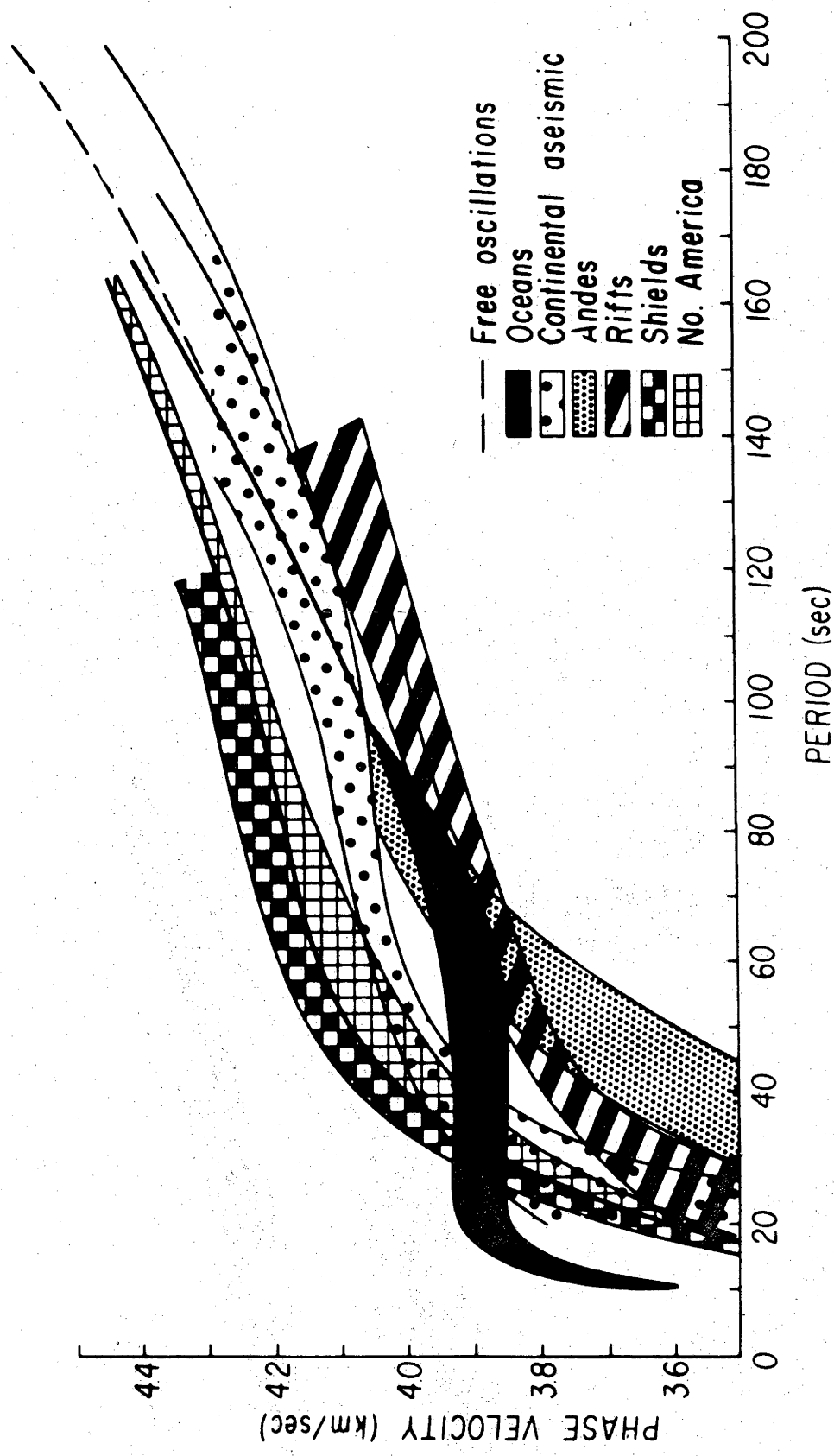


Figure 1.1: Knopoff's comparison of the span of Rayleigh wave phase velocities for standard regions.

In a series of papers Satō [1955, 1956, 1956] introduced Fourier analysis to surface wave studies and demonstrated that phase velocity could be measured in non-dispersive propagation, where the peak and trough method fails completely. Using a tripartite net to determine the direction of propagation of surface waves, Evernden [1953, 1954] showed that interference by waves refracted at oceanic-continental boundaries was responsible for the pulse-like departures from the smooth wave-trains predicted by theory. Variations in the Moho depth in Southern California were obtained by Press [1956], who developed the tripartite array technique, in which three stations are used to obtain phase velocity. This eliminated the necessity for the epicenter to be on some particular great circle path, and consequently more earthquakes could be used for analysis. The method, however, ignores azimuthal variations in the source function, which may introduce error.

Time-variant filters were introduced by Pilant and Knopoff [1964] to separate interfering dispersed wave trains. The interference can result from spatial or temporal separation at the source or from multipath propagation from a single source. The study of the Alpine region by Knopoff, Mueller and Pilant [1966] emphasized the difficulty involved in obtaining smooth phase velocity curves even when a high quality seismic net was used to gather data. Multipath propagation has been studied by Capon [1970, 1971], and Capon and Evernden [1971], using high resolution wave number analysis techniques on data supplied by LASA (the Large Aperture Seismic Array in Montana) to determine the direction of approach of propagating long period waves.

The combined use of time-variant filtering and Fourier analysis has been applied to many of the latest surface wave studies; the results of these studies are summarized by Knopoff [1972], who also gives an extensive source list.

Recognizing the limitations of the peak and trough method, Alexander [1963] digitized the seismograms and introduced the technique of obtaining group velocity by means of narrow-band, zero phase shift, digital filters; in this way he achieved separation of higher modes from the fundamental mode. Kanamori and Abe [1968] used band pass filters in the time domain to obtain group velocities in the presence of surface waves contaminated by body waves or by higher mode surface waves. These concepts were developed into a systematic process called 'moving window

analysis' by Landisman, Dziewonski and Sató [1969], who developed computer programs that convert a time series into a two-dimensional display of filtered signal amplitude (using either a linear or decibel scale) with group velocity or group arrival time plotted against the logarithm of period. The amplitude values are contoured by hand, and modes of propagation and group velocity can be inferred from the resulting contour diagram. This paper also introduced the concept of using cross-correlation of seismograms observed at two stations colinear (in the great circle sense) with the earthquake epicenter to determine phase velocity and group velocity.

The next advance in computer-based analysis was 'multiple filter analysis' [Dziewonski, Bloch and Landisman, 1969] which exploited the Fast Fourier Transform [Cooley and Tukey, 1965] and eliminated a phase shift problem intrinsic in moving window analysis, whilst retaining the same form for presentation of results. Filtering is performed in the frequency domain instead of the time domain. These methods are mathematically equivalent, and give essentially identical results.

Recently, several papers have extended 'multiple filter analysis'. Levshin's [1972] critique of the process gives an illustration of its noise-penetrating power, and also gives algorithms for speeding up the computations. Inston, Marshall and Blamey [1971] and Cara [1973] use the dispersion of the medium to obtain filter bandwidth variation with frequency for the purpose of maximizing the temporal resolution, although the 'residual dispersion' method [Dziewonski, Mills and Bloch, 1972] accomplishes the same end.

Bloch and Hales [1968] introduced some new techniques for the direct determination of phase velocity from seismograms recorded at a pair of stations, using a two-dimensional display similar to the multiple filter analysis of Dziewonski *et al.* [1969]. But Levshin [1972] points out that these more sophisticated techniques cannot yield any more information than is already contained in multiple filter analysis. Levshin's nomenclature is 'FTAN' (frequency time analysis) and this concise acronym will be used throughout this dissertation. FTAN has been used extensively in this study to obtain group velocity from cross-correlograms of seismic signals.

1.3 INVERSION

The ultimate goal of surface wave studies is to interpret the observed dispersion information in terms of possible structures and compositional properties of the Earth which have the same wave propagation characteristics as the observed data. It is recognized that there is a high degree of non-uniqueness associated with the inversion problem; i.e., there exist a multiplicity of different structures possessing dispersion characteristics which satisfy the data. An objective of inversion is to establish the possible existence of globally distinct (G-far) solutions, as opposed to solutions that differ only in their fine structure. An Earth model containing two low velocity channels would be globally distinct from a model with only one low velocity channel.

The longer the period of Love or Rayleigh waves, the more deeply they penetrate into the Earth. Anderson's [1964] Universal Love wave dispersion tables, computed via a variational approach combined with Haskell's [1953] matrix formulation, show that layers down to a depth of $1/2$ to $1/6$ of the surface wavelength have the most powerful influence on the phase velocity of the fundamental mode of Love waves. Similar studies give a corresponding factor of about 0.4 times surface wavelength of Rayleigh waves [Knopoff, 1972].

Early inversion attempts used a trial and error method of adjusting a starting Earth model to fit the observed data within some level of tolerance. A systematic procedural basis for the trial and error method is described by Haddon and Bullen [1969]. Worthington [1973] invokes 'the Principle of Maximum Simplicity' (which could also be termed 'the Principle of Least Astonishment') to describe the guiding rationale that leads to the least complicated model. The result of the trial and error method is a single model whose usefulness depends on the perseverance, intuition and judgement of the investigator.

With a single 'best' model as the defined objective of inversion, Dorman and Ewing [1962] used a least-squares curve-fitting technique and computed shear velocity partial derivatives at each step of the iterative procedure. Brune and Dorman [1963] employed the same methods in their definitive study of the structure under the Canadian Shield. They obtained a model which fitted their short period, long

period and higher mode Rayleigh wave data, as well as fundamental mode Love wave data. However, subsequent studies showed that their least-squares curve-fitting could create numerical instabilities [Takeuchi and Sudo, 1968; and Takeuchi, Dorman, and Saito, 1964].

Backus and Gilbert [1967, 1968, 1970] have formally examined the non-uniqueness of the general inverse problem of determining the structure of the Earth from free oscillation data. Since their mathematics is formidable, Parker [1970] may be read for a clear exposition of their work in relation to electrical conductivity in the mantle.

The Monte Carlo method, as first presented by Keilis-Borok and Yanovskaya [1967], puts the trial and error method of inversion on a firm statistical basis. Although demanding large amounts of computing time, Monte Carlo inversion gives a family of models that satisfy the observed data to some given level of accuracy; see for example, studies by Press [1968], Wiggins [1969], Anderssen, Worthington and Cleary [1972].

The envelope of all acceptable models produced by a Monte Carlo run can be achieved with significantly less computing expenditure by linear-programming techniques, as first applied to the geophysical problem by Johnson [1972] and later used by Worthington [1973]. However, LP inversion has been criticised for two reasons: (1) its complete reliance on the assumption of validity of linearization of the problem and (2) the extremal character of the derived models.

The poristic nature of the inverse problem in geophysics makes it difficult to see direct relations between the observed data (e.g., standard deviations, phase or group velocity, amplitude information) and the non-uniqueness bounds of possible solutions. Wiggins [1972] has studied this problem and uses the eigenvectors of the coefficient matrix to establish the resolving power and information distribution of free oscillation data. A pragmatic approach used by Dziewonski [1971] attempts to match 'pure path' dispersion information for Love and Rayleigh waves in the period range 150 to 325 s with models characterized by the smallest possible number of parameters. He showed that the distribution of shear velocity and density in the first 400 km may be adequately described by a set of four values corresponding to: (1) crust, (2) lid, (3) low velocity channel, and (4) bottom of low-velocity channel

to the 400 km discontinuity. In an earlier paper Dziewonski [1970a] showed that a high (negative) correlation exists between shear velocity partial derivatives and density partial derivatives in the upper mantle; non-uniqueness stems partly from this correlation since the computed functionals can be fitted to observed data by changing either density or shear velocity in the appropriate manner.

It may be noted here that difficulties have occurred in attempts to fit both Love and Rayleigh wave data simultaneously to a model. This problem was first encountered by McEvelly [1964] who proposed: (1) erroneous Love wave data, or (2) anisotropy (differences between horizontal and vertical shear velocity) as possible explanations for the problem.

Der *et al.* [1970] investigated the effects of observational errors on the inversion problem. They concluded that Love wave observations yield much less information than Rayleigh waves about the shear velocity distribution, and that higher mode observations increase the accuracy and resolution that may be attained. Furthermore,

'the most difficult part of conducting such a study is the estimation of errors. The propagation of errors in complicated digital processing and filtering operations, inability to estimate the effects of lateral refraction and lateral changes in the structure, and errors caused by instrumental phase shift all contribute to the overall measurement error in varying and often unknown amounts'.

1.4 THE PRESENT STUDY

In 1963 there were five WSSN stations operating in Australia: TAU-Hobart, MUN-Mundaring, CTA-Chartiers Towers, RIV-Riverview and ADE-Adelaide, making nine station pairs available for surface wave studies in this continent. (Permutation of five stations taken two at a time actually gives ten paths, but one of them, Hobart to Mundaring, is oceanic and will not be considered further.)

There have been few surface wave studies of the Australian continent. The author is aware of only two works that have looked for regional differences in Australia by this method, those of Bolt and Niazi [1964] and Thomas [1969], although the single path CTA-ADE has been used extensively to demonstrate new developments in numerical analysis of surface waves by Landisman *et al.* [1969]. Bolt and Niazi analysed

seismograms recorded at Perth, Brisbane and Charters Towers from earthquakes in the seismic belt from Banda Sea to Noumea. They used the peak and trough method to cover the period range 14 to 25 s for group velocities and 14 to 45 s for phase velocities of Rayleigh waves. They concluded that the crust of the path from Charters Towers to Perth closely resembles the structure of the Canadian Shield as determined by Brune and Dorman [1963]. But they noted the presence of regional differences in the Australian crust and a systematic decrease in group velocity between 15 and 25 s as the path from the selected earthquakes to Perth became more northerly. On the basis of Rayleigh wave dispersion, they concluded that the overall crustal thickness of Australia was probably between 30 and 35 km. The relatively short span of periods of their dispersion information does not permit investigation of the structure of the upper mantle.

Thomas selected a set of 35 earthquakes and attempted to ascertain if two-station analyses of Rayleigh waves over these nine paths would reveal any regional differences in surface wave dispersion. He used a variation of the peak and trough method to obtain phase velocities, and this limited the maximum period to 50 s, at best. Although a large number of events were successfully analysed, the scatter of the data prevented any definite conclusion about regional differences. Using Dorman and Ewing's [1962] inversion methods on polynomial smoothed data, Thomas concluded that: (1) if the crust were considered to be a uniform single layer the data indicated a Moho depth that was constant within 5% over the whole continent; and (2) if two layers were used in the starting model, the data would indicate considerable variation within the crust, although the depth of the Moho would be within 1 km of 40 km over the continent. It was obvious that inversion of fundamental Rayleigh wave phase velocities alone did not allow the crust-mantle structure to be uniquely determined.

Thus, in 1969, little was known about surface wave propagation across Australia. Love wave studies had never been attempted, and Rayleigh wave information was sparse and scattered, no information other than that for the path CTA-ADE was available for periods longer than 50 s.

The present study germinated from this situation. A study of surface wave dispersion across Australia was undertaken with the

objectives of: (1) extending the period range of Rayleigh wave information by using the recently developed numerical methods discussed in Section 1.2; (2) obtaining Love wave dispersion data; and (3) inverting this new information to establish possible crust-mantle structures. A concomitant more general objective was to attempt to extend the analysis range of direct surface wave observations to longer periods so that they would overlap with the average regional data obtained from studies of circumferential traverses and free oscillations.

The original set of earthquakes used by Thomas was re-examined. Early results obtained by summing cross-correlations looked promising, but indicated that more events with differing epicentral distances would have to be included in the summation of cross-correlograms in order to realize the full noise-reducing capability of this technique. The study was therefore expanded and seismograms from an additional 100 events were obtained from the Seismological Data Center, Washington, D.C. Particular attention was paid to the inclusion of earthquakes on both sides of a two-station pair. Group velocity was obtained over the period range 10 to 183 s, and phase velocities were derived both by integrating the group velocity and by Fourier analysis. Very smooth phase velocity curves are obtained by integrating group velocity. To the author's knowledge the method of obtaining phase velocity by integrating group velocity (see Chapter 3) has not been used in published surface wave studies. An explanation for its absence probably stems from the fact that group velocity is generally more susceptible to noise than is phase velocity. The discussion in Chapter 4 shows that further signal averaging can be obtained by combining the Frequency-Time-Analysis results for different paths belonging to the same regions, but this averaging does not permit the direct extraction of phase velocity by Fourier analysis. It does however yield an unbiased average of group velocity, which can then be integrated to obtain phase velocity.

The following chapter describes the methods used for data acquisition and management. A digitizing system was developed during the course of this study. Its ease of editing and close supervision of the processing stream of a large amount of data were essential factors contributing to the success of the study. Chapter 3 establishes the framework for the methods of digital analysis used to obtain group and phase velocity. Chapter 4 presents the results of the analysis of

surface wave dispersion across Australia and clearly shows differences between dispersion across western and eastern Australia. The problem of interference between the fundamental Love mode and higher Love modes is examined, and it appears that the method of summing cross-correlations gives a reasonably accurate measurement of Love wave phase velocities. Chapter 5 describes the Monte Carlo inversion of the dispersion results and presents feasible Earth models for western and eastern Australia.

The last chapter, 6, is concerned with the significance of the inversion results and their relation to other geophysical information.

CHAPTER 2

DATA ACQUISITION AND DIGITIZATION

Dziewonski and Landisman [1970] applied cross-correlation concepts, originally proposed by Landisman *et al.* [1969], to the analysis of world-circling waves. Specifically, they summed cross-correlograms after computing autocorrelograms of seismograms that had been digitized over intervals of more than 15 hours. The suggestion of summing cross-correlograms to reduce the interference of noise in direct observations (the two-station method) first appears in Dziewonski and Hales [1972]. The advantage of this method is that it affords a means of enhancing the phase information contained in seismograms before performing the non-linear operation of computing $\phi(\omega) = \arctangent[ImF(\omega)/ReF(\omega)]$, where $F(\omega)$ is the complex Fourier spectrum of either: (1) a station seismogram, or (2) a cross-correlogram of two seismograms. Apparently this method of summing cross-correlograms has not yet been used in published two-station studies of surface waves. To the author's knowledge, all surface wave studies appearing in the literature compute the phase curve for each event separately before averaging the results.

A deteriorating signal/noise ratio at longer periods causes the computational efficiency of $\phi(\omega)$ to deteriorate. By summing cross-correlograms, the signal/noise ratio is enhanced, particularly at longer periods. Destructive interference of signal-organized noise is achieved by including events with differing epicentral distances in the sum of cross-correlograms.

2.1 DATA SELECTION AND ACQUISITION

Phase and group velocity are obtained from surface waves generated by events that lie on or near the extension of the great circle between two stations. To obtain more events than Thomas used, a magnetic tape listing earthquakes from 1961 to 1970 was searched by a computer program for events with azimuths within 6.0° of the great circle azimuth

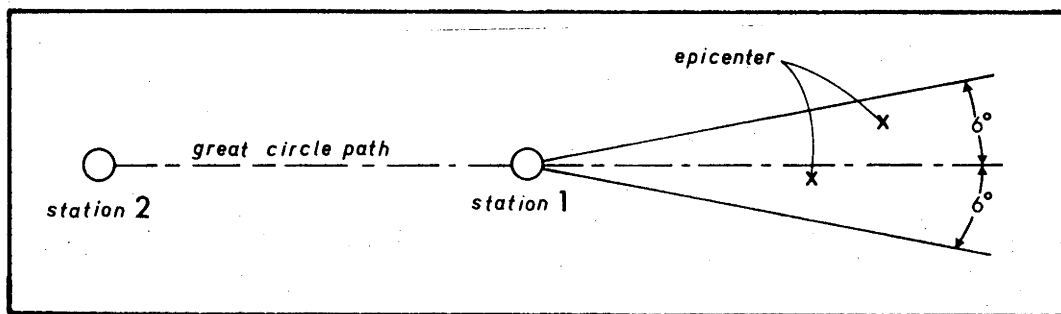


Figure 2.1: Sketch of two-station method.

at station 1, and with magnitudes greater than 5.5 (see Fig. 2.1). Knopoff and Schwab [1968] show that source phase shift is frequency-dependent and is also a function of the inclination of the source from the vertical. Thus, it is important to minimize the displacement of the epicenter from the great circle colinear with the two observing stations. The method of summing cross-correlations assumes that the event lies exactly on the great circle path defined by the locations of the two seismic observatories. If this assumption is not strictly true, an error related to the difference between the differential path length and the distance between the two stations is introduced. The error increases as the epicenter is located further off the great circle, and a similar error can be introduced in the case of very deep earthquakes. Fig. 2.2 shows the magnitude of the error. Events with locations that would have caused a gross error by being too far off the great circle were not included in the sum of cross-correlograms. This criterion prevented some of the events in Thomas's list from being included in the sum of cross-correlations. For example, his event number 31 lies 16° off the great circle connecting CTA-MUN. Correct phase velocities for these events can be obtained by using the proper differential path length in the computation of velocity [see Thomas, 1969], although source phase shift might introduce an error if the deviation is excessive.

In their definitive work on the Canadian Shield, Brune and Dorman [1963] report that phase velocities obtained from events with great circle azimuthal deviations between 4° and 7° varied considerably from each other and from those with azimuth deviations less than 4° , an effect they attributed to refraction. Therefore, they considered only those events with deviations of 4° or less. Since the present study employs methods of removing noise distortion which are more effective than the peak and trough method used by Brune and Dorman, a larger

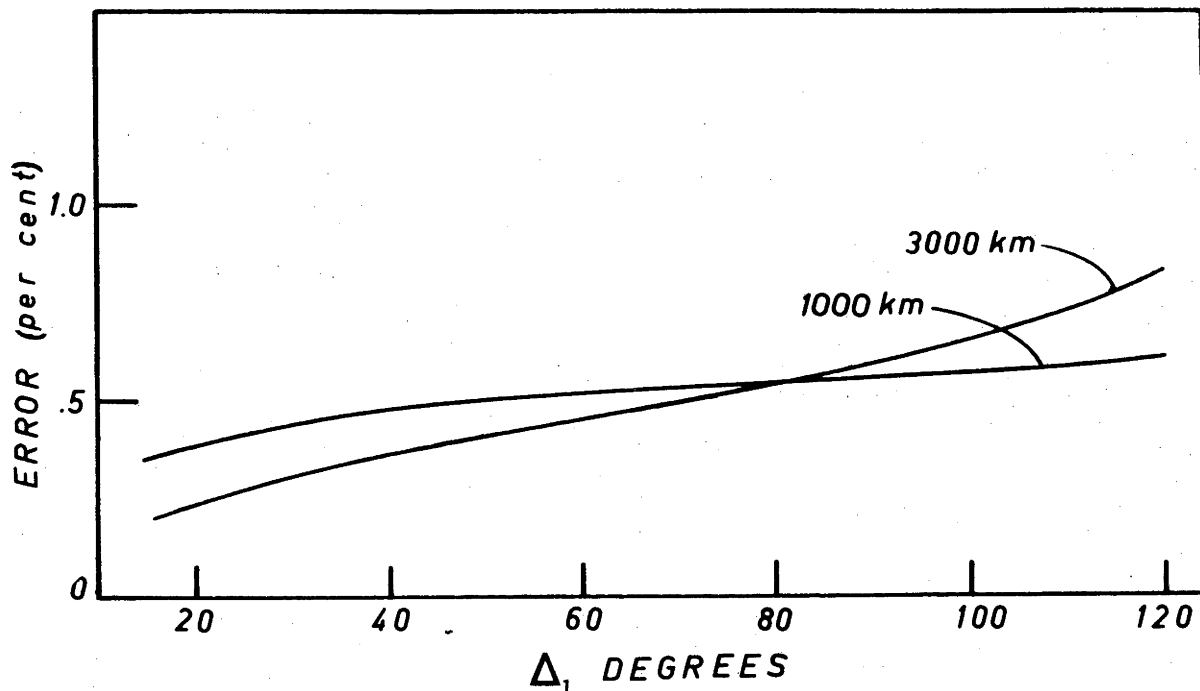


Figure 2.2: Error introduced into the sum of cross-correlations when the epicenter is 6° off the great circle defined by two seismic stations. The curves are for 1000 km and 3000 km inter-station path lengths.

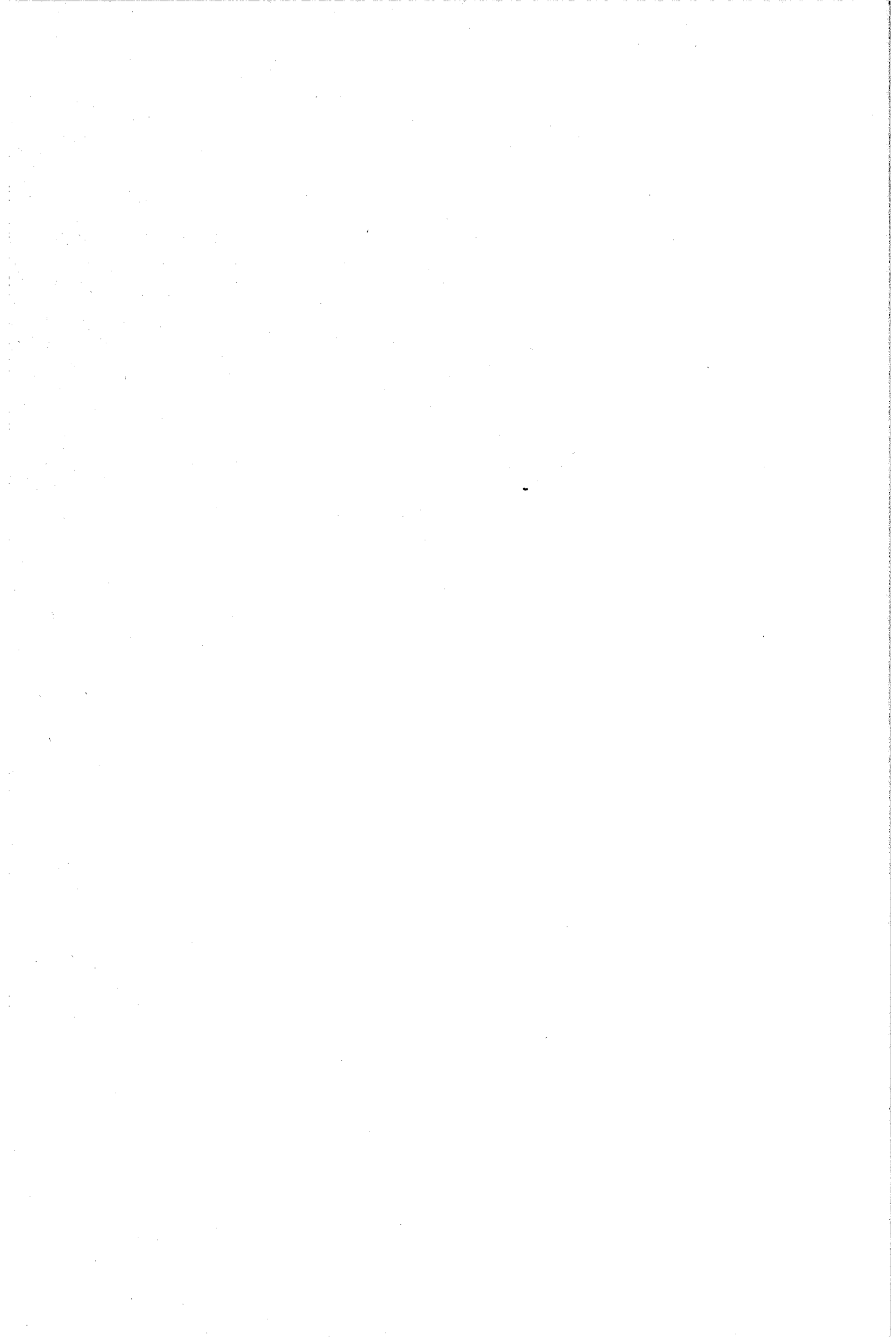
azimuthal window was used in the search in order to obtain sufficient events for consideration.

The search revealed the following numbers of earthquakes that passed the above criteria for the nine paths.

CTA-TAU	354
ADE-TAU	143
ADE-MUN	91
CTA-ADE	292
RIV-MUN	67
RIV-ADE	90
CTA-RIV	91
CTA-MUN	86
RIV-TAU	182

Ten events were selected from each of these sets according to the following criteria in the priority listed here:

- (1) five events on either side of the two-station path
- (2) different epicentral distances



- (3) large magnitude
- (4) small great-circle azimuthal deviation.

Copies of the vertical and horizontal component seismograms on 70 mm film chips were ordered from the Seismological Data Center, Washington, D.C. The full list of the earthquakes used in this study appears in Table 2.1. Event identification numbers from 1 to 40 correspond to the same numbering scheme used by Thomas. The numbers above 100 represent additional events. Fig. 2.3 shows the locations of these events on a stereographic projection of the Earth centered at Alice Springs (which is nearly the geographical center of Australia). The nature of the highly

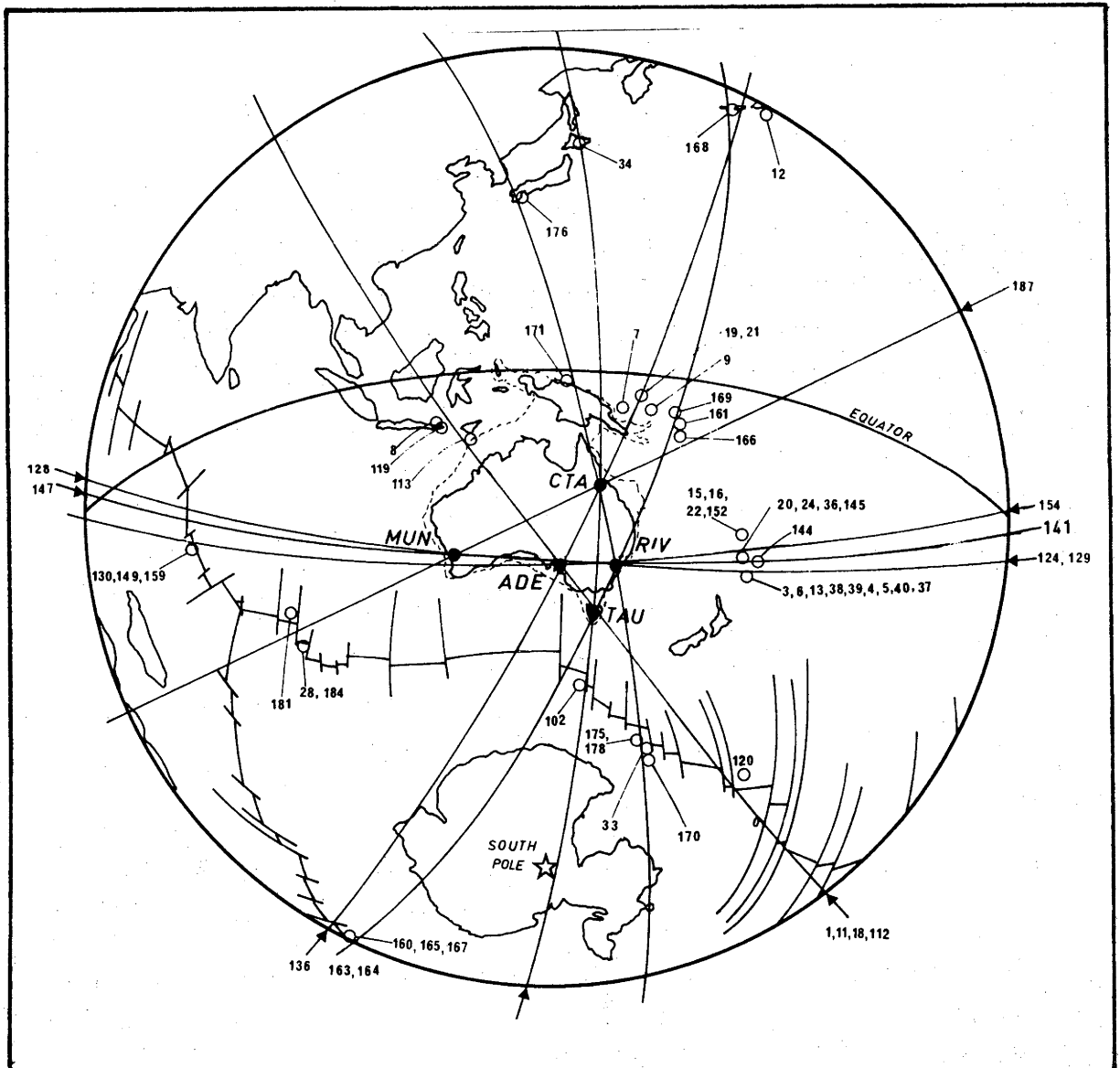


Figure 2.3: Stereographic world projection with locations of earthquakes used in this study.

Table 2.1

Identification number	Day	Mo	Yr	Hr	Min	Sec	Path	Epicenter	M _b	Deviation from great circle (°)	% Path length error	(R)ayleigh or (L)ove
34	16	3	1965	16	46	15.5	CTA to TAU	40.80 N 142.90 E	5.6	0.9	0.4	L
102	23	10	1965	8	33	47.4	TAU to CTA	55.00 S 146.20 E	5.7	5.6	0.0	RL
1	25	12	1962	12	9	45.6	TAU to ADE	36.20 S 100.20 W		6.3	0.2	R
8	18	5	1963	12	20	31.9	ADE to TAU	8.20 S 115.60 E	5.9	6.1	0.7	R
11	15	6	1963	15	30	37.7	TAU to ADE	36.30 S 98.90 W	4.9	5.5	0.0	R
18	24	9	1963	16	30	16.0	TAU to ADE	10.60 S 78.00 W	6.5	6.2	0.1	R
112	3	11	1965	1	39	3.1	TAU to ADE	9.10 S 71.40 W	6.2	1.0	0.5	L
113	12	10	1966	0	6	38.8	ADE to TAU	12.00 S 121.70 E	5.6	0.5	0.2	R
119	13	8	1970	4	22	38.5	ADE to TAU	8.89 S 117.98 E	6.0	3.4	0.3	RL
120	24	8	1970	12	30	19.5	TAU to ADE	56.59 S 142.48 W	5.9	4.0	0.0	R
39	28	3	1963	23	29	14.6	ADE to MUN	9.60 S 177.50 W	5.1	0.6	0.0	RL
38	31	3	1963	19	22	53.3	ADE to MUN	30.00 S 178.00 W	6.0	2.0	0.0	R
3	28	3	1963	11	12	31.3	ADE to MUN	30.20 S 177.80 W		2.4	0.0	R
6	2	4	1963	4	43	30.9	ADE to MUN	29.70 S 177.10 W		1.9	0.0	RL
13	14	7	1963	0	2	22.8	ADE to MUN	30.50 S 177.20 W	5.3	3.1	0.1	R
20	4	10	1963	2	47	32.1	ADE to MUN	20.70 S 174.00 W	5.3	8.8	0.8	R
24	31	10	1963	3	17	42.0	ADE to MUN	21.80 S 175.00 W	6.3	8.0	0.7	R
124	9	12	1965	6	7	47.7	ADE to MUN	17.30 N 100.00 W	6.0	0.2	0.1	RL
128	5	4	1969	2	18	29.9	MUN to ADE	12.15 N 41.20 E	6.2	3.1	0.2	RL
129	4	2	1970	5	8	48.0	ADE to MUN	15.53 N 99.48 W	6.0	2.3	0.0	RL
130	25	10	1970	12	0	35.2	MUN to ADE	13.69 S 66.26 E	5.8	5.2	0.4	RL
7	13	5	1963	22	48	10.3	CTA to ADE	6.00 S 150.10 E		7.2	0.5	R
9	2	6	1963	10	0	0.1	CTA to ADE	6.10 S 154.50 E	5.7	8.4	0.7	RL
12	24	6	1963	16	17	15.4	CTA to ADE	52.30 N 171.20 W	5.4	2.2	0.5	R
19	2	10	1963	3	31	27.0	CTA to ADE	5.40 S 152.00 E	5.6	1.0	0.1	R
21	26	10	1963	22	41	29.8	CTA to ADE	5.20 S 152.00 E	5.9	1.2	0.2	L
136	22	7	1968	5	9	15.7	ADE to CTA	54.62 S 1.74 E	5.6	2.6	0.3	RL
40	28	3	1963	23	29	14.6	RIV to MUN	19.60 S 177.50 W	5.1	12.8	1.4	RL
37	31	3	1963	19	22	53.3	RIV to MUN	30.00 S 178.00 W	6.0	6.4	0.3	RL
36	4	10	1963	2	47	32.1	RIV to MUN	20.70 S 174.00 W	5.3	7.8	0.5	R
141	17	5	1964	19	26	20.6	MUN to RIV	35.20 N 35.90 W	5.6	2.3	-	L
144	2	3	1965	9	19	41.6	RIV to MUN	27.20 S 177.90 W	5.6	0.6	0.0	R
145	27	12	1967	16	22	48.5	RIV to MUN	22.30 S 174.80 W	6.1	5.9	0.3	RL
147	5	4	1969	2	18	29.9	MUN to RIV	12.15 N 41.20 E	6.2	5.1	0.4	RL
149	25	10	1970	12	0	35.2	MUN to RIV	13.69 S 66.26 E	5.8	3.2	0.1	R
4	28	3	1963	23	29	14.6	RIV to ADE	29.60 S 177.50 W	5.1	9.4	1.0	R
5	31	3	1963	19	22	53.3	RIV to ADE	30.00 S 178.00 W	6.0	10.0	1.1	R
15	13	8	1963	21	52	37.4	RIV to ADE	19.30 S 173.70 W	5.1	6.1	0.5	R
16	14	8	1963	2	46	44.1	RIV to ADE	21.40 S 175.20 W	4.7	4.1	0.2	R
22	27	10	1963	10	38	49.0	RIV to ADE	22.80 S 175.20 W	4.8	1.8	0.1	R
152	21	7	1965	2	51	39.0	RIV to ADE	20.90 S 175.70 W	5.7	5.4	0.4	RL
154	9	12	1965	6	7	47.7	RIV to ADE	17.30 N 100.00 W	6.0	5.0	0.5	RL
159	25	10	1970	12	0	35.2	ADE to RIV	13.69 S 66.26 E	5.8	1.2	0.0	RL
160	27	6	1965	9	45	48.7	TAU to RIV	54.70 S 5.20 E	5.9	1.8	0.4	R
161	17	7	1965	7	20	30.7	RIV to TAU	9.70 S 159.80 E	6.4	3.0	0.3	R
163	16	8	1965	12	36	23.6	TAU to RIV	0.50 S 19.90 W	6.2	1.3	0.8	L
164	19	10	1966	8	1	33.8	TAU to RIV	1.50 S 15.40 W	6.2	4.4	0.4	L
165	22	7	1968	5	9	15.7	TAU to RIV	54.62 S 1.74 E	5.6	0.0	0.5	RL
166	18	8	1968	18	38	30.6	RIV to TAU	10.11 S 159.86 E	6.2	3.5	0.3	L
167	26	11	1968	0	3	14.3	TAU to RIV	57.53 S 6.79 W	5.6	5.7	0.0	RL
168	31	10	1969	11	33	4.8	RIV to TAU	51.32 N 179.01 W	6.0	0.9	0.5	RL
169	25	6	1970	5	13	58.6	RIV to TAU	7.92 S 158.69 E	6.1	0.5	0.2	RL
170	17	6	1963	18	30	54.3	RIV to CTA	65.70 S 179.30 W	5.6	1.2	0.2	RL
33	30	12	1964	13	19	47.4	RIV to CTA	62.60 S 165.80 E	5.2	5.5	0.1	RL
171	24	8	1965	14	3	16.0	CTA to RIV	3.20 S 141.00 E	5.5	1.0	0.2	L
175	26	5	1968	14	41	52.0	RIV to CTA	63.34 S 170.70 E	5.5	2.3	0.1	RL
176	21	4	1969	7	19	27.5	CTA to RIV	32.19 N 131.86 E	6.1	1.5	0.3	R
178	29	6	1969	17	9	13.9	RIV to CTA	62.78 S 166.27 E	5.5	5.2	0.1	R
28	20	8	1964	12	48	47.7	MUN to CTA	37.40 S 78.30 E		4.1	0.0	RL
181	17	2	1966	11	47	56.8	MUN to CTA	32.20 S 78.90 E	6.4	5.9	0.2	RL
184	10	7	1968	11	16	44.6	MUN to CTA	36.81 S 78.54 E	5.7	2.9	0.0	RL
187	22	10	1969	22	51	33.5	CTA to MUN	34.83 N 121.34 W	5.9	2.6	0.4	R

structured seismic activity of the Earth is apparent. Most earthquakes occur in small belts of activity, and thus a restriction is imposed on fulfilment of the condition that surface waves from a full range of epicentral distances be cross-correlated and summed for each two-station path.

It is worthwhile to point out the necessity for continual scrutiny in the data-preparation stage. For example, Thomas's events 34 and 35 produced virtually identical seismograms at both CTA and TAU even though the second event occurred 13 days after the first. There would be no signal/signal-generated-noise enhancement derived from analysing both events. The possibility of analysing replicate seismograms is reduced if, within an active seismic zone, events are chosen for maximal separation and this precaution was observed throughout the data-selection stage.

The above selection criteria provided 90 events suitable for further processing. Since a two-station analysis of both Love and Rayleigh waves requires digitization of six seismograms for each event, there were potentially 540 more seismograms to be digitized. Clearly, some thought had to be given to methods of digitization and management of this large amount of data, or the capabilities of a single investigator would have been inadequate. The next section in this chapter describes how an efficient digitizing method was developed for this project.

It is perhaps first necessary to discuss the reasons for analysing so much data when, in principle, 'a single seismogram contains all the information needed for a fairly detailed structural interpretation' [Anderson, 1967, p.360]. The primary reason is, of course, the objective of extending the range of reliable phase velocity measurement, hopefully to a period as long as 200 s. Great earthquakes, particularly deep ones, are efficient generators of mantle (i.e. mantle-sensing) waves; the problem is that the trace of the direct observation of the waves from great earthquakes is almost always driven off-scale by the magnitude of ground motion, so that the earlier signals of world-circling waves usually cannot be read. Therefore we are forced to use seismograms from smaller earthquakes, in which mantle-wave amplitudes may be so small as to be imperceptible by visual examination. Only by processing and summing a number of records can the mantle-wave amplitude be enhanced on such records.

At shorter periods, although the signal strength is high, the seismogram may be contaminated by signal-organized noise. Thomas's phase measurements became rather scattered and unreliable above 40 s for some paths. In gathering dispersion information, the common practice has been to examine a number of records to obtain for analysis those that contain clear dispersed wave trains with minimal evidence of beats indicating refraction. But what if no such clear records are ever observed?

An example is the CTA-TAU path. No clear vertical component records from events located north of CTA were observed, but the events located south of TAU generated relatively clear signals at both TAU and CTA. There are probably other station locations on the Earth where, for similar reasons, clear uncontaminated wave trains are not observed, and in these cases signal enhancement processing methods by summing many records would be of great use.

Some of the sources of noise contamination of long period records are:

- (1) refraction at continental boundaries causing later arrival of energy at either or both stations.
- (2) multi-path propagation or reflection from continental boundaries [see Capon, 1970, 1971].
- (3) multiple or extended source functions in time and space that generate overlapping wave trains.
- (4) higher mode propagation.
- (5) contamination by body waves; for example, core reflections can arrive in the midst of a dispersed surface wave train.
- (6) seismic and instrumental background noise, significant in the low-amplitude portions of the signal spectrum.

It is rather difficult to identify with certainty which of these mechanisms might be contaminating a seismogram, but an example of later arrival at station 1 can be seen in Fig. 3.2, where an energy peak at 21 s period is clearly visible about 2.5 min after the main dispersed wave. The later arrival of this energy (probably due to multi-pathing) at station 1 cross-correlates with energy at station 2, giving a shorter time lag and consequently a higher velocity at 21 s. The group velocity

analysis of this cross-correlogram in Fig. 3.4 shows anomalously high group velocity at 21 s. Furthermore, the ridge crest that defines group velocity is disturbed between 20 and 30 s. The processing used to generate these FTAN diagrams is described in Chapter 3.

2.2 DIGITIZING AND MANAGEMENT OF DATA

In view of the lack of digitizing facilities in Canberra suitable for processing the large number of records required in the study, a digitizing program was developed about a PDP-15 computer and its peripheral devices, primarily a 12-bit A/D converter and a Calcomp Model 565 Incremental Plotter. Initially, this computer had 16 K words of memory (later upgraded to 32 K); its use was restricted to staff and students of the Department of Engineering Physics. Any limitations imposed by its relatively small size were found to be compensated by its availability and by the close supervision of the processing stream afforded by the single-user concept. This computing installation provided on-line graphical interaction with the data processing, with both hard and soft copy available as output. The need for quick graphical output in seismic data processing work can hardly be overstressed. This kind of 'hands on' service is seldom available at large multi-user computing centers.

Digital Equipment computers use file-oriented Dectape for semi-permanent storage of programs and data. A standard format was used that denoted the number of the event, the name of the recording station and the seismograph component in the title of the file. The file contained a 1024-point digitized seismogram, the start time of digitizing and information about the sampling rate. This data-management system avoided the bulk associated with cards and paper tape, and there was less chance of mistaken identification of data files than in storage on magnetic tape.

The following sections (extracted from the author's paper 'Computer-Aided Digitization of Chart Records', published in *Journal of Physics E*, Jan, 1974) describe the PDP-15 digitizing system and also describe how signals recorded on non-rectilinear instruments can be conveniently digitized.

2.3 DIGITIZING INSTRUMENTS

Commercial XY-digitizing instruments increment along one axis, and when a predetermined sampling point is reached, record signal displacement perpendicular to that axis. They are suited to the digitization of chart records with rectilinear, orthogonal axes. However, many recording instruments do not operate in this orthogonal, rectilinear mode: for example, more data can be recorded on the same area of paper by writing the trace on a recording medium that has been wrapped around a rotating drum, which is being continuously advanced by a lead screw. This helical recording mode is used by many observatories to record continuously the variation of some quantity (such as ground motion) and in particular is used by the World-Wide Standard Seismic Network to obtain a complete day's earthquake activity on a single manageable record.

Two points arise when these signals are to be digitized:

(1) the time axis is not parallel to the edge of the paper; (2) the signal axis is not perpendicular to the time axis. The angle between the signal axis and the time axis differs from 90° by the pitch of the lead screw that advances the drum; let this angle be θ_0 . Although θ_0 is usually rather small, typically only 0.3° in WWSSN recordings, James and Linde [1971] showed that significant errors can be introduced into any subsequent Fourier analysis if it is ignored during digitizing.

A serious digitizing problem occurs when chart records are made on instruments in which the pen is directly attached to a moving-coil galvanometer. The signal axis is curvilinear instead of rectilinear, because the pen is constrained to move in a circle with radius equal to the length of the galvanometer arm. When this type of chart record is digitized with a rectilinear-digitizing instrument, the signal can sometimes erroneously appear to be multiple-valued. The proper digitization of this type of chart record is a time series of the galvanometer deflection angle θ_i at discrete time intervals t_i . Table 2.2 lists the characteristics of four common types of recording instruments and Fig. 2.4 shows how their axes are arranged.

Digitizing instruments are commercially available, but their high cost has encouraged some workers to construct their own instruments. Howell [1966] mounted seismograms on a screw-fed milling table which served as a basis for an inexpensive laboratory-constructed digitizer. Wickens and Kollar [1967] used a modified drum recorder and tracked the

Table 2.2

Type	Galvanometer arm length	Usual offset angle ($^{\circ}$)	Type of trace (see Fig. 2.4)
XY recorder	effectively infinite	0	Straight (a)
Drum	1 m	0.3	Straight (c)
Drum (heated stylus)	7 in	1.7	Curved (d)
Portable strip chart	2 in	0	Curved (b)

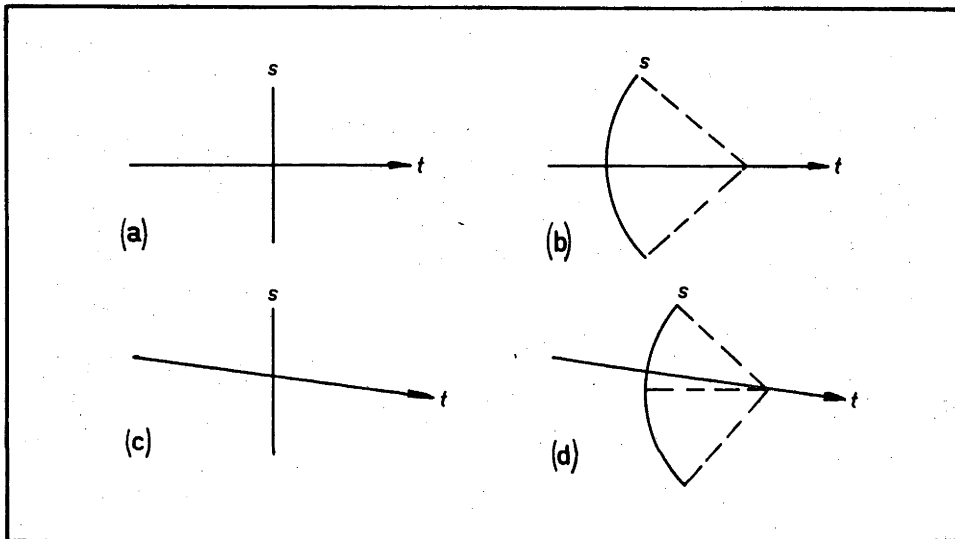


Figure 2.4: The appearance of the axes of some types of recording instruments. (a) XY recorder, (b) strip chart recorder, (c) drum in helical recording mode with light beam, (d) drum and heated stylus. s is signal axis, t is time axis.

signal with a microscope. They found that variable drum speed and sampling interval, and optical magnification, were features that improved accuracy as well as reduced the associated tedium. Goodspeed and Savage [1968] describe an electromechanical digitizer designed to process large amounts of meteorological data.

Experience has shown that certain human engineering factors should be considered when designing a digitizing system. It is considered best to move the recorded trace along its time axis under a

graticule, since the operator's point of focus is then stationary, and he can devote his complete attention to tracking the signal amplitude, preferably with just one control. When small amplitude parts of the record are being followed, it should be possible to increase the speed of the record under the cross-hair and thus sample at a faster rate. A control for this function should be available so that the operator need not take his eyes from the moving record. It is highly desirable that samples be taken at uniform time intervals, and that this be done automatically without the necessity for conscious action on the part of the operator.

2.4 DIGITIZING SYSTEM

The digitizing problems discussed above can be met by using an incremental plotter under computer control to simulate the geometry and behavior of the recording instrumentation. Two potentiometers, interfaced to the computer via analogue-to-digital converter channels, give on-line control of the plotter drum and pen carriage.

Consider now the digitization of a seismogram recorded on a helical drum recorder with a galvanometer arm seven inches long. The seismogram is taped to the drum of an 11 in. Calcomp plotter, with alignment being achieved by ensuring that the start of one trace and the end of the previous trace are coincident. After the plotter pen assembly has been replaced by a lens engraved with cross-hairs, the appropriate offset angle can be input to the computer.

The variables to be digitized (time t and galvanometer deflection θ) are related to the XY coordinates of the chart record by the equations:

$$x = vt + R(1 - \cos \theta) \quad (2.1)$$

$$y = -vt \sin \theta_0 + R \sin \theta \quad (2.2)$$

where v is the paper velocity, R is the length of the galvanometer arm and θ_0 is the offset angle. Voltages generated by two potentiometer controls 'A' and 'B', are converted by an analogue-to-digital converter and are fed into a computing loop as shown in Fig. 2.5. The chart on the drum moves under the cross-hairs at a speed proportional to the product of Δt and T , where Δt is proportional to the setting of potentiometer 'A' and T is the cycle time of the computing loop. An operator tracks the

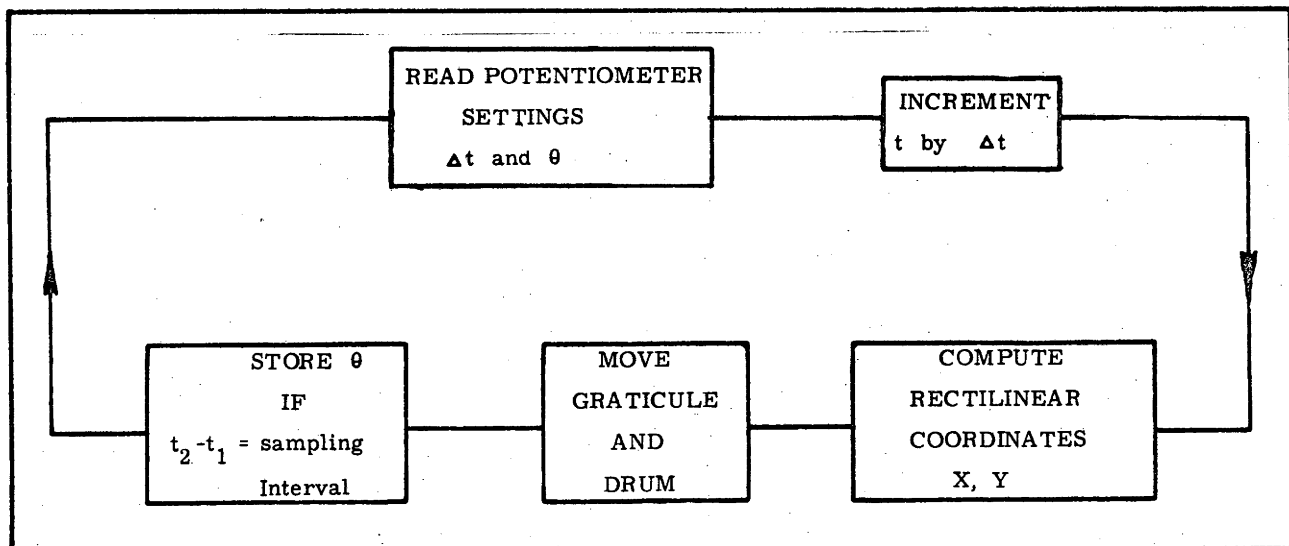


Figure 2.5: Flow chart showing how the computer models the recording instrument while an operator tracks the seismogram trace.

signal by adjusting potentiometer 'B', which generates trial values for θ . A value for θ_i is deposited into memory at predetermined intervals. The digitized time series can be read later and stored on a peripheral device. Potentiometer 'A' can be used to set a negative Δt so that both the chart on the drum and simulated time move backwards. This conveniently allows 'on-line' editing and correction of errors, since it becomes possible to go back and re-digitize a section that has been tracked with unacceptably large errors. Any previous stored data are simply overwritten in core memory. When potentiometer 'A' is set so that $\Delta t = 0$, the drum stops and the operator can suspend a digitizing session to insert new data or to take a rest.

The system described above has worked satisfactorily, and has been used to digitize hundreds of seismograms. The system is capable of obtaining an equispaced time series from analogue data for further digital processing, even though the data may be recorded on charts or graphs which do not have rectilinear or orthogonal axes. A drum-type plotter is probably best suited for this use, since the operator's point of focus stays on a line, but it would be possible to use the same concepts with a computer controlled flat-bed plotter.

Finally it is important to point out that the accuracy and resolution of this system, limited only by the plotter specifications, is 0.005 in., which is about three times better than many commercial

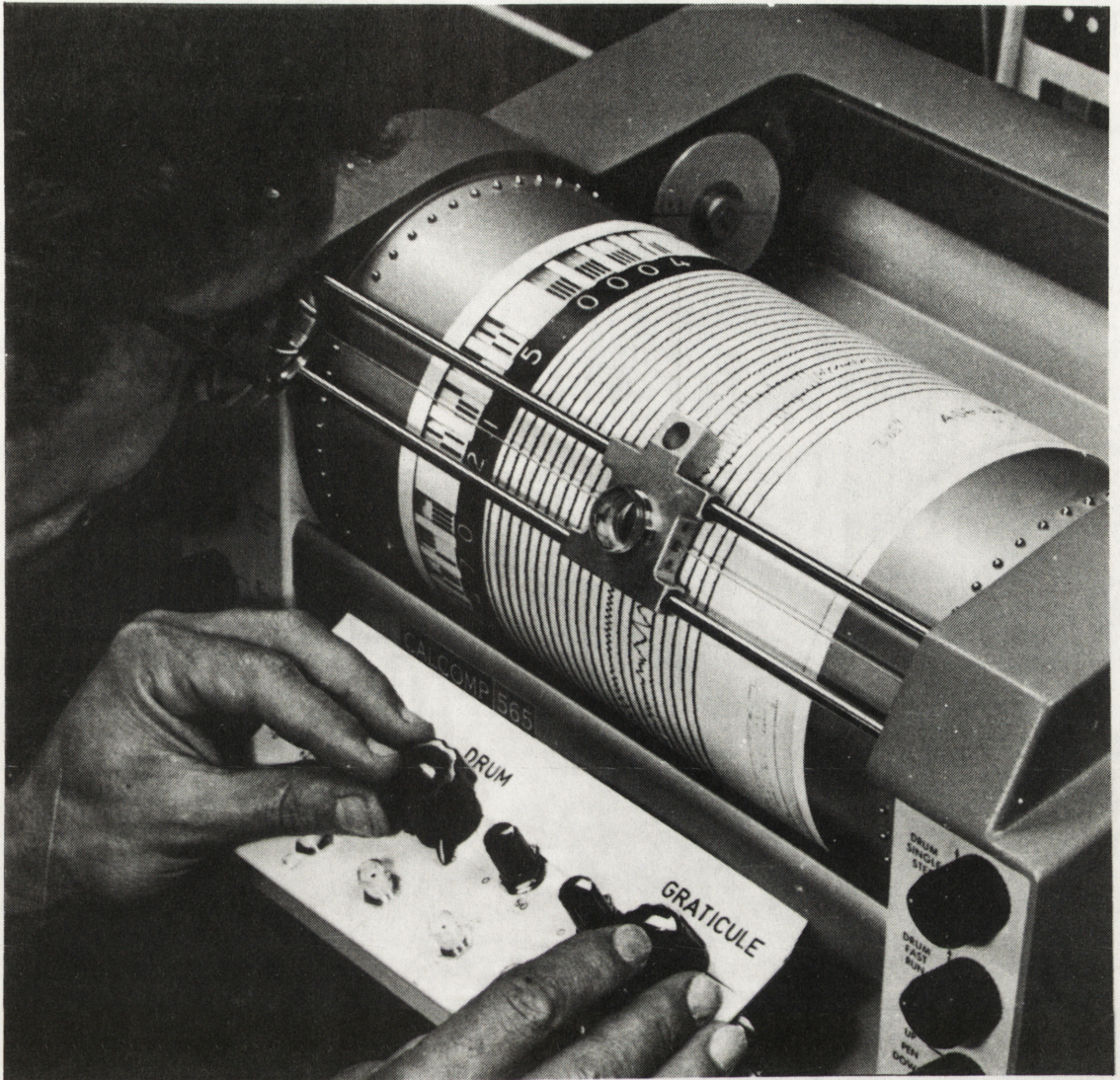


Figure 2.6: Calcomp 565 incremental plotter under computer control in use as a digitizing instrument.

digitizers. The concept of overall computer control decidedly eases the problems associated with management of large amounts of data.

The apparatus in use is shown in Fig. 2.6.

CHAPTER 3

NUMERICAL ANALYSIS OF DISPERSED SEISMIC SIGNALS

3.1 INTRODUCTION

The observed dispersion of surface waves is a direct consequence of the change in the elastic properties of the Earth with depth; compressional velocity α , shear velocity β , and density ρ tend to increase with depth because of the increase of pressure, although reversals may occur because of the contrary effect of the increase of temperature [cf. Stacey, 1969, p.107]. The phase velocity of a monochromatic surface wave is determined by the properties of the medium through which it travels to a depth roughly equal to its wavelength, with maximum influence exerted by the properties and structure of the Earth at a depth around one-half of the wavelength. At the present time it is not possible to examine directly the constituents of the Earth below a few km; thus most of the information about these properties is provided by ground motion recorded at the surface of the Earth by seismometers. From surface wave information, an attempt is made to deduce properties at depth that are responsible for the dispersion observed on the surface. (Information is also provided by body wave data, but will be treated only incidentally here.)

Since the two-station method eliminates the complications introduced by frequency-dependent phase shift at the source, it has become the most reliable method of determining the phase and group velocities pertaining to the crust and upper mantle underlying a path between two locations on the surface of the Earth.

Extraction of precise dispersion information is made difficult by the distortion due to the presence of noise and by a WWSSN seismometer response that peaks at 25 s period, with the consequence that the signal/noise ratio of longer period parts of the spectrum becomes progressively

weaker. In 1965 the peak response of WSSN long period seismometers was reduced to 15 s, with additional loss of long period signal strength.

However, under certain conditions, it is possible to observe extremely long period wave trains. Mantle waves consisting of energy at periods longer than 100 s can sometimes be seen clearly after multiple circumferential passages, because the combined effects of dispersion and attenuation reduce the proportion of shorter period energy generated by large earthquakes.

In this chapter, methods of extracting phase and group velocity from surface wave observations are presented in detail, and known limitations are discussed. The discussion uses a combined theoretical and practical approach and describes programs developed to run on a PDP-15 computer.

The analysis presented in Section 3.2 mainly follows that of Dziewonski and Hales [1972], with certain exceptions which are noted in the course of the exposition. It should be mentioned that three errors were found in their treatise, Section IIIA, 'Dispersion Parameters': (1) Eqn (7) should be integrated from $-\infty$, not 0. If the time domain signal is finite, the frequency band must be infinite. (2) The line after Eqn (10) should read $t_{ph}(\omega) = r/C(\omega)$; not $t_{ph} = C(\omega) \cdot r$. (3) Eqn (15) and the explanatory sentence preceding it are not clear when taken together. The equation is correct, but the sentence implies that one must seek independent means of obtaining $k(\omega)$ when $C(\omega)$ is known. The statement would be true if 'phase' and 'group' were interchanged to read 'phase velocity can be uniquely derived from group velocity if $k(\omega)$ at some frequency is known', followed by Eqn (3.21) of this text. These points will be clarified in the next section.

3.2 PHASE VELOCITY AND GROUP VELOCITY

The ground displacement produced by a single-mode propagating dispersed wave train at time t , distance r , and azimuth θ from the source may be represented by

$$f(r,t,\theta) = \frac{1}{2\pi} \int_{-\infty}^{\infty} F(\omega) e^{i\omega t} d\omega, \quad (3.1)$$

where $F(\omega)$, the complex frequency spectrum of the signal, can be considered as a function of both amplitude and phase, i.e.

$$F(\omega) = A(r, \theta, \omega) e^{i\phi(r, \theta, \omega)} . \quad (3.2)$$

The amplitude $A(r, \theta, \omega)$ exhibits a complex dependence on the source mechanism and the properties of the propagation medium. However, the phase is simpler and may be expressed as the sum of three terms:

$$\phi(r, \theta, \omega) = -k(\omega) \cdot r + \phi_o(\theta, \omega) + \phi_i(\omega) ; \quad (3.3)$$

where $k = 2\pi/\lambda$ is the wave number, $\phi_o(\theta, \omega)$ is a source phase shift that may vary with both azimuth and frequency, and $\phi_i(\omega)$ is the seismometer phase shift.

The treatment is simplified if we assume that ϕ_o and ϕ_i are zero and take the inverse Fourier transform of Eqn (3.2):

$$f(r, t, \theta) = \frac{1}{2\pi} \int_{-\infty}^{\infty} A(r, \theta, \omega) e^{i(\omega t - kr)} d\omega \quad (3.4)$$

to obtain the familiar travelling wave equation, where the phase $\Psi = \omega t - kr$ is a function of the independent variables ω and t . (The formalism of taking the total derivative at this point is due to the present author. It differs from the usual exposition of group velocity based on the integration of Eqn (3.4) over a narrow band of frequencies or, alternatively, the use of two monochromatic waves closely spaced in frequency.) The conditions for stationary phase are obtained by setting the total differential of Ψ equal to zero:

$$d\Psi = \frac{\partial\Psi}{\partial t} dt + \frac{\partial\Psi}{\partial\omega} d\omega = 0 . \quad (3.5)$$

For a monochromatic wave of frequency ω_1 , $d\omega = 0$ and the second term drops out. Then

$$\frac{\partial\Psi}{\partial t} = \omega_1 - k \frac{dr}{dt} = 0 \quad (3.6)$$

defines the phase velocity $C(\omega_1)$ of a wave of that frequency:

$$C(\omega_1) = \frac{dr}{dt} = \frac{\omega_1}{k(\omega_1)} . \quad (3.7)$$

Now, consider a snapshot of the wave train at time t_1 , in which case $dt = 0$. Then

$$\frac{\partial\Psi}{\partial\omega} = t_1 - r \frac{dk}{d\omega} \quad (3.8)$$

defines the group arrival time t_1 in terms of the distance r and a differential relation involving k and ω . A group velocity may now be defined as:

$$U(\omega) = \frac{d\omega}{dk} = \frac{r}{t}, \quad (3.9)$$

and M.A. Biot [1957] has established a general proof that group velocity is the same as the velocity of energy transport.

If phase velocity is independent of frequency $\omega/k = a$,

$$\frac{d\omega}{dk} = a, \quad (3.10)$$

and therefore group velocity is the same as phase velocity. This is non-dispersive propagation.

Seismic surface waves exhibit dispersion; that is, $C(\omega) \neq \text{constant}$ and, in general, group velocity is a function of frequency.

In some cases group velocity may be constant over a limited range of frequency, and an analytic expression giving phase velocity in terms of group velocity may be derived as follows. (Love waves exhibit nearly constant group velocity from about 100 to 300 s period.) Since

$$U(\omega) = U_0 = \frac{d\omega}{dk}, \quad (3.11)$$

$$\omega = \int U_0 dk = U_0 k + b_1 \quad (3.12)$$

and thus [combining with (3.7)]:

$$C(\omega) = \frac{U_0}{1 - b_2/T}, \quad (3.13)$$

where $b_2 = b_1/2\pi$ and T is the period. This approximation was given by Toksöz and Ben-Menahem [1963].

Group velocity and phase velocity are not independent dispersion parameters, of course, and some useful relations between them in terms of λ and T , are given here. For example, since $\omega = 2\pi C/\lambda$ and $k = 2\pi/\lambda$ we can write

$$U = \frac{d(2\pi C/\lambda)}{d(2\pi/\lambda)} \quad (3.14)$$

$$= \frac{\lambda dC - Cd\lambda}{\lambda^2} \bigg/ \left(-\frac{d\lambda}{\lambda^2} \right) \quad (3.15)$$

or

$$U = C - \lambda \frac{dC}{d\lambda} . \quad (3.16)$$

Proceeding in a similar manner we obtain the following useful relations for group velocity:

$$U = \frac{\lambda^2}{T^2} \frac{dT}{d\lambda} \quad (3.17)$$

and

$$U = \frac{C}{1 + \frac{T}{C} \frac{dC}{dT}} . \quad (3.18)$$

Eqns (3.16) and (3.17) appear in standard physics texts; Eqn (3.18), not so well known, appears in Toksöz and Ben-Menahem [1963].

On the other hand, if group velocity is known, phase velocity can be obtained by integration, although not uniquely, since there is a constant of integration. Eqn (3.9) is integrated as follows:

$$\int_{k_1}^k dk = \int_{\omega_1}^{\omega} \frac{d\omega}{U(\omega)} , \quad (3.19)$$

giving an integral expression for the wave number

$$k(\omega) = \int_{\omega_1}^{\omega} \frac{d\omega}{U(\omega)} + k(\omega_1) , \quad (3.20)$$

where $k(\omega_1)$ is the wave number at the lower limit of the integral and may not be accurately known. From Eqn (3.7), this gives

$$C(\omega) = \frac{\omega}{\int_{\omega_1}^{\omega} \frac{d\omega}{U(\omega)} + k(\omega_1)} . \quad (3.21)$$

For numerical work it is convenient to use $f = \omega/2\pi$, and Eqn (3.21) can be rewritten as:

$$C(f) = \frac{f}{\int_{f_1}^f \frac{df}{U(f)} + \frac{k(f_1)}{2\pi}} . \quad (3.22)$$

If the phase velocity $C(\omega_2)$ is known for a shorter period, then $k(\omega_2)$ is known and $k(\omega_1)$ can be obtained from

$$k(\omega_1) = k(\omega_2) - \int_{\omega_1}^{\omega_2} \frac{d\omega}{U(\omega)} . \quad (3.23)$$

This last equation is the basis for the final determination of phase velocity from group velocity as presented in Chapter 4. Fourier analysis is used to obtain an estimate of phase velocities at shorter periods, and this estimate is then used to obtain the wave number at longer periods.

3.3 THE TWO-STATION METHOD

Consider a seismogram recorded at station 1 of waves from an earthquake located a distance Δ_1° away. The approximate time of arrival of the dispersed wave train was printed out from a list of the events by a computer program using the relation

$$t_1' = t_0 + \frac{\Delta_1}{U_m}, \quad (3.24)$$

where t_0 is the time of origin and U_m is the approximate maximum group velocity, taken as 2.4° per min for Rayleigh waves and 2.64° per min for Love waves. The seismograms were examined in the vicinity of t_1' , and those showing a readable signal were selected for digitizing. Digitization commenced at t_1 (two or three min earlier than t_1') to ensure inclusion of low-amplitude long period waves present in the beginning of the dispersed wave train. A standard sampling rate of one per s, high enough to eliminate aliasing and low enough to include all of the wave train within 1024 s (about 17 min), was used. The horizontal component seismograms were combined according to the relation

$$f(t)_{\text{transverse}} = f(t)_E \cos \theta - f(t)_N \sin \theta \quad (3.25)$$

to obtain ground motion transverse to the direction of propagation. $f(t)_E$ is the east-west component, $f(t)_N$ is the north-south component and θ is the azimuth from the station.

Standard preliminary signal processing was applied to all time series [see, for example, Bendat and Piersol, 1971, p.289] for trend removal and end tapering.

Fourier phase spectra were then computed, using the Fast Fourier Transform (FFT), and phase velocities were computed from the relation

$$C(T) = \frac{D_2 - D_1}{t_2 - t_1 + T \left(\frac{\phi_2 - \phi_1}{2\pi} + m \right)} \quad (3.26)$$

in which the subscripts denote station 1 or 2, D is the epicentral

distance in km, t is Greenwich Mean Time at the start of the digitizing, T is the period, ϕ is the phase angle in radians and m is an integer reflecting the uncertainty due to the periodicity of trigonometric functions. The correct value for m was determined by a program that permitted convenient interaction with the data, which is briefly described here.

Discrete Fourier analysis quantizes the phase and amplitude of a continuous distribution of energy into resolvable frequency bands of width approximately 0.001 Hertz in this case. A period T_j can be associated with the band by the relation

$$T_j = \frac{1024}{j-1}. \quad (3.27)$$

Eqn (3.26) is used to compute a discrete phase velocity $C(T_j)$ at periods from 14 s ($j=74$) to 79 s ($j=14$). It is reasonable to assume that the phase velocity at 79 s should have a value close to 4.0 km/s. This value is used in Eqn (3.26) to obtain an integer value for m_0 , which is usually a small positive integer or zero. m_0 gives a starting point to plot phase velocity for $j=14$ to $j=74$. At each increment of j , the program examines $C(T_{j-1})$ for three test values of m (they are m , $m+1$, $m-1$) and the current value for m is changed to the one from this subset which minimizes the change in $|C(T_{j-1}) - C(T_j)|$, thus obtaining the smoothest possible phase velocity curve that the data will permit.

If the resulting phase velocity curve is unacceptable the above procedure is repeated on the same plot with unit change in m_0 , giving a family of phase velocity curves (see Fig. 3.1) from which the most geophysically realistic one can be chosen. Greater separation between the curves at periods longer than 50 s facilitates the selection of the correct one. This early stage of simple harmonic analysis was performed on Thomas's [1969] 35 earthquakes. While it was possible to extend his results to periods somewhat longer than 50 s, it was obvious that not much reduction of the scatter in phase velocity results was achieved. At this point, considerable attention was focused on time-varying filtration to improve the phase information; this is elaborated in the next section.

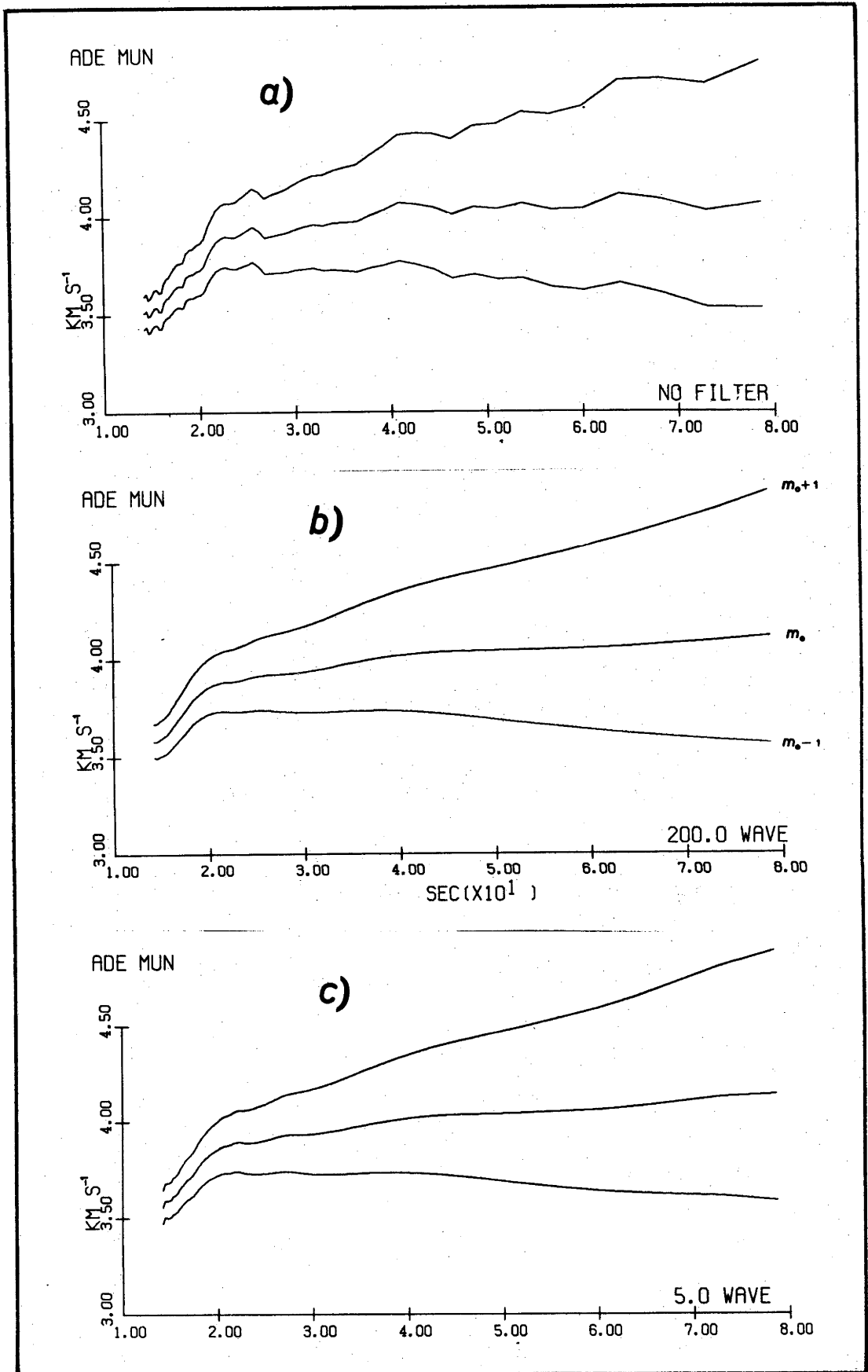


Figure 3.1: Phase velocity curves for ADE-MUN event 3 showing the effect of ambiguity in the number of wavelengths between two recording stations. (a) unfiltered, (b) 200 s window used in time-variant filtering, (c) window width is five times the period of a Fourier component.

3.4 TIME-VARYING FILTRATION (TVF)

Knopoff and Pilant introduced TVF as a procedure to reduce the distortion of phase measurements caused by noise energy whose arrival-time on a frequency-time plane is significantly different from that of the signal. Landisman *et al.* [1969] discussed the implementation of various window functions in both the time domain and the frequency domain. Frequency domain filtering only will be considered here.

The first step in TVF is to construct an FTAN contour diagram of the signal, as shown in Fig. 3.2a, which displays event number 3 recorded at Adelaide. Fig. 3.3a shows the record at Mundaring. These typical examples of seismograms used in this study show the following points:

- (1) The main dispersed signal is clearly visible. It is plotted in terms of group arrival-time against log period. Time increases from the top of the diagram downwards.
- (2) The ridge crest denoting the dispersed wave train is clearly evident.
- (3) Isolated plateaus of noise such as that marked 'a' are apparent.
- (4) The region marked 'b' is the first higher oceanic shear mode of propagation.

In Fourier analysis, these extraneous noise regions distort the true phase of the signal at the same frequency.

The heavy line on the FTAN diagram is the best estimate of group arrival-time. The location of this line is a subjective operation that depends on the skill and experience of the analyst. However, he can use all the information in the FTAN diagram to decide where to place the estimated group arrival time line.

The FTAN contour plot is remounted on the 565 Calcomp plotter and, with the aid of a program similar to the digitizing program described in Chapter 2, 42 discrete coordinates of group arrival-time are entered into the computer and appended to the file containing the digitized seismogram. This technique of graphical interaction expedited the design of a large number of TVFs.

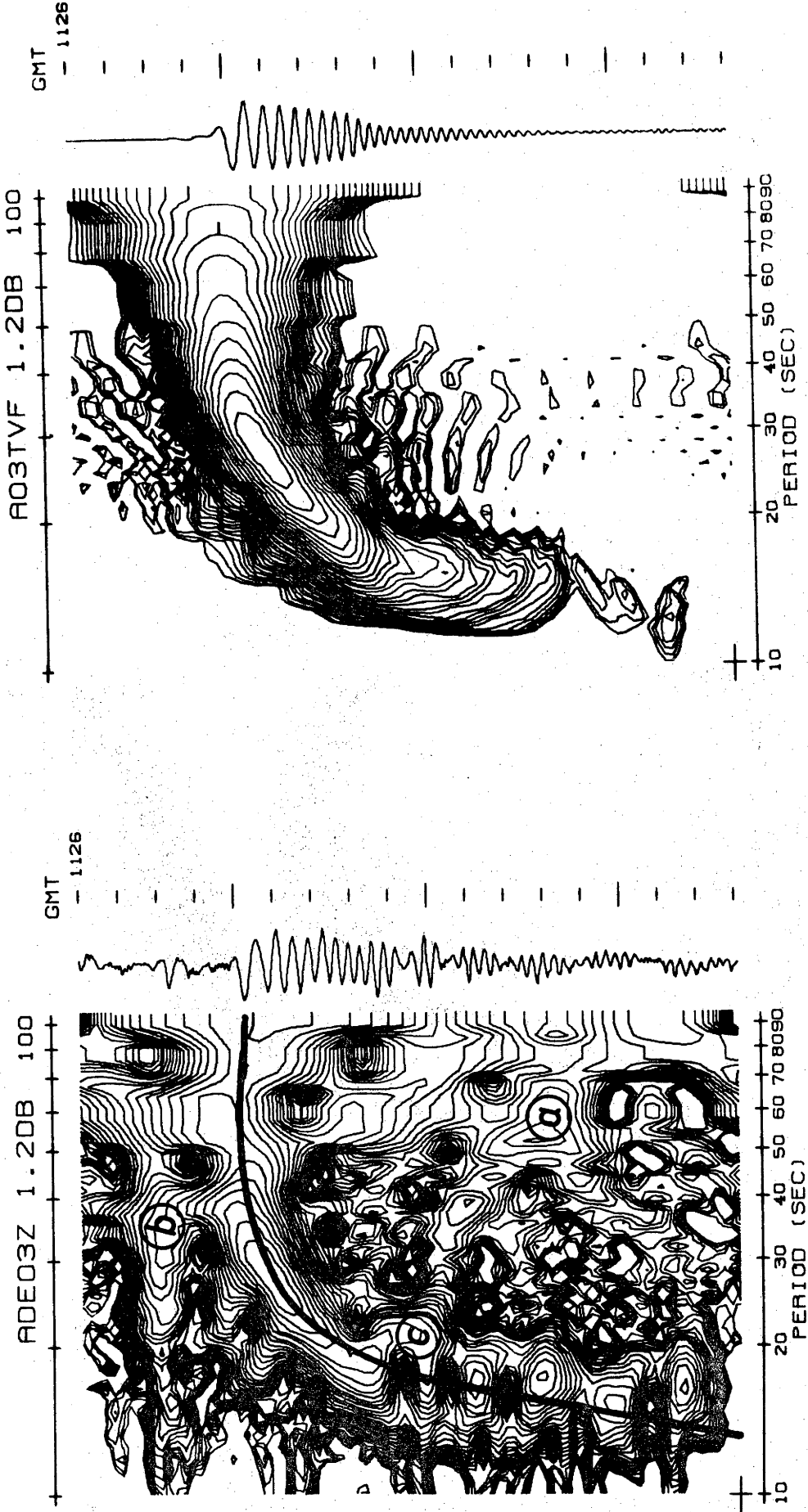


Figure 3.2: Frequency time analysis of event 3 at Adelaide (left); the same seismogram after time-variant filtering (right). Notice later time arrival of energy at 'c'.

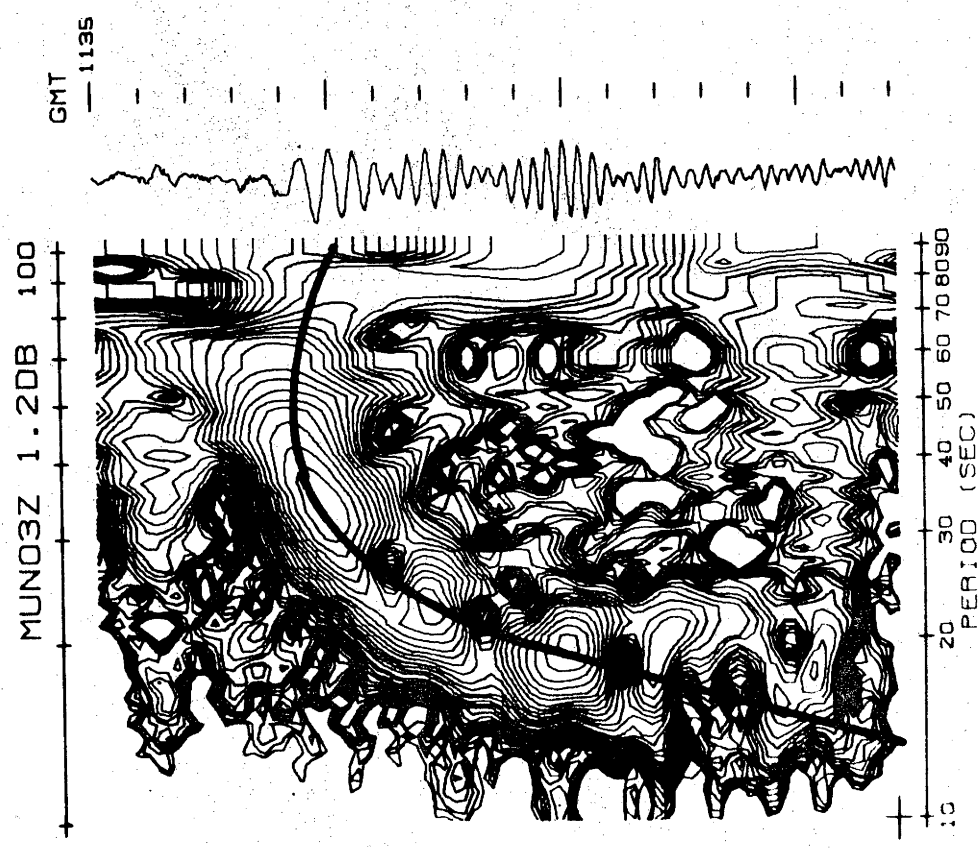
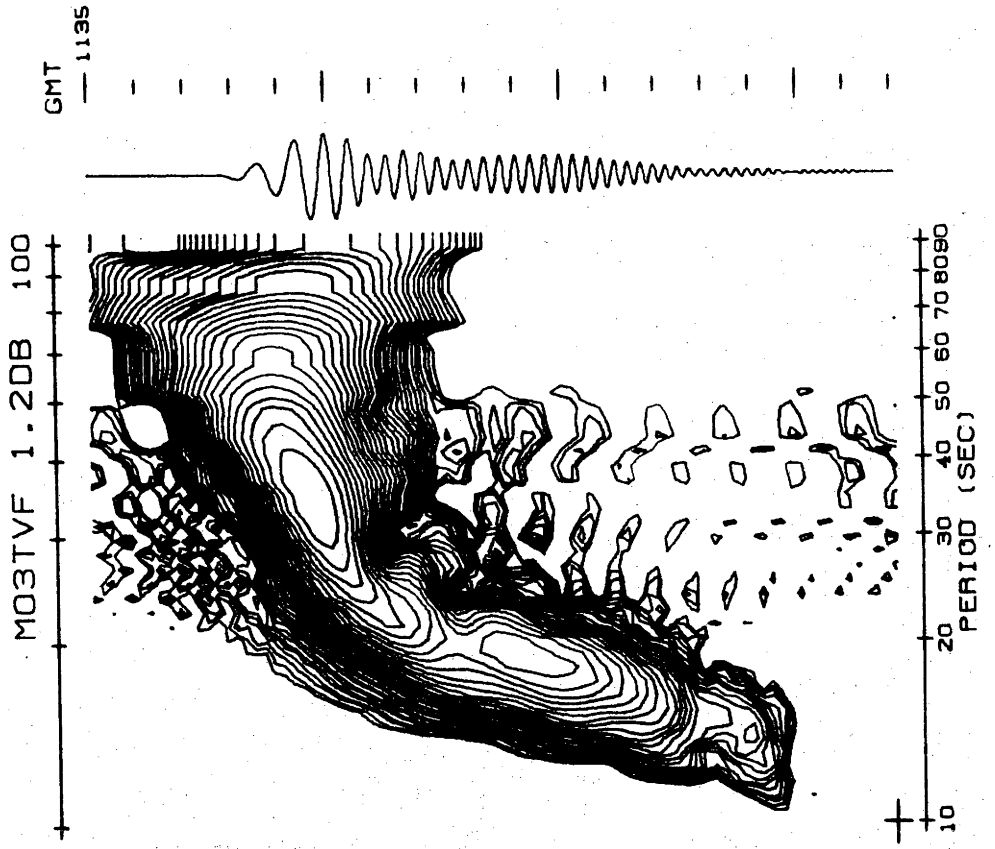


Figure 3.3: Frequency time analysis of event 3 at Mundaring (left); the same seismogram after time-variant filtering (right).

The file containing the digitized seismogram is now ready to be processed by the TVF program, which performs the following computations:

- (1) A discrete Fourier transform is computed, from which Fourier amplitude coefficients are obtained.
- (2) Each Fourier component, taken as a pure sinusoidal time function, is windowed symmetrically by a cosine window with its midpoint at the group arrival time of that frequency.
- (3) The windowed sinusoidal components are added in the time domain to synthesize a TVF'd seismogram.

An FTAN plot of the results of TVF is shown in Figs. 3.2b and 3.3b. Notice that the noise located away from the main signal wave train is no longer present. However, the comparison of phase velocity curves for this event before and after TVF, shown in Fig. 3.1, deserves some critical comments.

Bias can be introduced by the subjective choice of estimated group arrival time on the FTAN plot. Furthermore, it is difficult to establish general criteria for the width of the window as a function of period. Numerical experiments showed that, when the signal/noise ratio was low (as at the longer periods), the computed phase curve after TVF was sensitive to both the choice of group arrival time and the window function. A slightly different estimate of group arrival time, say earlier at station 1, would produce a lower phase velocity after TVF because the windowing advances the phase at station 1, making the computed phase delay greater.

Two kinds of window functions were thoroughly investigated, (1) a constant window width within the range 100 to 400 s, and (2) a window width equal to a constant between 2 to 10 times the period of the Fourier component. Fig. 3.1 shows some results for event 3 with windows of (1) 200 s and (2) five times the period. While both curves have been smoothed compared to the unfiltered phase velocity curve, the differences between them show that the results of TVF are susceptible to the choice of windowing function.

If the signal/noise ratio is too small, no amount of processing will bring out the phase information from a single event. On the other hand, when the signal/noise ratio is large, TVF is an effective method of smoothing the phase velocity curve.

After Thomas's set of events had been processed as outlined here, it was concluded that TVF would not attain the objective of extending the phase velocity curves to longer periods. This objective can be achieved by the method of summing cross-correlograms suggested by Dziewonski and Hales [1972], which is discussed in the next section.

3.5 CROSS-CORRELATION

Consider the Earth between two seismic stations to be a linear filter that modifies an input signal $f_1(t)$ to produce $f_2(t)$ observed at the second station. Using electrical circuit terminology, the properties of a linear filter can be completely specified by a transfer function $H(\omega)$. Furthermore, if $F(\omega)$ is the Fourier transform of $f(t)$, then

$$F_2(\omega) = H(\omega) F_1(\omega) . \quad (3.28)$$

Multiplying both sides of this equation by $2\pi F_1^*(\omega)$, the complex conjugate of $F_1(\omega)$, gives

$$2\pi F_1^*(\omega) F_2(\omega) = H(\omega) \cdot 2\pi F_1^*(\omega) F_1(\omega) . \quad (3.29)$$

The left hand side of Eqn (3.29) is recognized as the Fourier transform of the cross-correlation $f_{12}(\tau)$, where

$$f_{12}(\tau) = \int_0^{\infty} f_1(t) f_2(t+\tau) dt . \quad (3.30)$$

Similarly, the right hand side is the transfer function $H(\omega)$ multiplied by the Fourier transform of the autocorrelation of $f_1(t)$ [see, for example, Lee, 1966, p.4]. Since the phase of an autocorrelation is zero, the phase spectrum of the left hand side must be the same as the phase spectrum of $H(\omega)$. The left hand side may be expanded as

$$2\pi A_1(\omega) A_2(\omega) e^{i(\phi_2(\omega) - \phi_1(\omega))} , \quad (3.31)$$

which demonstrates that the cross-correlogram of two signals is a function whose phase spectrum is the difference of the phase spectra of the two signals. In other words, the Fourier transform of the complete cross-correlogram $f_{12}(\tau)$ yields the same phase spectrum as the difference between the phase spectra of $f_1(t)$ and $f_2(t)$.

The most important advantage derived from the cross-correlation method is 'normalization' of the path. Since the cross-correlogram

contains the phase function of the path, this normalization makes it possible to add directly the cross-correlograms of an arbitrary number of events in order to achieve signal enhancement, especially at longer periods.

When performed in the time domain, the computation of a cross-correlogram used about 5 min of computer time and yielded a time series 2047 points in length. The mid-point of the cross-correlogram corresponds to a time lag equal to the difference between the start times of the digitized seismograms. This fact is used to line up the cross-correlograms to a common time lag for one path so that they can be added. Prior to summation, the cross-correlograms were normalized to a maximum value of unity. This operation weights each event equally, rather than a weight that would depend on the signal strength.

Because of the small core size of the PDP-15, all Fast Fourier Transforms were restricted to time series 1024 points long, and it was necessary to truncate the 2047-point cross-correlogram to 1024 points. This was accomplished by locating the absolute maximum of the sum of cross-correlograms and extracting 512 points on either side of the point. The phase spectrum derived from the truncated series has to be corrected by the relation

$$\bar{\phi} = \phi_{tr} - \frac{2\pi\Delta t}{T}, \quad (3.32)$$

where $\bar{\phi}$ is the desired phase spectrum of the full cross-correlogram, ϕ_{tr} is the phase spectrum derived from the truncated cross-correlogram, Δt is the time shift between these two time series and T is the period of a Fourier component. Phase velocity for the two-station path under consideration could now be computed according to Eqn (3.26) where, now, $\bar{\phi} = \phi_2 - \phi_1$.

Landisman *et al.* [1969] showed that it was possible to evaluate group velocity directly from the cross-correlogram. They regard the inter-station cross-correlogram as an approximation to the temporal response of the inter-station medium when a delta function is applied to the first station and recorded by a distortionless detector at the second station. They suggest that the cross-correlogram should contain the group delay times for all wave components common to the two original recordings. Note that the phase delay function of the cross-correlogram is identical with the phase delay function of the impulse response of the inter-station

medium and, according to Eqn (3.5) *et seq.*, this observation is sufficient to define group velocity. The amplitude function of the cross-correlogram is $A_1(\omega) \cdot A_2(\omega)$, whereas the amplitude function of the impulse response is given by $A_2(\omega)/A_1(\omega)$. In general the latter expression cannot be computed satisfactorily because of instabilities in the amplitude spectrum. Furthermore, it implies non-divergence of energy, in that it is implicitly assumed that the change observed in the wave from station 1 to station 2 is completely due to the intervening medium. This assumption is not strictly accurate in view of arrival of energy by paths other than the direct path.

3.6 FREQUENCY TIME ANALYSIS (FTAN)

The evolution of FTAN as applied to seismic signals was described briefly in Chapter 1, Section 1.2. The basic approach of determining group arrival time by narrow-band filtering of the seismic signal was first used by Alexander [1963]. Early attempts to systematize methodology were made by Archambeau *et al.* [1965, 1966]. Difficulties associated with time domain filtration were obviated by Dziewonski *et al.* [1969] who exploited the Fast Fourier transform. Later Dziewonski *et al.* [1972] gave an explicit analytical representation for the filtered seismogram using first order Taylor series expansion for $A(\omega)$ and $k(\omega)$, and, more recently, Herrmann [1973] extended the theoretical analysis to treat the occurrence of multiple modes and to include the second term in the Taylor series expansion. He concluded that 'narrow band-pass filtering of a dispersed surface wave can be used to determine the group velocities and spectral amplitudes of the various modes composing the signal under certain conditions: namely that the group arrivals of the individual modes are well enough separated in time that their contributions to the filtered signal do not interfere' [Herrmann, 1973, p.670].

Since FTAN is thoroughly described in the above works, it will not be presented in full detail here. A concise formulation of the method, similar to that given by Levshin [1972], will be given. In the present study FTAN was used extensively, not only for analysis and determination of group and phase velocities, but also for designing time-variant filters and as an aid in pre-selection of events. All seismograms were subject to FTAN after being digitized. The compendium

of all these contoured arrival times is an extremely interesting exhibit of the 'wealth of information contained in ordinary seismograms' [Landisman *et al.*, 1969]. It is hoped that sufficient examples are included in the next chapter and Appendix D to illustrate this quotation.

Following Levshin [1972], consider the expression describing an inverse Fourier transform

$$Y(t, \omega) = \frac{1}{2\pi} \int_{-\infty}^{\infty} H\left(\frac{\lambda - \omega}{\omega}\right) F(\lambda) e^{i\lambda t} d\lambda, \quad (3.33)$$

where t = time

ω = circular frequency

$F(\lambda)$ = Fourier spectrum of preprocessed seismogram

λ = dummy circular frequency

$H(x)$ = narrow band filtering kernel centered on $x = 0$.

At the present time, no analytical methods are known that enable a continuous evaluation of the complex function $Y(t, \omega)$. Therefore the continuous filter kernel $H\left(\frac{\lambda - \omega}{\omega}\right)$ is partitioned into a bank of discrete narrow-band Gaussian filters

$$H_i(\lambda, \omega_i) = e^{-\alpha \left(\frac{\lambda - \omega_i}{\omega_i}\right)^2}. \quad (3.34)$$

The envelope of the filtered seismic signal is equal to the magnitude of the complex function $Y_i(t, \omega_i)$. It is computed by the equation

$$|Y_i| = \sqrt{Y_i^2 + \hat{Y}_i^2}, \quad (3.35)$$

in which \hat{Y} is the Hilbert transform of Y . Deutsch [1969, p.107] discusses envelope functions of analytic signals and shows that they are well defined provided that the carrier frequency is above the bandwidth of the modulating signal. The Hilbert transform, also known as the 'quadrature function', advances the phase of each Fourier component by 90° . That is, if $S(T) = \cos T$ then $\hat{S}(T) = \sin T$, and if $S(T) = \sin T$ then $\hat{S}(T) = -\cos T$. The envelope function is displayed in contiguous columns to give a two-dimensional representation of amplitude on a time vs. logarithmic frequency plane. Envelope samples were decimated to eliminate too many data points as required.

Dziewonski *et al.*'s [1969] algorithm produced a display of signal amplitudes as a matrix of two-digit numbers output on a line printer. The matrix was subsequently contoured by hand. Since this operation would have been too laborious to process a large number of events, the present study used a contouring program kindly furnished by Mr J.A.B. Palmer of the Division of Computing Research, CSIRO, Canberra, A.C.T., to contour the FTAN results prior to output. Both Dziewonski's algorithm and Palmer's contouring program were developed to run on large computers, and some changes had to be made to permit them to run within the 16 K memory of the PDP-15. However, these did not seriously affect their scope, and appropriate modifications permitted a maximum FTAN contoured plot of 42 period samples by 85 time (or velocity) samples to be output. This constitutes a period range of 10 s to 90 s, with period samples spaced 15% apart. Where required, extension of the period range to 200 s was accomplished by re-filtering the seismograms over the period range 20 to 200 s; the overlapping FTAN sections were then superimposed to obtain a 10 s to 200 s period coverage.

In order to fit these programs in the 16 K memory of the PDP-15, only one complex Fortran array is used in the computer program to implement the filtering implied in Eqn (3.33), as contrasted to Dziewonski's algorithm, which uses three Fortran arrays of the same size. The digitized seismogram is read into the real part of a complex array and its FFT is computed and stored on disc. For each Gaussian filter, the FFT is read back into the same Fortran array and frequency windowing is performed in place. The need for one array is eliminated by storing the Fourier transform on disc rather than holding it in core. Y_1 and its Hilbert transform \hat{Y}_1 are simultaneously computed and returned into the same complex array by an algorithm later discovered to exist in McCowan [1966]. Computer serendipity led the author to discover this time and space saving artifice before McCowan's documentation was pointed out to him. This method of computing the Hilbert transform obviates the third Fortran array. Briefly stated, the procedure is to zero the second half of the FFT, and half-weight the end and middle points before computing the inverse transform. Y_1 is in the real part of the complex array and \hat{Y}_1 is in the imaginary part. The envelope function is computed by Eqn (3.35) in the same Fortran array, and is stored on disc until it is scanned later by the contouring program.

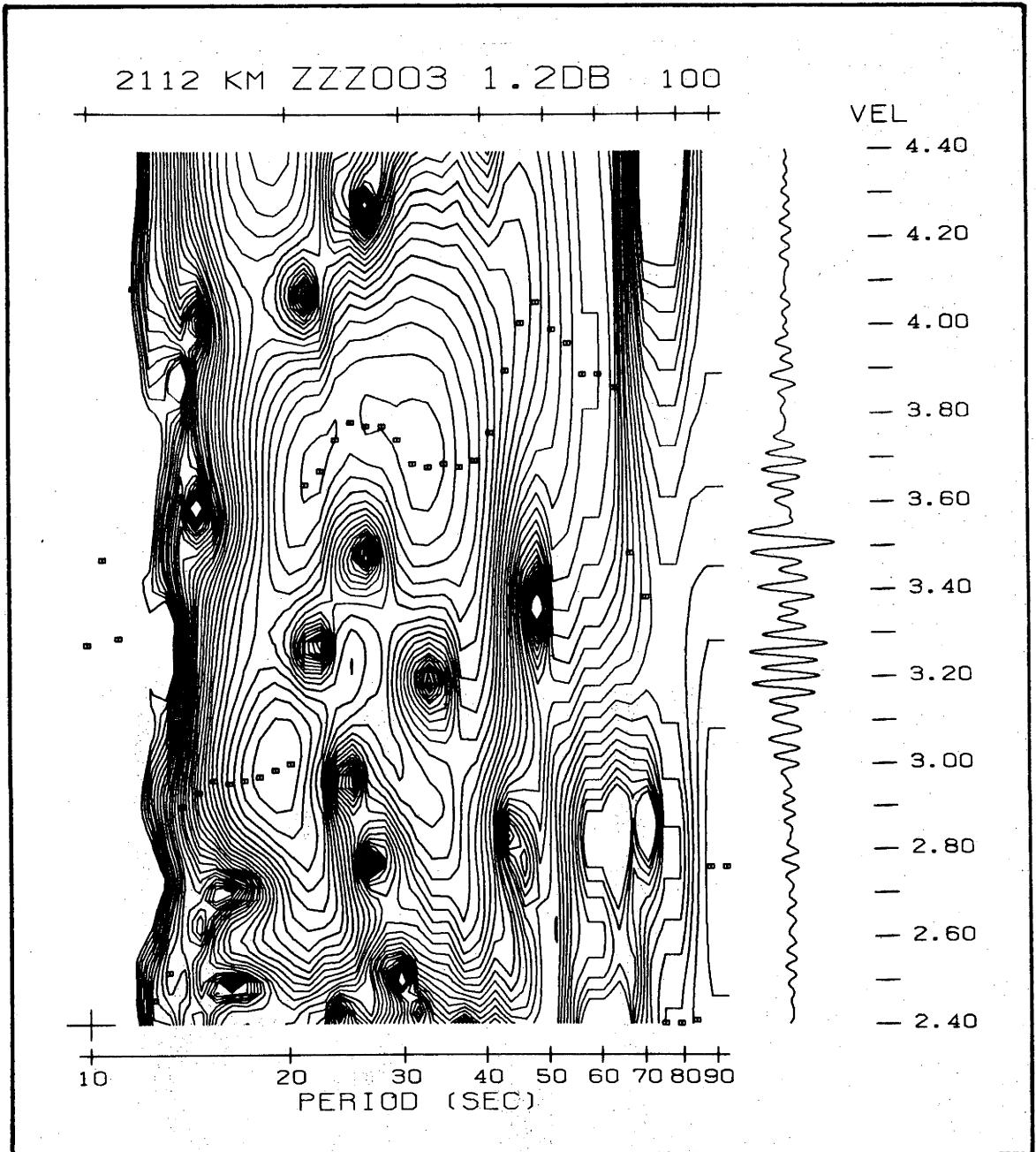


Figure 3.4: Frequency-time analysis of the cross-correlation of event 3 to infer group velocity for ADE-MUN path. See Section 2.1 for discussion of anomalously high group velocity at 20-30 s period.

An FTAN plot required about 13 min to produce, depending on the desired number and spacing of the contour intervals. By using program segmentation software supplied by Digital Equipment Corporation (CHAIN and EXECUTE), an overlay scheme was developed that enabled the computer to process a number of data files without the need for operator presence. A flow chart of FTAN procedure is shown in Fig. 3.5.

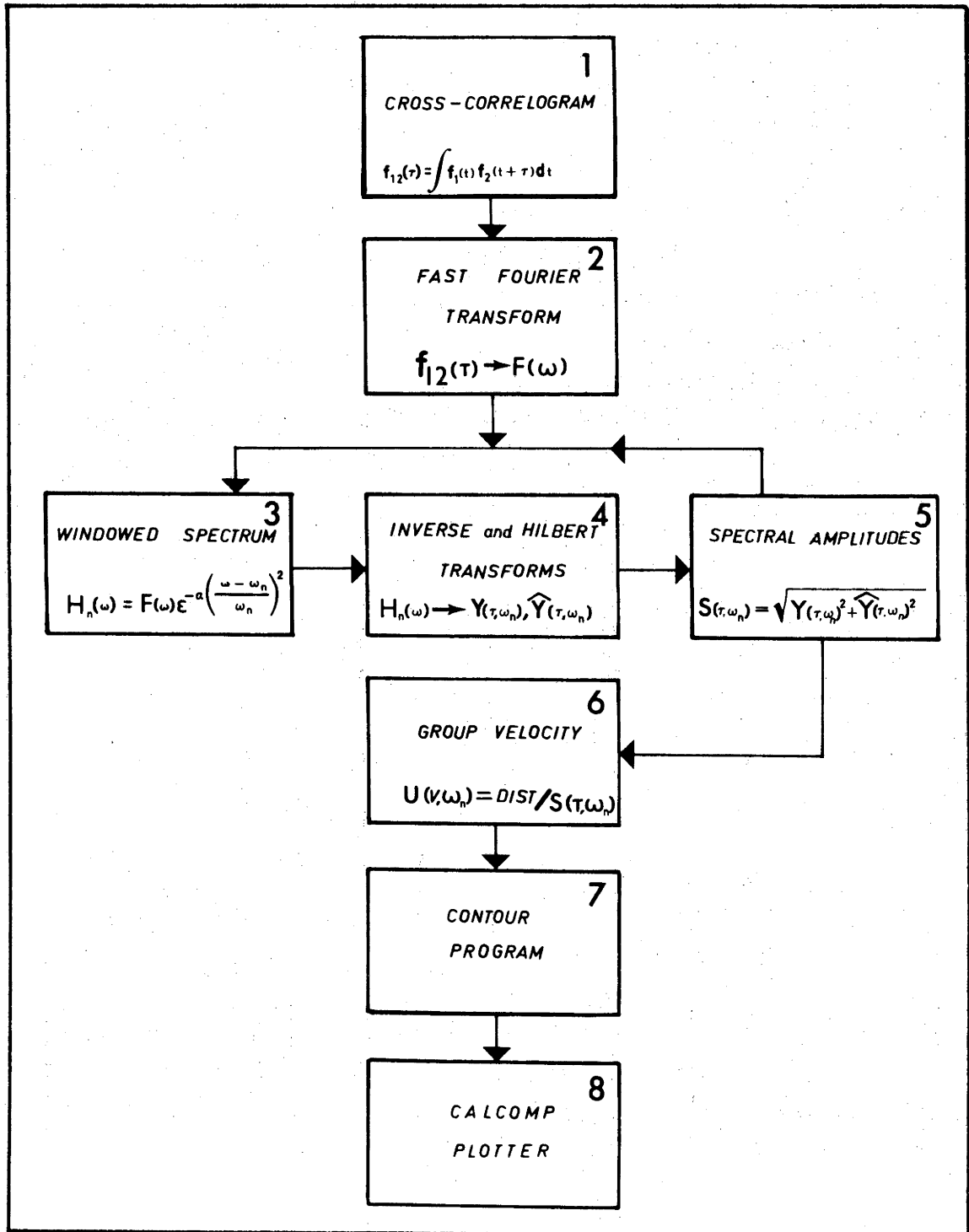


Figure 3.5: Flow chart for obtaining group velocity from contour plot of frequency-time analysis (FTAN) of cross-correlogram.

CHAPTER 4

ANALYSIS OF OBSERVED DISPERSION

4.1 INTRODUCTION

Methods of numerical analysis used to calculate surface wave dispersion from seismograms recorded at two stations were described in the preceding chapter. Given five WWSSN recording stations situated more-or-less uniformly around the coast of Australia, there are nine continental paths that can be studied. These were shown in Fig. 2.3. The aim of this investigation is to determine if differences exist in the dispersion across these nine paths, which would indicate variations in the crust-upper mantle structure throughout Australia. To do this, the dispersion must be measured with sufficient precision to render the uncertainties of the measurement less than the differences that might exist. This chapter is devoted to presentation and discussion of the results of analysis of the dispersion observed in the nine Australian paths.

A remark about the presentation, particularly about the amount and detail of results, is in order at this point. On the average, there are six events included in the determination of dispersion for each of the nine paths. Each event requires three FTAN diagrams, two for the seismograms and one for the cross-correlation analysis. Thus, some 162 FTAN diagrams would be needed for a complete documentation of the work done on Rayleigh waves alone. Love wave analysis would add another 111 diagrams.

The inclusion of these FTAN diagrams in totality would be confusing and would unnecessarily increase the length of this dissertation. Therefore, one path, CTA-ADE, was selected for which the analysis and results are presented in full detail. This path was selected because it has been extensively analysed by other workers during the past few years, and Rayleigh wave phase velocity information for comparison exists in the literature. The general quality of the data and

analytical results for this path are typical of the other eight paths, and it is believed that full documentation of this one path will serve to illustrate the treatment given to all.

4.2 THE PATH CTA-ADE: RAYLEIGH WAVES

Six earthquakes were analysed for the CTA-ADE path, of which five were located to the north. Their epicentral distances and magnitudes are listed in Table 4.1.

Table 4.1

Identification number	Epicentral distance ($^{\circ}$)	Magnitude
7	14.5	-
9	16.1	5.7
12	81.0	5.4
19	15.6	5.6
21	15.8	5.9
136	83.4	5.6

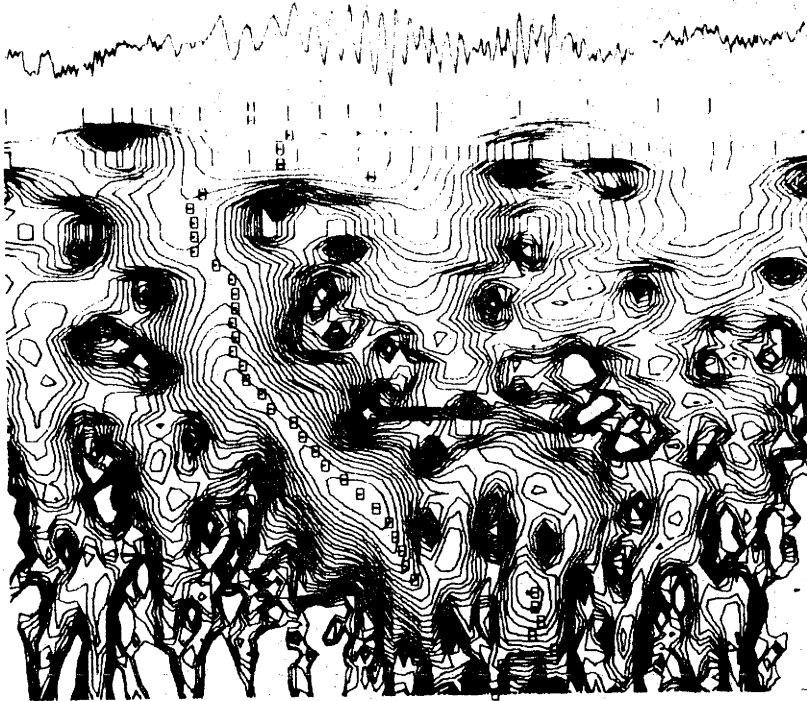
FTAN diagrams of group arrival times for the six events are shown in Figs. 4.1 to 4.6, with the figure on the left side showing the FTAN analysis of the surface wave train at the first of the two-station pair. The dispersions observed at the first station for events 7, 9, 19 and 21, which are all nearly 15° distant, are similar and typical of an oceanic path. In each of these cases the FTAN diagram at station 2 is markedly different from that at station 1, as a result of the wave train having traversed a continental inter-station path.

Early efforts in this study were devoted to time-variant filtration of separate events in an attempt to extend the period range and to smooth the phase curve. Results of time-variant filtering of five events are shown in Fig. 4.7. Event 136 is not shown in this figure because it is not one of Thomas's set of events, and only the events used by Thomas were time-variant filtered, because it was subsequently found that an analytical program using the sum of cross-correlations without TVF was preferable. These results indicated that time-variant filtering

ADEC72 1.20B 100

GMT

- 2254

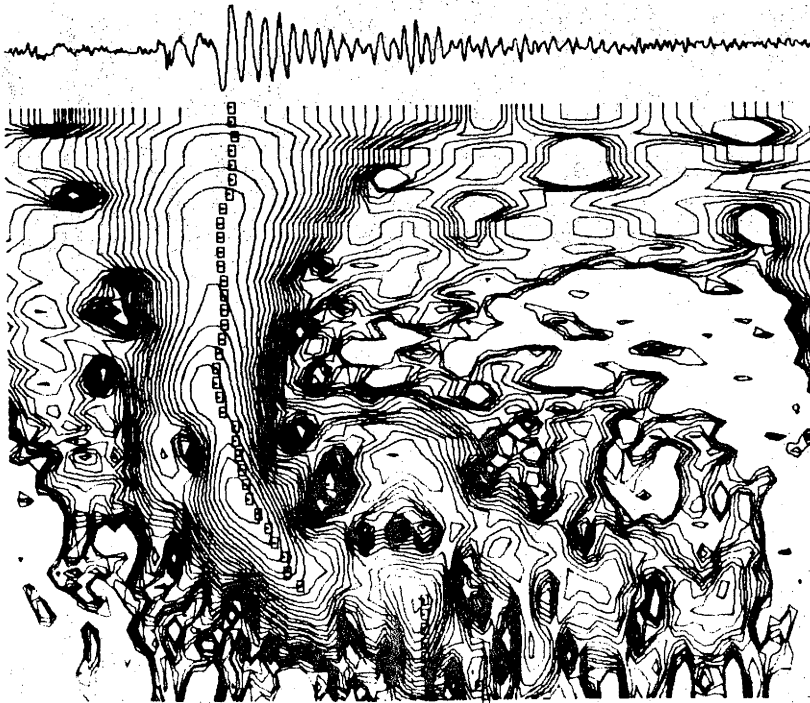


10 20 30 40 50 60 70 80 90
PERIOD (SEC)

ADEC72 1.20B 100

GMT

- 2251



10 20 30 40 50 60 70 80 90
PERIOD (SEC)

Figure 4.1: Frequency time analysis of event number 7 vertical component recorded at station 1, CTA (left), and station 2, ADE (right). Seismogram uncorrected for instrument response, G.M.T. is Greenwich Mean Time start of digitization. Small squares indicate maximum amplitude at constant period. There are 24 contour intervals spaced 1.2 db apart.

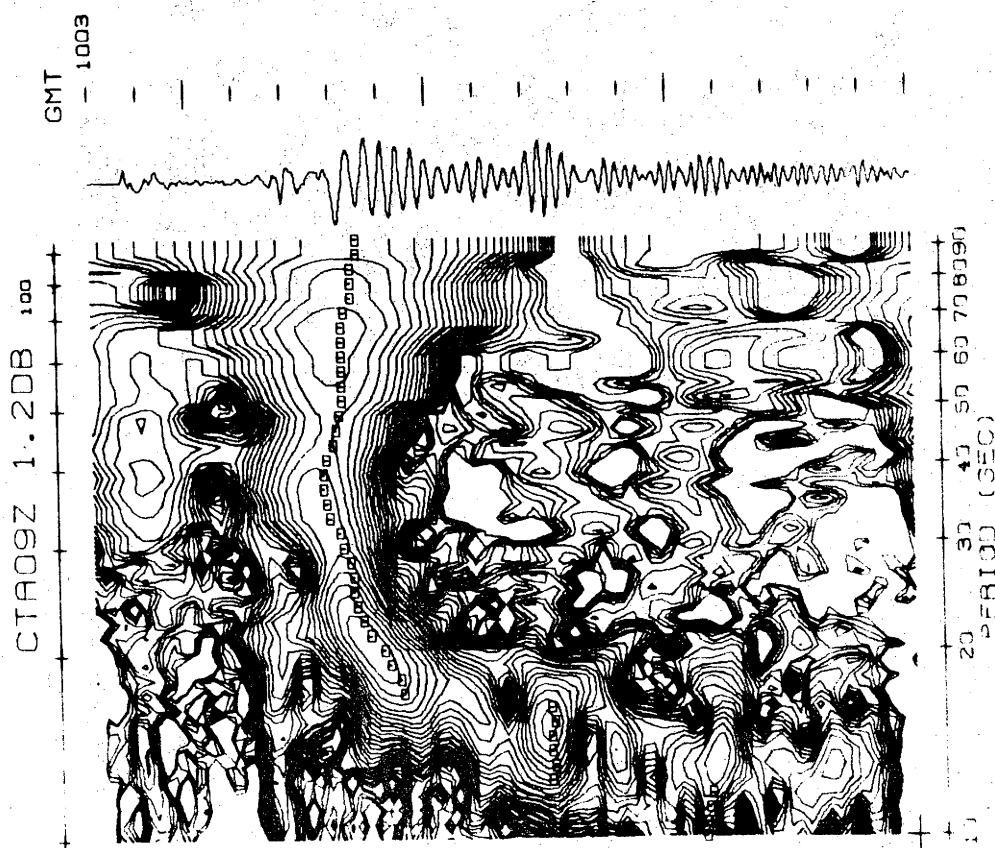
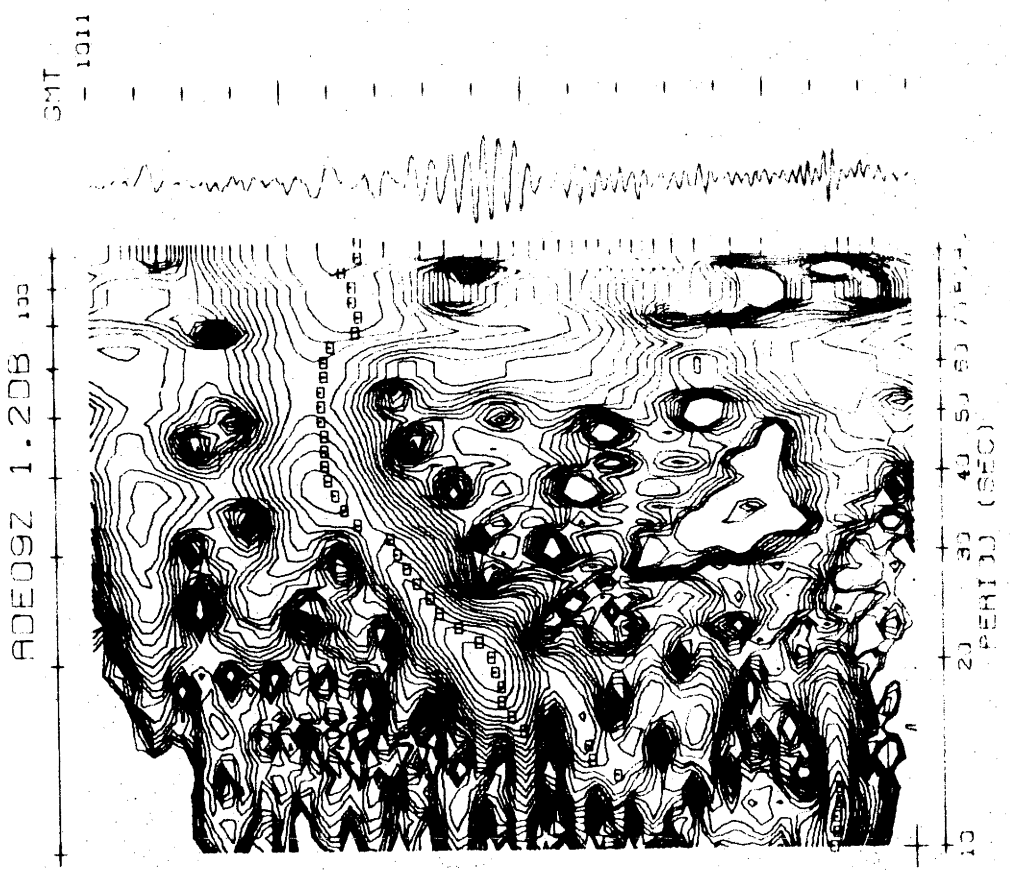


Figure 4.2: FTAN analysis of event number 9 vertical component. For details see caption to Figure 4.1.

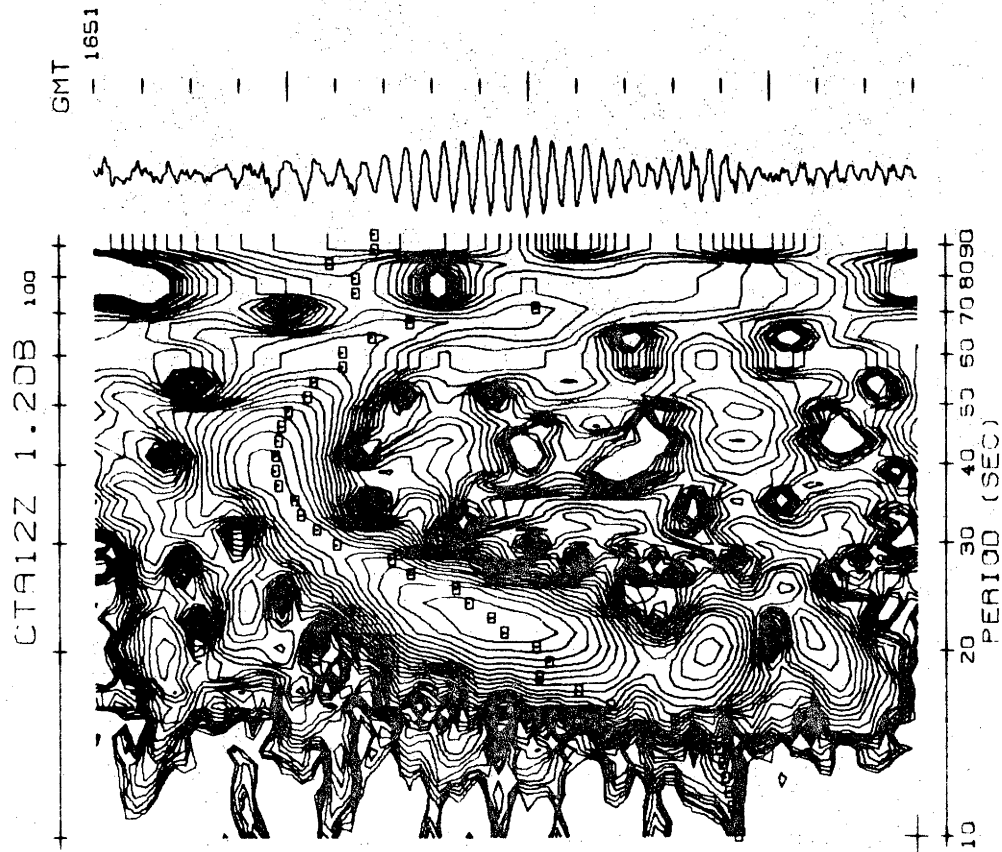
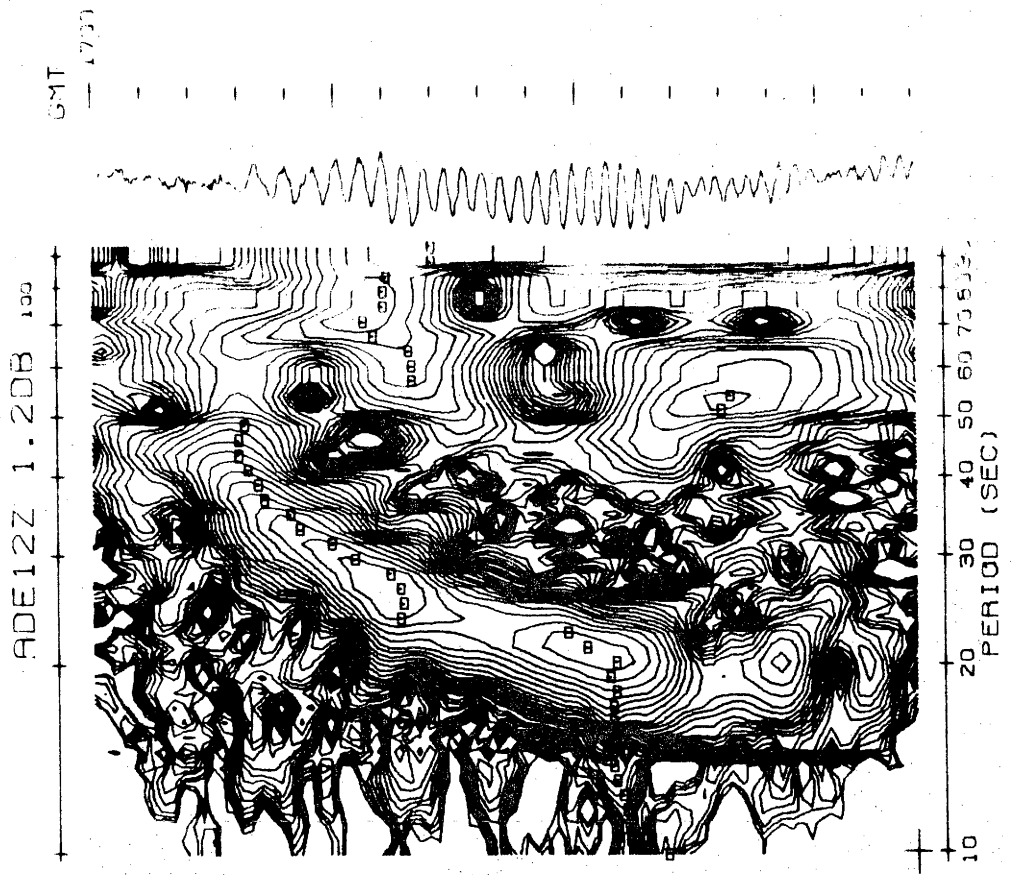


Figure 4.3: FTAN analysis of event number 12 vertical component. For details see caption to Figure 4.1.

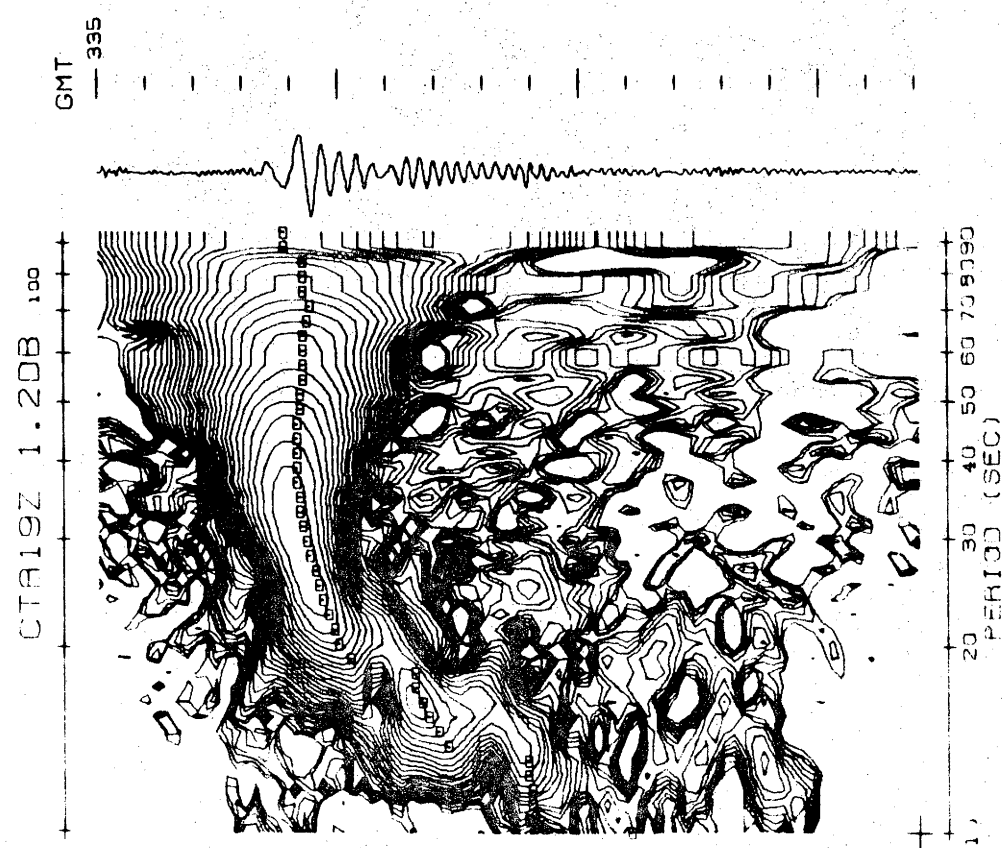
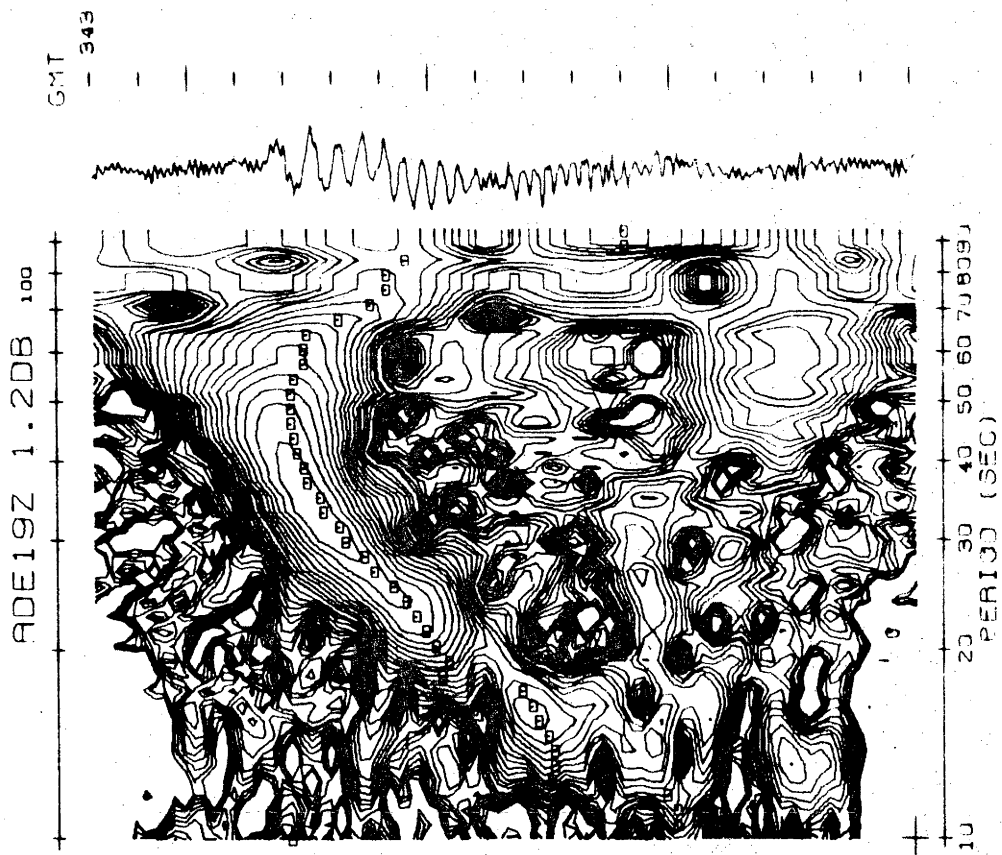
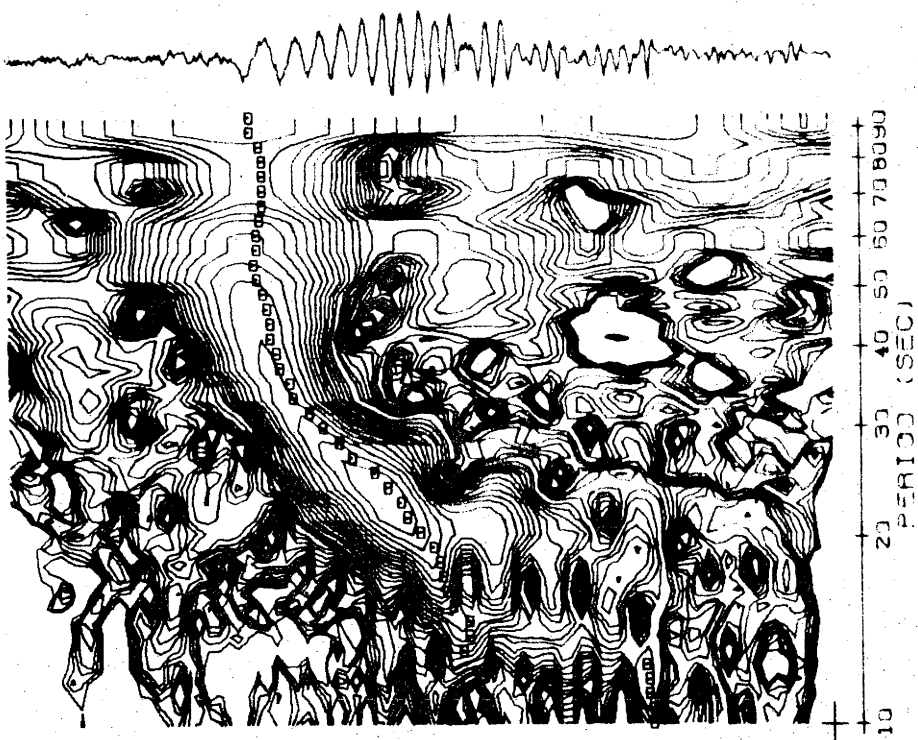


Figure 4.4: FTAN analysis of event number 19 vertical component. For details see caption to Figure 4.1.

A0E21Z 1.2DB 100

GMT
- 2252



CTA21Z 1.2DB 100

GMT
- 2245

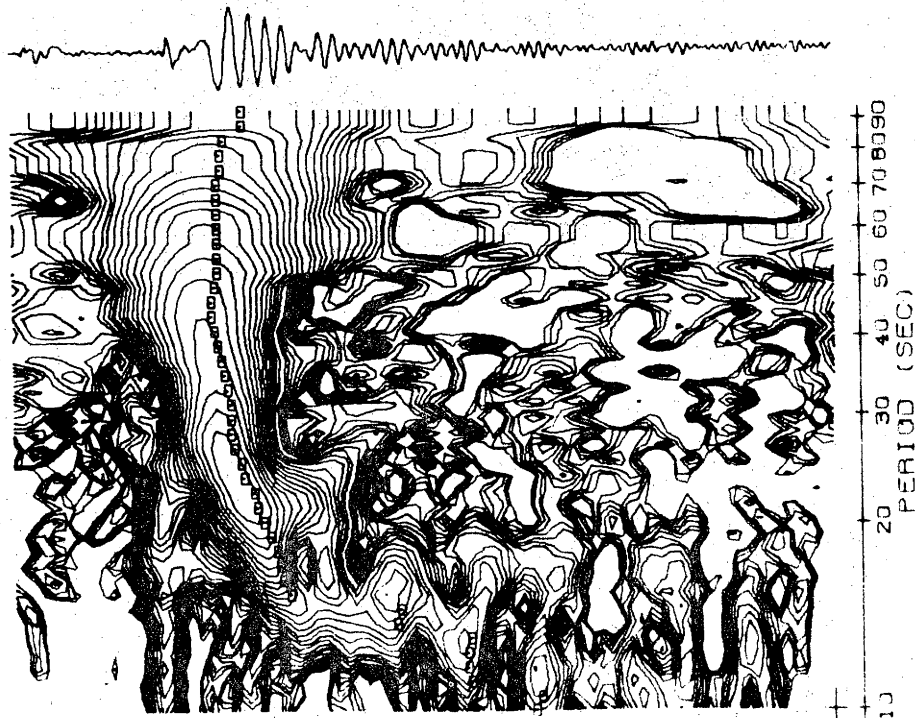


Figure 4.5: FTAN analysis of event number 21 vertical component. For details see caption to Figure 4.1.

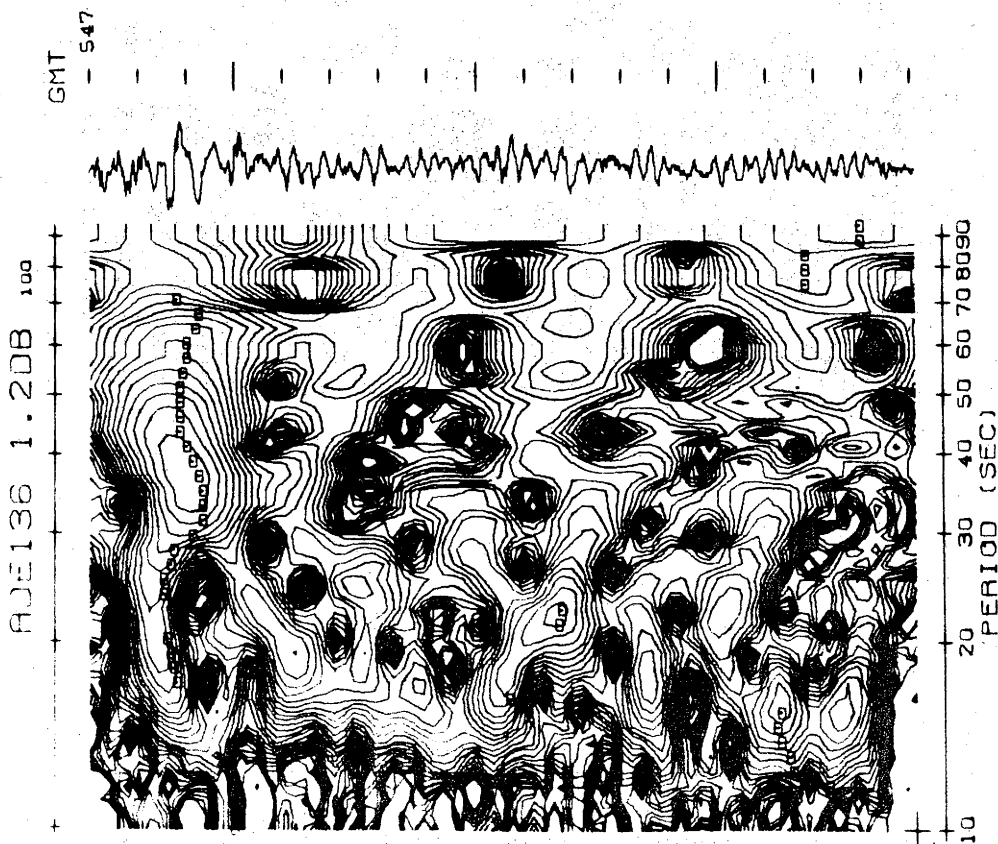
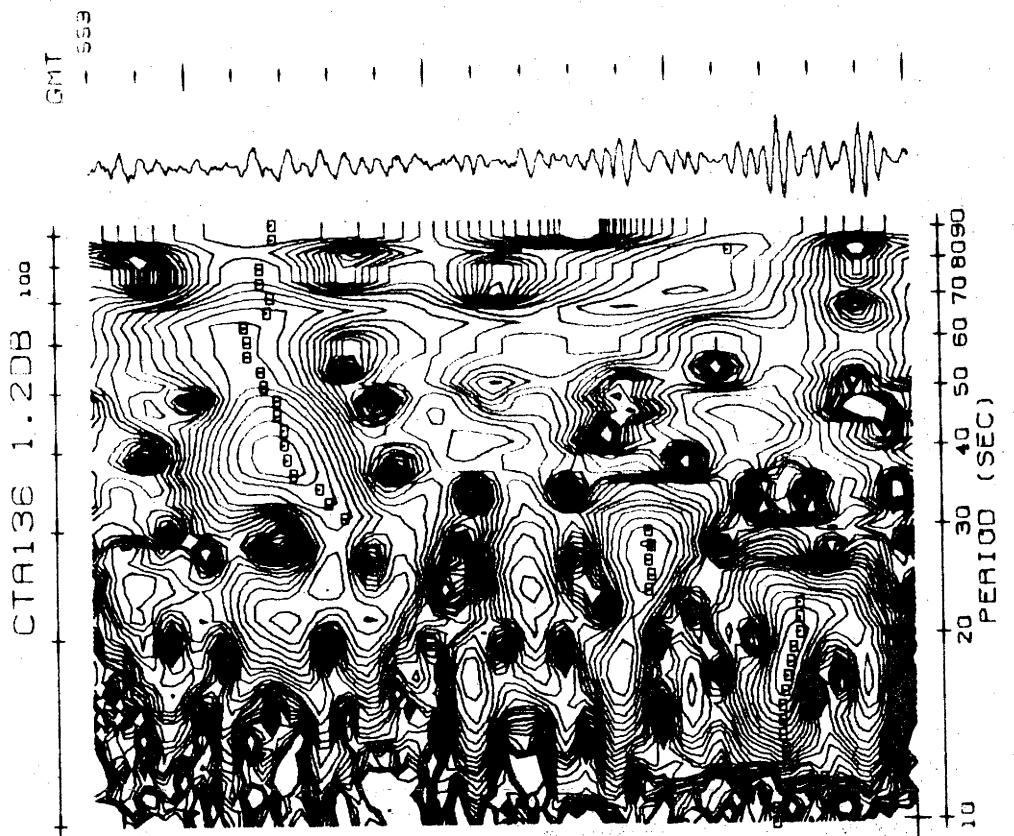


Figure 4.6: FTAN analysis of event number 136 vertical component. For details see caption to Figure 4.1.

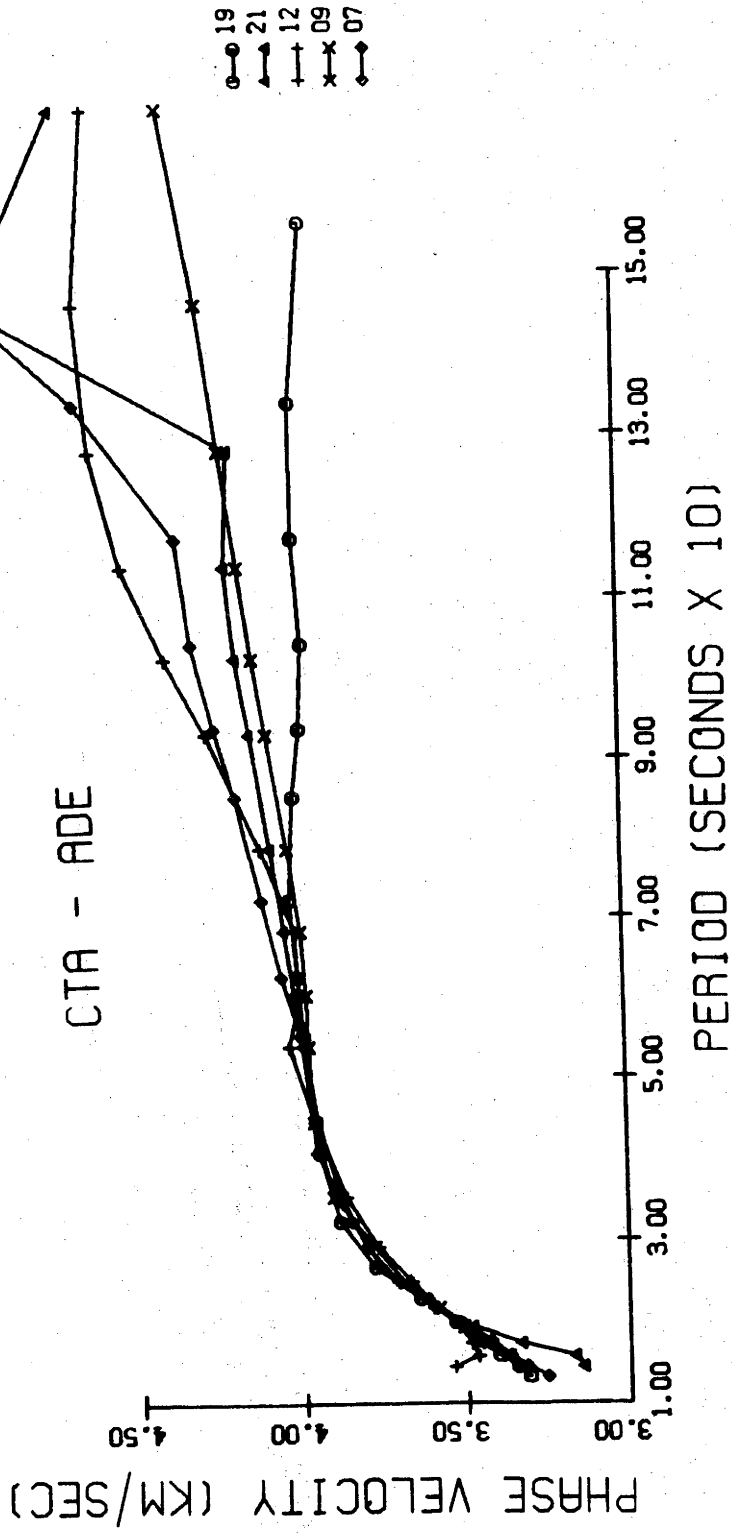


Figure 4.7: Phase velocity curves for path CTA-ADE. Five seismograms were time-variant filtered at both stations before Fourier analysis.

was effective in smoothing the phase velocity curve in the period range where signal/noise ratio was high, but was much less effective in extending the range of measurement to longer periods, where the signal/noise ratio is low.

The results of time-variant filtering the CTA-ADE events shown in Fig. 4.7 are typical of the results obtained for the other eight paths. For any one path the individual phase curves obtained from separate events generally exhibit self-consistency over the period range 14 to 70 s, but show serious divergence at periods longer than 70 s. When it was realized that TVF would not appreciably reduce the uncertainty in phase velocity measurements at long periods, the technique was abandoned in favor of cross-correlation summing. Before proceeding directly to summation, however, it was of interest to examine the results of cross-correlation analysis of each event individually.

Cross-correlation analyses of the six events used for CTA-ADE are shown in Figs. 4.8 to 4.10. In these figures group velocity has been computed and contoured for each event separately. It was expected that the information contained in the individual group velocity diagrams would assist in determining if that event would contribute to the enhancement of signal during the summation of cross-correlations. However, the scatter in group velocity at periods longer than 70 s made it impossible to discriminate between events in this manner. This scatter is mainly a manifestation of low signal/noise ratio at long periods; in addition it demonstrates that group velocity is less immune to noise than is phase velocity.

In view of these results, all available cross-correlations were added without further attempts at data selection. The individual cross-correlations were normalized to a maximum value of unity, aligned to a common time lag, and summed. Unity normalization assigns equal weight to each event rather than a weight that would depend on the signal level.

FTAN analysis of the sum of cross-correlations for the CTA-ADE path is shown in Fig. 4.11. Considerable smoothing has been achieved by summing. The contours are smooth and regular from 12 s to 90 s; at periods longer than 90 s the contours tend to become disorganized.

Phase velocity was computed by Fourier analysis of the sum of cross-correlations and is shown in Fig. 4.12. For comparison, the

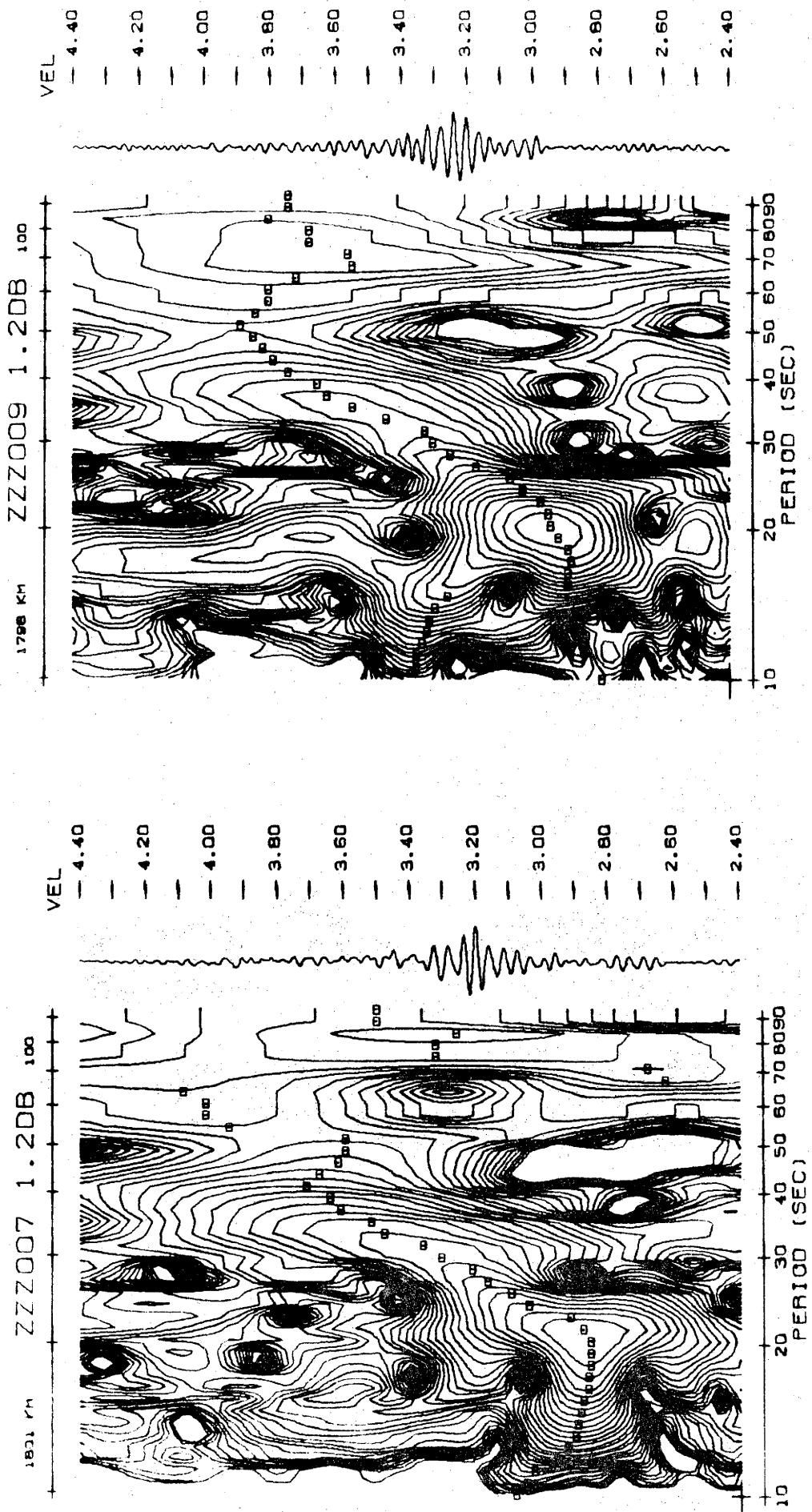


Figure 4.8: Group velocity determined from FTAN contour diagrams of the cross-correlogram of event 7 (left) and that of event 9 (right) CTA-ADE.

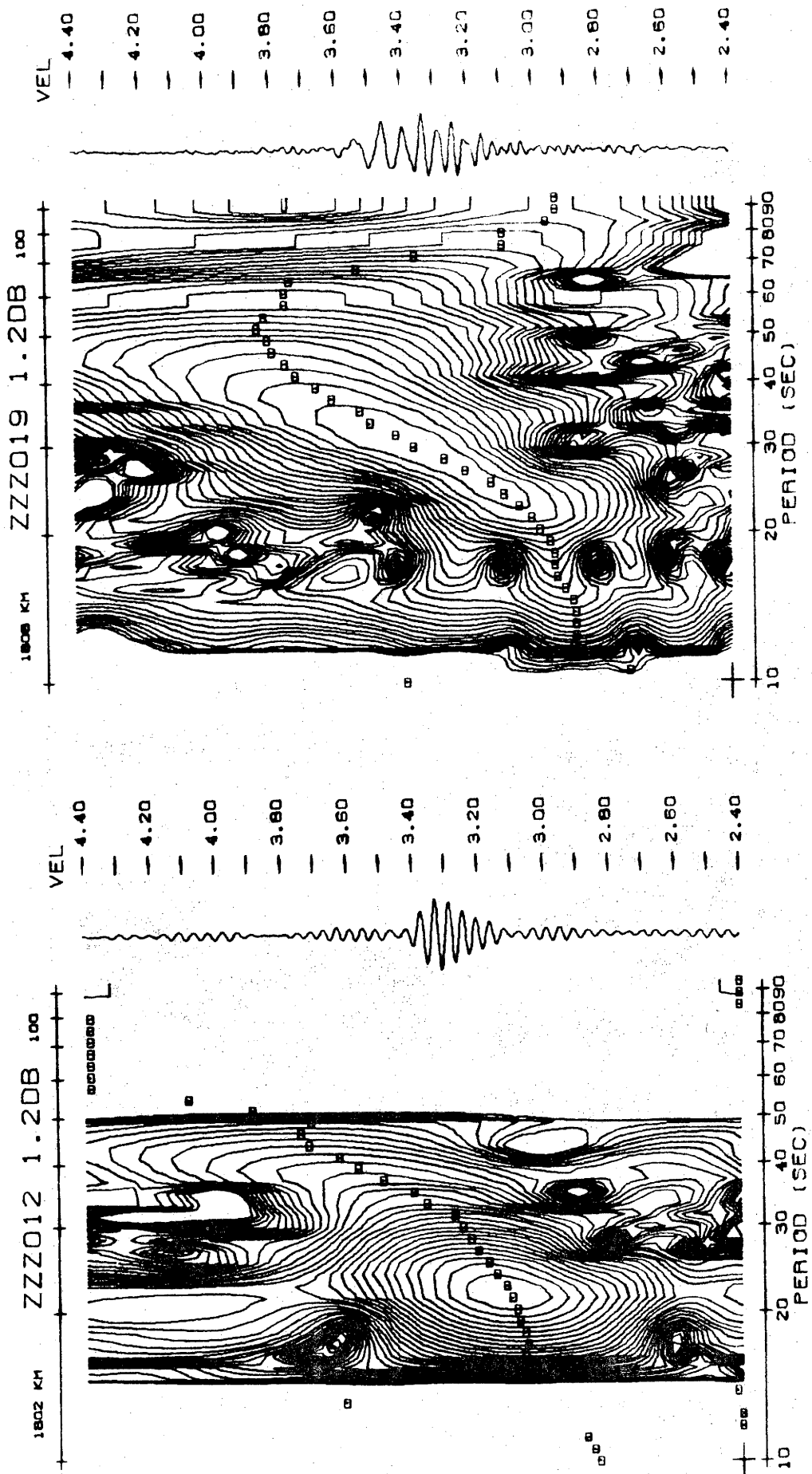


Figure 4.9: Group velocity determined from FTAN contour diagrams of the cross-correlogram of event 12 (left) and that of event 19 (right) CTA-ADE.

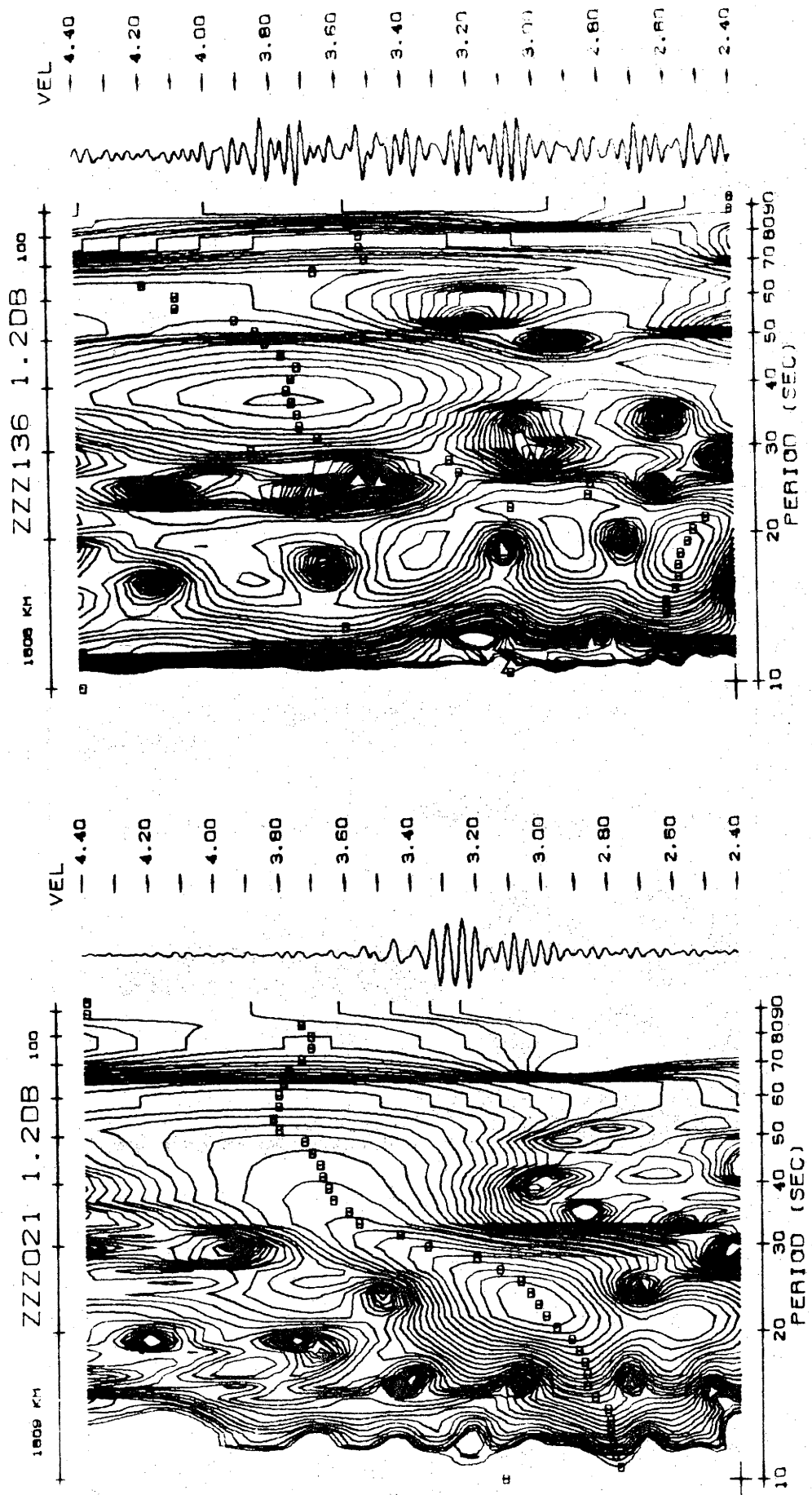


Figure 4.10: Group velocity determined from FTAN contour diagrams of the cross-correlogram of event 21 (left) and that of event 136 (right) CTA-ADE.

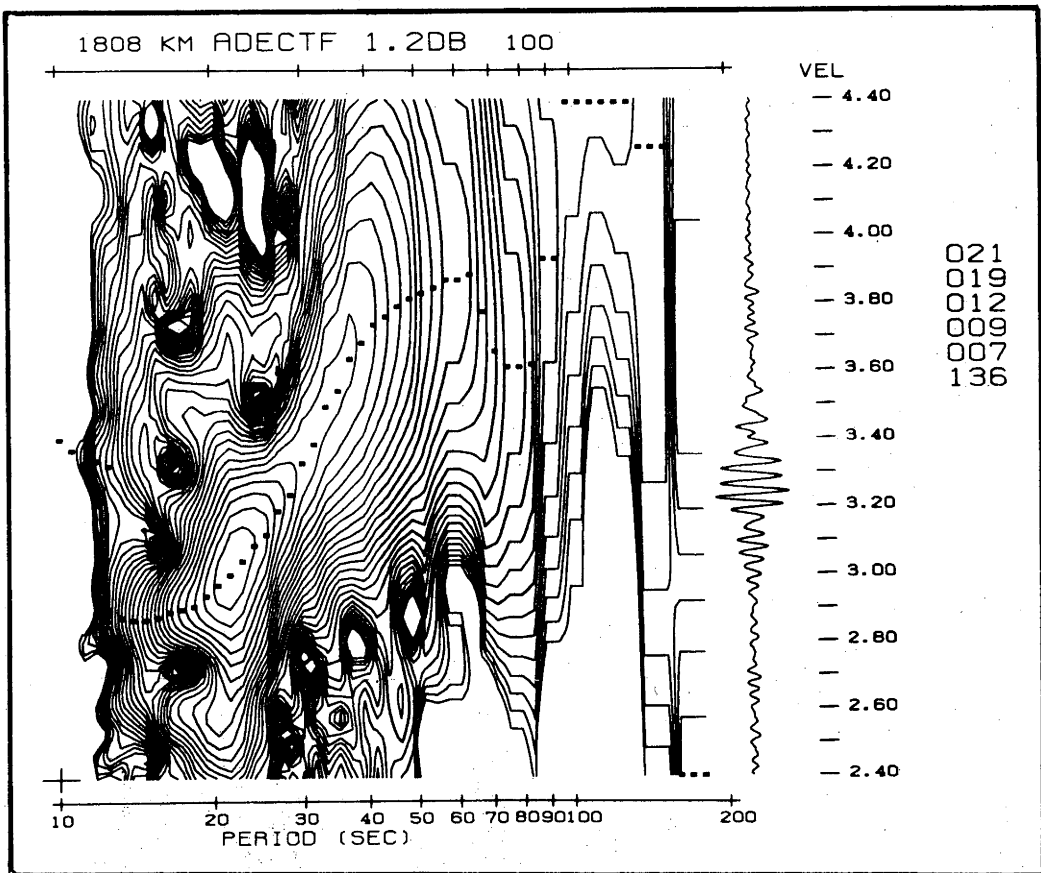


Figure 4.11: Group velocity inferred from the sum of six cross-correlograms for CTA-ADE path. Contour analysis extended to 183 s.

results of Landisman *et al.* [1969] and Thomas are shown for the same path. The present study and Landisman's results are virtually identical over the period range 14 to 80 s. Thomas's phase velocity data, covering a much shorter period range, appear to be consistently too high.

It is apparent from Fig. 4.7 that the uncertainty in the author's phase velocity measurements increases at longer periods, as evidenced by the divergence of the curves obtained by Fourier analysing individual events. The uncertainty is about 0.5 km/s at a period of 150 s. If the noise were completely random, the summation of n signals could, at best, be expected to improve the signal/noise ratio by \sqrt{n} in amplitude, if the signal/noise ratios are the same. For this path $n=6$, so the uncertainty might be reduced to about 0.2 km/s. This is

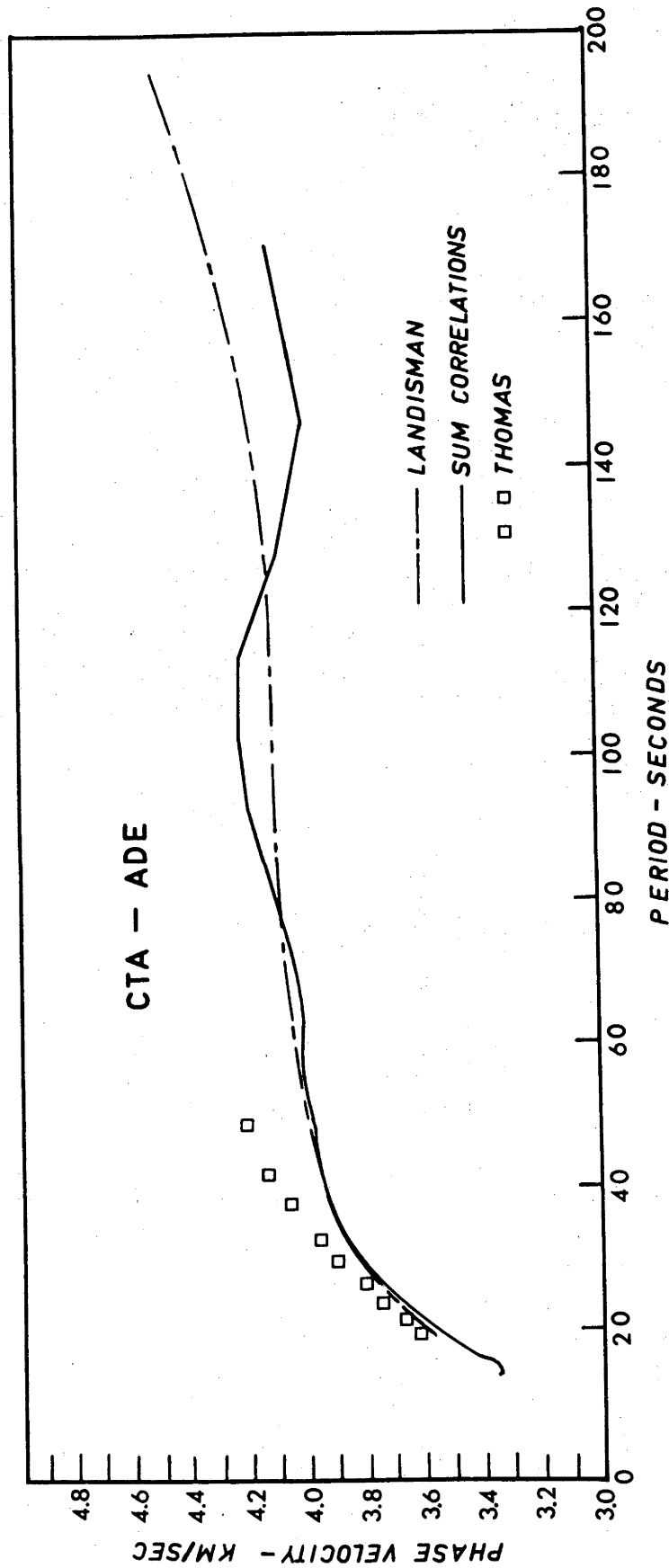
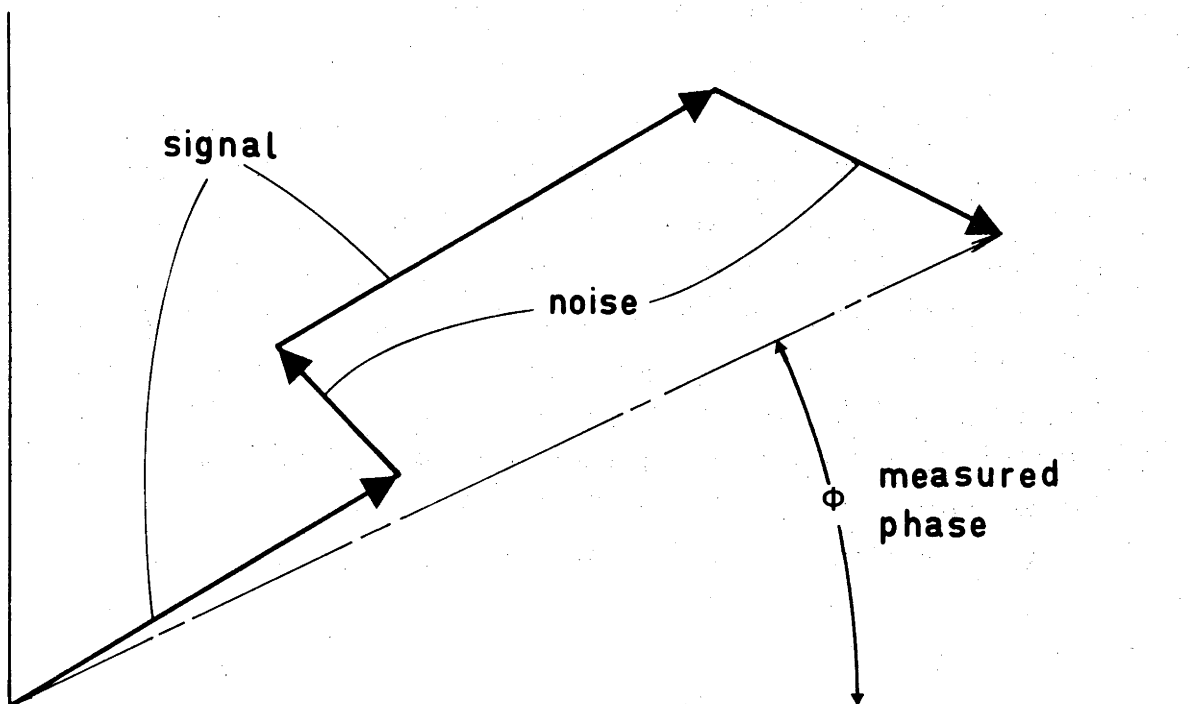


Figure 4.12: Phase velocity for CTA-ADE path obtained from Fourier analysis of sum of cross-correlations, compared with Landisman's and Thomas's results.

approximately the magnitude of the discrepancy between Landisman's and the present results.

Landisman's phase velocity curve for the CTA-ADE path, derived from a time-variant filtered cross-correlogram of a single event, is notable for its smoothness and its extension to long period. It is perhaps fortuitous that this event generated waves of sufficiently large amplitude to permit analysis to such long periods. The magnitude m_b of the event was 5.9, with an epicentral distance of 77° . It may be noted that event number 9, with magnitude 5.7, distance 16° , gives a phase velocity curve in close agreement with Landisman's to periods as long as 170 s.

The calculation of the Fourier phase spectrum $\phi(\omega) = \arctan[\text{Im}F(\omega)/\text{Re}F(\omega)]$, used to determine phase velocity according to Eqn (3.26), is not linear; that is, $\arctan(s+n)$ does not equal $\arctan(s) + \arctan(n)$. It is assumed that within a frequency interval resolvable by Fourier analysis, the phase of the signal is invariant among the cross-correlations of events common to one path. The signal amplitudes in this frequency interval will differ, of course. It is further assumed that the noise is random in both phase and amplitude, although it is difficult to test this assumption. By summing cross-correlations, several measurements are made of the same invariant



SIGNAL PHASE IS INVARIANT, NOISE IS RANDOM

quantity, namely phase, in the presence of noise. If the noise is truly random it will destructively interfere, whilst the signal will be enhanced. A simple average of the individual phase spectra obtained from individual events gives equal weight to the phase computed by a non-linear process, whereas when the phase is determined from the sum of cross-correlations, the signal component and noise component of all events are added vectorially. This represents a linear averaging process.

If the noise is not random, it is possible for the results from summed cross-correlations to be inferior to a single event with a low signal/noise ratio.

It can be concluded that summing cross-correlations succeeds in obtaining an unbiased measurement of phase velocity, but the uncertainty in the measurement at long period is still relatively large.

4.3 OTHER AUSTRALIAN PATHS: RAYLEIGH WAVES

The points made in the preceding discussion apply generally to the remaining eight Australian paths. Group velocity analyses of summed cross-correlations for each path are shown in Figs. 4.13 to 4.16. In general, the contours remain coherent and relatively well-organized to periods as long as 90 s. The contours of individual event cross-correlations for these eight paths (not shown herein) are markedly less well-organized (see previous examples for the CTA-ADE path). Bloch [1969] and Bloch, Hales and Landisman [1969] also found that FTAN group velocity analysis of a single cross-correlation was restricted to periods less than 50 s; at longer periods the contours became too disorganized.

Phase velocities computed from the sum of cross-correlations are shown on a common velocity scale in Fig. 4.17, and in Fig. 4.18 the same curves are displaced to facilitate individual identification. The only filtering applied to these data was a group velocity window between 2 and 5 km/s. The set of phase velocity curves thus represents an unbiased measurement of regional phase velocity in Australia.

Whilst there is still residual scatter in these phase velocity curves, a systematic increase in Rayleigh wave phase velocity can be seen from 'East' Australia to the shield region in 'West' Australia (see map, Fig. 4.19). In the period range 30 to 70 s, above the 'knees' of the curves, the phase velocities for the three paths involving Mundaring in

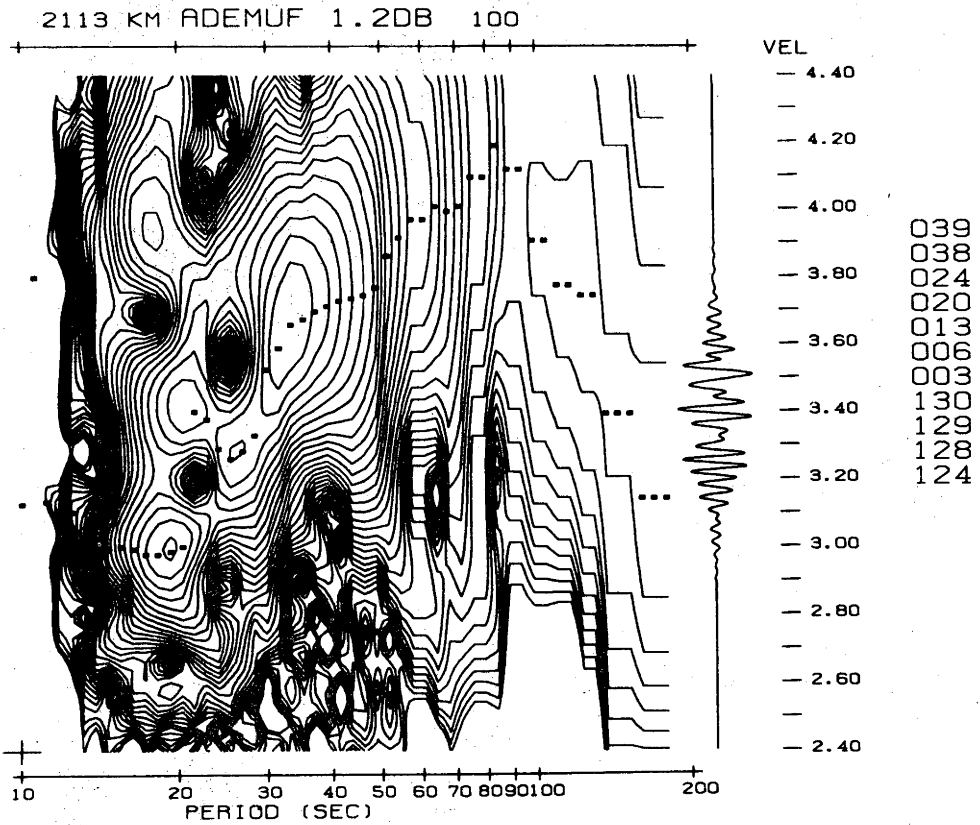
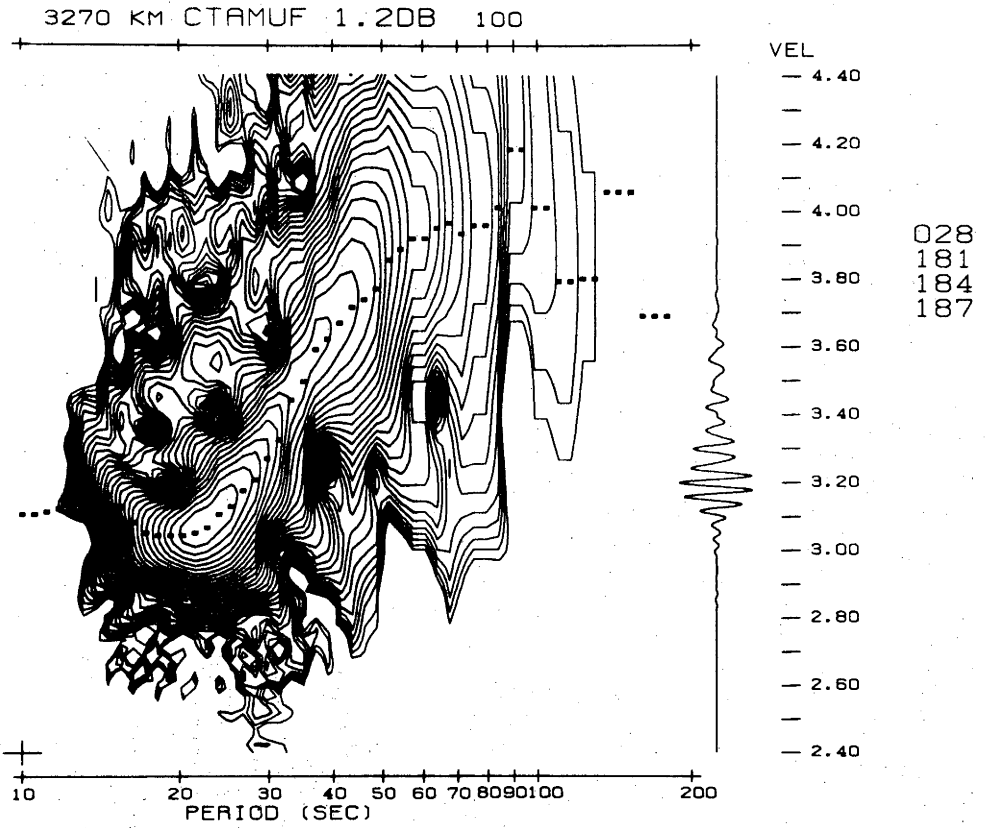


Figure 4.13: Frequency time analysis of sum of cross-correlograms for CTA-MUN ('WAL') and ADE-MUN.

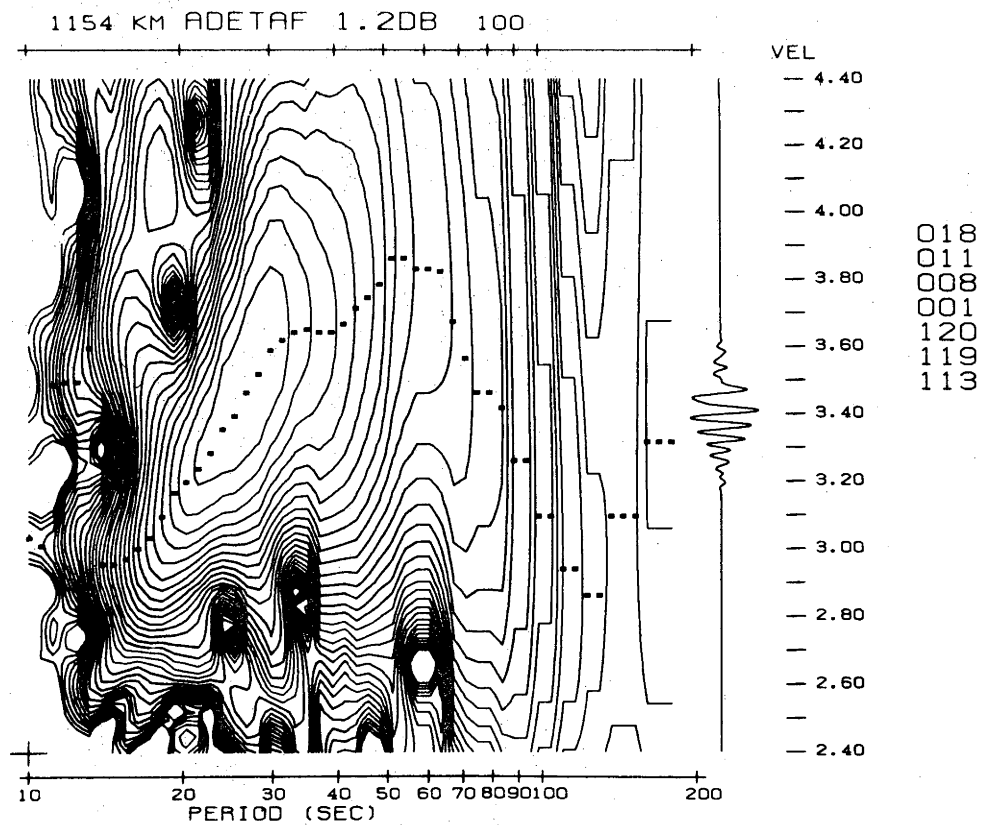
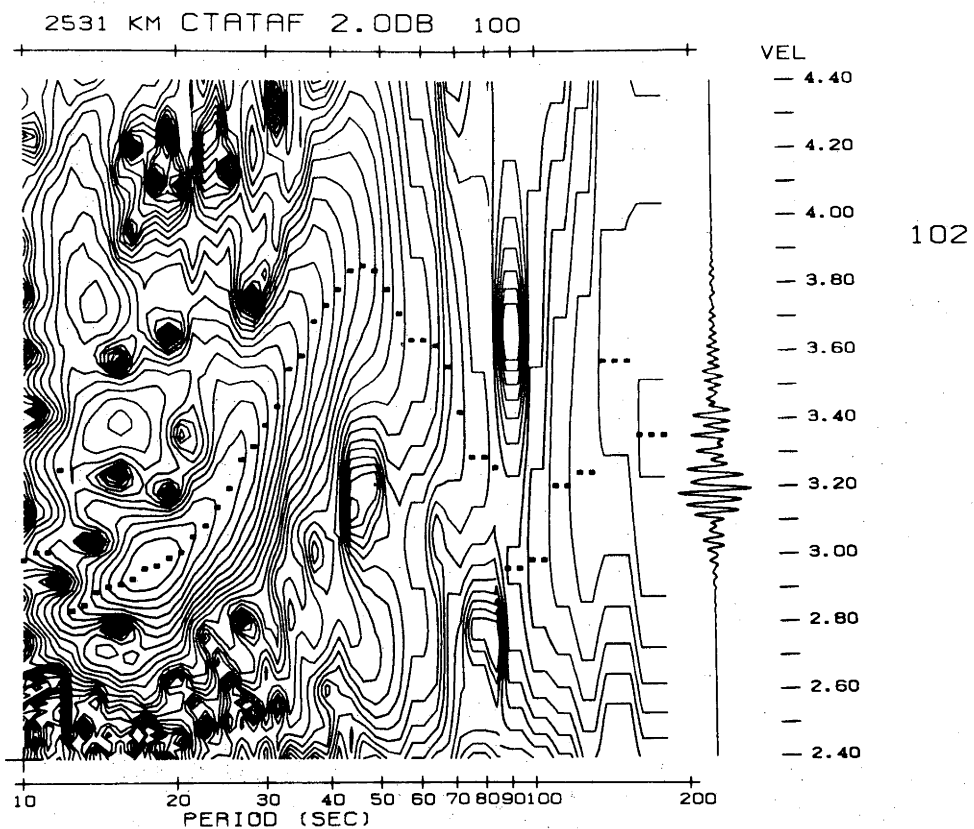


Figure 4.14: Frequency time analysis of sum of cross-correlograms for CTA-TAU and ADE-TAU.

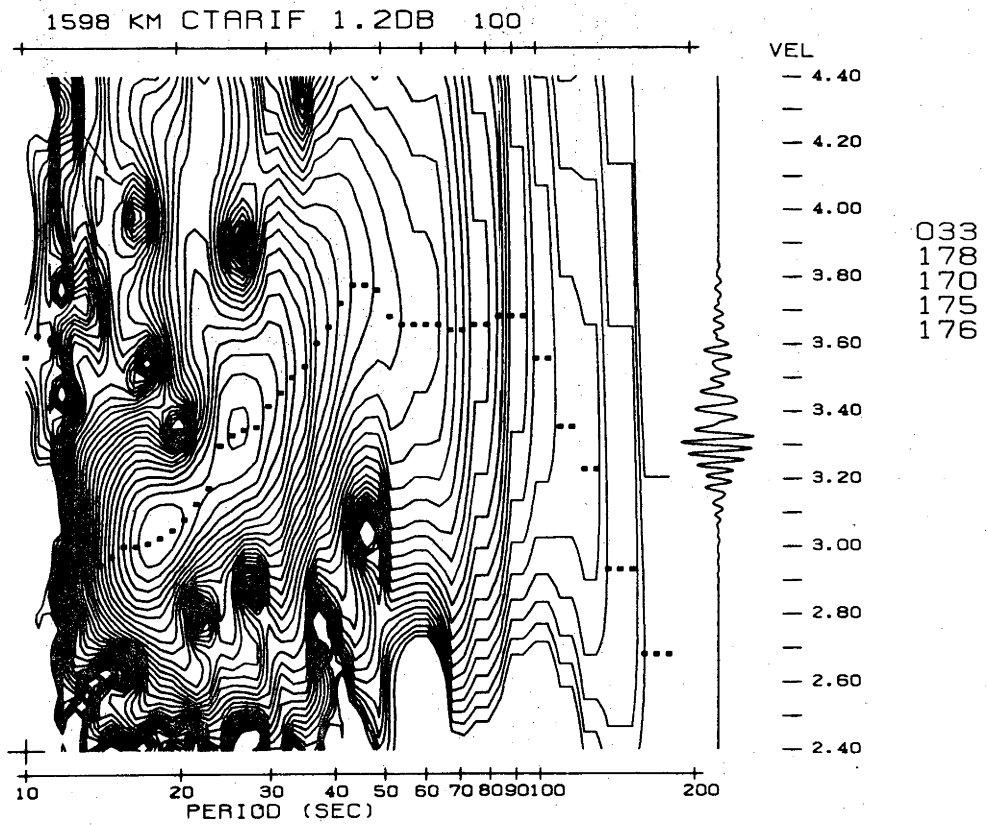
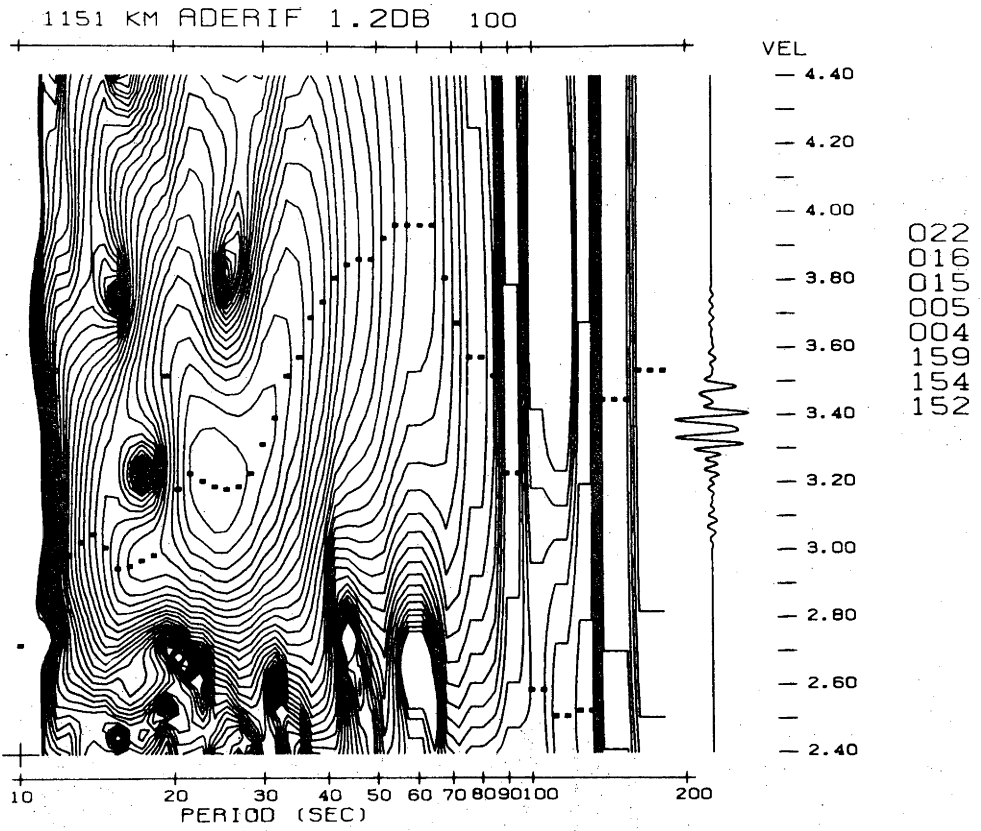


Figure 4.15: Frequency time analysis of sum of cross-correlograms for ADE-RIV and CTA-RIV.

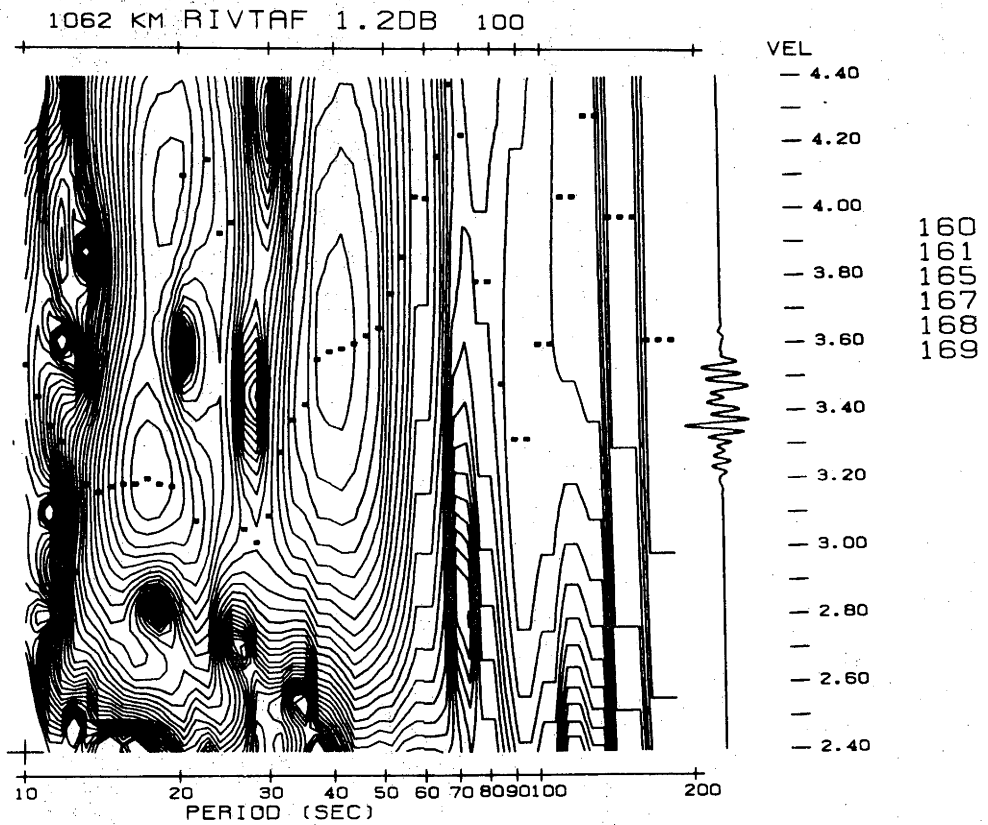
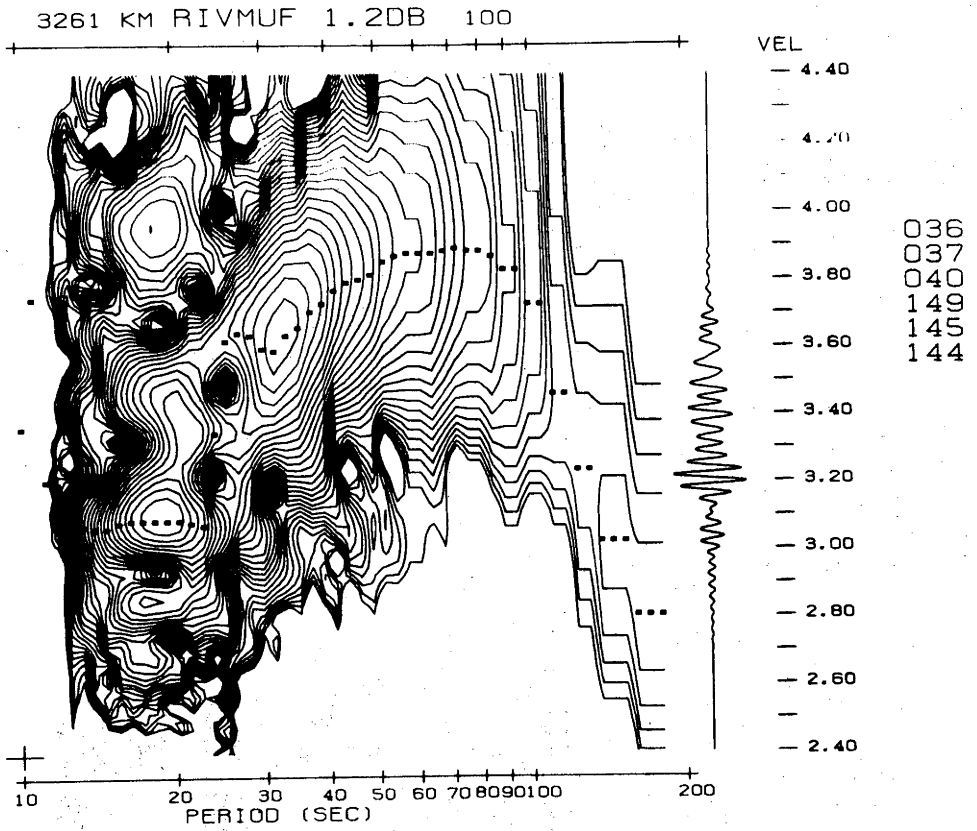


Figure 4.16: Frequency time analysis of sum of cross-correlograms for RIV-MUN to RIV-TAU.

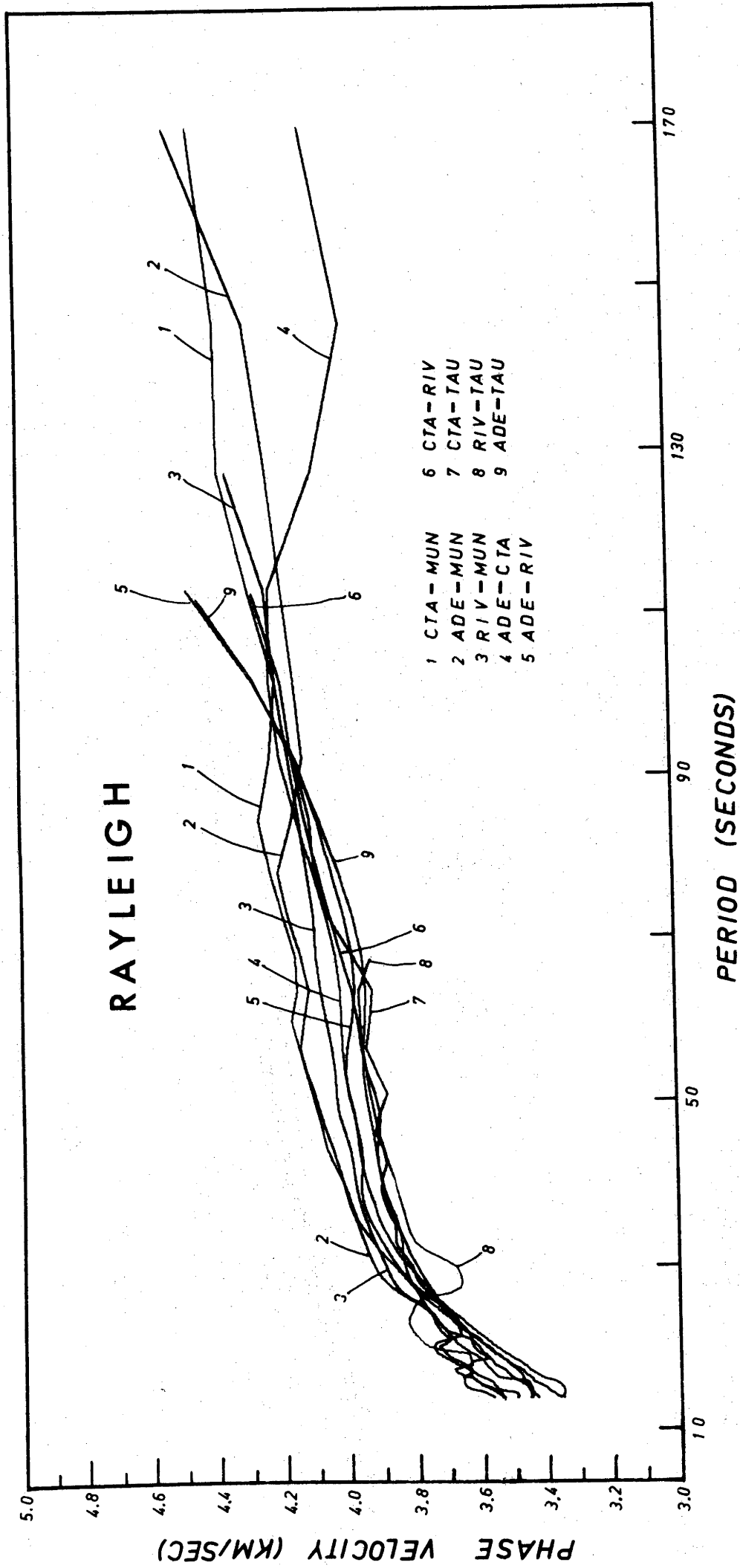


Figure 4.17: Rayleigh wave phase velocity for nine Australian paths obtained by Fourier analysis of sum of cross-correlations. No filtering has been used to obtain these results.

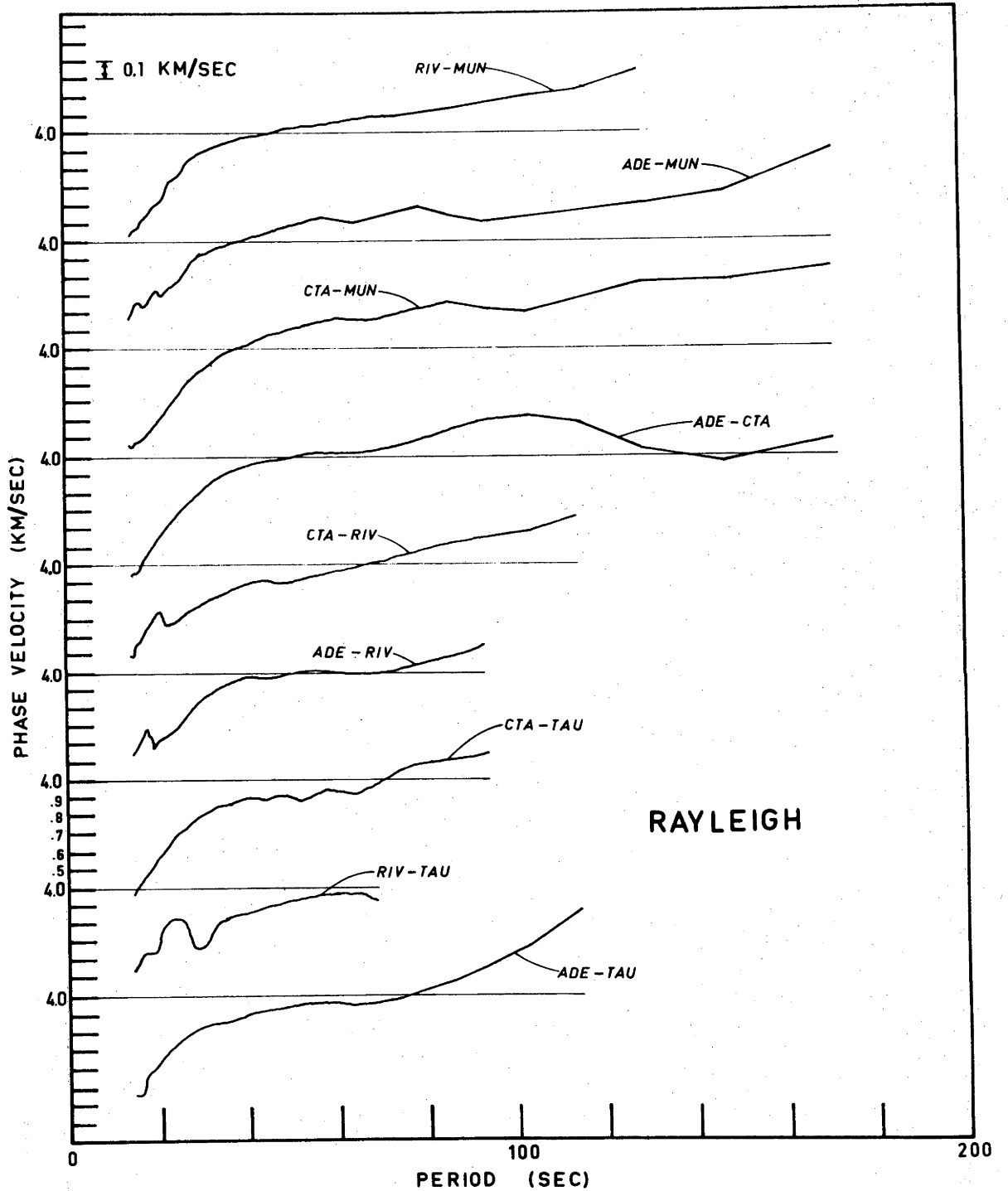


Figure 4.18: Rayleigh wave phase velocity for nine Australian paths obtained by Fourier analysis of sum of cross-correlations. This is the same information as shown in Fig. 4.17. The curves are displaced here to facilitate their identification.

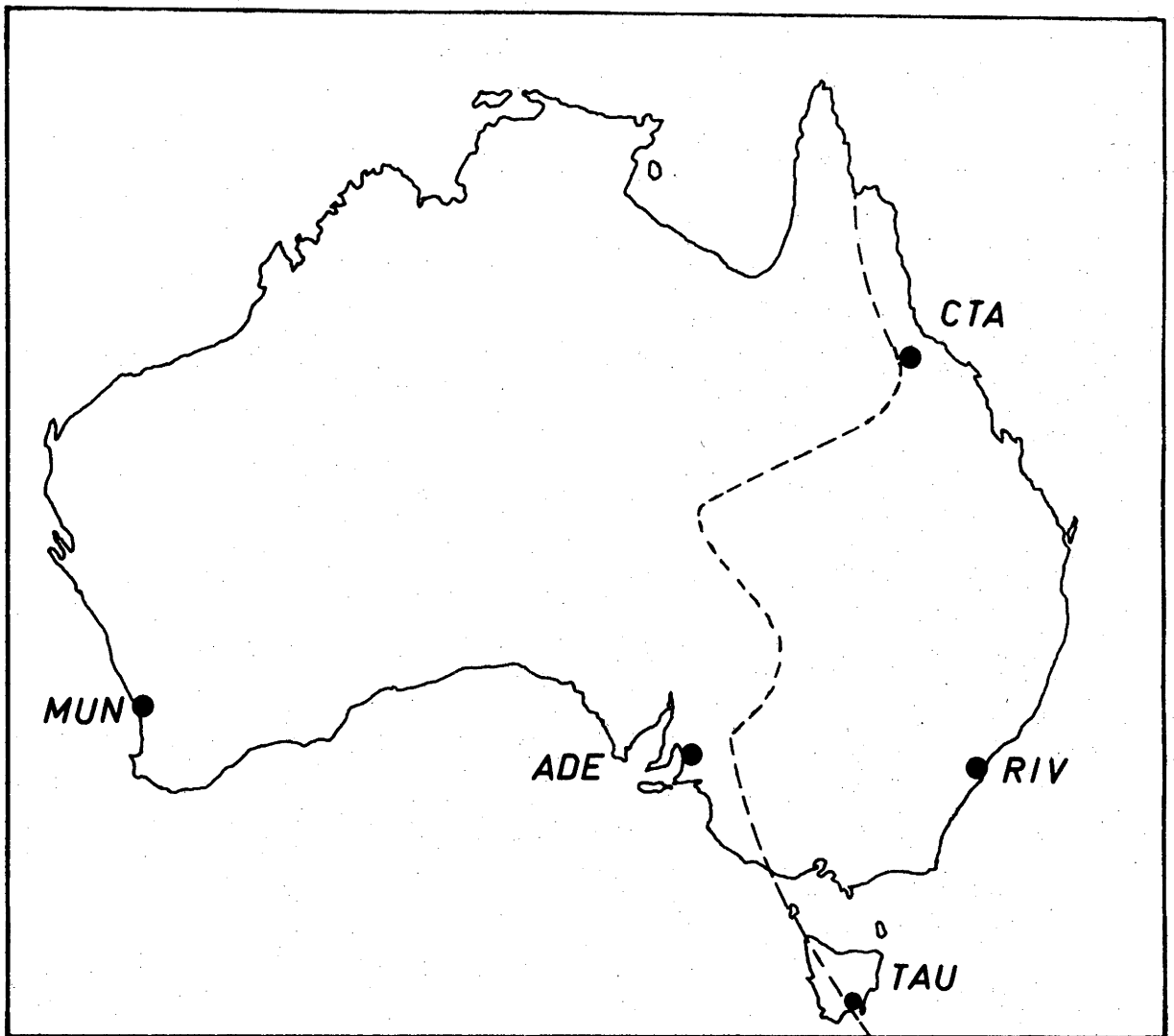


Figure 4.19: Sketch map of Australia showing the eastern limit of pre-Cambrian rocks [Howard and Sass, 1964].

Western Australia lie above the other six paths located in East Australia. The path RIV-MUN, as might be expected, appears to average the lower eastern velocity and the higher western velocity, since it lies roughly midway between the ADE-MUN and CTA-MUN paths on the one hand, and the six eastern paths on the other. There is some indication that all nine phase velocity curves tend to merge to a common value of 4.15 km/s at a period of 100 s.

Close inspection of the phase velocity curves shown in Fig. 4.17 suggests that the six East Australia paths might be further subdivided into two groups. The three paths that involve TAU (7, 8, 9)

lie below the paths involving ADE (4, 5); the amount of the difference is about 0.06 km/s between 30 and 60 s period. This observation could be explained by the location of ADE, involving greater penetration into the higher velocity shield area, although definite conclusions are hampered by low geographical resolution of the shield boundary and residual uncertainty in the phase velocity curves.

Thomas's study does not show this systematic increase in velocity: in fact, his phase velocity for CTA-ADE is virtually identical to that for CTA-MUN (see Figs. 4.20a and 4.20b) whereas the author's results indicate the CTA-MUN velocity to be 0.2 km/s higher than ADE-CTA over the period range 30 to 80 s. It can be concluded that relatively large inaccuracies or high susceptibility to noise perturbation, inherent in the peak and trough method used by Thomas, precluded this observation.

Figs. 4.21 and 4.22, reproduced from Knopoff's [1972] summary of surface wave dispersion, show Rayleigh wave phase velocities observed for some shield areas and 'aseismic platforms' of the world. They show a difference of about 0.2 km/s between these two categories, similar to the results here. Knopoff uses the FLO-GOL data as a reference curve, and it has been superimposed on Fig. 4.29, which will be discussed later in this chapter, to enable comparison with the author's results.

The designation 'aseismic platform' in Knopoff's nomenclature seems to correspond approximately to East Australia (and he includes Landisman's CTA-ADE curve in this group). However, the region may also be classified as 'tectonic' according to the nomenclature of Dziewonski [1971].

The grouping of paths into 'West' and 'East' Australia can be seen in their group velocities as well as their phase velocities. For comparison purposes, a direct tracing of the group velocity maxima at constant period for the nine paths is shown in Fig. 4.23. These maxima define the ridge crest from which group velocity may be inferred. Although the scatter in group velocity is greater than that exhibited by phase velocity, there is a clear indication that the group velocities for the three paths involving Mundaring, located in the State of Western Australia, tend to reach higher values at long periods than do the group velocities for the six 'East' paths. Again, the RIV-MUN results tend to lie between those of the 'pure shield' West paths and the East paths.

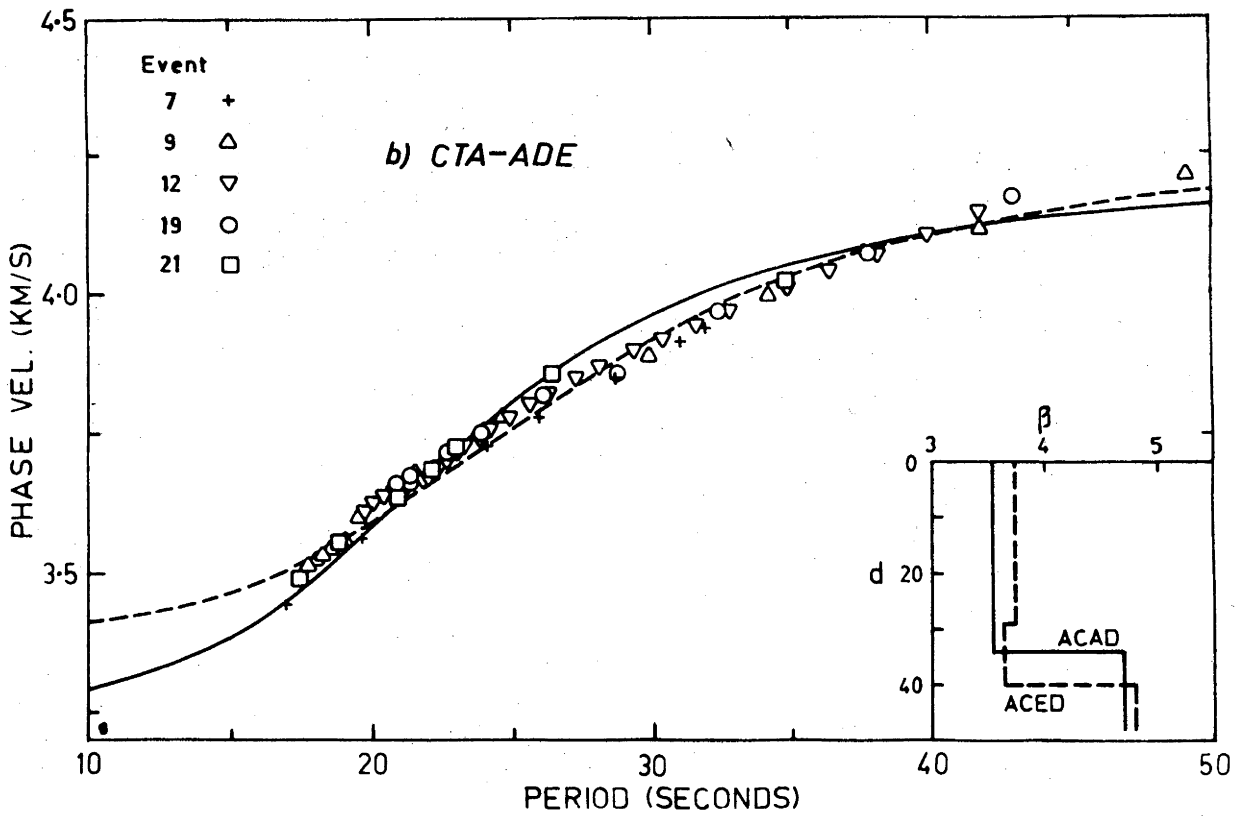
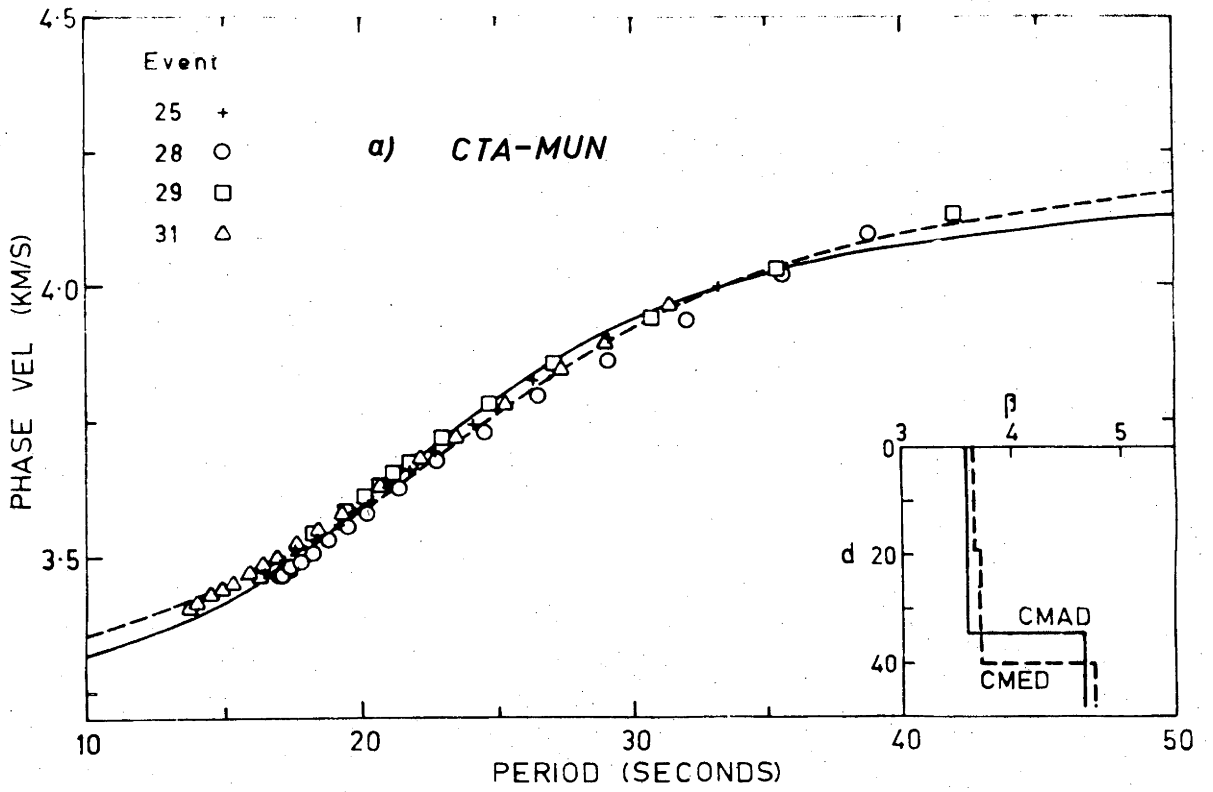


Figure 4.20: Thomas's results for Rayleigh wave phase velocity for CTA-MUN and CTA-ADE.

Group velocities for the six East paths attain a maximum value between 40 and 60 s.

4.4 FURTHER SIGNAL AVERAGING

It is evident that considerable noise reduction, signal enhancement and unbiased averaging are obtained by summing the cross-correlograms of seismograms common to a path. It is quite probable that further improvement of the author's results, particularly in reducing the uncertainty of information at longer periods, would be obtained by increasing the number of events included for each path; but a much larger quantity of data would probably be required to achieve a significant improvement.

On the other hand, further signal averaging can be carried out by averaging the results of the paths common to the regions discussed in the preceding section. Cross-correlations cannot be added for paths with different lengths, but signal averaging can be performed by summing the complete FTAN matrix point by point. (There are 42 discrete period samples with 85 discrete velocity intervals in the FTAN matrix. The FTAN matrix is comprised of positive numbers only, normalized to a maximum value of 99).

The FTAN matrices for the 'West Australian' paths CTA-MUN and ADE-MUN were combined in this way. The resulting contoured matrix is shown in Fig. 4.24 and is called 'WA2'. (Note, 'WA1' will refer to the single pure shield path CTA-MUN.) In the same manner 'EA1' refers to the summation of five FTAN matrices for the 'East Australian' paths CTA-RIV, CTA-TAU, ADE-RIV, ADE-TAU and RIV-TAU (Fig. 4.25). For reference

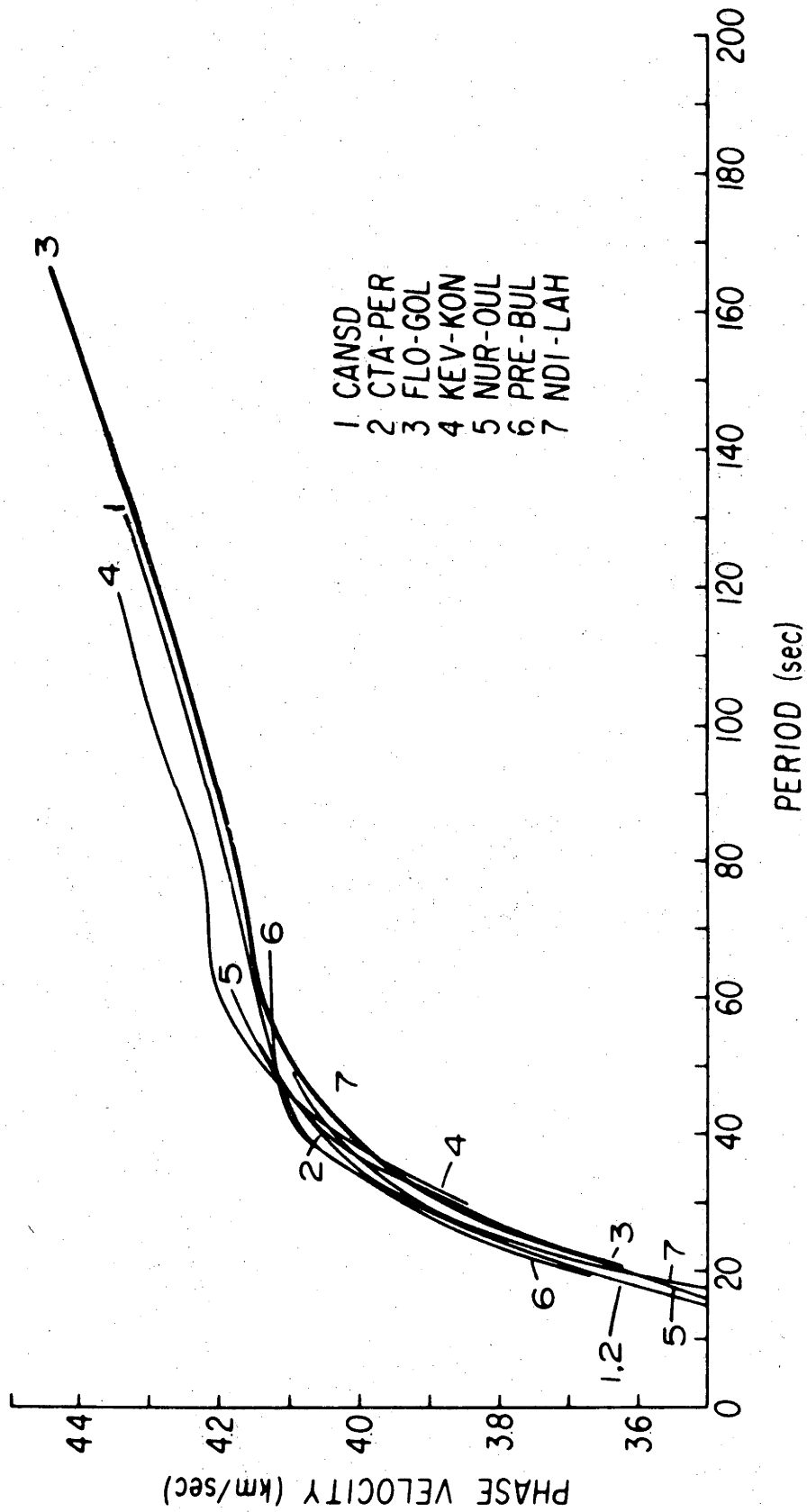


Figure 4.21: Knopoff's Rayleigh wave phase velocities for some of the shield areas of the world.

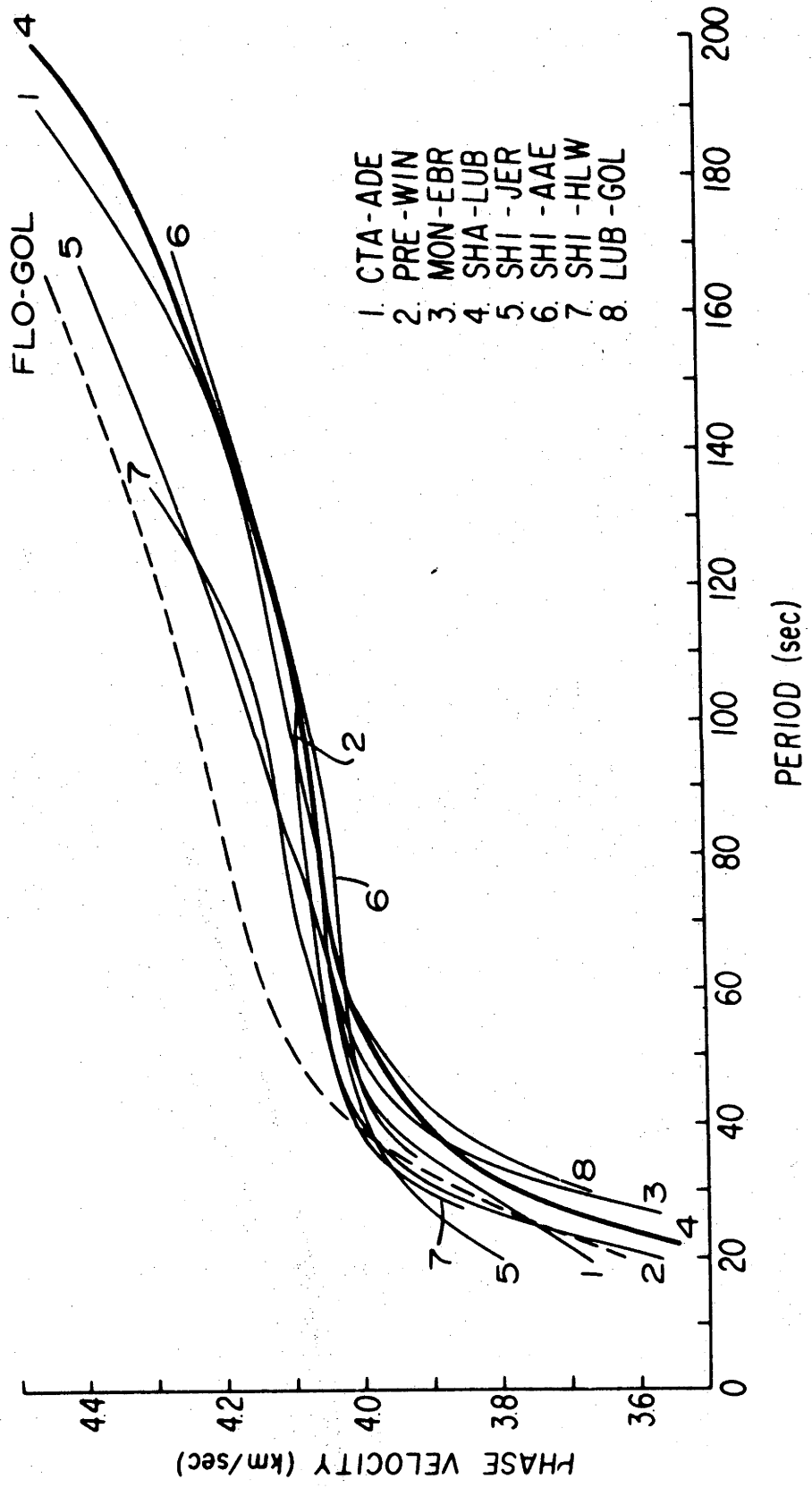


Figure 4.22: Knopoff's Rayleigh wave velocities for 'aseismic' platforms.

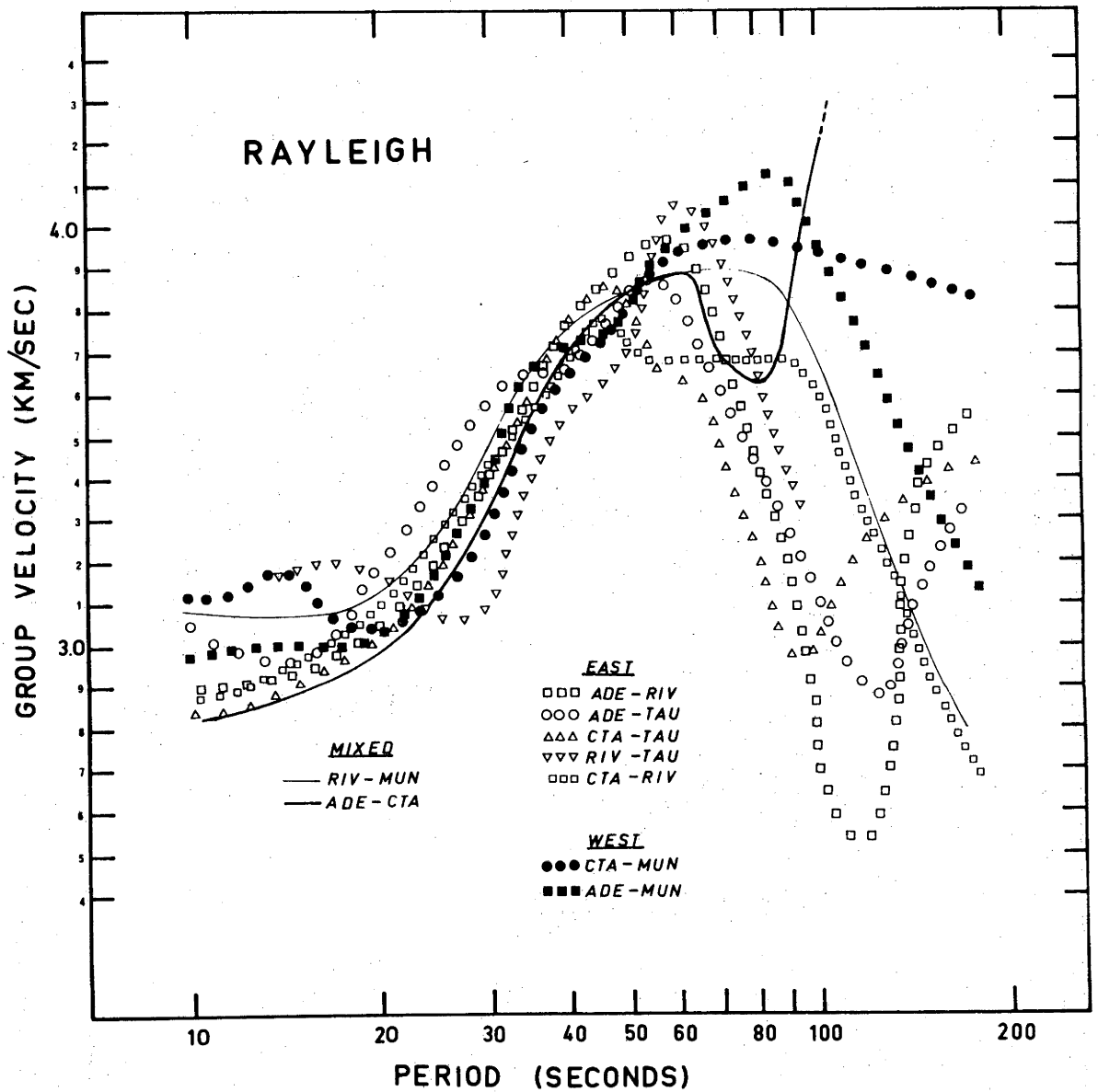


Figure 4.23: Rayleigh group velocity for nine Australian paths. This information is taken directly from the FTAN plots 4.13 to 4.16.

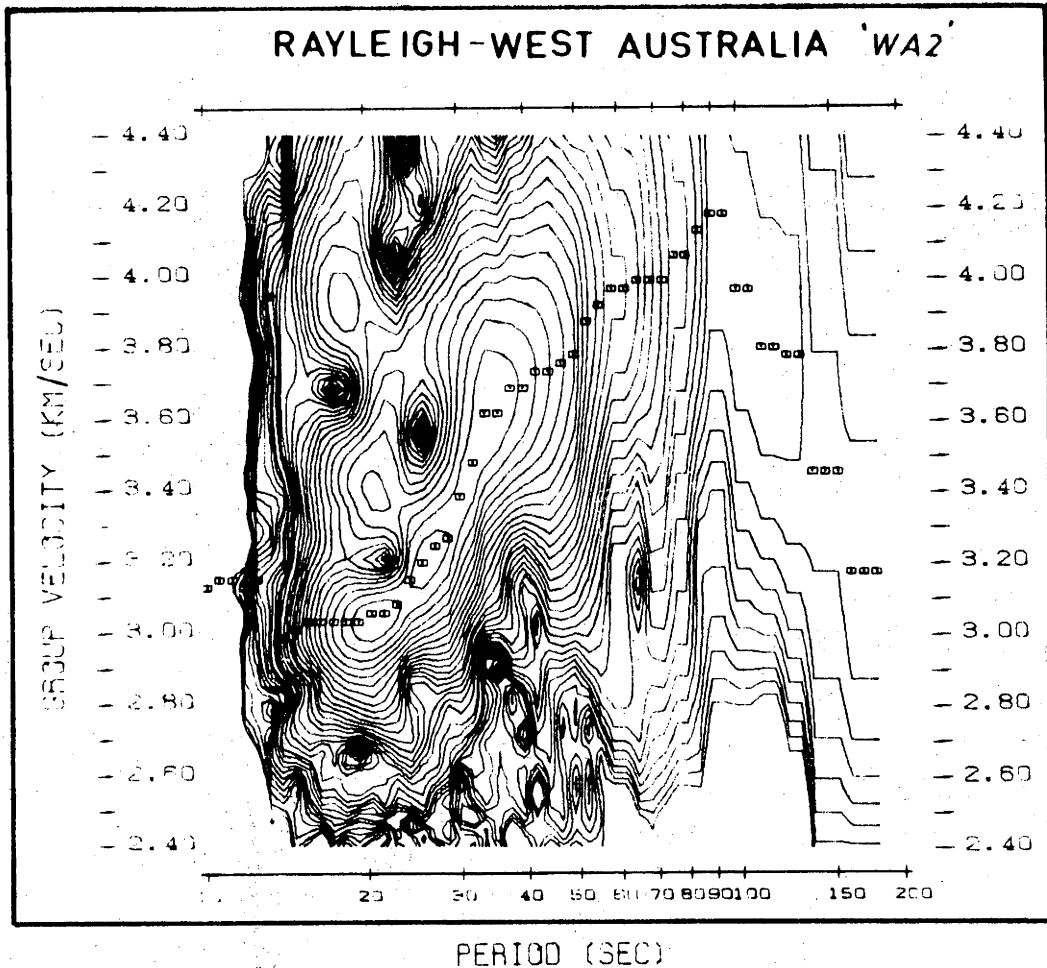


Figure 4.24: Group velocity for western Australia 'WA2' after further signal averaging by adding together the FTAN matrices for CTA-MUN and ADE-MUN.

purposes, 'Total Australia' refers to the summation of all nine paths (Fig. 4.26), although it is emphasized that this information is derived from a collection of mixed paths. The grouping thus corresponds to the division into the 'Shield' and 'Tectonic' regions of Australia indicated on the map of Australia (Fig. 4.19).

For the East Australian paths, the curves for ADE-RIV and CTA-TAU are reasonably self-consistent in that they all show a dip in group velocity at about 110 s period followed by a systematic increase at longer periods. The group velocities at periods longer than 100 s for the RIV-TAU path are too scattered to allow meaningful interpretation. CTA-RIV, on the other hand, shows a steady decrease in group velocity from about 100 s. Although there is no *a priori* reason for discarding the data from this path, it may be considered suspect because of

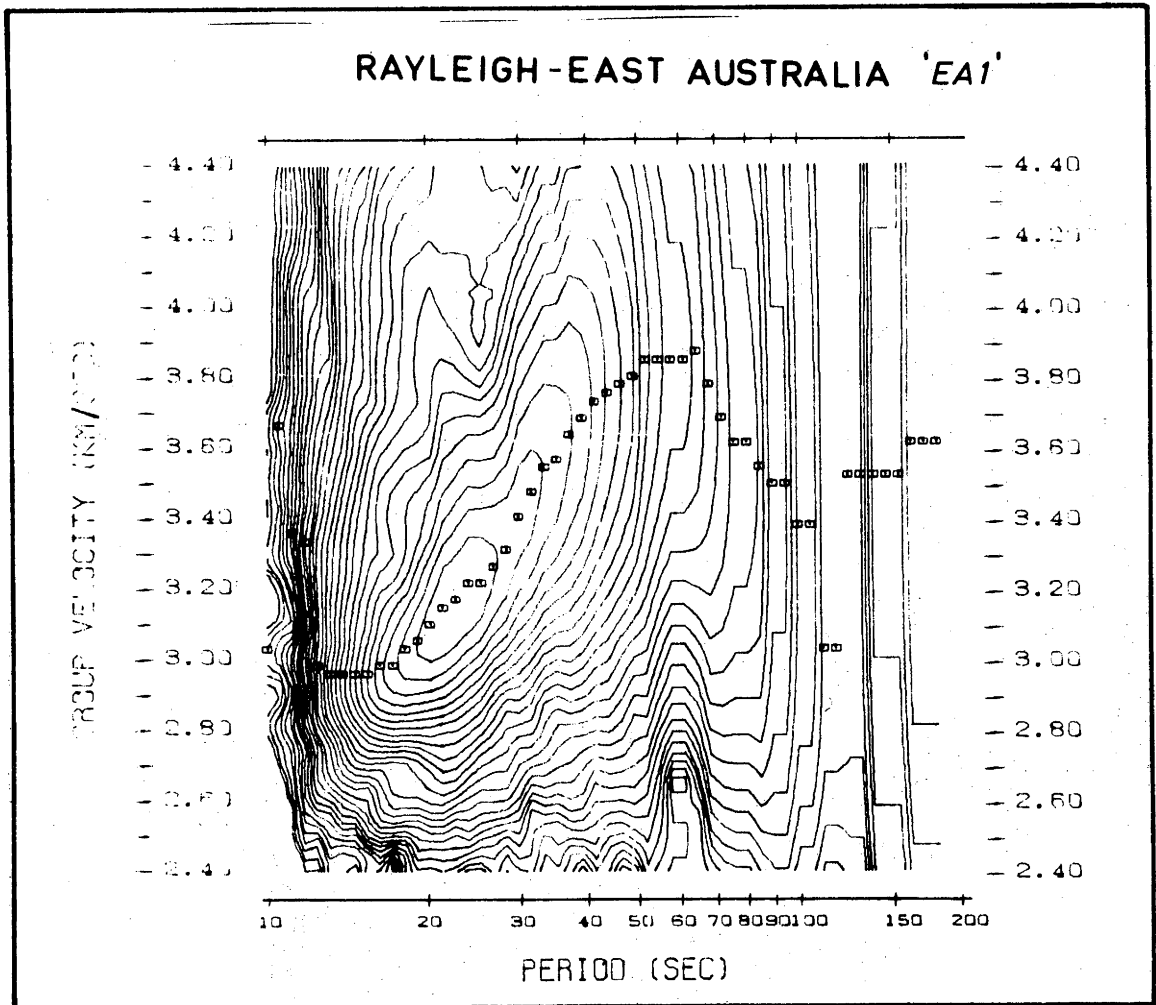


Figure 4.25a: Group velocity for eastern Australia 'EA1' after further signal averaging by adding the FTAN matrices for ADE-TAU, CTA-TAU, ADE-RIV, CTA-RIV and RIV-TAU.

(a) lack of consistency with the other paths, and (b) low group velocities at periods beyond 150 s, which (as will be seen) are inconsistent with the results of other workers. For this reason another summation of the FTAN matrices for only ADE-RIV, ADE-TAU and CTA-TAU was made. It is labelled 'EA2' and is shown in Fig. 4.25b.

Of the sets of West Australian data, CTA-MUN is an undoubted 'pure shield' path, whereas ADE-MUN incorporates the edge of the continental shelf for a large proportion of its length (see Fig. 4.19). It has already been noted in Section 2.1 that interference problems were encountered at shorter periods due to a multi-path effect in this region. For this reason a separate curve for the CTA-MUN path has been included in Fig. 4.27. It is labelled 'WA1'.

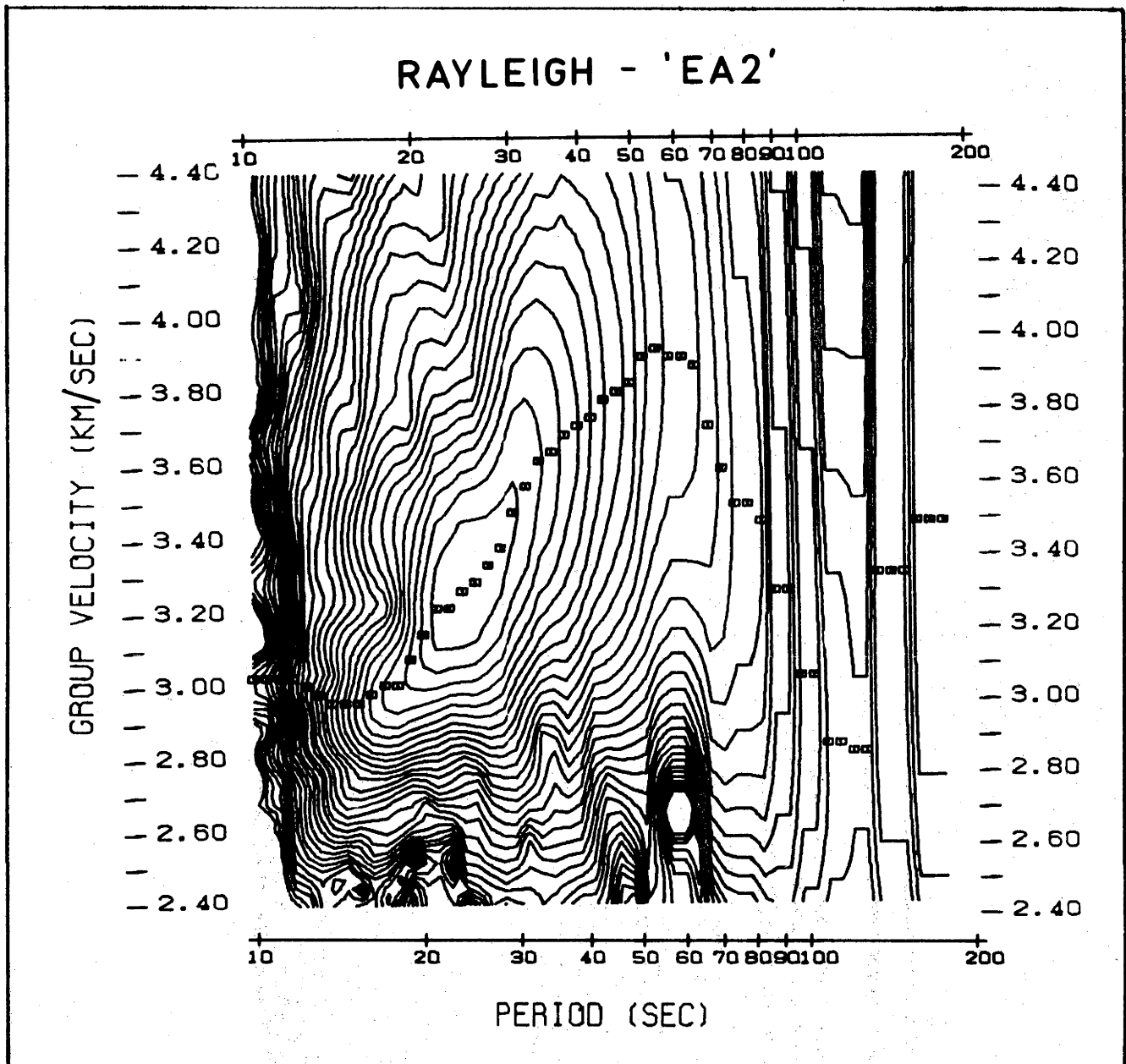


Figure 4.25b: Group velocity for eastern Australia 'EA2' after further signal averaging by adding the FTAN matrices for ADE-TAU, CTA-TAU and ADE-RIV.

Signal averaging in this manner trades off geographical resolution in the hope of achieving higher precision as well as extending velocity information to longer periods.

As a result of this additional signal averaging the contour diagrams of group velocity displayed in Figs. 4.24 to 4.26 show further improvement in the coherence of contours, both to longer periods and to shorter periods. It is possible to discern a ridge crest down to a period as short as 10 s, although the ridge crest may not necessarily

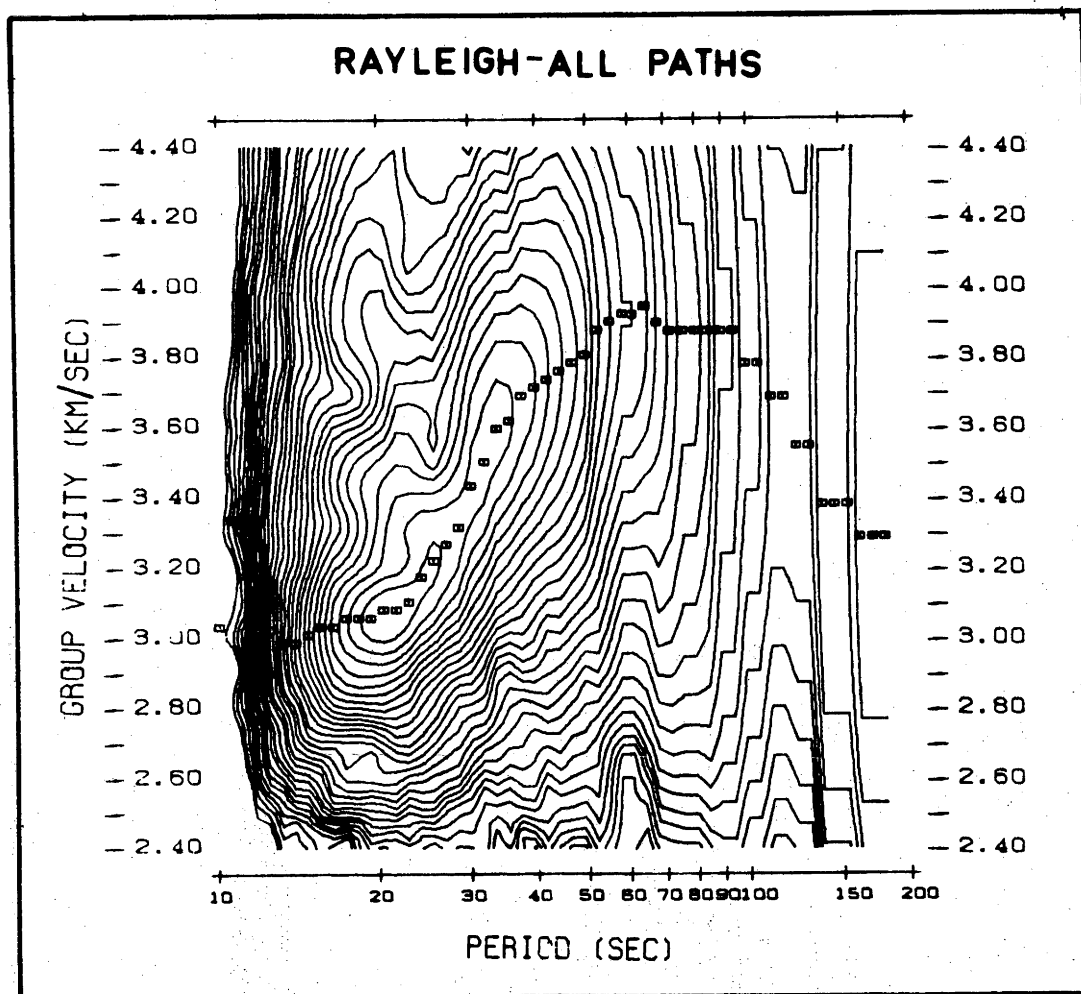


Figure 4.26: A reference group velocity for 'total' Australia obtained by adding FTAN matrices for nine Australian paths.

coincide with the maxima at constant period indicated by small squares on the contour diagrams. This is probably due to the presence of higher modes that have group velocities higher than that of the fundamental mode in the period range 10 to 15 s.

At longer periods the group velocity contour diagrams deteriorate, for a number of reasons. The signal grows progressively weaker at long periods, an indirect consequence of the inability to make use of the strong mantle waves generated by great earthquakes in the two-station direct observation method. An attempt is made to locate local maxima in a two-dimensional region of extremely small gradients; this situation is further degraded by the low resolution of FTAN which diffuses the signal both in time and in frequency. The accepted practice in harmonic analysis is to use a time series of length 5 to 6 times the maximum period of interest. Thus a 1024 s time series permits analysis

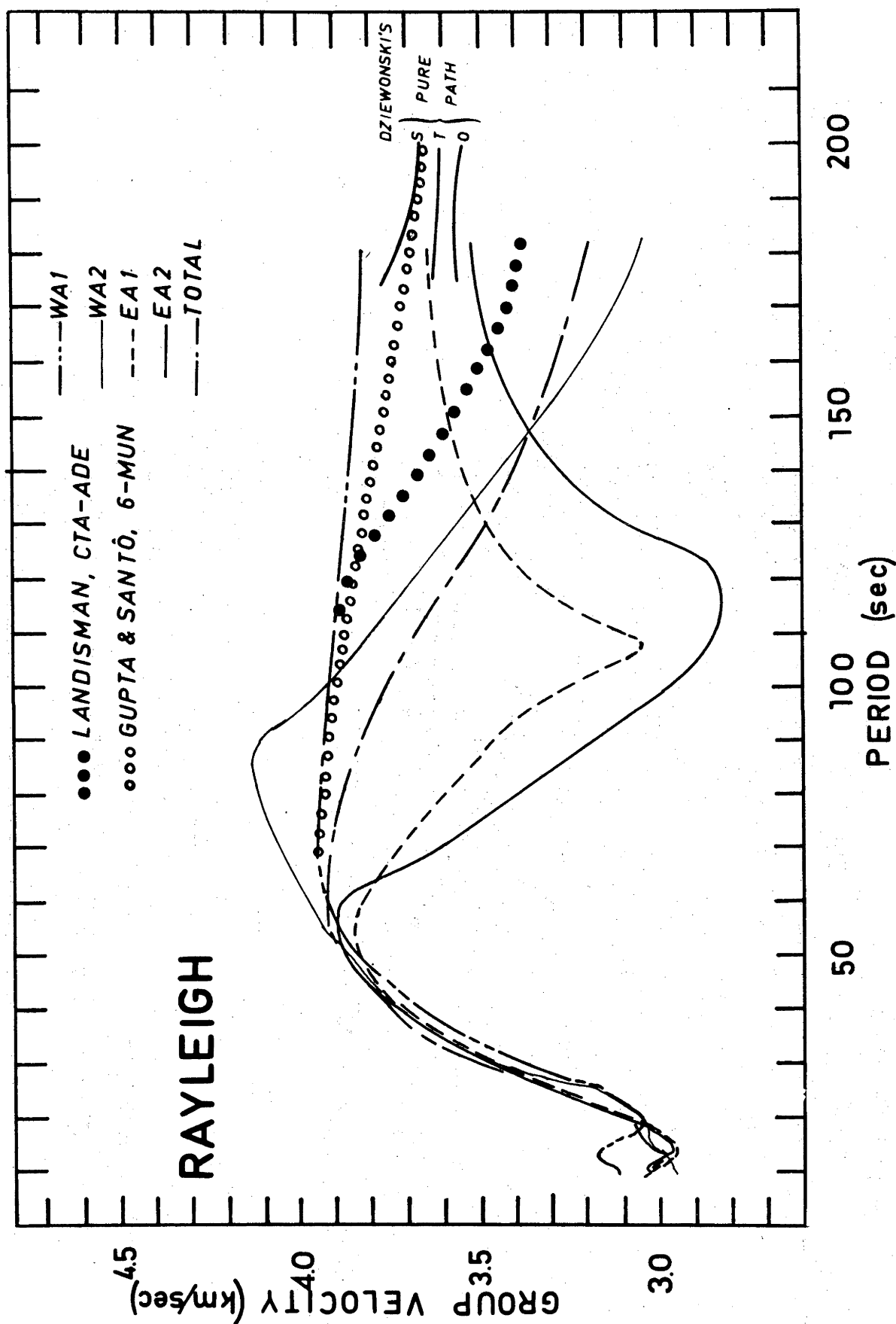


Figure 4.27: Group velocity curves for Australia plotted against a linear period axis. Comparison with data from Landisman and world-circling waves by Dzierwonski, and Gupta and Santó.

only to 160 to 200 s. In other words, the use of the 1024 s time series is being pushed to its limit.

The maxima at constant period, shown as small squares on the FTAN diagrams, exhibit regularity to 183 s period, except for 'EA1' and 'EA2', which show a pronounced dip at about 120 s. A notable feature of these diagrams is the manner in which group velocity reaches its maximum value at a much longer period in 'WA1' and 'WA2' compared to 'EA1' and 'EA2'. Also, note that the magnitude of the second derivative of the group velocity curve at its maximum is much greater for the East curves than for the West curves. This characteristic proved to be a powerful discriminant in testing models in the Monte Carlo inversion, described in Chapter 5. These observations are shown more clearly in Fig. 4.27, where the group velocity curves are plotted against a linear period scale to avoid the compression of a logarithmic abscissa. It is also quite apparent that little difference in group velocity exists over the period range from 10 to 50 s. This observation indicates great uniformity in the composition and depth of the crust over the whole continent of Australia.

The results at periods longer than 100 s must be treated with caution, for the reasons already given. Nevertheless, the results graphed in Fig. 4.27 show that group velocities of mantle waves having periods of up to 200 s can be measured directly within specific geographical regions, as distinct from deriving this information from world-circling waves.

For a comparison with the author's results, three studies have been included in Fig. 4.27: (1) Dziewonski's [1970b] pure path data, which extend down to periods as short as 150 s, (2) Gupta and Santô's [1973] world average data, which extend down to 90 s period, and (3) a group velocity curve obtained by differentiating Landisman's phase velocity curve shown in Fig. 4.12. Dziewonski's data are representative of Fourier analysis of world-circling waves; his data agree closely with other free oscillation studies and are not expected to change significantly as new information becomes available. Gupta and Santô attempted to extend the analysis of world-circling waves to shorter periods by careful selection of seismograms that showed inverse dispersion sufficiently clearly to permit the use of the peak and trough method. Landisman's result was discussed earlier and represents phase

velocity extracted by the two-station method. The present author calculated the 'Landisman' group velocity curve in Fig. 4.27 by differentiating his phase velocity curve according to Eqn (3.19).

Thus, the group velocity curve derived from Landisman, and that of the author, constitute direct measurements of group velocity in a limited geographical area. The data of Dziewonski, and of Gupta and Santô, constitute group velocity determined from surface waves that have travelled completely around the Earth. The 'WA2' curve is not congruent with the 'shield' curve of Dziewonski in the range 150 to 200 s, although it is less discrepant with the Landisman curve. 'WA1', on the other hand, agrees well with both the Dziewonski and the Gupta and Santô results. Curves 'EA1' and 'EA2' both join reasonably well with Dziewonski's tectonic curve at about 180 s. Even at these periods, then, the data are not necessarily in conflict with the data arrived at by other methods, and may be taken to confirm that systematic differences exist between group velocities for shield and tectonic regions in the period range 100 to 200 s. The suggestion of a dip in group velocity at about 120 s across tectonic regions certainly warrants further investigation.

At periods shorter than 100 s the precision and accuracy of group velocity measurements are much better, and, when the large number of events that have been included by a linear averaging process is taken into account (54 events are included in the Rayleigh wave analysis for 'total Australia'), considerable confidence can be placed in the measurements at periods less than 100 s. The profiles of group velocity must be evidence of systematic changes in the characteristics of the low velocity channel, and in Chapter 5 the results of inversion of this information are discussed with regard to information gained about the LVC.

4.5 DERIVATION OF PHASE VELOCITY CURVES BY INTEGRATING GROUP VELOCITY

The phase velocity curves of Fig. 4.17 obtained by processing all available data are not suitable for use in the inversion study discussed in the next chapter; they must be smoothed. Accepted smoothing techniques such as moving average or polynomial fitting do not add information to the data. Group velocity measurements contain additional information about the slope of the phase velocity curve since they are obtained by a different process. In the present study, the

combination of summing cross-correlations from an ensemble of events and adding FTAN matrices has produced group velocity curves that can be integrated, and thus integration is the preferred method of smoothing.

Phase velocity was obtained from the regionalized group velocity curves by numerical integration according to Eqn (3.22). There is an unknown constant of integration k_1 , the wave number at the lower limit of integration. The wave number at this period is not known accurately because of uncertainty in phase velocity at long periods. Determination of a value for k_1 was made on the basis of the observation that the complete phase velocity curve derived by integration could be specified if the wave number was known at one frequency (cf. Eqn (3.23)).

It appears that the most accurate, unbiased phase velocity information is in the period range 40 to 80 s obtained by Fourier analysis of summed cross-correlations, as shown in Fig. 4.17. This assumption was used to determine a value for k_1 in the following way:

The regionalized group velocity curves were numerically integrated with k_1 varied in steps of 0.0001π s/km in each successive integration. A family of phase velocity curves was thus obtained, and an example, 'WA2', is shown in Fig. 4.28a. Note that each of these phase velocity curves has the same group velocity curve. This family of curves was compared with the CTA-MUN and ADE-MUN phase velocity curves in Fig. 4.17 in the period range 40 to 80 s, and the value for k_1 that gave the best fit in this period range was found by visual interpolation. Proceeding in the same manner, regional phase velocity curves for 'WA1' and 'EA1' were obtained by integrating group velocity and are shown in Fig. 4.29. Significant features of this presentation are:

- (1) Between 40 and 80 s period the phase velocities in 'West Australia' are about 0.2 km/s higher than those in 'East Australia'.
- (2) The curves merge to a common value, 4.15 km/s, at 110 s period.
- (3) In the period range 10 to 25 s the phase velocities for 'East' and 'West' Australia are nearly the same, there being less than 0.05 km/s difference.

This last comment cannot be applied to the phase velocities determined from Fourier analysis of summed cross-correlations, which show

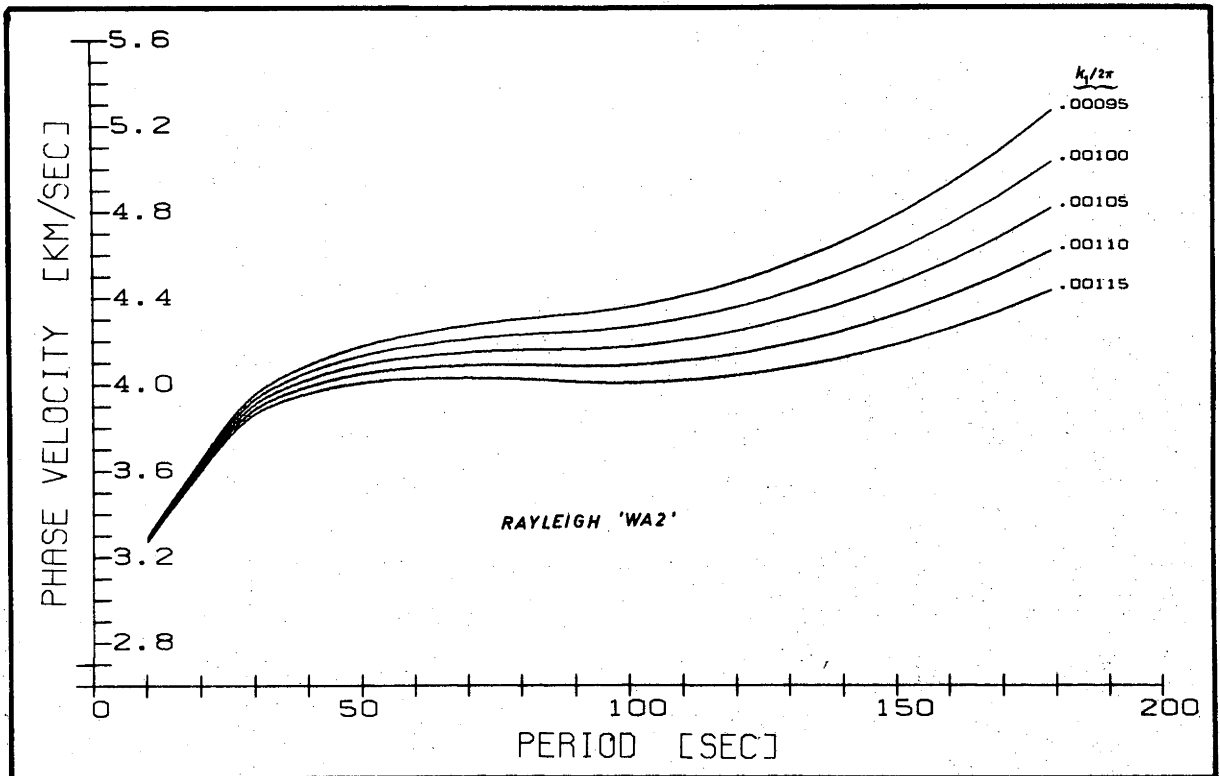


Figure 4.28a: Family of phase velocity curves obtained by integrating the group velocity curve 'WA2'. Wave number at 183 s is not known accurately. This family of curves was visually compared with Fig. 4.17 to obtain a value for k_1 .

considerable scatter at short periods. It can be concluded that FTAN summation of paths of different length followed by integration of group velocity is an effective way of obtaining a smooth phase velocity curve from noisy data.

Fig. 4.29 shows three phase velocity curves obtained by integrating group velocity:- 'WA1' (this is the single path CTA-MUN), 'WA2' (combined FTAN matrices for CTA-MUN and ADE-MUN), and 'EA1' (FTAN matrices for all six East paths). One more family was computed:- 'EA2', a selection of certain eastern paths, characterized by a broader and lower dip in group velocity than 'EA1' exhibits. The family of phase velocity curves obtained by integrating 'EA2' is shown in Fig. 4.28b. It is apparent that there is a difficulty in attempting to justify a reasonable wave number at the longest period and at the same time maintain agreement with Fourier phase velocities in the 40-80 s range. For this reason 'EA2' has not been included in Fig. 4.29.

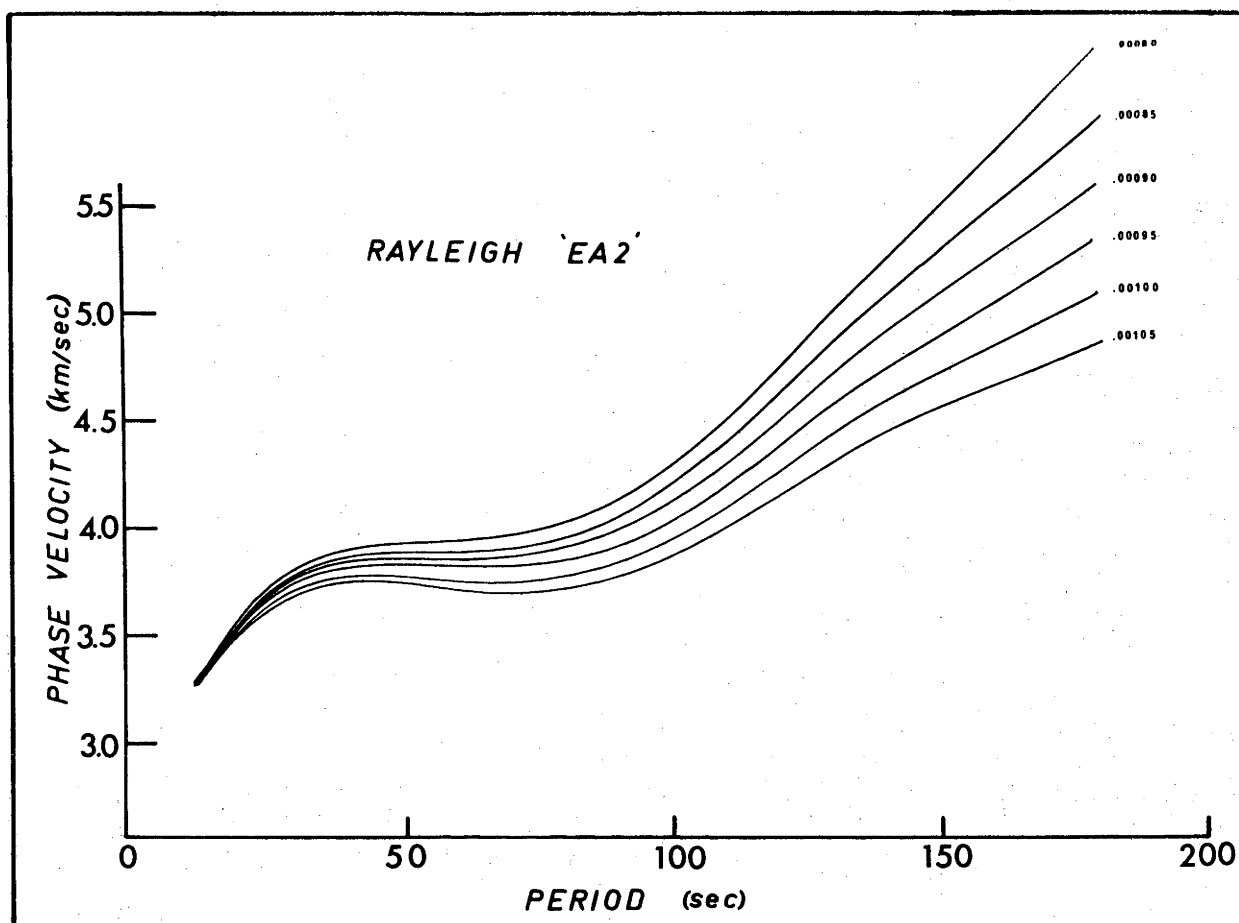


Figure 4.28b: Family of phase velocity curves obtained by integrating the group velocity curve 'EA2'.

4.6 DISCUSSION: RESULTS AT LONG PERIODS

The feasibility of the dip at 110 s exhibited by Rayleigh wave group velocity in Fig. 4.29 for the paths in eastern Australia will now be examined. A summary of pertinent information is presented to determine if this unexpected behaviour of group velocity might be real.

Firstly, Figs. 4.17 and 4.18 show that the two paths, ADE-MUN and CTA-MUN, which are located to the west of the boundary defined by the CTA-ADE path (see map, Fig. 4.19), can be more-or-less successfully analysed by the cross-correlation method to obtain reasonable phase velocities to periods as long as 170 s. On the other hand, these figures also show that this type of analysis becomes unreliable at 100 s or less for the six paths located to the east of this line. The analysis for the mixed path RIV-MUN, which traverses both regions, appears satisfactory to 130 s. These observations lend confidence to the ability of the sum of cross-correlations method to enhance signal strength in the 100 to 200 s

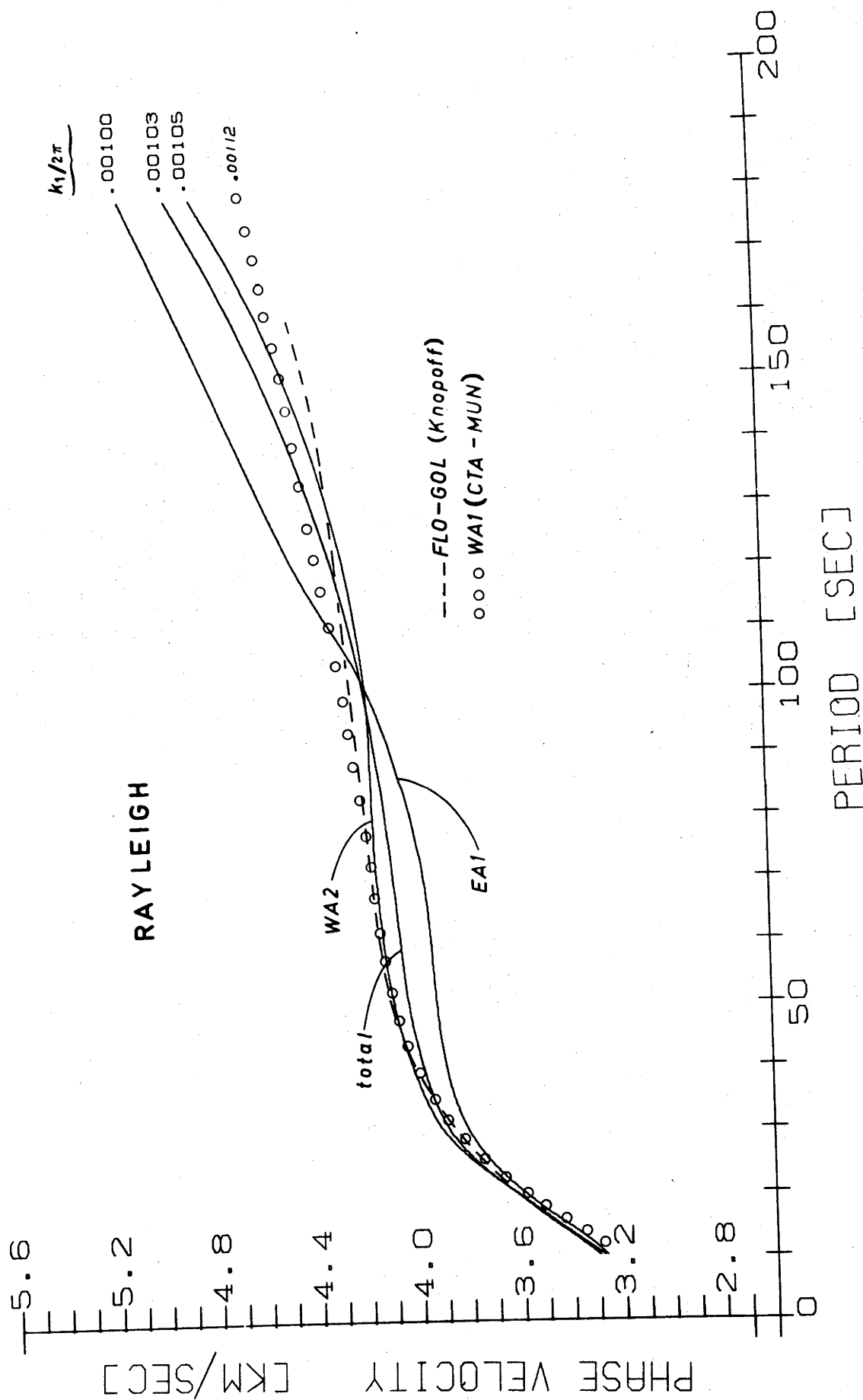


Figure 4.29: Rayleigh wave phase velocity curves for Australia obtained by integrating group velocity curves.

range, and suggest that there is something unusual about Rayleigh wave propagation in eastern Australia.

Events 4 and 5 are interesting because the same seismograms were used in the analysis of RIV-MUN (East), ADE-MUN (West) and RIV-MUN (traversing both East and West). Using the same surface waves, the latter two paths can be analysed to longer periods than the RIV-ADE path, which is contained entirely in eastern Australia. This tends to rule out the hypothesis that a loss of long period signal strength associated with the events used in the analysis of eastern Australia might be responsible for the unusual dispersion observed there at periods between 100 and 200 s. The CTA-ADE path, which skirts the shield boundary, was successfully analysed to long periods, but note that its group velocity tends to drop below that of the pure shield path CTA-MUN, as though partially influenced by the peculiarities of the eastern region. (This is confirmed also by Landisman's results in Fig. 4.27.)

Fig. 4.17 shows that the phase velocity curves for the eastern paths tend to cross the curves for the shield region at about 100 s, and the small amount of information at longer periods than this (see 5, 6 and 9 in Fig. 4.17) indicates that they continue to remain above the shield curves at longer periods. This tendency is shown clearly in Fig. 4.29, by the 'EAL' phase velocity curve. This curve was obtained by integrating the 'EAL' group velocity curve, and it fits the individual path data, as determined by Fourier analysis of summed cross-correlations, quite well to 110 s.

Were these unusual observations more limited, an explanation might be sought in proposing a localized singularity such as the channel geometry of the Gulf of California [Thatcher and Brune, 1973] where lateral variations exert a complicating effect on the dispersion observed. The unusual group velocities observed here, however, are seen in a span of crossing paths over a wide area, roughly 1500 km in extent, and thus any proposed small-scale heterogenous structures can be eliminated.

These arguments do not verify the reality of the questionable dip in group velocity; they serve mainly to demonstrate that the phase velocity and group velocity results are consistent.

The present study shows two distinctly different group velocity profiles in the 100 to 200 s period range, namely (a) a steady decrease

from 4.1 km/s to 3.6 km/s, and (b) the suggestion of much lower group velocity, perhaps as low as 3.2 km/s, before rising to the values near 3.7 km/s obtained from analysis of world-circling waves.

Other studies have presaged a pronounced group velocity dip. Landisman's extended phase velocity curve for CTA-ADE, when differentiated, yields a group velocity of 3.3 km/s at 190 s. Similarly, SHI-HLW (curve 7 in Fig. 4.22 from Knopoff) for northern Arabia bears a similarity to the East Australia curve in Fig. 4.29, and, upon differentiation, yields group velocities about 0.4 km/s below (a) above.

A possible counter-argument is that the Love wave results do not show a corresponding dip in group velocity (see Fig. 4.43). Note that, when instrumental response is included, the spectrum of Love wave energy peaks at 60 s compared to 25 s for Rayleigh waves, and consequently there is less chance of there being a weak signal problem in the 100-200 s range (cf. Figs. 4.34 to 4.39 for spectral amplitudes).

For reasons to be mentioned, the Love wave results must be considered less reliable than those obtained for Rayleigh waves. However, a more important point is that the presence of a hypothetical low shear velocity layer responsible for the dip in Rayleigh wave group velocities would not necessarily produce a similar dip in the Love wave curve. This statement is supported by Fig. 4.47 from Bloch [1969], which shows partial derivatives with respect to shear velocity for Rayleigh and Love fundamental modes. Since Love waves sample the Earth less selectively than do Rayleigh waves, a localized low shear velocity layer would not be expected to produce a marked perturbation on the Love wave dispersion curve, as it might for Rayleigh waves.

Here again, this reasoning does not directly support the reality of the group velocity dip, but shows that a consistent overall data set is possible.

The group velocity results can therefore be tentatively accepted at face value. It remains to be established whether a realistic model can be obtained by inversion.

4.7 LOVE WAVES

The preceding sections have described the methods of analysis used to obtain regionalized phase velocity curves for Rayleigh waves. In

general, the same methods were applied to the analysis of Love wave data. However, four readable seismograms are required for Love wave analysis whereas only two are needed for Rayleigh waves. In some instances the lack of one readable horizontal component seismogram prevented that event from being analysed. Consequently, only 35 events were analysed, considerably less than the 54 for Rayleigh waves.

The measurement of Love wave dispersion may have large uncertainties due to interference of the higher modes with the fundamental mode. Thatcher and Brune [1969] showed that for many Earth structures the fundamental, first and second higher mode group velocities were so close together that these modes do not separate in time on the seismogram. A beat phenomenon between the modes occurs, with a beat wave length on the order of 1000 and 2000 km. Rapid fluctuations in apparent phase velocity would be expected if the recording station were located in the vicinity of a beat node. They suggest that such rapid phase velocity fluctuations have not been reported because such results would have been judged to be of poor quality and would have been discarded before final reporting.

In a companion paper, Boore [1969] concluded that 'the first higher mode can be an important contaminant of the fundamental (Love) mode, but that interstation phase velocities measured over an ensemble of events should show scatter but no strong bias'. His analysis of the problem showed that phase velocities for the fundamental mode perturbed by the higher mode would oscillate about the unperturbed value and the length of the oscillation would increase at longer periods.

In the present study no attempt at pre-selection of Love wave data has been made; all readable horizontal seismograms were cross-correlated and included in the sum for the appropriate path. The theoretical predictions mentioned above appear to be observationally verified by the results of Fourier analysis shown in Figs. 4.44a and 4.44b. Some paths such as CTA-ADE show violent phase velocity fluctuations, others such as ADE-RIV and CTA-RIV appear to exhibit oscillations about a mean curve, the length of the oscillation increasing at long periods.

The analysis for one path, CTA-ADE, is presented in full detail. The east-west and north-south horizontal components were combined

according to Eqn (3.25) to obtain ground motion transverse to the direction of propagation. FTAN contour plots of the transverse components for the CTA-ADE path are shown in Figs. 4.30 to 4.32. The results of group velocity analysis of the cross-correlograms for each event used for this path are shown in Figs. 4.33 and 4.34. Group velocity analyses of summed cross-correlograms for the nine paths are shown in Figs. 4.35 to 4.39. They are markedly more disorganized than Rayleigh wave contour diagrams, as might be expected when the fundamental and higher modes are interfering. Time-variant filtration was not applied to Love wave data for the reasons expressed in Section 3.4.

The philosophy used for Rayleigh waves was applied to the summation of FTAN matrices according to 'West' (CTA-MUN and ADE-MUN), 'East' (ADE-RIV, ADE-TAU, CTA-RIV, CTA-TAU and RIV-TAU) and 'Total' (all nine paths) in an attempt to achieve similar reduction in noise interference. The results of this regional signal averaging by summing the FTAN matrices is shown in Figs. 4.40 to 4.42. The fundamental and first higher Love wave group velocity modes of Earth models resulting from inversion (see Chapter 5) are shown also on these figures. It is probable that these modes are mutually interfering and consequently cannot be separated by FTAN.

In these diagrams, it is possible to infer a coherent ridge crest indicating group velocity for Love waves much more readily than in the contour diagrams for the separate paths. The ridge crests exhibit changes in the slope of group velocity between 20 and 40 s. West Australia shows a gradient reversal at 35 s. This is due to interference from higher modes, and the FTAN results will be sensitive to the spectral amplitude ratios of the interfering modes.

The ridge crests are graphed against a linear period scale in Fig. 4.43, together with other data. Here again, it is of interest to see how the attempted extension of two-station dispersion compares with data from world-circling waves. Dziewonski and Landisman's [1970] results for their Path 1 are shown in Fig. 4.43. This path is primarily oceanic and would be expected to give group velocities less than those observed for continental regions. Thus, although the uncertainties in the author's measurements are large, it appears that the results are not inconsistent with dispersion obtained by a different method, although the

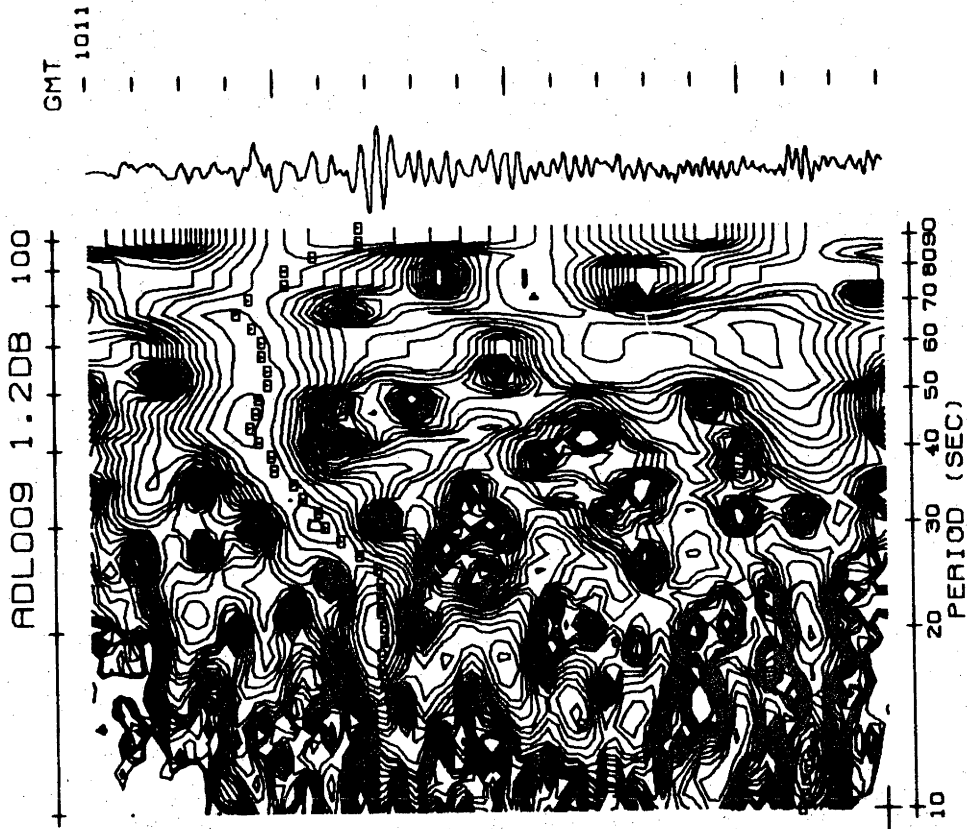
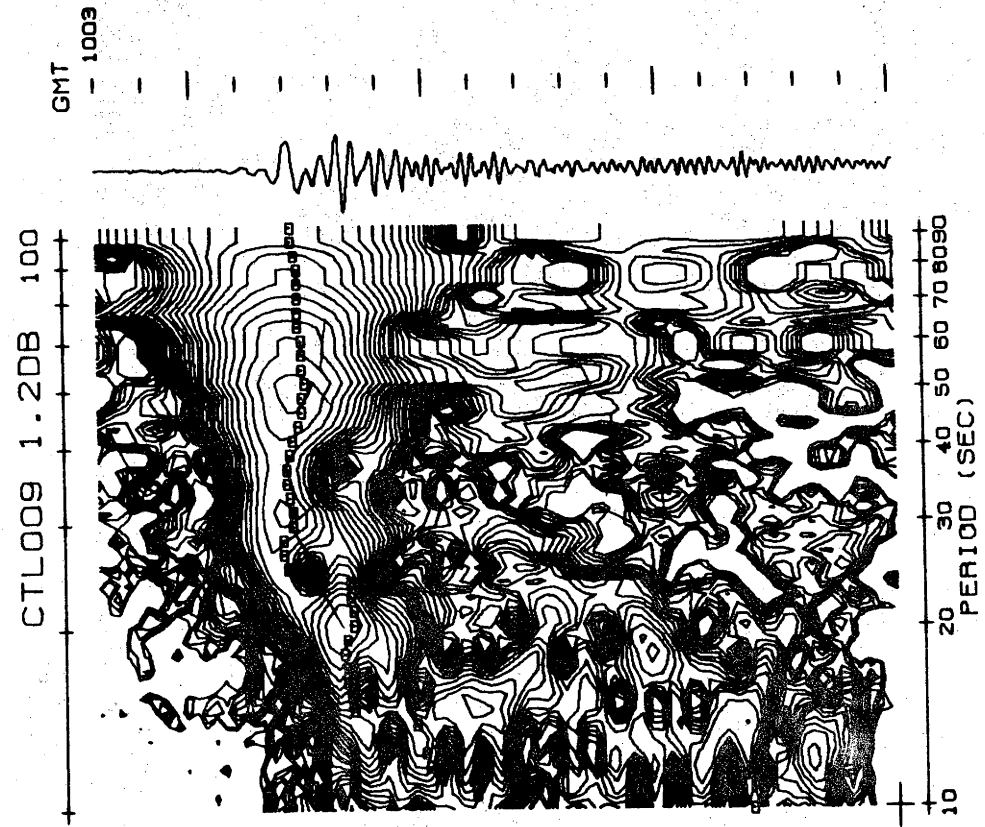


Figure 4.30: Frequency time analysis of group arrival time of event 9, Love waves, at CTA (left) and ADE (right).

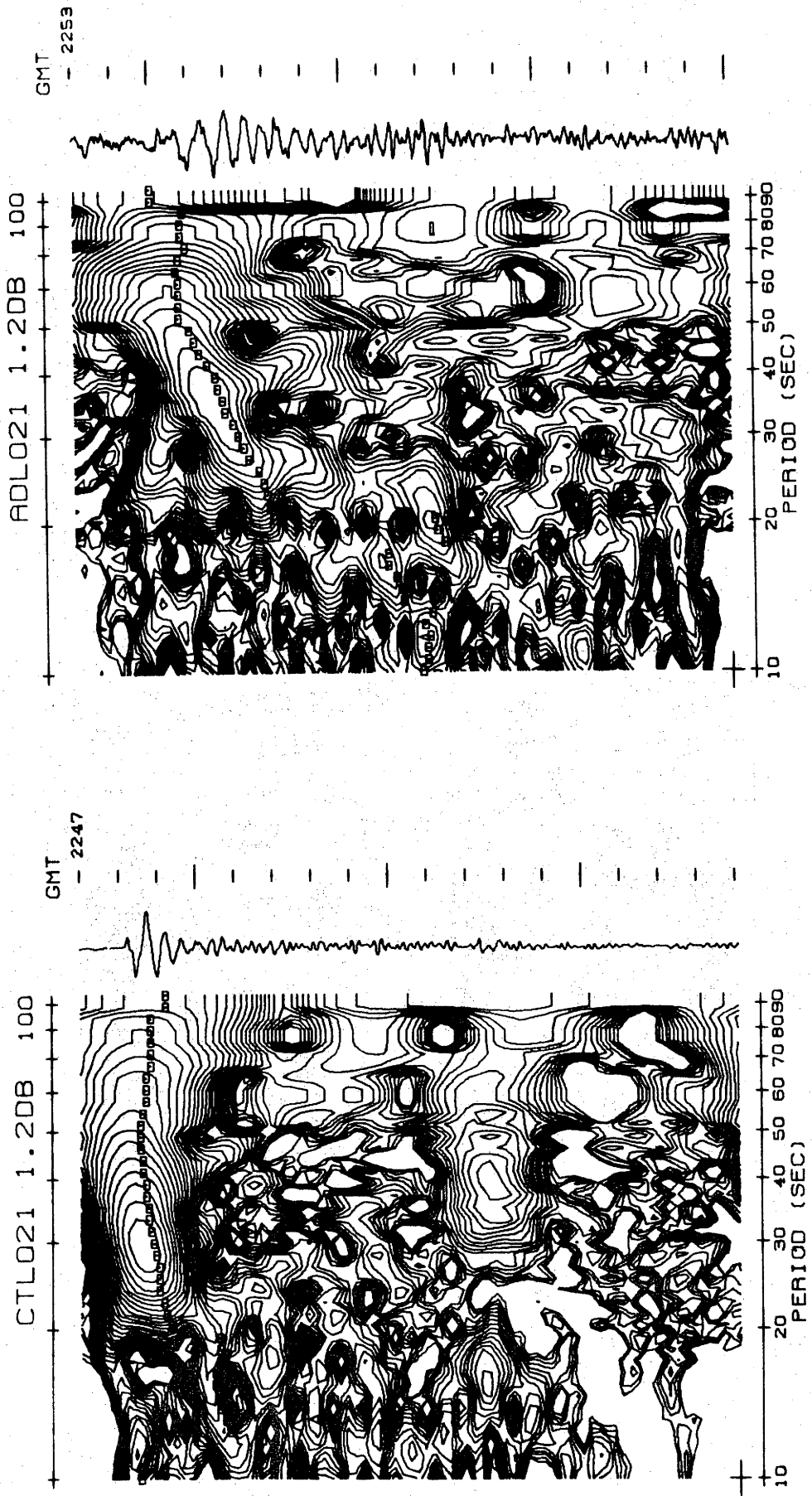


Figure 4.31: Frequency time analysis of group arrival time of event 21, Love waves, at CTA (left) and ADE (right).

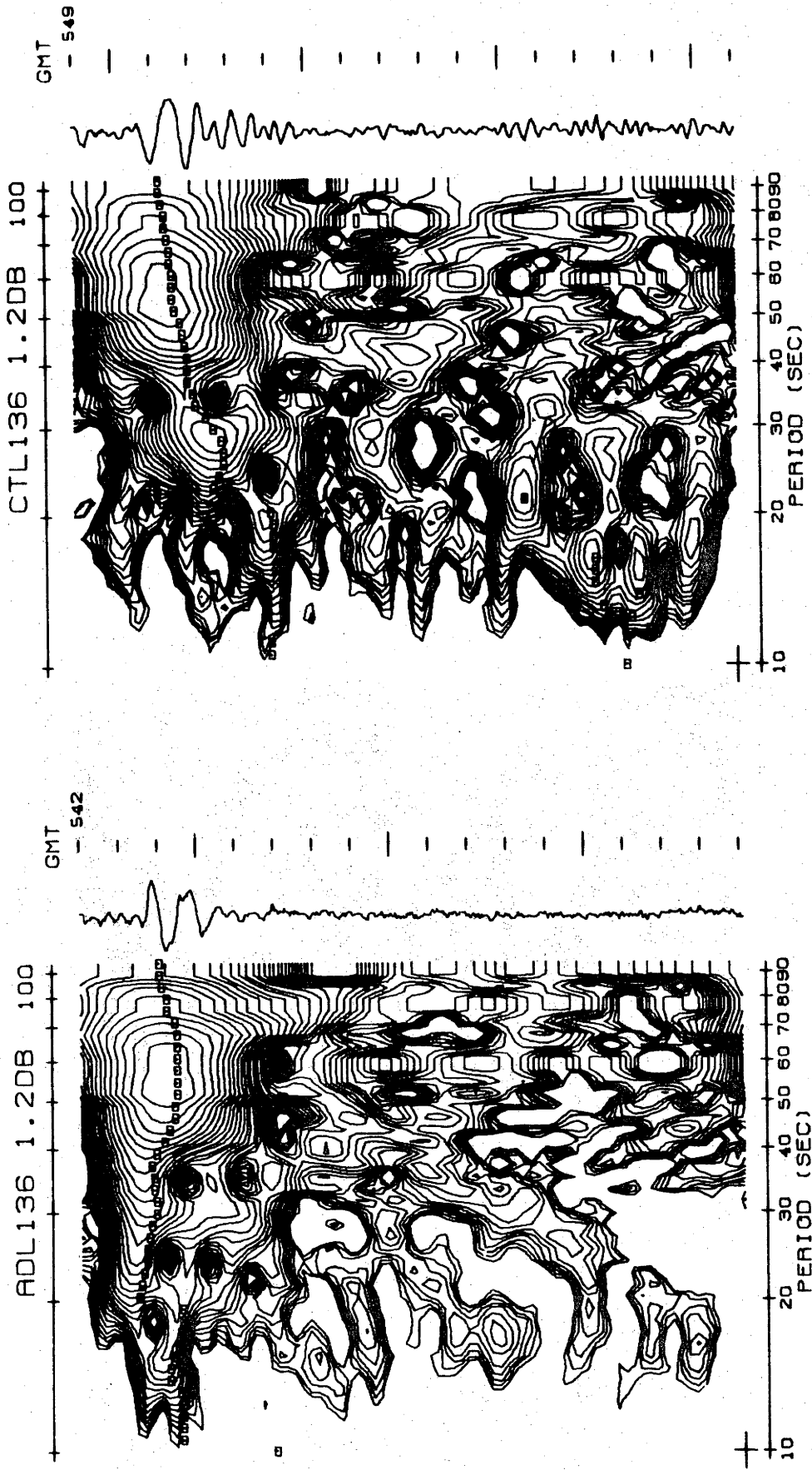


Figure 4.32: Frequency time analysis of group arrival time of event 136, Love waves, at CTA (left) and ADE (right).

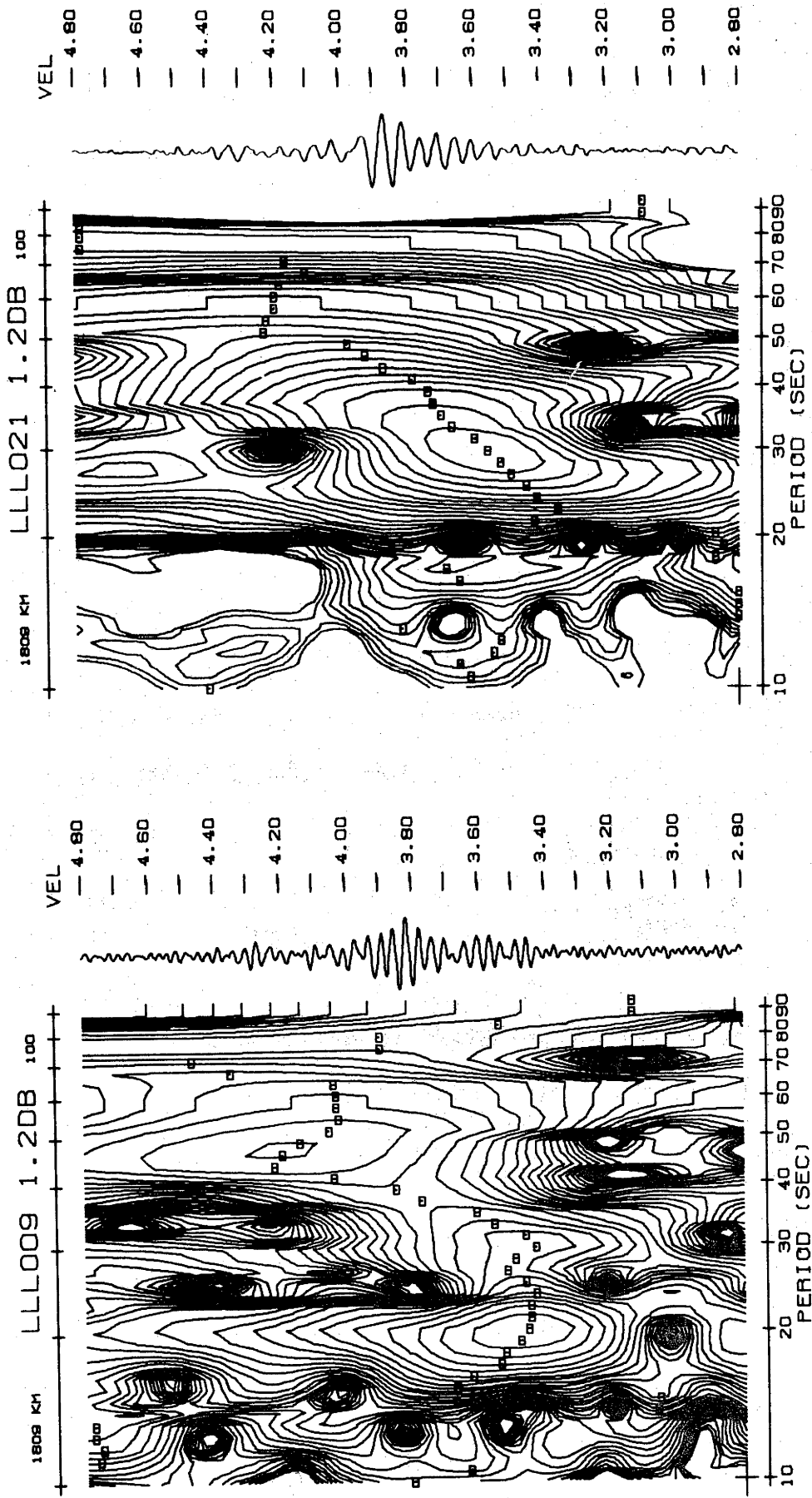


Figure 4.33: Love wave group velocity from FTAN contour diagram of event 9 (left) and event 21 (right).

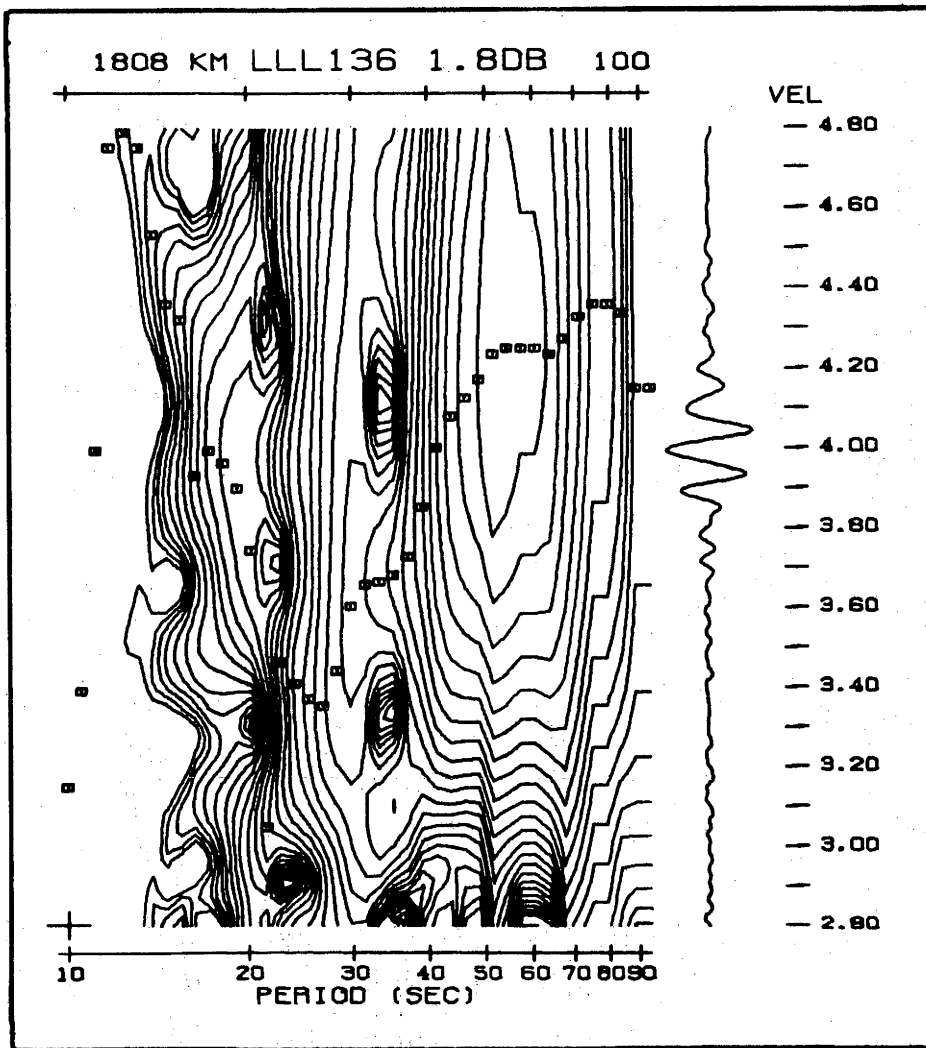


Figure 4.34: Love wave group velocity from FTAN contour diagram of event 136.

ridge crest denoting group velocity is almost certainly biased to higher values at longer periods by the proximity of the first higher mode.

Data from Brune's [1969] summary of crustal structure are also included in Fig. 4.43 for comparison. Although extending only to 60 s period, these curves agree qualitatively with the author's results at these shorter periods.

Although recognizing that the group velocity curves for Love waves shown in Fig. 4.43 could not be considered true measurements of the fundamental Love mode, the author felt it would be a worthwhile exercise to integrate them in the same manner as Rayleigh waves to see if any information could be gained from the resulting phase velocity curves. The constant of integration k_1 was chosen so that all three phase

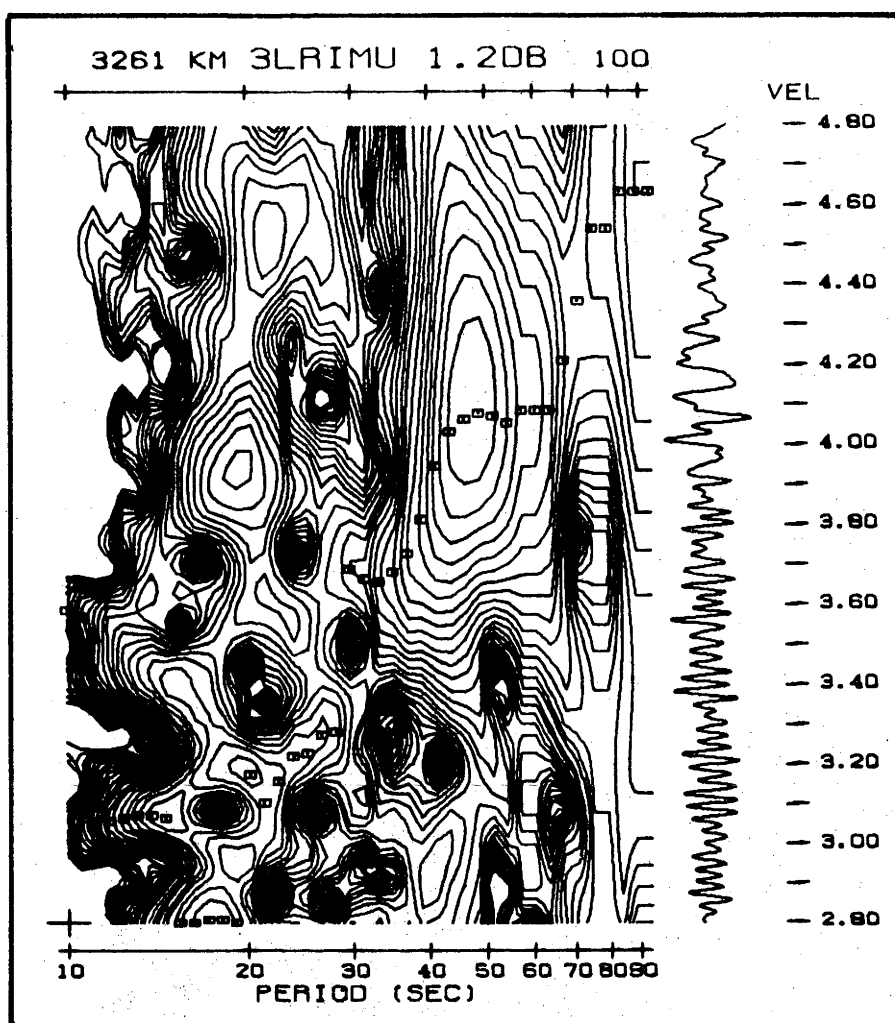


Figure 4.35: Love wave group velocity from sum of five cross-correlograms for path RIV-MUN.

velocity curves ('West', 'East' and 'Total') tended to a common value of 5.1 km/s at 183 s period. This appeared to be a reasonable assumption based on the results of Fourier analysis shown in Fig. 4.44a. The results of the integration are shown in Fig. 4.45, and an example of the family of phase curves obtained from one group velocity curve ('East' in this case) is shown in Fig. 4.46. With Rayleigh wave data it was possible to find an acceptable fit of the phase velocity curves derived by integrating group velocity to the phase velocity curves obtained from Fourier analysis of cross-correlations. In the Love wave case, this was not possible. The curves derived by integration lie consistently above those derived from Fourier analysis. This exercise confirms the belief that the group velocities obtained by FTAN analysis are too high because of interference by the higher modes.

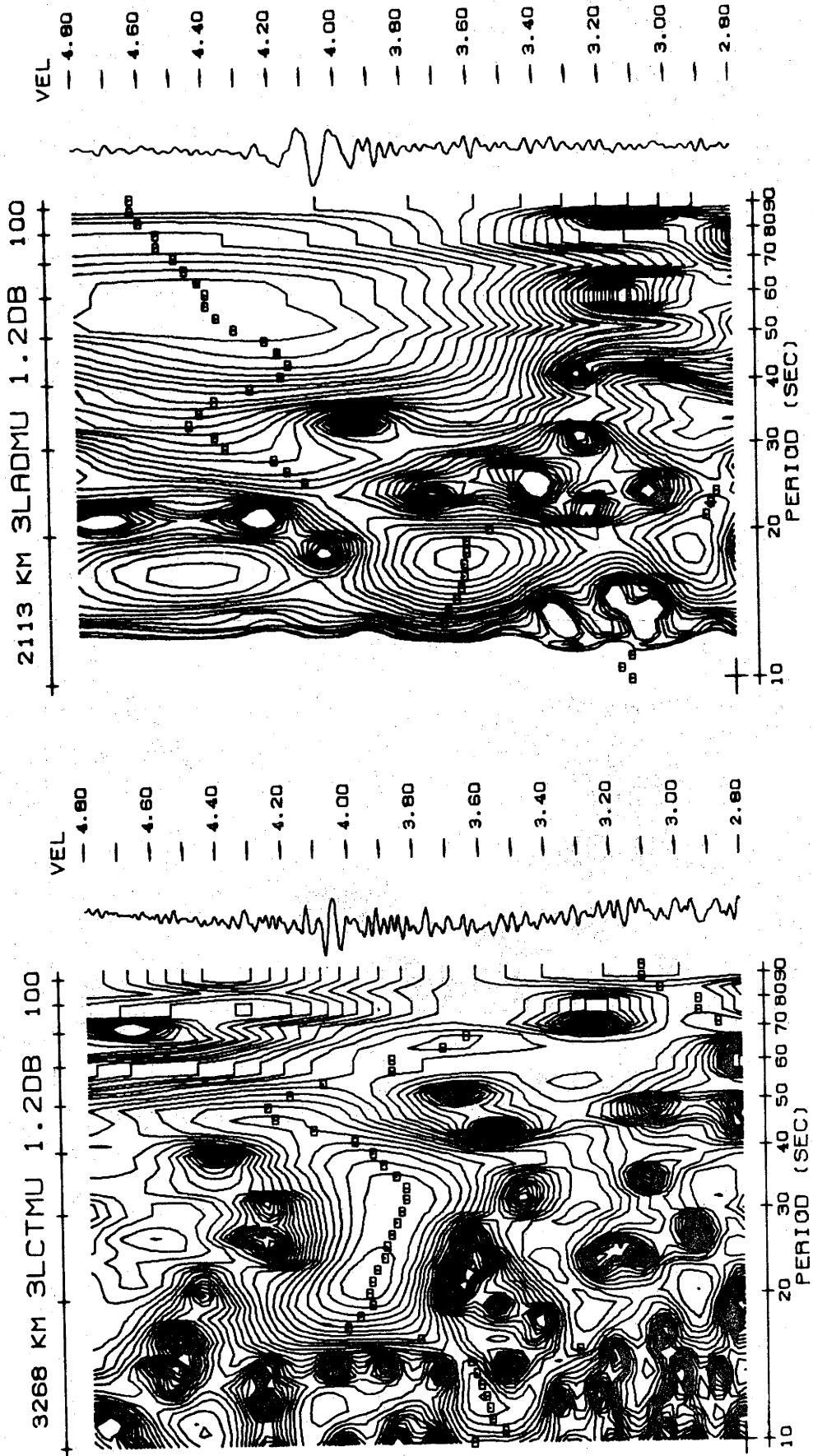


Figure 4.36: Love wave group velocity from sum of five cross-correlograms for CTA-MUN (left) and six for ADE-MUN (right).

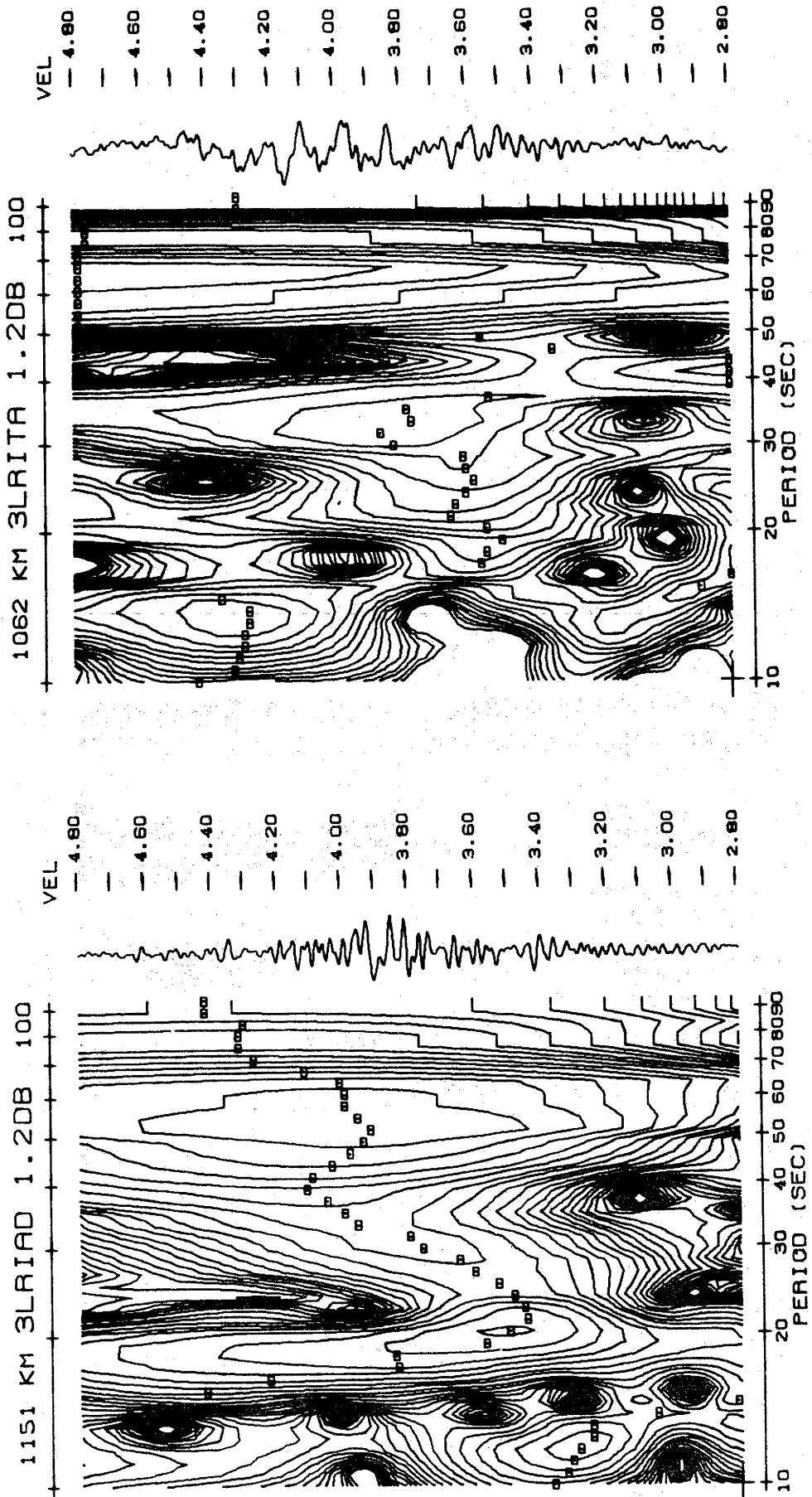


Figure 4.37: Love wave group velocity from sum of three cross-correlograms for RIV-ADE (left) and seven for RIV-TAU (right).

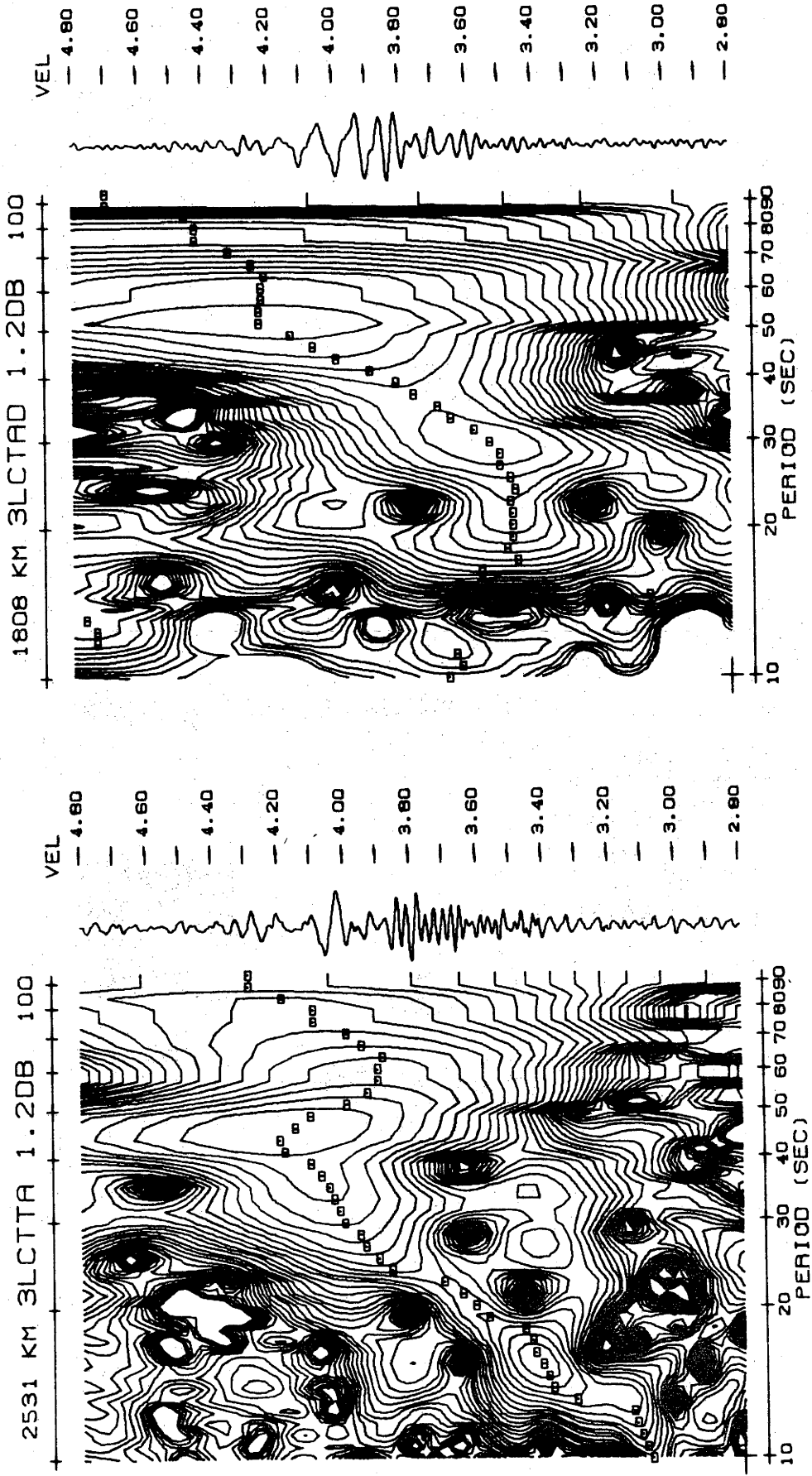


Figure 4.38: Love wave group velocity from sum of two cross-correlograms for CTA-TAU (left) and three for CTA-ADE (right).

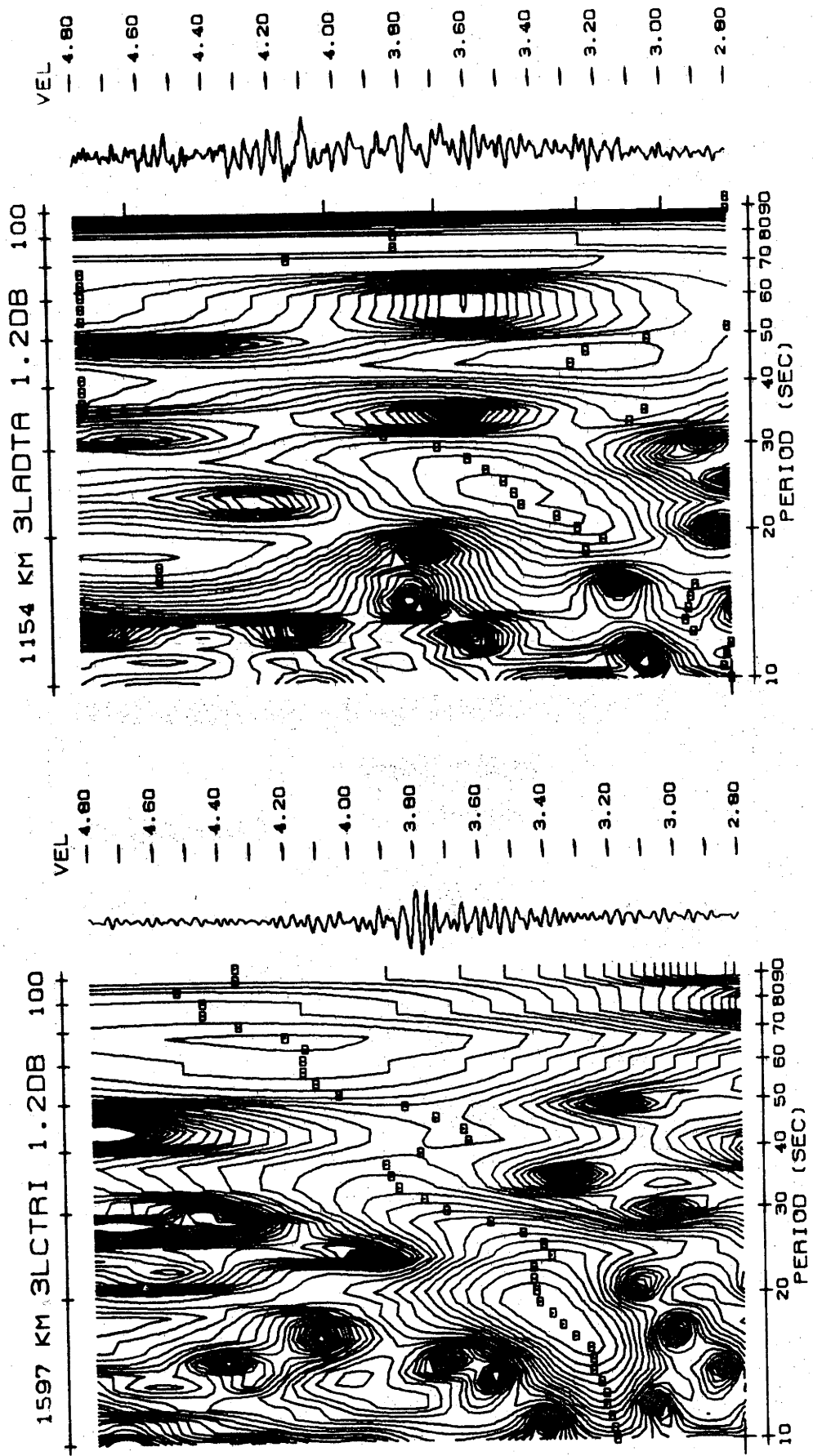


Figure 4.39: Love wave group velocity from sum of four cross-correlograms for CTA-RIV (left) and two for ADE-TAU (right).

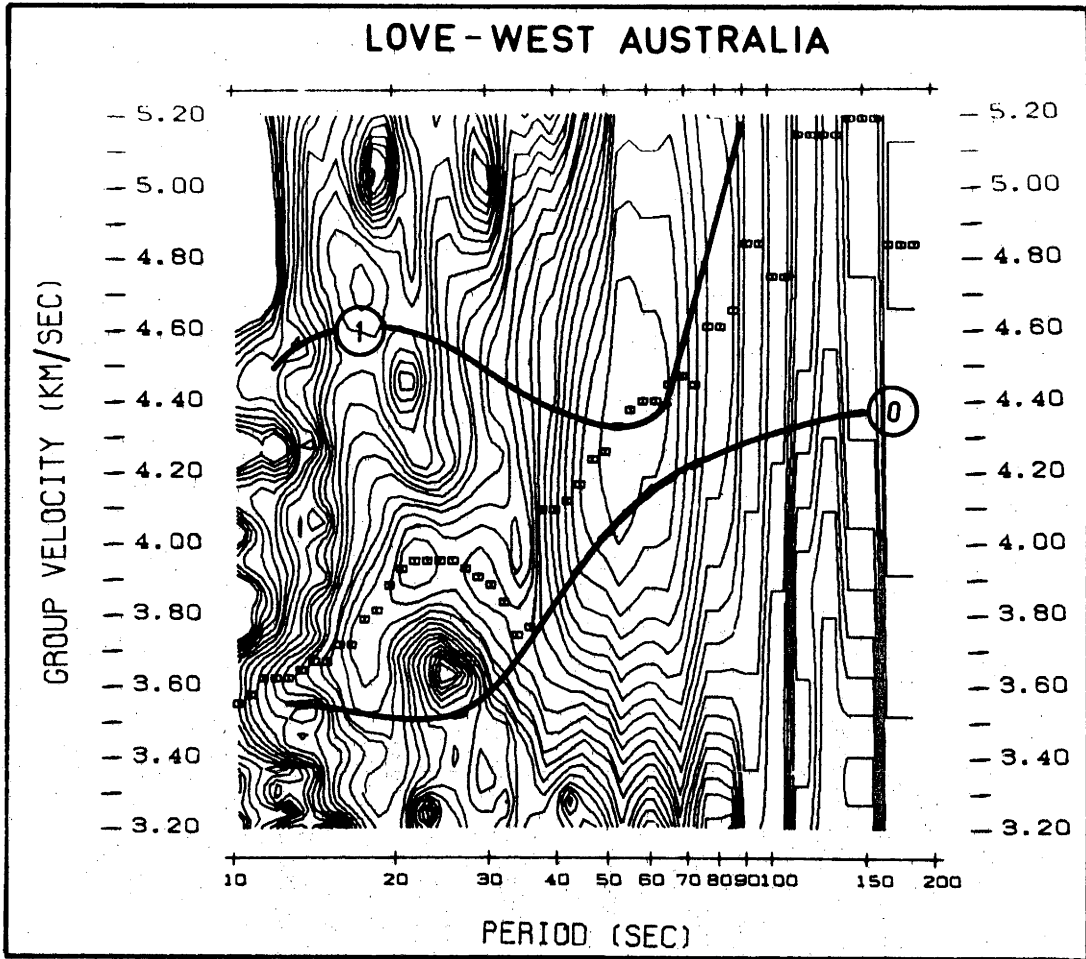


Figure 4.40: Love group velocity for 'West' Australia after further signal averaging by adding the FTAN matrices for CTA-MUN and ADE-MUN. 0 indicates the Love wave fundamental mode from a 'West' Monte Carlo model and 1 indicates the first higher Love mode.

Further evidence that the integrated Love phase velocity information shown in Fig. 4.45 is unreliable was revealed by inversion. It was impossible to find Earth models that would fit the integrated Love phase velocity curves. However, it was possible to fit models to the phase velocity information derived from Fourier analysis.

The obvious conclusion is that, until methods are found that will permit the higher modes to be resolved from the fundamental mode, any Love wave group velocity information obtained by frequency time analysis must be considered unreliable. However, it appears that averaging an ensemble of events via the 'sum of cross-correlations' method does permit reasonably accurate fundamental Love wave phase velocities to be obtained using Fourier analysis.

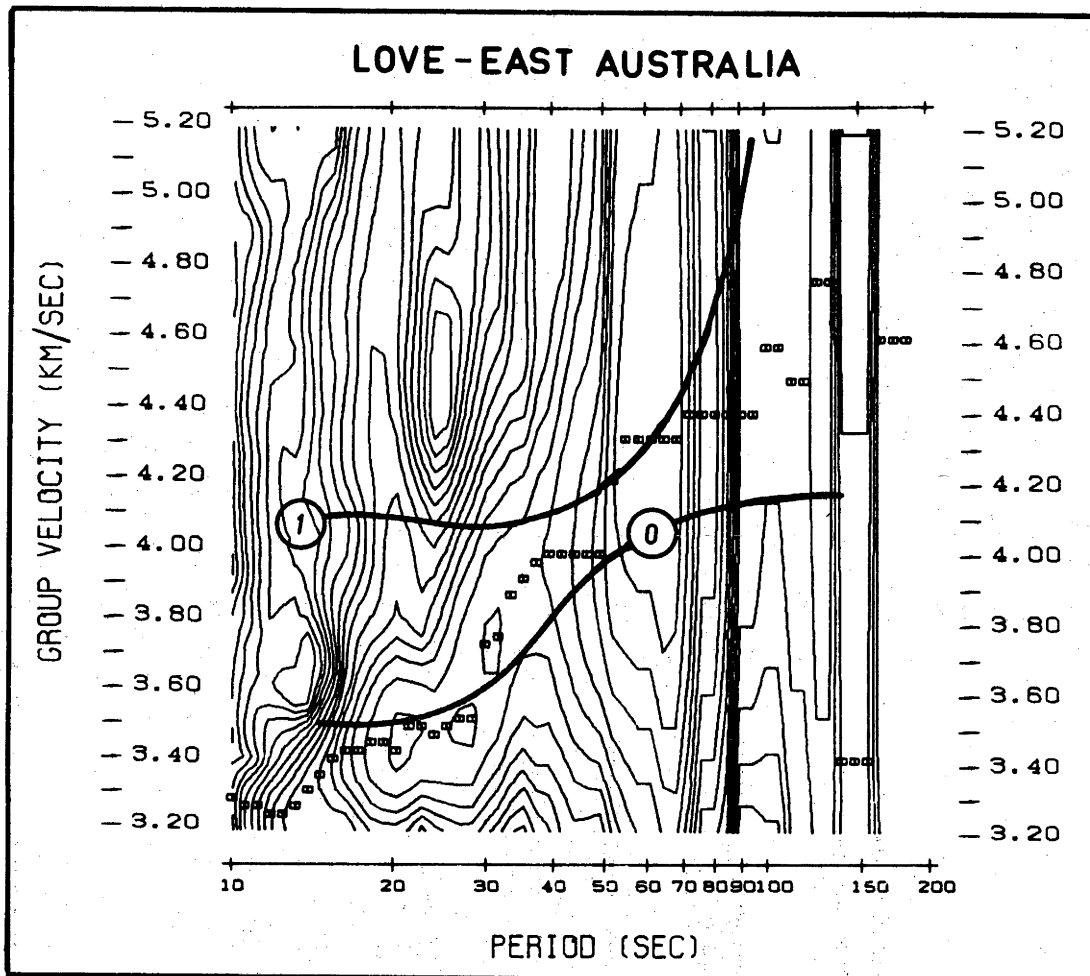


Figure 4.41: Love group velocity for 'East' Australia after further signal averaging by adding the FTAN matrices for ADE-TAU, CTA-TAU, ADE-RIV, CTA-RIV and RIV-TAU. Fundamental and first higher Love wave modes shown were calculated for an 'East' Monte Carlo model.

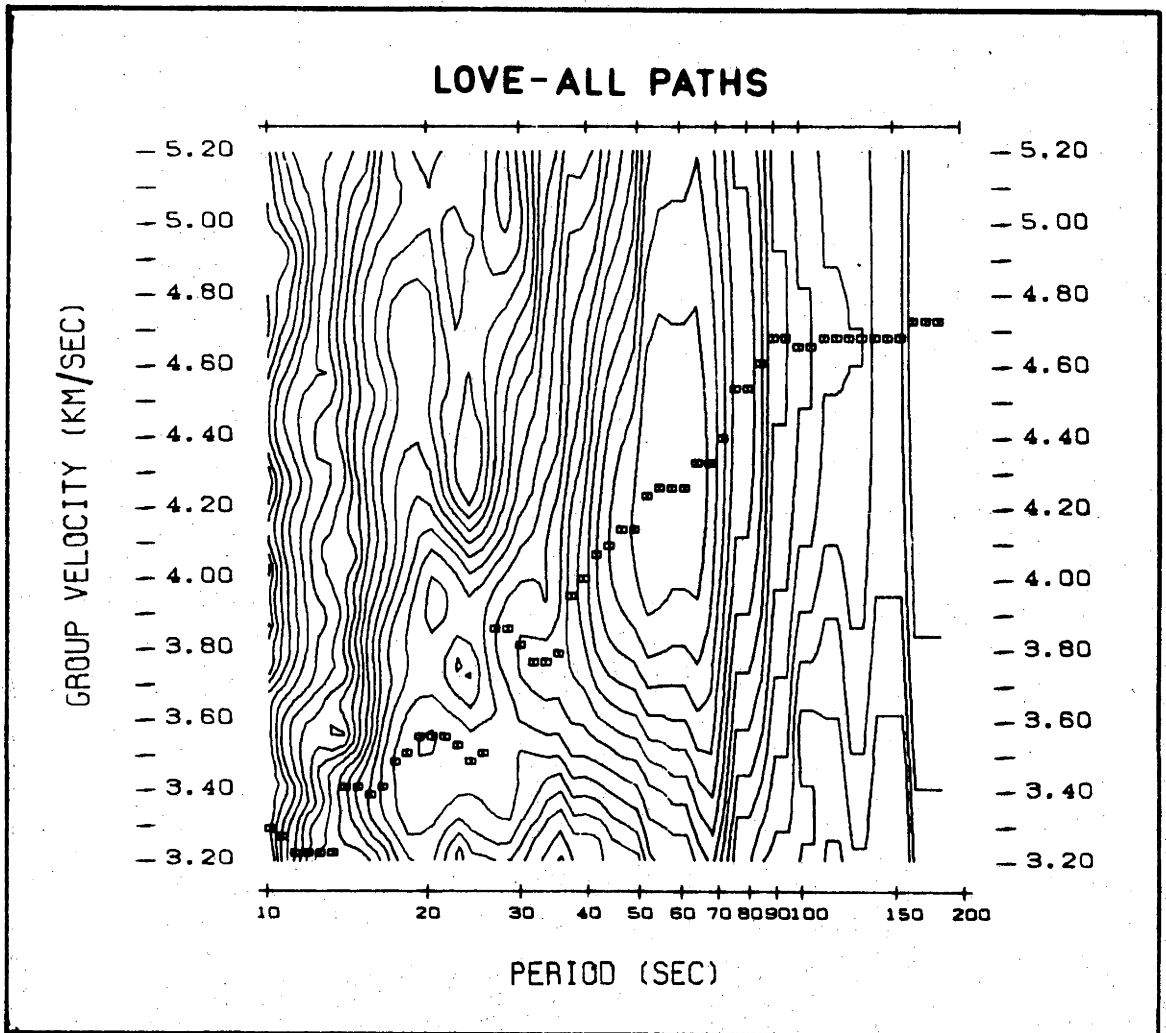


Figure 4.42: A reference Love group velocity for 'Total' Australia by adding FTAN matrices for all nine Australian paths.

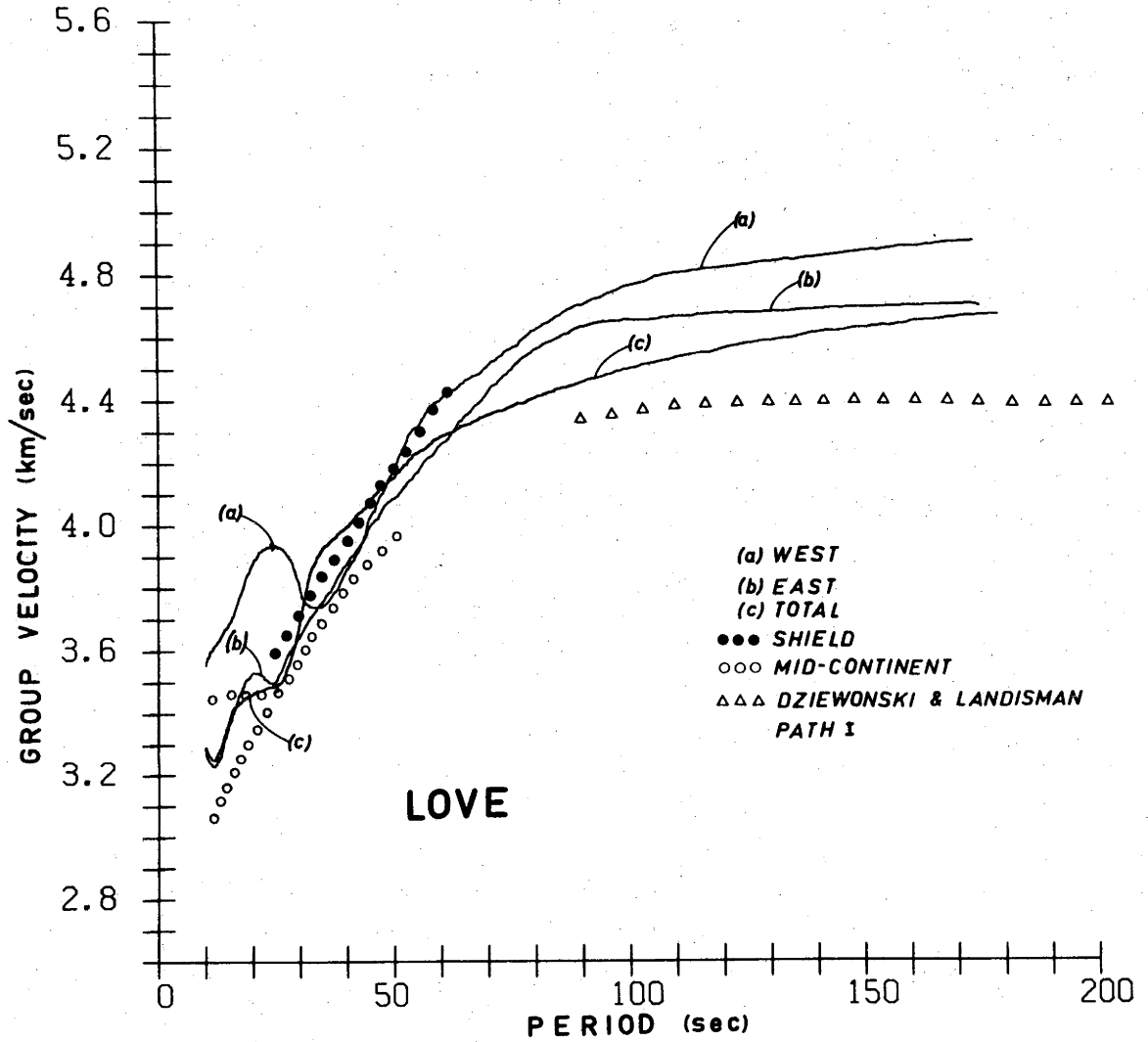


Figure 4.43: Love wave group velocity obtained for Australian regions by summing FTAN matrices. Comparison with other data.

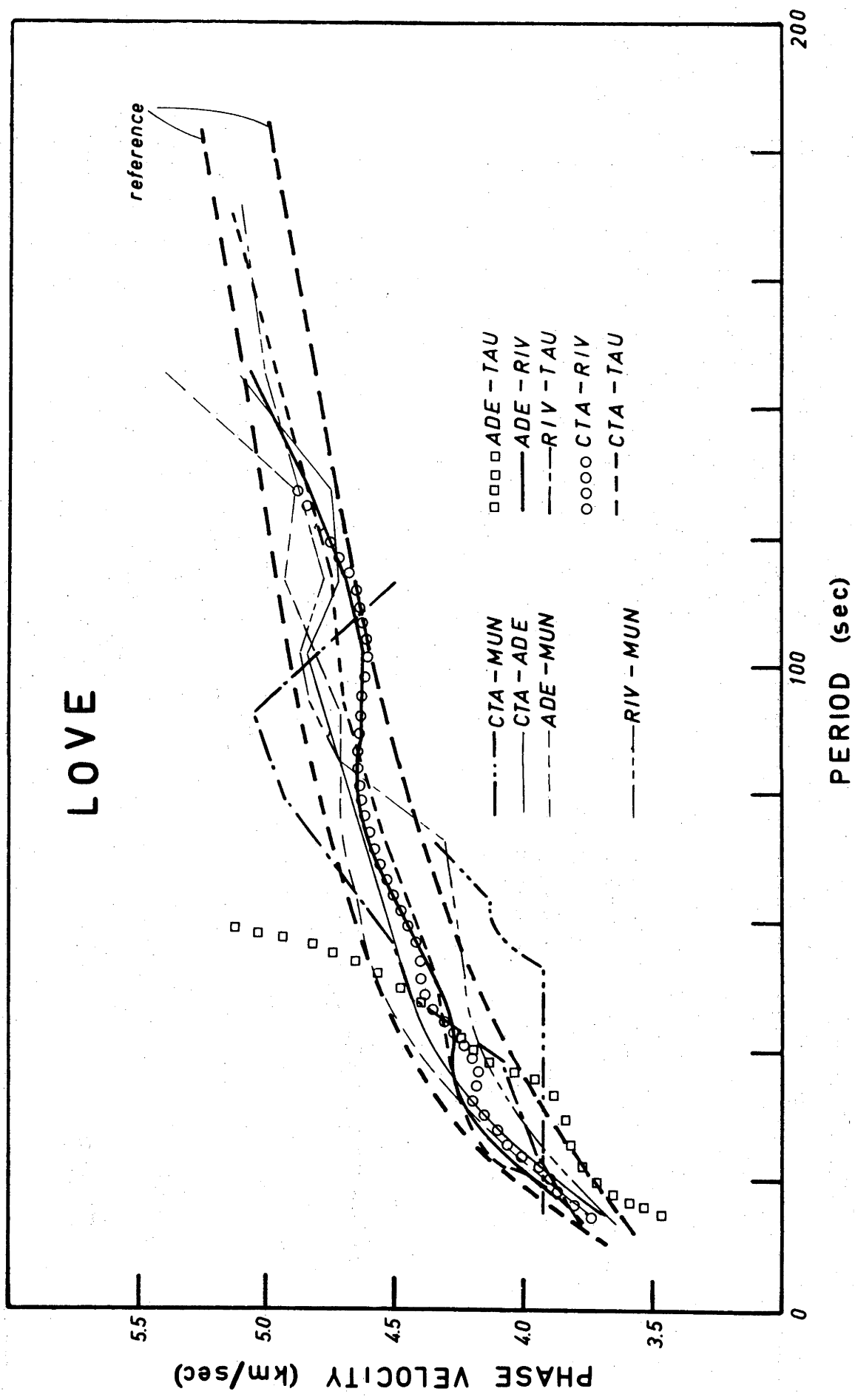


Figure 4.44a: Love wave phase velocities obtained by Fourier analysis of sums of cross-correlations. See Section 4.7 for explanation of scatter.

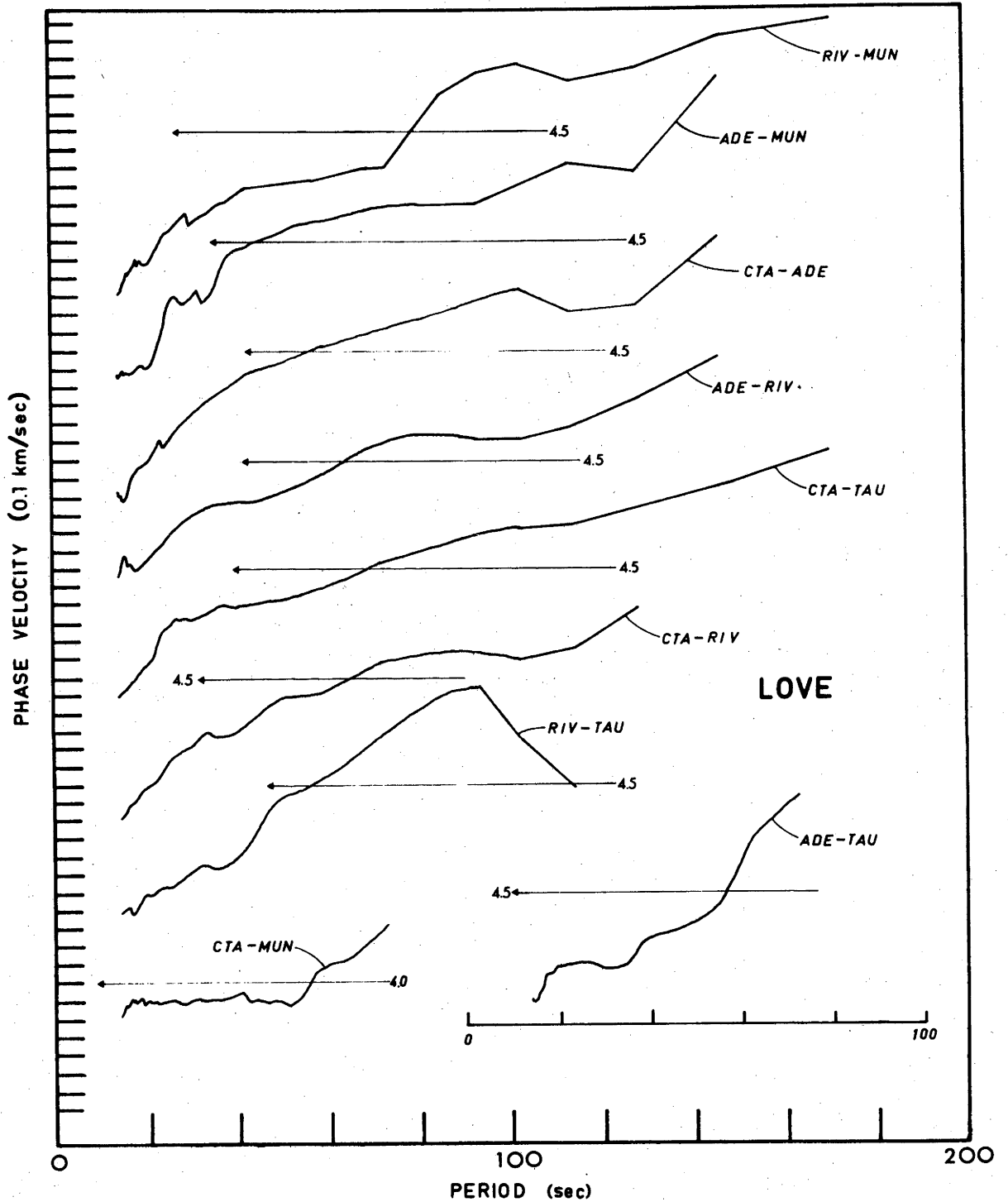


Figure 4.44b: Same information as Fig. 4.44a presented on displaced axes to facilitate identification.

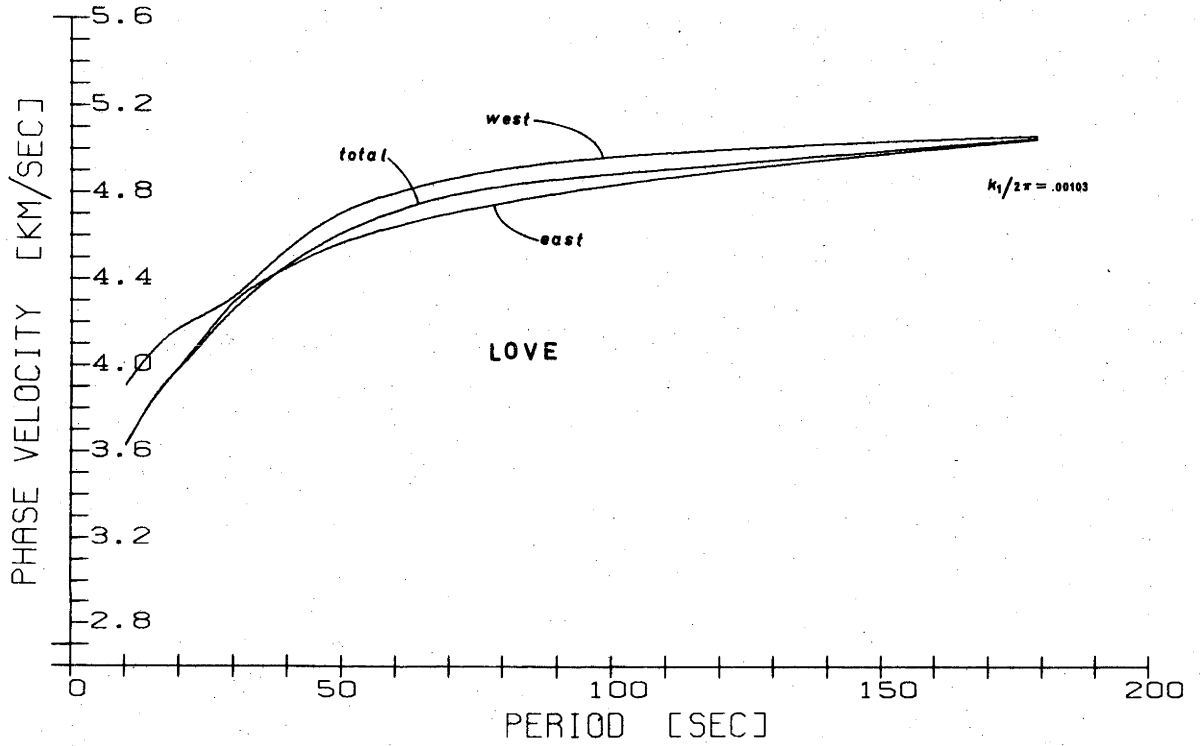


Figure 4.45: Love wave phase velocity for 'West', 'East' and 'Total' Australia obtained by integrating group velocity. This information is not reliable, see text Section 4.7 for explanation.

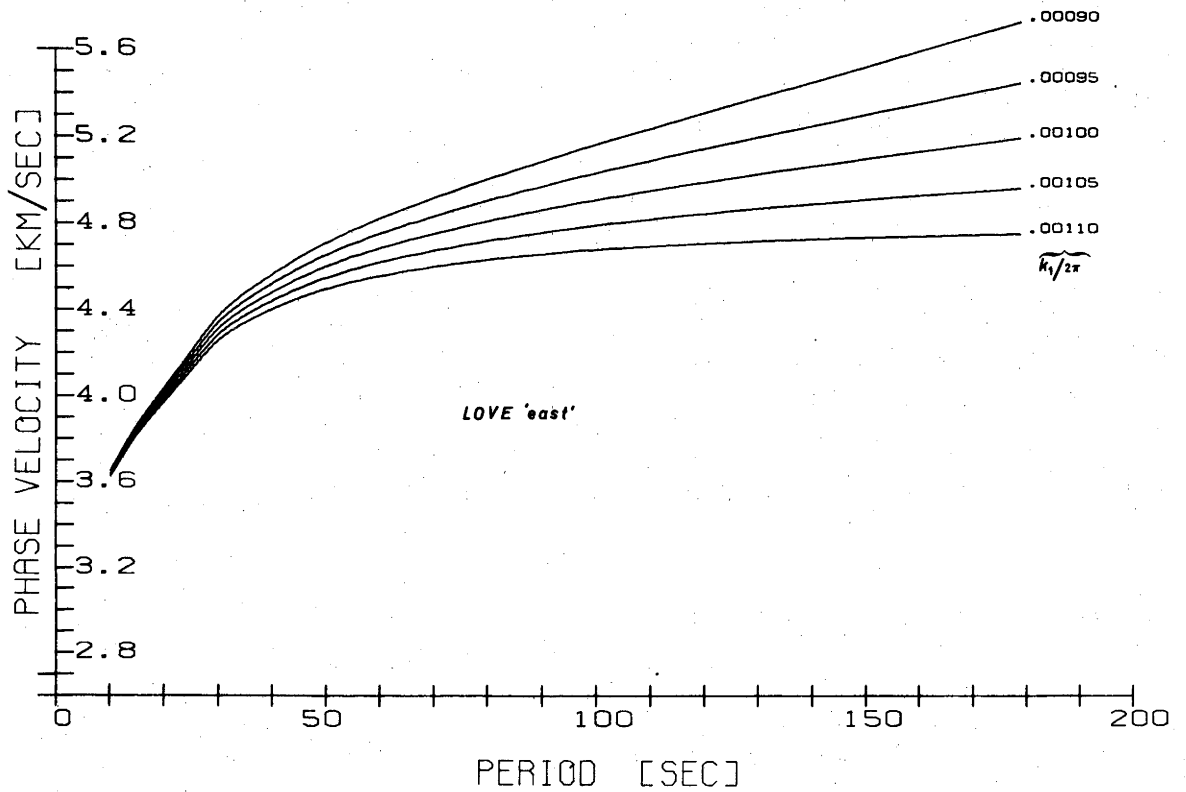


Figure 4.46: Obtaining phase velocity by integrating the Love group velocity curve 'East'. Wave number at 183 s is not known accurately. This family of curves was to be visually fitted to Figure 4.44, but were found to be unreliable because of higher mode interference.

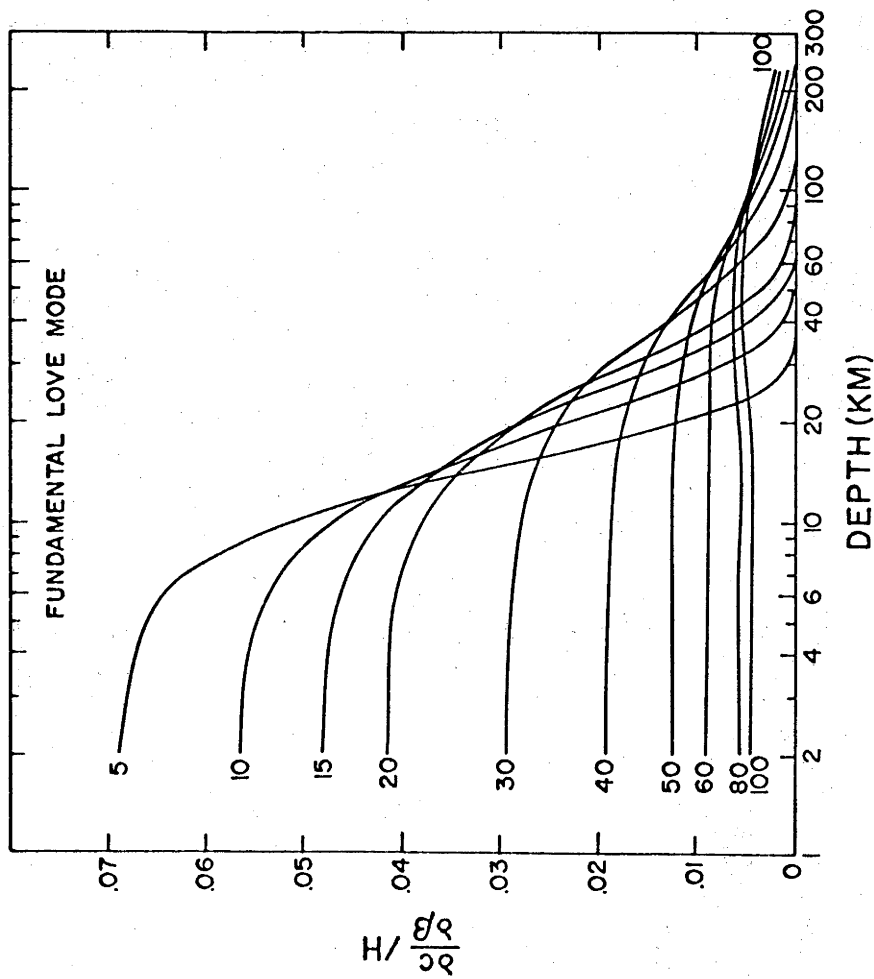
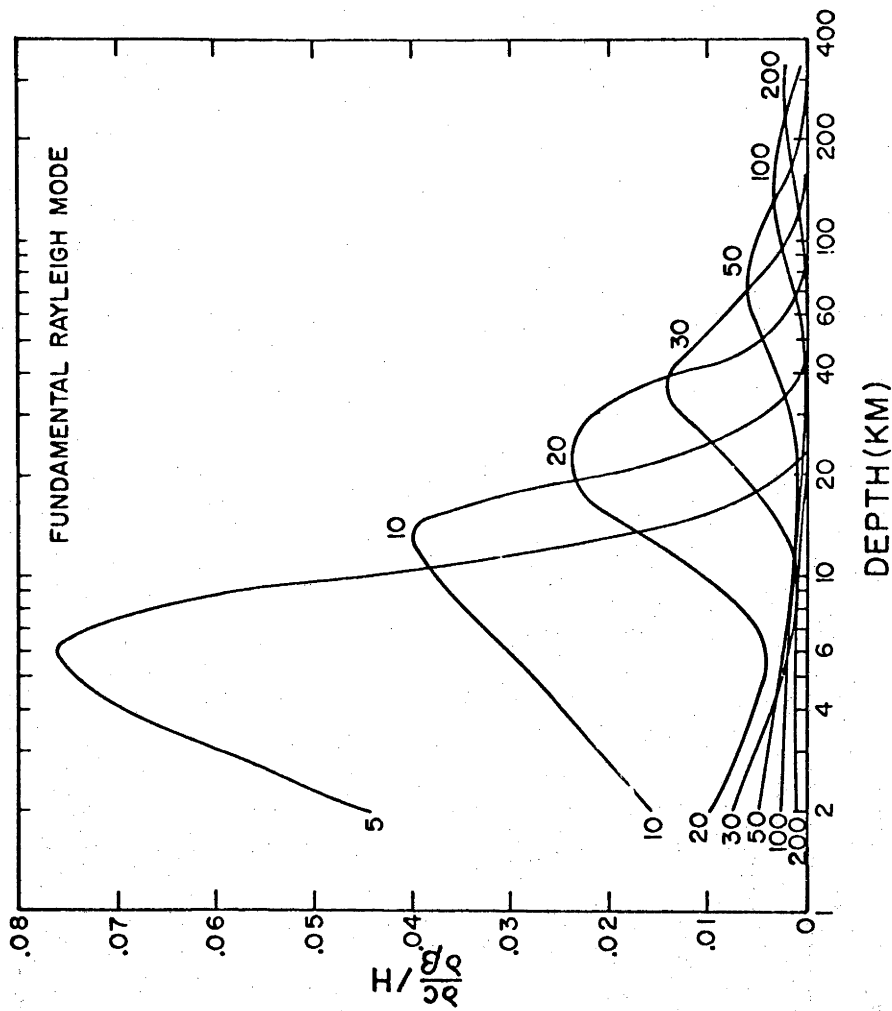


Figure 4.47: Fundamental mode Rayleigh and Love wave partial derivatives with respect to shear velocity, from Bloch [1969].

CHAPTER 5

INVERSION

This chapter describes the Monte Carlo inversion (MCI) program developed to invert the observed surface wave information for Australia presented in the preceding chapter, and the results obtained from the inversion of the data. A Fortran program TEQUILA was used to compute the dispersion characteristics of Earth models. Program TEQUILA, written by Dr R. Massé and amended later by James Fix, is based on papers by Haskell [1953], Dorman [1962], Rosenbaum [1964], Dunkin [1965] and Biswas *et al.* [1970].

5.1 THE WORKING MODEL

A working model with the least number of layers needed to satisfy the data is optimal for an inversion study, for a number of reasons. Firstly, the computational efficiency of the inversion program is much better. It was observed that the CPU (Central Processing Unit) time required by Program TEQUILA was proportional to the number of discrete periods at which dispersion was computed and, more importantly, was approximately proportional to the square of the number of layers in the model. (These observations were deduced from five- and seven-layer models.) Since MCI requires the computation of dispersion for a very large number of models, it is obviously desirable to formulate the task in terms that will minimize the CPU time needed for each execution. Secondly, if it can be shown that a particular number of layers is sufficient to fit the observed data within some given accuracy bounds, then there is no further information to be gained by increasing the number of layers in the model. Indeed, an increase in the number of layers will almost certainly produce models which fit the data but which must be rejected because oscillations in shear velocity from layer to layer are geophysically unacceptable.

Investigating the uniqueness of upper mantle models upon inversion of 'pure path' dispersion data in the 150 to 325 s period range, Dziewonski [1971] concluded that

'the distribution of shear velocity in the first 400 km may be adequately described by a set of four values, the first of which is fixed and corresponds to the crust. The remaining three correspond to the lid, the low velocity channel, and the layer from the bottom of the low velocity channel to the 400-km discontinuity. The density distribution between the crust-mantle boundary and the 400-km discontinuity can be described by one average value, which is not unique because of its interaction with shear velocities between 400 and 650 km (Dziewonski, 1970a)'.

Inclusion of shorter period information will permit more resolution in the crust, but Der *et al.* [1970] showed that not more than three layers are warranted in the crust if only fundamental modes are inverted. Their conclusions were based on the inversion of dispersion information from 5 to 80 s period range. Since the present study commences at 10 s, it was assumed that a two-layer crust would be sufficient. These considerations dictated a working model with five layers above a half-space.

The primary objective of the inversion was to investigate the structure in the upper mantle, particularly the characteristics of the upper mantle low velocity layer and the variations in these characteristics implied by the differences in the dispersion curves for eastern and western Australia. For this, the amount of variability in the crust was restricted, especially since body wave studies of the crust have shown no significant differences between these two regions [cf. Cleary, 1973]. Two layers, each 20 km thick, were taken to comprise the crust, thus fixing the Moho at 40 km [Cleary, 1973]. The shear velocity in the first layer was fixed at 3.6 km/s (cf. values of 3.55 ± 0.04 km/s by Bolt *et al.* [1958] and 3.59 ± 0.01 km/s by Doyle and Everingham [1964], for regions within the shield, and one of 3.62 ± 0.03 km/s found in southeastern Australia by Doyle *et al.* [1959]).

In the second layer the velocity was allowed to vary from 3.6 to 3.85 km/s. The next layer, the lid, commenced at 40 km. Its lower boundary was permitted to range from 50 to 150 km, thus allowing a lid thickness ranging from 10 to 110 km. In the lid thus defined, the allowable range of V_S was 3.8 to 4.9 km/s. The depth of the bottom of

the next layer, the potential low velocity layer, was made variable between 160 and 390 km. The model construction therefore permitted a low velocity channel whose thickness could range from 10 to 240 km and whose mid-point could be located between 95 and 270 km. Shear velocity was constrained between 4.0 and 5.1 km/s in this fourth layer and also in the fifth layer, which is the layer between the bottom of the low velocity channel and the 400 km discontinuity. The sixth layer is a half-space commencing at 400 km, with shear velocity allowed to range between 4.8 and 5.5 km/s.

A possible constraint at the 400-km discontinuity would have been to incorporate the suggestions of Liebermann [1973] based on laboratory investigations of the elasticity behaviour of the olivine-spinel and olivine-beta phase transitions. He offers specific recommendations for jumps in shear velocity and density at the 400-km discontinuity, but time did not permit the inclusion of his recommendations into the MCI.

The behaviour of partial derivatives of Rayleigh and Love wave phase velocities gives valuable insight into the relative significance of V_S , V_P and ρ at various depths. Several workers have published information about this behaviour [McEvelly, 1964; Anderson, 1964; and Bloch, 1969]. Transverse Love waves are completely insensitive to variations in V_P . The partial derivatives for both Rayleigh and Love waves with respect to V_S are 5 to 10 times greater than the corresponding partials with respect to density. The partials of Rayleigh wave phase velocity with respect to V_P are smaller than those with respect to density.

In view of these considerations, shear velocity only was inverted. Values for compressional velocity and density were interpolated from Wang's [1972] Earth model. These are shown in Table 5.1.

A pseudo-random number generator was used to generate random models within the bounds described above, and simple computation converted the variable depths into layer thicknesses for input to TEQUILA.

Table 5.1

Layer	Compressional velocity	Density
1	6.30	2.84
2	6.60	3.36
3	7.70	3.37
4	8.35	3.39
5	8.35	3.49
6 (half space)	8.90	3.90

5.2 TESTING PROCEDURE

The computation of Love wave dispersion from a model requires half the CPU time needed to calculate Rayleigh wave dispersion for the same number of period samples. In the interests of computational efficiency, therefore, models were tested first against Love wave criteria, and successful models stored for later testing against Rayleigh wave criteria. The resulting models were then further tested against group velocity data as described below.

The fundamental Love wave phase velocity curve was computed for each randomly-generated model, and standard deviation for the model was computed from the differences at eleven sample points logarithmically spaced between 10 and 150 s period on the mean curve defined by the reference lines shown in Fig. 4.44a. The magnitude of the standard deviation was used to decide whether the model would be discarded at this point, or accepted for further testing against Rayleigh wave phase velocity. In order not to bias the selection of possible models, a relatively large standard deviation of 0.16 km/s for Love phase velocity was used as a 'go, no-go' test.

For models tentatively accepted on the basis of Love wave dispersion characteristics, Rayleigh wave phase velocity curves were computed, and standard deviations were derived using as references the 'EA1' and 'WA1' phase velocity curves (see Fig. 4.29). The test limits were reduced to 0.06 km/s in this case, and feasible models were sorted into 'East' and 'West' files. (Note that in this context 'West'

designates central and western Australia and corresponds approximately to the region west of the limit of exposed Precambrian rocks shown by the dotted line in Fig. 4.19.) There were still a relatively large number of feasible models (about 200 'West' and 60 'East') at this stage.

Program TEQUILA was then used again to compute group velocity according to Eqn (3.18). This computation takes about 4 s CPU time, compared to 2 s in the preceding process, because 30 points on the phase velocity curve had to be computed in order to obtain group velocity. The 'East' set was scanned for models with a group velocity maximum between 40 and 85 s period and with a large value of the second derivative at the maximum. This test was a powerful discriminant in the selection of models characterized by a sharp maximum and a tendency to possess low values of group velocity between 100 and 200 s period. The testing stages just described produced, from an initial 4500 random trials, six models giving the best fit to all the available 'East' information. The six 'East' models are shown in Fig. 5.1 and a comparison of their dispersion with observed Rayleigh and Love wave dispersion is shown in Figs. 5.2 and 5.3. These models are referred to as 'low contrast' models. The 'high contrast' models are discussed in Section 5.3.

The subset of 'West' models was refined by comparison with 'WAl' group velocity. A useful discriminant for this set was found to be the requirement that group velocity at 150 s be less than 4.1 km/s. Many models tended to possess a rather high value for both group and phase velocity at the longer periods. The combination of these 'West' tests netted about 40 models from an initial randomly-generated set of 4000. From these 40, eight were selected by visual inspection as the closest approximation to the 'WAl' group velocity curve. It should be noted that this final set of eight models, as shown in Fig. 5.4, appears biased toward group and phase velocities slightly higher than the observed Rayleigh wave dispersion (see Fig. 5.5), but that the models do encompass the observed dispersion at periods longer than 80 s. The fit of the 'West' models to observed Love wave phase velocities is displayed in Fig. 5.6.

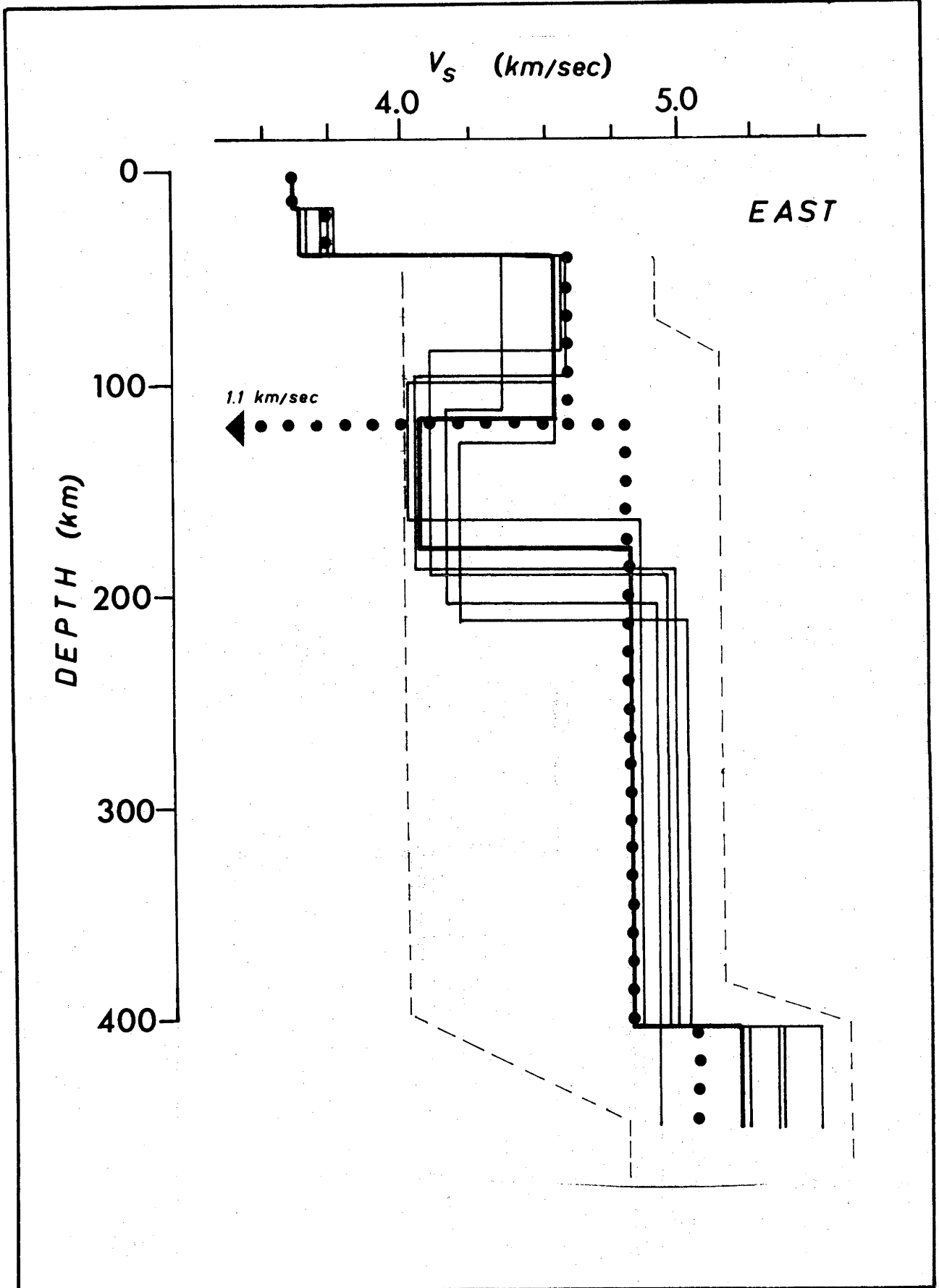


Figure 5.1: 'East' upper mantle models found by Monte Carlo inversion showing a well-defined low velocity layer for eastern Australia.

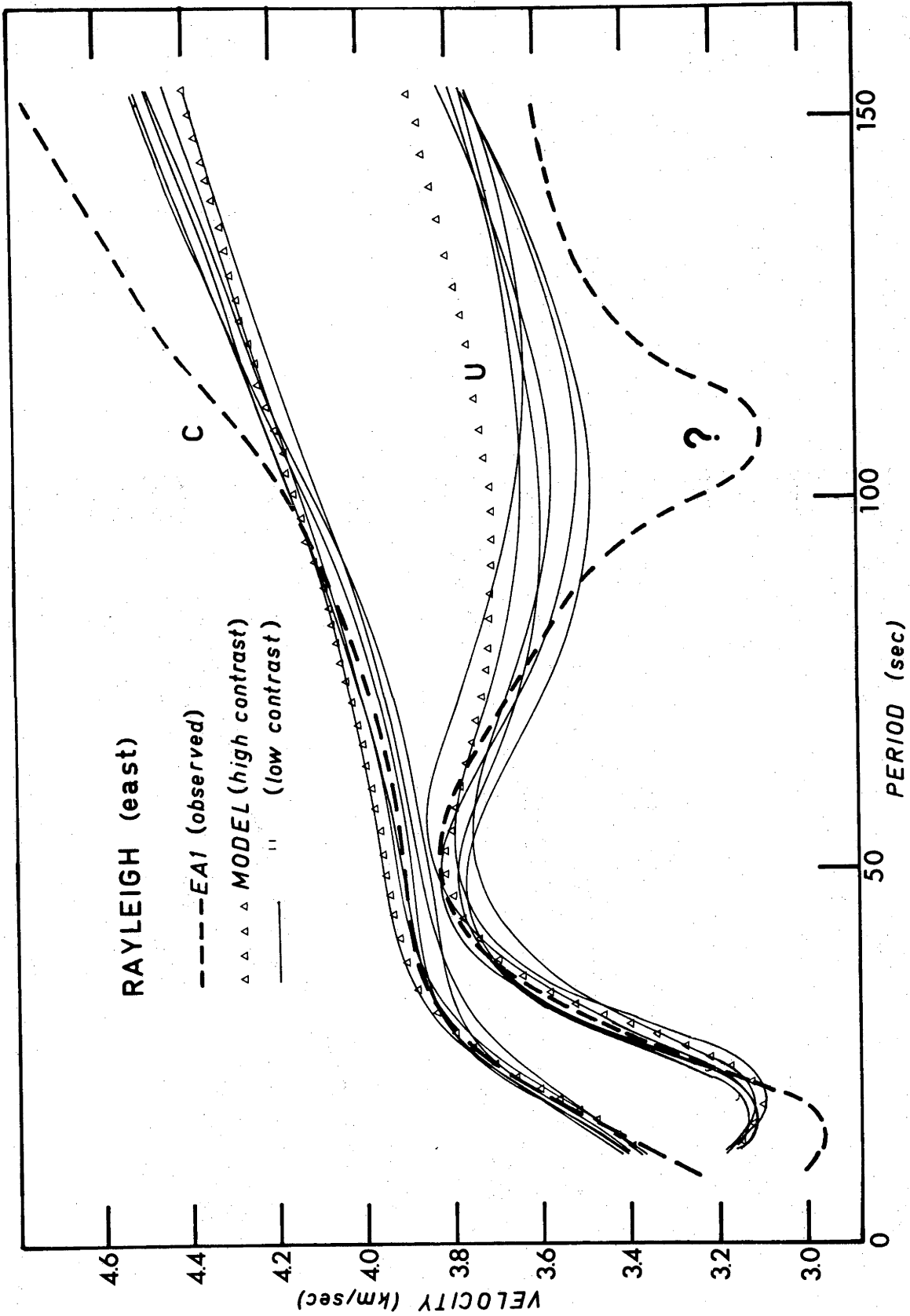


Figure 5.2: Comparison of the calculated dispersion of 'East' models with observed Rayleigh wave dispersion.

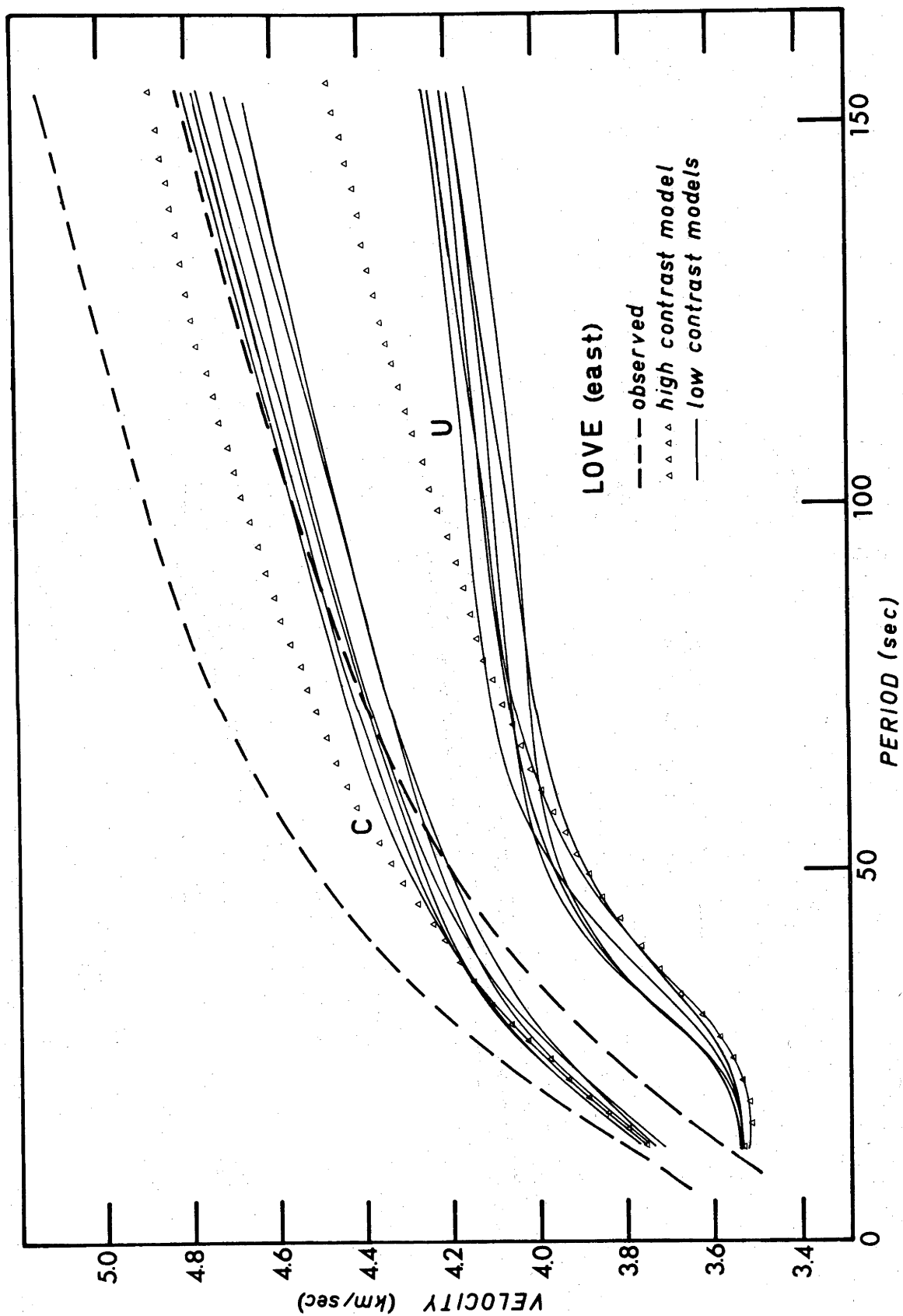


Figure 5.3: Comparison of the calculated dispersion of 'East' models with observed Love wave dispersion.

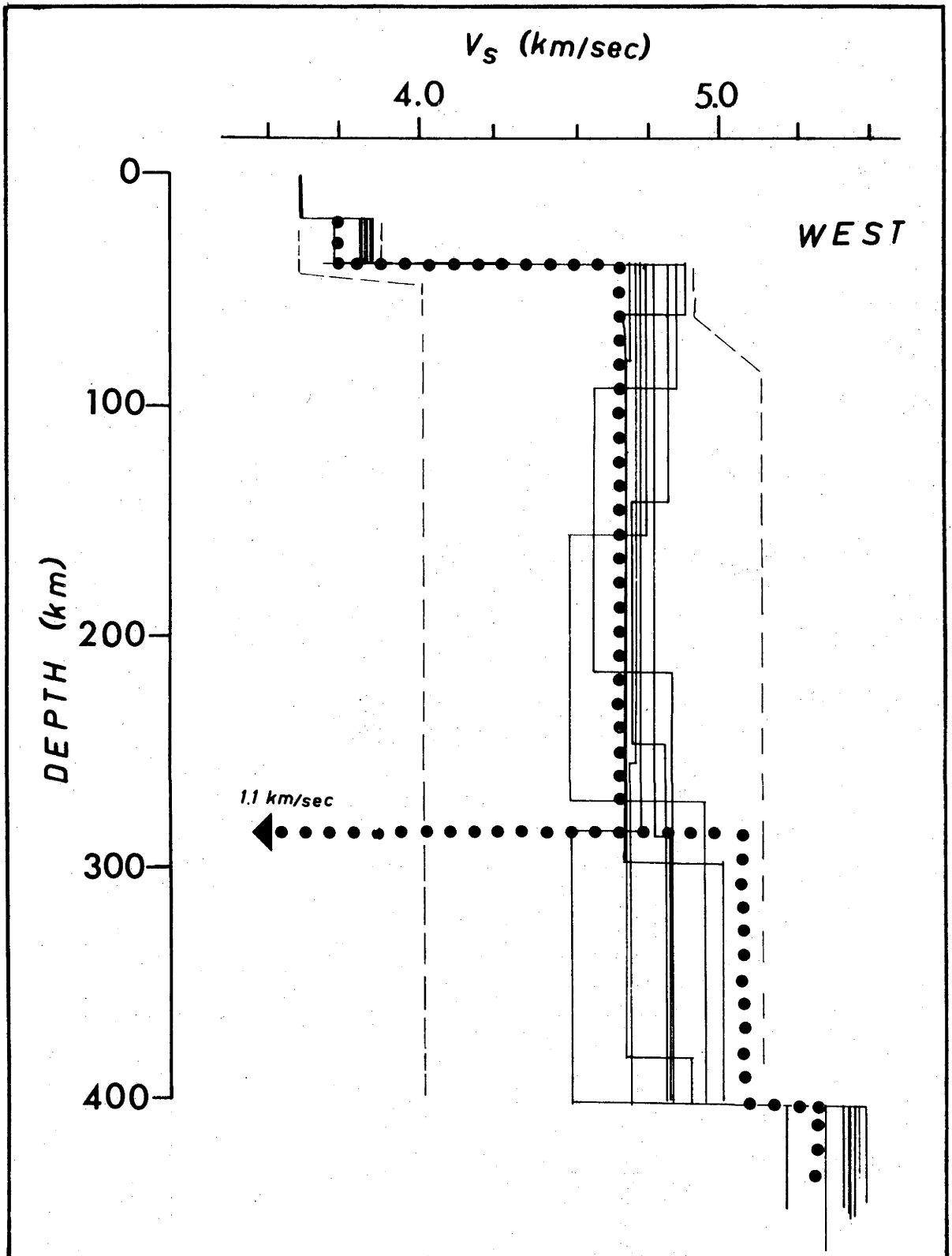


Figure 5.4: 'West' upper mantle models for western Australia found by Monte Carlo inversion. Note absence of well-defined low velocity layer.

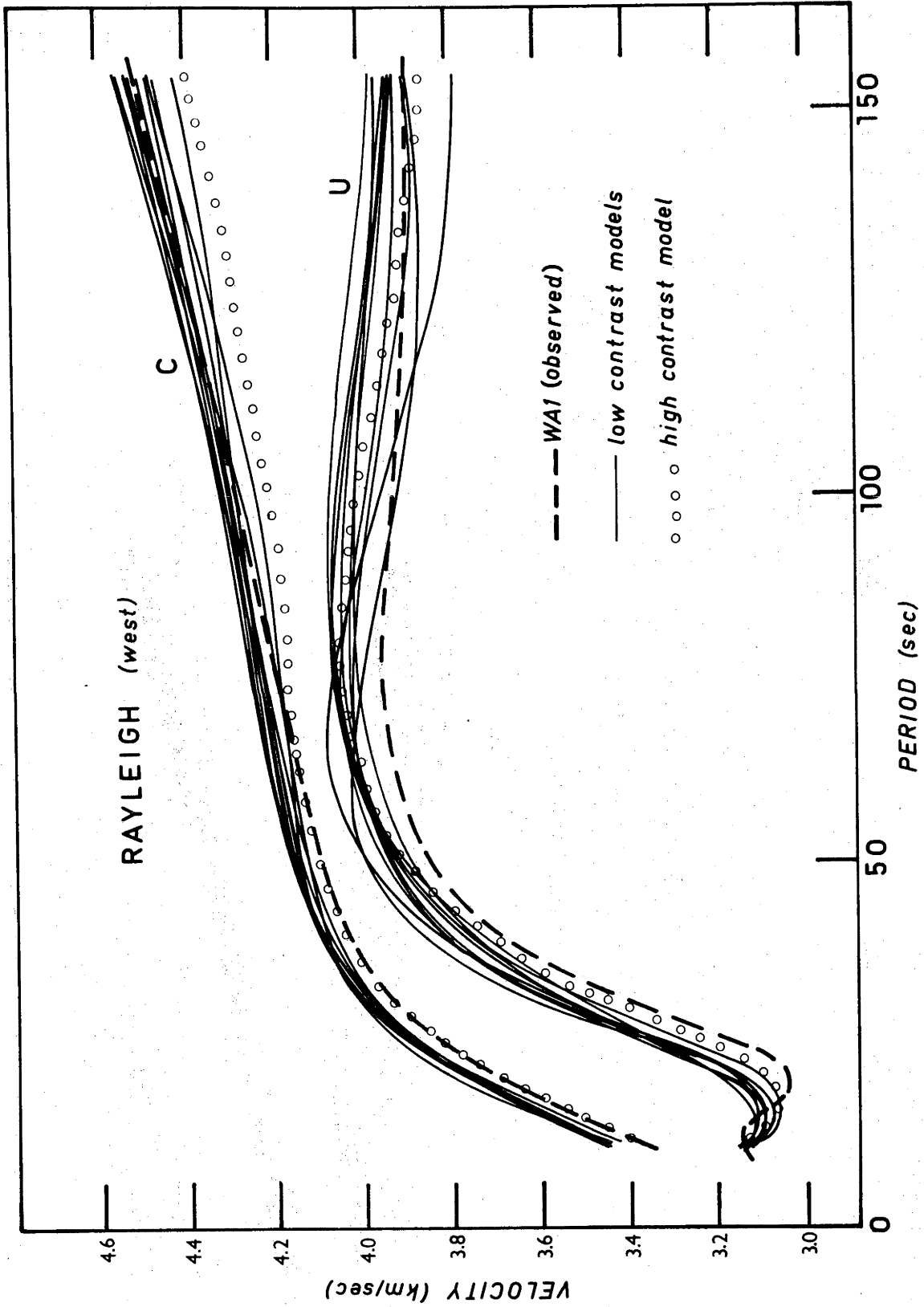


Figure 5.5: Comparison of the calculated dispersion of 'West' models with observed Rayleigh wave dispersion.

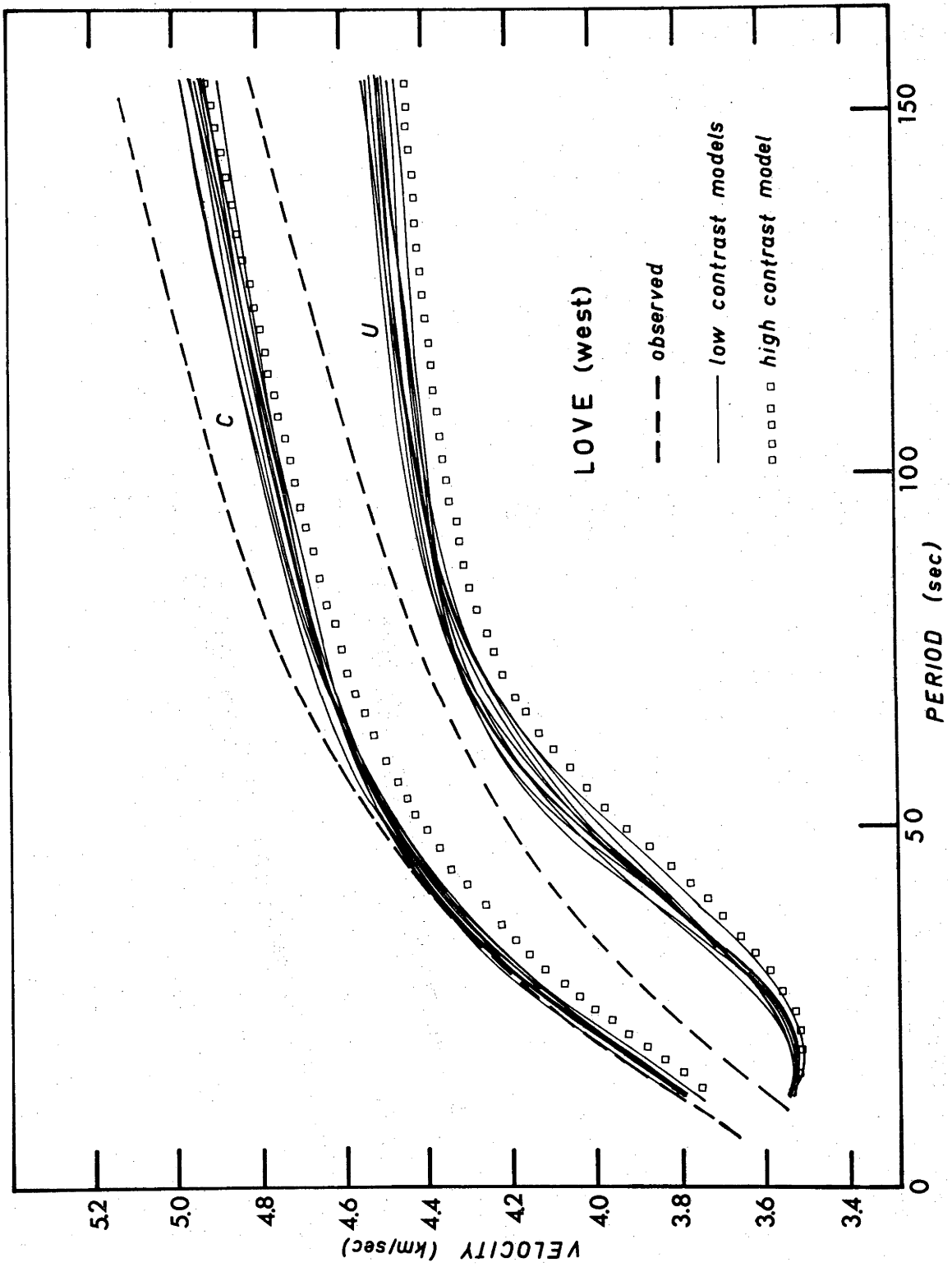


Figure 5.6: Comparison of the calculated dispersion of 'West' models with observed Love wave dispersion.

5.3 HIGH CONTRAST MODELS

In agreement with results obtained earlier by Aki [1968], Bloch, Hales and Landisman [1969] found that inclusion of a 'high contrast' thin layer enabled a better fit of Earth models to the surface wave dispersion observed in Africa. In a later paper, Hales and Bloch [1969] reviewed the evidence indicating that the low velocity layers might be thin throughout the Earth's upper mantle, suggesting a thickness of 0.5 to 2.0 km with shear velocity of the order of 0.55 to 1.1 km/s in the layer. They pointed out that a high contrast model giving the same Rayleigh wave dispersion as a low contrast model will not exhibit the same Love wave dispersion. If the dispersion in the real Earth is caused by a thin low velocity channel, it will not be possible to fit observed data for both Rayleigh and Love waves by a model having a single thick low contrast low velocity layer. This is just what has been observed in Japan [Aki, 1968] and the central United States [McEvelly, 1964] and, as is seen in Section 6.4, in Australia by the present author.

Time permitted only a brief investigation of this interesting question. The working model was recast so that the fourth layer (the low velocity layer) was 2.0 km thick with a shear velocity of 1.1 km/s. (These rather arbitrary values were suggested by the Hales and Bloch [1969] paper.) The position of the layer was allowed to range between a depth of 50 km and a depth of 390 km, and an MCI run of 3500 random models was initiated. The other model parameters and their ranges were as stated in Section 5.2. Using the same testing procedure as before, three possible models were found for the 'East' subset. The high contrast LVC in these models was at depths of 119, 132 and 156 km; that is, not surprisingly, they appeared close to the center of gravity of the LVC of the low contrast models. One model, with the high contrast layer at 119 km, was selected on the basis of a slightly larger value of the second derivative at the group velocity maximum, and is included in Fig. 5.2. Note that, except for marginally higher group velocity between 100 and 150 s, this model has the same Rayleigh wave dispersion as the low contrast models.

As is evident from Fig. 5.3, however, the Love wave dispersion of the high contrast 'East' model differs considerably from that of the low contrast models. Whilst it remains essentially identical with the latter at periods from 10 to 40 s, the high contrast model exhibits higher

values of fundamental Love wave phase velocity at longer periods, and for this reason fits the observed Love wave dispersion much better. In the problem of fitting both Love and Rayleigh wave dispersion, the observed Love wave phase velocities are always higher than those calculated from models that fit the Rayleigh wave dispersion curve. Anisotropy in shear wave velocity has been postulated to explain the discrepancy, but it appears that a thin high contrast layer accomplishes the same effect.

Returning now to the tentative set of 'West' high contrast models, it was observed that the thin high contrast layer always appeared at depths below 200 km in the 22 models remaining at this stage. As these models exhibited rather similar dispersion characteristics, one sample, displayed in Fig. 5.4, has been selected for comparison with the low contrast models. The selection was based on a slightly better fit to observed 'West' Rayleigh wave phase velocity from 10 to 80 s, although the fit at periods longer than this suffers a marginal degradation. Overall, the Rayleigh wave group velocities for the high contrast models were very similar to those of the low contrast models.

The fit of the high contrast 'West' model to the observed Love wave dispersion was considerably improved in a manner similar to that observed for the 'East' group. The 'West' high contrast model gives somewhat lower Love wave phase velocities from 10 to 100 s than shown by the low contrast models. Here again, the inclusion of a high contrast LVC permits a better simultaneous fit to both Love and Rayleigh wave observed dispersion than is possible with six-layer low contrast models.

5.4 HIGHER LOVE MODES

It was of interest to use Program TEQUILA to compute the higher Love modes for the 'East' and 'West' models, and to compare the predictions of the models with the observed group velocities shown on the FTAN diagrams in Figs. 4.40 and 4.41. The fundamental and first higher Love modes for the model indicated by the heaviest line in Fig. 5.1 were computed and superimposed on the 'East' FTAN group velocity diagram in Fig. 4.41. This comparison emphasizes the mode interference problem for Love waves reported by Thatcher and Brune [1969], although it is not clear that this is the only problem. There is a suggestion that the first higher mode is almost resolved by FTAN in the 10 - 25 s period range. This is perhaps more strongly suggested in the 'West' group velocity FTAN

diagram, Fig. 4.40. In both diagrams, in the period range 40 to 200 s the observed ridge crest lies between the two modes, suggesting that their spectral excitation ratio is of the order of unity in this period range. (Harkrider [1970] gives theoretical spectral ratios and this value is plausible.) In the 'West' diagram there is a marked discrepancy between the observed ridge crest and the fundamental Love mode of this model in the 18 - 35 s period range. Considerable speculation could be advanced concerning the reason for this discrepancy but the safest comment may be that it needs further investigation.

It was found impossible to use program TEQUILA to compute the second higher Love mode for the 'West' models. Furthermore, none of the higher modes for the high contrast models could be computed with this program. Time did not permit a thorough investigation of this difficulty. Suspecting that a small number of layers may have created computational difficulties, the author tried computation with a 20-layer model (maintaining the same shear velocity profile), but this failed also.

The first higher Rayleigh mode lies well above and outside the range of group velocities shown in these FTAN diagrams. The second higher mode for some 'West' models contained a branch that had values for group velocity of about 4.2 km/s at 20 s period. Although there is no information about the spectral excitation of the second higher mode, perhaps it is responsible for the energy plateau that persistently appeared near this region on some FTAN diagrams (cf. results for CTA-ADE path, Figs. 4.1 to 4.6).

5.5 CONCLUSIONS

The incorporation of Rayleigh wave group velocity as a constraint in MCI markedly reduced the non-uniqueness bounds of possible models that fit the 'East' Australia observed data. Although the pronounced 'dip' at 110 s must remain questionable, it was found that the characteristics of the LVC in the 'East' models shown in Fig. 5.1 were well constrained by the requirement only that they exhibit a sharp maximum in group velocity between 40 and 85 s. In this period range the observed data are much more reliable. The LVC in eastern Australia appears to begin at about 90 km and to terminate at about 200 km. Inverting a similar profile (but using phase velocity only), Knopoff

[1972] found that the LVC in 'aseismic' areas commenced at about 100 km, but its bottom was poorly defined.

The 'East' models fit the observed data well except, as can be seen in Fig. 5.2, the group velocity at periods between 10 and 20 s. The calculated dispersion matches the Rayleigh wave group velocity curve at its maximum reasonably well, but it was found impossible, using six-layer models, to duplicate the pronounced 110 s 'dip' in group velocity. At 150 s, however, the calculated group velocity has a value consistent with the values obtained from analysis of world-circling waves. Since the Rayleigh wave phase velocity curve is derived from group velocity it shows similar fitting difficulties. The discrepancy at short periods suggests that a three-layer crust might be needed in the model. More sophisticated modelling techniques are probably required to improve the fit at long periods.

It can be concluded that group velocity is a more sensitive test of possible upper mantle structures than is phase velocity, and it follows that further advance of our knowledge of upper mantle structure is critically dependent on more numerous and more accurate group velocity measurements.

The measurements must extend to beyond 200 s if the upper mantle is to be well-defined down to the 400-km discontinuity. A simple experiment showed that the group velocity curve from its maximum to 150 s, computed from a six-layer model, was not independent of the value of V_S in the half space.

The 'West' Australia models show a minor fitting problem in the period range from 10 to 80 s. Both the Rayleigh wave phase and group velocities shown by all models are consistently higher than the observed data by about 0.04 km/s. Perhaps this, too suggests that a three-layer crust is called for, or it may be that the model values of V_P and density should be adjusted in the upper 100 km. Higher mode Rayleigh wave information would help to resolve this point.

It has been shown that models with a thin high contrast layer with shear velocity appropriate to an almost-liquid state fit both Love and Rayleigh wave observations better than low contrast models. This is true for the shield area in central and western Australia, although it is more pronounced in eastern Australia. Fig. 5.3 shows that Love wave

phase velocities for the low contrast 'East' models fall outside the reference lines at periods longer than 100 s. The adjustment of a thin high contrast layer does not seem to be as necessary for the 'West' models, as has been found for the Canadian Shield by Brune and Dorman [1963]. Note, however, that a later inversion of CANSD data by Massé [1973] increased the discrepancy between the observed and calculated Love wave dispersion, suggesting the same type of Love wave fitting problem as observed here in the Australian Shield.

The clear indication of a low velocity layer in eastern Australia and the absence of a definite low velocity layer in central and western Australia are discussed in detail in the next chapter.

CHAPTER 6

DISCUSSION OF RESULTS

The present study has shown that it is possible, using ordinary seismograms, to extend the period range of surface wave observation and analysis to almost 200 s, and thereby bridge the gap that has existed between studies of dispersion of world-circling waves on the one hand, and of dispersion across geographical regions of limited extent on the other. Summation of cross-correlations, using the two-station method, succeeds in this because it provides a means of enhancing the weak long period spectrum, while at the same time signal-associated noise can be randomized by averaging an ensemble of events with differing epicentral distances.

The study has shown that the continent of Australia comprises at least two regions with distinctly different upper mantle structures. The 'West' region shows small variations in shear velocity down to 400 km while the 'East' region gives positive indication of a pronounced LVC between depths of about 100 and 200 km. The two regions thus differentiated are also geologically distinguishable in that the former is a shield area containing exposed rocks of Precambrian age, while the latter is apparently Palaeozoic in age and has been subject to moderate uplift on a number of occasions, including the period from the late Tertiary to the present [cf. David, 1950, p.642].

Comparison of Figs. 5.1 and 5.4 of this work with Figs. 9 and 8, respectively, of Knopoff [1972] (reproduced here in Fig. 6.1), makes it clear that a close similarity in upper mantle structure exists between the shield regions of the United States and Australia, and between the 'continental-tectonic' (or, in Knopoff's terminology, 'aseismic platform') regions of the western United States and eastern Australia. This finding parallels the agreement between values of travel-time anomalies found for these two types of regions in each continent [cf. Cleary and Hales, 1966; Cleary, 1967; and the discussion in the following section].

Using a different method of decomposing the world-circling path, Kanamori [1970] obtained 'pure path' group and phase velocities for both Rayleigh and Love waves, as well as an estimate of attenuation in the upper mantle. He too found phase velocities for tectonically active areas to be significantly lower than those for ocean and shield. Dziewonski [1970b] obtained 'pure path' phase and group velocities which differed significantly from Kanamori. He corrected the equation for averaging phase velocities used by Kanamori, and avoided the use of different path compositions for phase and group velocity measurements by obtaining both from the auto-correlogram of the digitized signal. Errors associated with the epicentral location, origin time, instrumental response and initial phase shift were also avoided. In deriving upper mantle models from 'pure path' data Dziewonski [1971] points out that there are

'... significant differences between dispersion curves for oceanic and shield areas, whereas Kanamori reported that these differences were not statistically meaningful. Also, the 'tectonic' phase velocities of Dziewonski (1970b) are not consistently lower than the shield or oceanic values ...'

Shield models and tectonic models from the above three works are shown in Figs. 6.2 and 6.3 respectively, with an example of one of the Monte Carlo models for each region from the present study. The general characteristics of the models agree but there are differences in their details. Shear velocity in the lid in shield areas is higher than in tectonic areas, although Dziewonski's values for the two regions are systematically lower than those of the others. Shield areas are characterized by little or no low velocity zone. If one is indicated, it is spread over a large depth range.

In the tectonic models the lid velocity is significantly lower than it is in the shield models. Tectonic models are characterized by a rather shallow low velocity zone with a pronounced velocity contrast. Both Dziewonski's and the present results favor a shallower, higher contrast LVC than those of Kanamori and Toksöz *et al.*

Alexander and Sherburne [1973] have recently studied the shield area of South America using Rayleigh and Love wave phase and group velocity dispersion measurements. They remark on the close similarity of all shield areas down to depths of about 400 km, and comment that the lateral movement of shields must involve a much greater thickness of lithosphere than that proposed for oceanic plate segments.

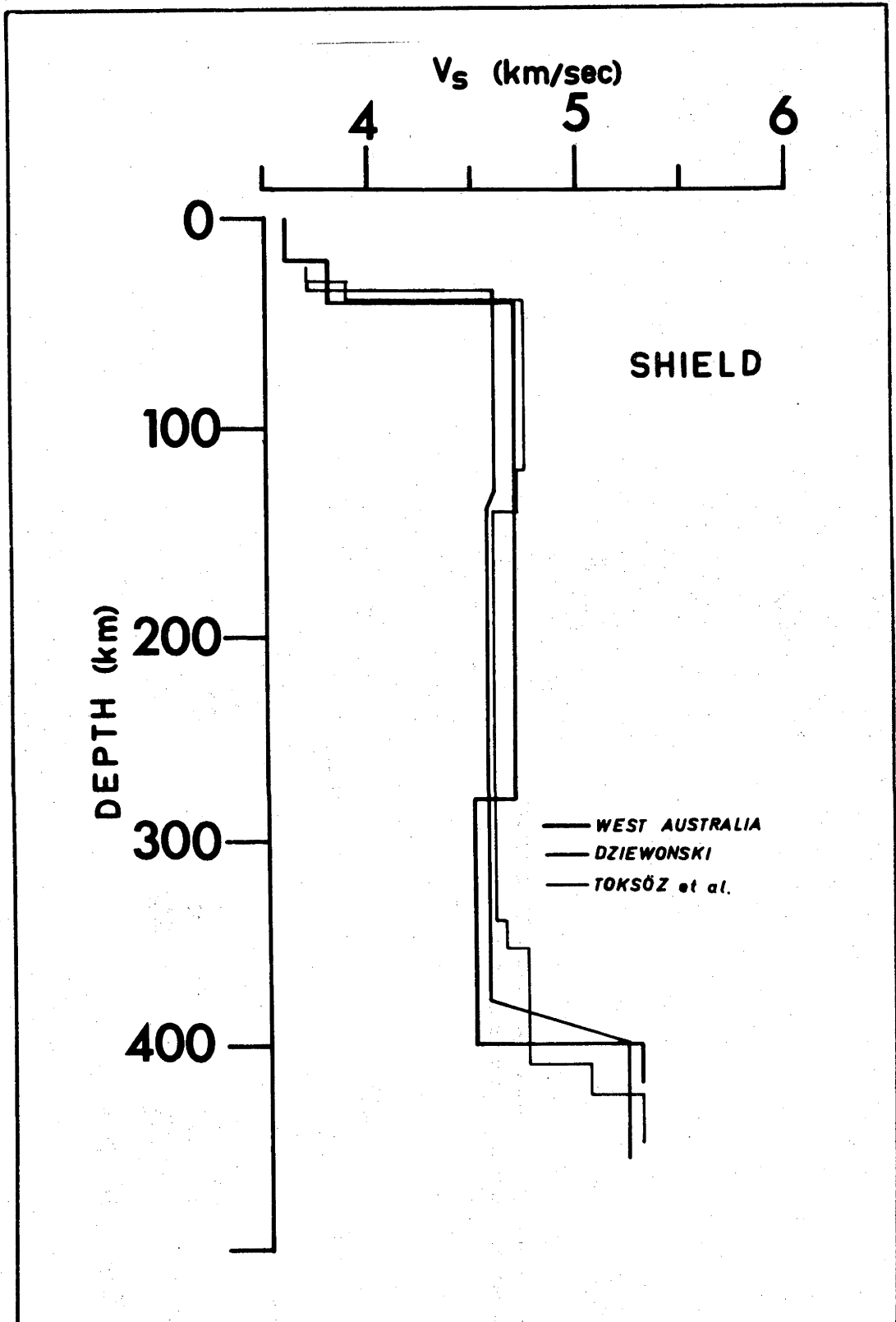


Figure 6.2: Comparison of 'West' Australia model with other shield models.

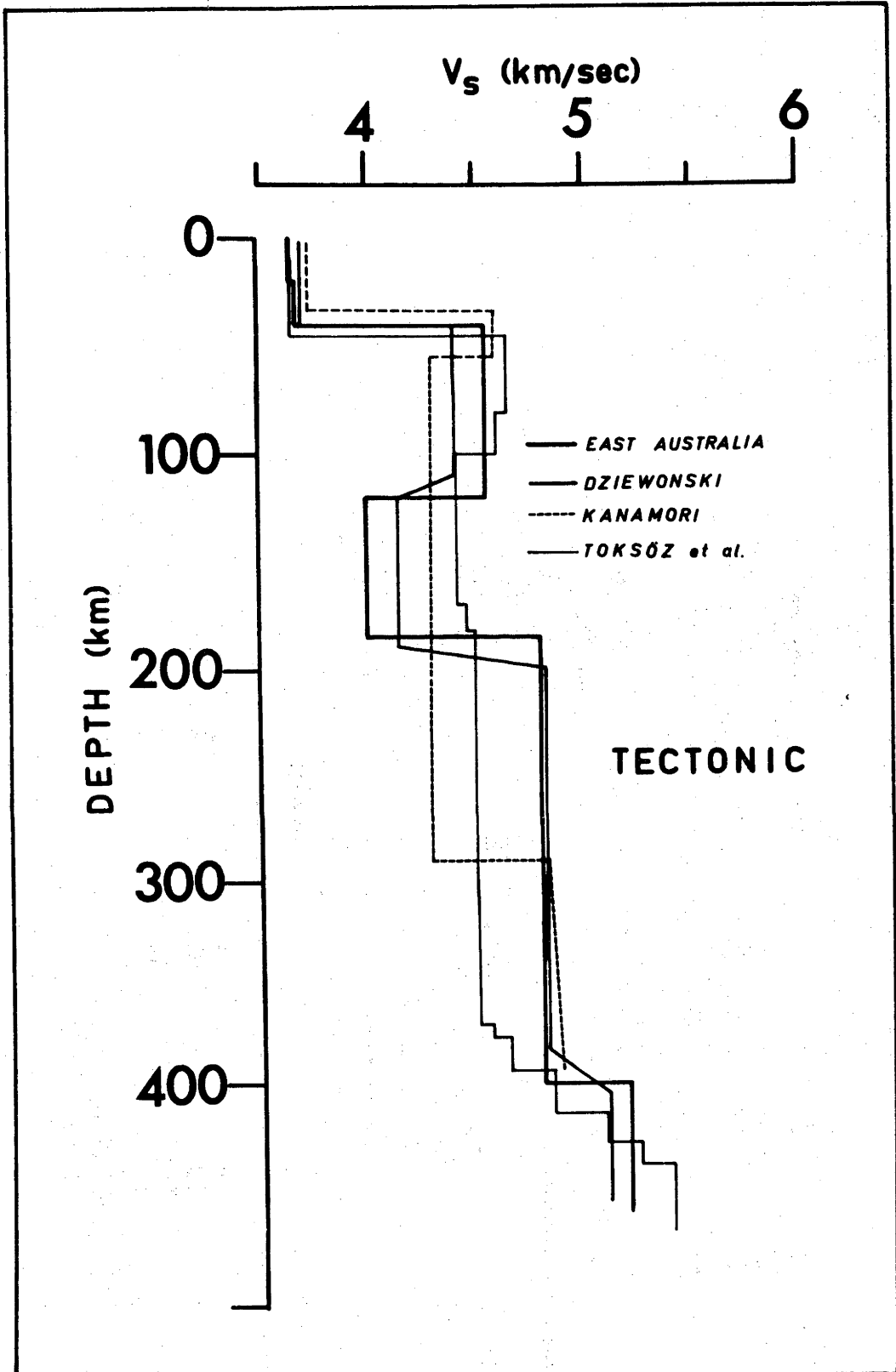


Figure 6.3: Comparison of 'East' Australia model with other tectonic models.

Thus, the general picture is similar for most studies, but the present results tend to show a better overall agreement with Knopoff's results (Fig. 6.1), in which direct observations of surface waves, rather than decomposed world-circling waves, are used. The thinner LVC in the 'East' Australia models, compared with Knopoff's 'aseismic' models, results from the use of the pronounced maximum in Rayleigh wave group velocity near 70 s, which had the effect of eliminating models like those of Knopoff.

6.2 COMPARISON WITH AUSTRALIAN BODY WAVE STUDIES

S_n

For the shield region, Bolt *et al.* [1958] derived an S_n value of 4.75 ± 0.01 km/s, which is in conformity with the range 4.75 - 4.9 km/s for the sub-Moho velocity given by the Monte Carlo models for 'West' Australia. S_n is well recorded in the shield, suggesting a positive S gradient in the upper mantle. From large explosions at the Ord River damsite in northwest Australia in 1970 and 1971, Denham *et al.* [1972] recorded S arrivals out to 19.5° on short period vertical instruments. From these data, Simpson [1973] tentatively suggested that an apparent break in the travel time curve at about 8° might be due to the presence of a low velocity zone, but the data did not justify the construction of a model.

In southeast Australia arrivals are weak or absent [Doyle *et al.*, 1959; Cleary and Doyle, 1962; Doyle *et al.*, 1966], suggesting a zero or negative V_S gradient immediately beneath the Moho. Using five weak S_n arrivals in southeast Australia from the 1961 Robertson earthquake, Cleary and Doyle formally derived a value of 4.7 ± 0.2 km/s for S_n . This value is higher than the range 4.45 - 4.55 km/s given by the Monte Carlo models for 'East' Australia, but the uncertainty limits of the two results overlap. Of the five observations, one has a large (3.6 s) residual. If this reading is excluded, the remaining observations give an S_n velocity of 4.6 ± 0.1 km/s, in better agreement with the present results. The Robertson data indicate that S_n disappears at some distance between 10° and 15° , which suggests that the critical negative velocity gradient (at which downgoing rays cease to be refracted back to the surface) is exceeded at a depth between 60 and 90 km.

P_n

Cleary [1973] has summarized P_n results from several studies in Australia. He found that the data in southeast Australia were compatible with the P_n value of 7.84 km/s from a reversed profile by Doyle *et al.* [1966] in the area, and observed a tendency for a systematic increase in P_n in a westerly direction across the shield region, with an 'average' value of about 8.2 km/s. Such a result is in conformity with the finding of this study that the S velocity beneath the Moho is of the order of 0.2 km/s lower in 'East' Australia than it is in the 'West' region.

From a study of P times from Australian earthquakes, Sutton and White [1966] found evidence of a low velocity layer in southeast Australia, commencing at a depth of 62 km. Their 'flat Earth' model consisted of a 32 km crust with $P_1 = 6.03$ km/s, underlain by a 30 km layer with $P_n = 8.21$ km/s, and with $V_p = 7.95$ km/s beneath. The model needs revision in the light of Cleary's [1973] summary, but the evidence for a lower velocity layer for P in the region is probably valid. The value for the depth of the commencement of the LVC is in approximate agreement with that suggested by the S_n observations in southeast Australia. Although low velocity layers in the models in Fig. 5.1 commence at somewhat greater depths than this, the results are not necessarily in conflict, because the modelling was restricted to the production of discontinuous layers rather than smoothly varying profiles.

White [1971] analysed travel times from earthquakes across the Australian Shield, and derived a model in which the P velocity decreases from 8.43 km/s at 200 km depth to 8.29 km/s at 300 km, rising again to 8.93 km/s at 380 km. He observes rightly that 'this layer is deeper and much less pronounced than [the Sutton and White] low-velocity layer ... for southeastern Australia'. That such a model is not inconsistent with the results of the present study can be seen from Fig. 5.4, where models with deep but weakly developed LVCs appear as valid solutions. Simpson [1973, p.86] queried White's results on the basis of a study of arrivals at the Warramunga array [Denman *et al.*, 1972], and derived an alternative shield model with no LVC, but with small (approx. 0.1 km/s) discontinuous increases in V_p at 85 km and 175 km. Once again, this does not appear to be inconsistent with the range of shear velocity models shown in Fig. 5.4. The differences observed between the P velocity models in the two regions are thus supported and strengthened by the present study, although the

finer details of upper mantle structure in both regions remain to be established.

Travel Time Anomalies

In North America Cleary and Hales [1966] found that P phases from teleseismic events arrive up to 2 s earlier at stations in shield regions than at stations in continental areas of recent uplift. They showed that this difference must be due largely to differences in upper mantle structure beneath the two types of regions. Doyle and Hales [1967] found a similar result for S waves in the same region. From the observation that the S anomaly is, on average, 3.7 times as great as the P anomaly, Hales and Doyle [1967] concluded that a model in which shear modulus alone varies (the compressibility remaining sensibly constant) fits the data best. They inferred that the difference between P and S anomalies was probably due to partial melting in the LVC in 'continental-tectonic' regions.

In a study of P times to Australian stations from nuclear explosions, Cleary [1967] found differences in P anomalies of up to 2.5 s between the continental-tectonic 'East' region and the shield region to the west. As mentioned in the previous section, this range of differences is similar to that observed by Cleary and Hales [1966] in the U.S.A. In a further study, Cleary *et al.* [1972] deployed portable seismic stations at intervals of approximately 100 km in a line which crossed the eastern boundary of the Australian Shield, and which was orientated at right angles to the direction of the 1971 nuclear explosion CANNIKIN on Amchitka Island. Although there was a relatively high scatter of about 0.4 s between adjacent stations, they found a consistent westward trend towards earlier P arrivals, with a range in station anomalies of about 1.5 s. Following Green and Hales [1968], they interpreted this as a wedging out of the low velocity zone in the upper mantle as the shield boundary is approached. Such an interpretation is consistent with the models in Figs. 5.1 and 5.4.

The S wave travel time for a vertical ray for each of the 'West' models in Fig. 5.4 was computed for the depth range between 400 and 40 km, and the set was found to have an average value of 76.0 s, with a standard deviation of 0.5 s. Similarly, the average S wave travel time for the set of 'East' models was 77.8 s, with an SD of 0.5 s. These

results give a difference in S anomalies of 1.8 s, with an SD of 0.7 s. The difference is in the right sense but the value appears to be quite low. From the data of Cleary [1967] and Cleary *et al.* [1972], it seems reasonable to suggest that the average difference between the P anomalies is about 1.5 s, which, if the results of Hales and Doyle [1967] are valid also in Australia, would correspond to an S anomaly of about 5.5 s. It may be noted here that Knopoff's 'shield' and 'aseismic' models also give a difference of only about 2.0 s in S anomalies. The LVC must, it seems, be even more pronounced than that shown in the models — as indeed is suggested by the group velocity curves of Fig. 4.27.

This point was further investigated by another MCI run in which the *a priori* bounds of the LVC were changed to 1.5 and 3.6 km/s, to test if there were possible models between the high and low contrast sets discussed previously. Seven 'medium contrast' models from an initial 5000 trials were found which fit the 'East' Rayleigh wave phase and group velocity curves in a manner very similar to the low contrast models. Five are shown in Fig. 6.4 (two are omitted because they are almost identical to those shown). A conclusion to be drawn from this additional MCI run is that Rayleigh wave dispersion data can establish only an upper limit to the thickness of the LVC, and not a lower one, since a quasi-continuous set of models can be found in which the thickness of the LVC ranges from 100 km to 2.0 km.

The average S time for the set of medium contrast models is 78.1 s with an SD equal to 0.8 s, which is slightly larger than that of the low contrast models. Taking the longest time in this set, and the shortest from the 'West' set, an S travel time difference of 3.7 s for vertical rays is obtained. This is still not as large as might be expected from the P station anomalies, but it might be interpreted as another indication that the LVC is rather thin and of high contrast.

The above remarks apply to the models where most of the time difference is an effect of the presence of a low velocity channel in the 'East' set of models. In the high contrast models, on the other hand, although the LVC is at very different depths in the two regions, its width and velocity, and therefore its contribution to the vertical S travel time, are the same for both. It can be seen that the S velocity profiles for these differ considerably over the entire 400 km: nevertheless the S travel time anomalies calculated from them differ by

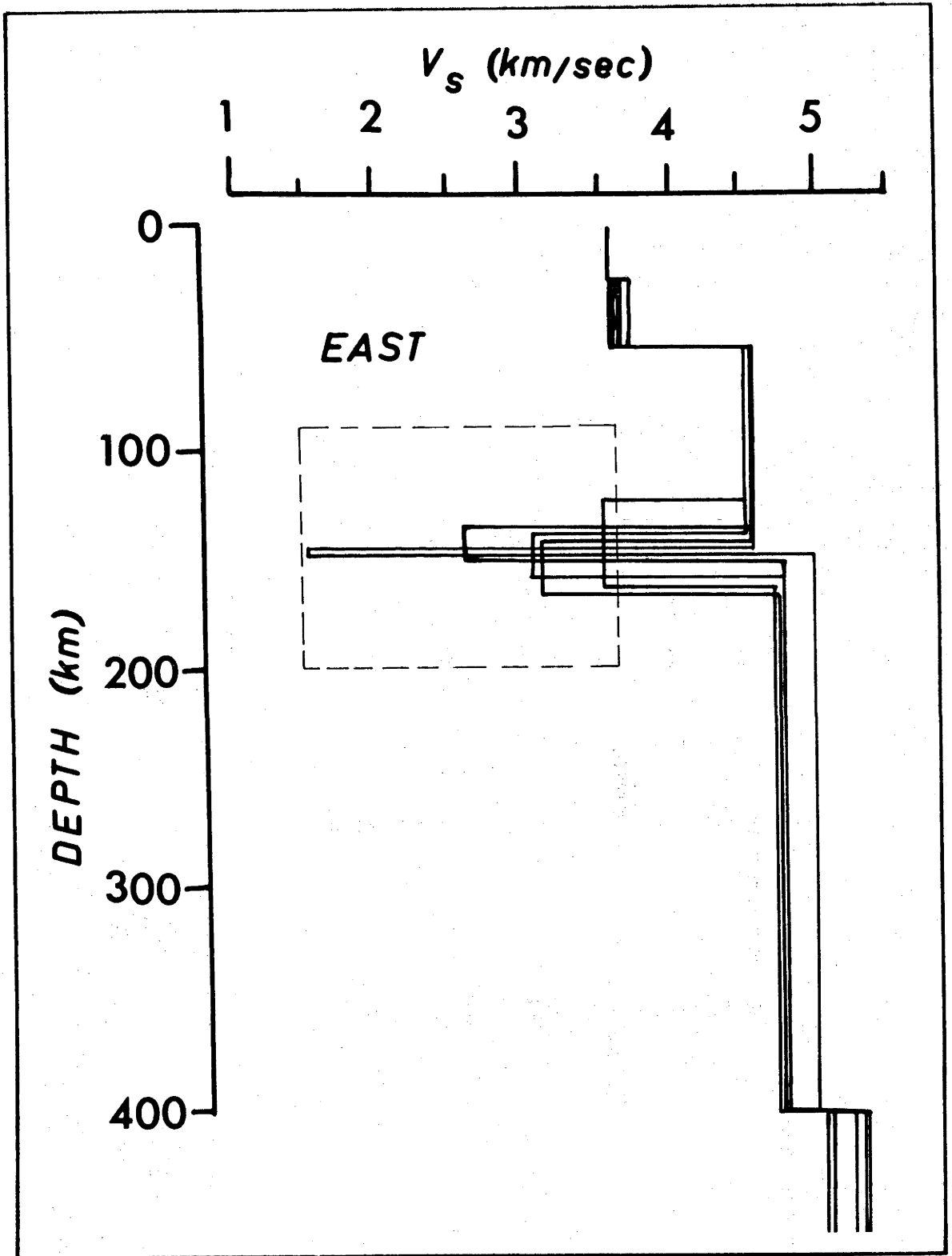


Figure 6.4: More 'East' Monte Carlo models with *a priori* bounds of low velocity layer changed to 1.5 to 3.6 km/s. The LVC in these models is shallower and shows greater shear velocity contrast than those in Fig. 5.1.

only about 1.5 s. In this respect, therefore, they are less satisfactory than the low contrast models. Small variations in the thickness of the LVC would of course produce appreciable changes in the S anomalies. In investigating the effect of the contrast of the LVC on models, it would be desirable to permit the layer thickness to vary and to use the observed values of the S anomaly as an additional constraint. It has been noted earlier that the 'East' high contrast model is more appropriate than its 'West' counterpart. However, the combination of the 'East' high contrast model with the low contrast model in the 'West' set that yields the earliest S time gives a difference in S anomalies of only 1.5 s.

6.3 RELATION TO OTHER AUSTRALIAN GEOPHYSICAL DATA

The verification in this study that the differences between the two parts of the continent persist into the upper mantle confirms that the eastern part of Australia is not simply a buried portion of the shield, but has in all probability a completely independent history. This lends weight to recent theories by Oversby [1971] and others of the accretion of the eastern part of the continent onto the shield, based on the concept of plate tectonics. McElhinny and Embleton [1974] have investigated Australian palaeomagnetic data in the light of this approach, and have pointed out that early palaeozoic pole paths for a region of southeast Australia approach those for northern and central Australia from the opposite direction, and converge with them during the Devonian. They conclude that this result is consistent with the accretion hypothesis — at least for the area from which the palaeomagnetic data were derived — in that it implies a relative rotation of about 120° between the two regions during the Silurian to Devonian period.

Heat flow studies in the Archaean Shield of Western Australia by Howard [reported by Howard and Sass, 1964] were the first to indicate that heat flows in shield areas were less than those in younger areas. In contrast to the value of about 0.9 microcal/sq cm s reported by Howard and Sass for the Archaean Shield, heat flows of about 2.0 microcal/sq cm s have been obtained for the Snowy Mountains region of southeast Australia by Beck [1956], Howard and Sass [1964] and Sass *et al.* [1967]. Ringwood [1962a,b] interpreted the low heat flow observations in terms of a model in which continental crusts evolved through partial melting and

metamorphism, resulting in a strong upward concentration of radioactive elements, which are subsequently removed by erosion of the surface layer to form a shield crust depleted of radioactive heat-producing elements. Ringwood, and also Clark and Ringwood [1964], pointed out that on this interpretation the temperature in the upper mantle beneath shields would be $100^{\circ} - 300^{\circ}$ lower than at the same depth below non-shield areas, and suggested that as a consequence seismic velocities would be higher beneath shields, and that the LVC would be less pronounced or absent. Although these predictions have been confirmed for other continents, especially by the work of Dziewonski [1970b, 1971]. Knopoff [1972] and others, it is satisfying to find such excellent agreement in data obtained from the same continent as were the heat flow data which helped provide the initial impetus for the model.

In this connection, it is interesting to note the presence of volcanism in eastern Australia during the late Tertiary, and in some parts of Victoria and eastern Queensland almost up to the present [David, 1959, p.637]. Although there is no current volcanism in these regions, the occurrence of volcanic activity depends upon the operation of tectonic forces as well as the existence of magma in the upper mantle, and the evidence for recently-existing partial melts beneath eastern Australia from the volcanic history of the region is certainly significant.

6.4 DISCUSSION: ANISOTROPY

Anisotropy in the upper mantle has been invoked by several workers to explain the difficulty encountered in fitting models simultaneously to observed Love and Rayleigh wave dispersion. Direct observation of anisotropy with respect to compressional waves in the upper mantle has been made in the Hawaiian area by Morris *et al.* [1969]. Olivine, believed to be a major constituent of the upper mantle, has been shown to be anisotropic for compressional and shear waves by Verma [1960]. In surface waves the anisotropy problem is complicated by the difficulty of obtaining reliable measurements of Love wave dispersion. Knopoff's [1972] summary of observation and inversion of surface wave dispersion prefers to 'delay the discussion of Love waves until such time as the corrections due to higher mode interference can be determined'. Consequently he considers only data obtained from the inversion of

Rayleigh wave phase velocities. Similarly, Thatcher and Brune [1973] do not attempt to fit Love wave data in their study of surface waves and crustal structure in the Gulf of California region. Thus there is some disagreement between workers on this subject, since Aki [1968], McEvelly [1964] and more recently James [1971b] prefer to include Love wave observations in their modelling. The Andes study by James [1971a,b] deserves some comment. He found anomalous G_1 waves that implied 15% anisotropy in the upper mantle. However, G_3 from the same earthquake exhibited 'normal' dispersion. He concludes that in this case anomalous Love wave phase velocities resulted from higher mode interference, and used the G_3 information solely.

This problem is less noticeable in pure shield areas, and Brune and Dorman [1963] found it possible to fit a model with no anisotropy to both Love and Rayleigh wave dispersion data, although the Love wave data extend only to 60 s. However, a more recent inversion of the Canadian Shield data by Massé [1973] has resulted in a model with a calculated dispersion that fits the Rayleigh wave phase velocities more closely, but now tends to lie below the Love wave observations.

Boore [1969] considered that Love wave phase velocities measured by an ensemble of events should exhibit scatter but no bias, even though there is interference between modes. This is precisely equivalent to the method of summation of two-station cross-correlograms used in the present study. Let us, therefore, proceed on the assumption that the Love wave phase velocities obtained by harmonic analysis represent 'true' fundamental Love wave phase velocities in the sense that the data oscillate about the unperturbed dispersion curve.

Hales and Bloch [1969] pointed out that surface wave studies indicate a universal, world-circling, moderately thick low velocity zone, but that P body wave studies do not in general confirm this model. They suggested that the low velocity layers in shield areas might be very thin and thus escape detection by the latter type of investigation. They reviewed Aki's [1968] result that a laminated mantle (or, alternatively, a single thin high contrast layer) produced effects similar to anisotropy. An interesting paper by Takeuchi *et al.* [1968] showed that effective anisotropy between Love shear velocity (β_L) and Rayleigh shear velocity (β_R) is produced in an upper mantle structure containing oblate magma pockets. They show that flat ellipsoids favor high values of anisotropy

at low liquid/solid volume fractions. A volume fraction of less than 5% produces an effective $(\beta_L)/(\beta_R)$ ratio of 6%, and is quite reasonable from a petrological point of view. The picture of discrete magma pools (or partial melts) appears conceptually more probable than a thin liquid-like layer existing continuously over a vast region.

An interesting observation by Cleary *et al.* [1972] was that the station-to-station scatter along their P anomaly traverse became less at the eastern (Canberra) end than it was along the remainder of the traverse. This observation may suggest that in the more eastern part of the region the occurrence of partial melts is greater, or may even be continuous, so as to produce a more homogeneous upper mantle than in the transition region of the shield boundary, where the more random distribution of partial melts could cause a greater scatter of P anomalies. This hypothesis is admittedly speculative, but a similarly dense traverse in Western Australia should establish whether the inter-station P anomaly scatter tends to be smaller within the presumably more homogeneous shield region.

6.5 A SUGGESTION FOR FURTHER WORK

The dip in Rayleigh wave group velocity appearing in some eastern Australian paths deserves further study. On 13 October, 1963, (05h 17m 57.1s) a great earthquake occurred in the Kurile Islands (see Dziewonski and Landisman [1970] for details and great circle analysis). Its epicenter is close to the great circle path containing CTA and TAU. Although the early phases are unreadable at these stations, later signals provide clear strong mantle waves for a two-station cross-correlation study for this path. Such a study should use a time series longer than 1024 s and may either verify or disprove the dip in group velocity. Some complications may arise from the presence of numerous aftershocks.

The above earthquake was not included in this study because the magnitude of the event was not included in the USCGS listing, and consequently the event was not detected by the search program described in Chapter 2.

Even if the dip in group velocity can be verified, conventional one-dimensional layered models may not be able to duplicate the sharpness of the dip in group velocity shown in Figs. 4.23 and 4.27. This may be a

phenomenon that can best be studied with more sophisticated modelling techniques such as the finite element technique [Drake, 1972].

APPENDIX A

Tabulation of observed Rayleigh wave phase velocity (Fig. 4.29)
and mean Love wave phase velocity (Fig. 4.44a) used to test
Monte Carlo models

Period (s)	W1 (km/s)	E1 (km/s)	Love (km/s)
10.0	3.20	3.26	3.61
13.1	3.29	3.35	3.68
17.2	3.36	3.48	3.79
22.5	3.63	3.68	3.92
29.5	3.85	3.80	4.08
38.7	3.97	3.89	4.23
50.7	4.09	3.92	4.39
66.6	4.16	3.96	4.56
87.3	4.22	4.05	4.72
114.4	4.33	4.37	4.85
150.0	4.48	4.80	5.02

APPENDIX B

Shear velocity tabulation for Monte Carlo models

N.B. The first layer in all models is 20 km thick
with a shear velocity equal to 3.6 km/s.

'East' Low Contrast

Layer	Model 1 Thickness (km)	Model 2	Model 3	Model 4	Model 5	Model 6
2	20.0	20.0	20.0	20.0	20.0	20.0
3	56.6	40.2	84.7	57.3	69.0	73.1
4	87.9	108.3	85.7	65.7	91.9	64.7
5	215.4	211.5	189.7	237.0	199.1	222.3
Half space	5.36	5.23	5.33	5.49	4.90	5.21

'East' High Contrast

Layer	Model 7	Model 8*	Model 9*
2	20.0	20.0	20.0
3	79.4	92.1	114.0
4	2.0	2.0	2.0
5	278.6	265.9	244.0
Half space	5.01	5.17	5.34

'East' Medium Contrast

Layer	Model 10	Model 11	Model 12	Model 13	Model 14	Model 15*	Model 16*
2	20.0	20.0	20.0	20.0	20.0	20.0	20.0
3	84.3	93.8	79.1	81.8	68.9	92.7	66.8
4	22.4	7.5	16.6	20.8	36.9	27.6	37.9
5	253.3	258.7	264.3	257.4	254.2	239.7	255.2
Half space	5.14	5.26	5.03	5.35	5.30	5.50	5.31

* These models not graphed in text

'West' Low Contrast

Layer	Model 17 Thickness (km)	V_S (km/s)	Model 18	Model 19	Model 20
2	20.0	3.83	20.0 3.73	20.0 3.84	20.0 3.80
3	79.5	4.80	95.2 4.77	88.4 4.72	50.2 4.81
4	121.8	4.69	151.7 4.75	116.1 4.75	72.8 4.67
5	158.8	4.85	113.1 4.80	155.5 4.71	237.0 4.67
Half space		5.49	5.41	5.36	5.35

	Model 21	Model 22	Model 23	Model 24
2	20.0	20.0 3.86	20.0 3.82	20.0 3.83
3	39.7	54.7 4.86	108.0 4.79	97.8 4.74
4	297.1	118.7 4.56	119.2 4.45	148.4 4.72
5	23.0	186.6 4.81	132.7 4.96	113.8 4.48
Half space		5.38	5.44	5.21

'West' High Contrast

Layer	Model 25
2	20.0 3.72
3	244.8 4.67
4	2.0 1.10
5	113.2 5.16
Half space	5.31

APPENDIX C

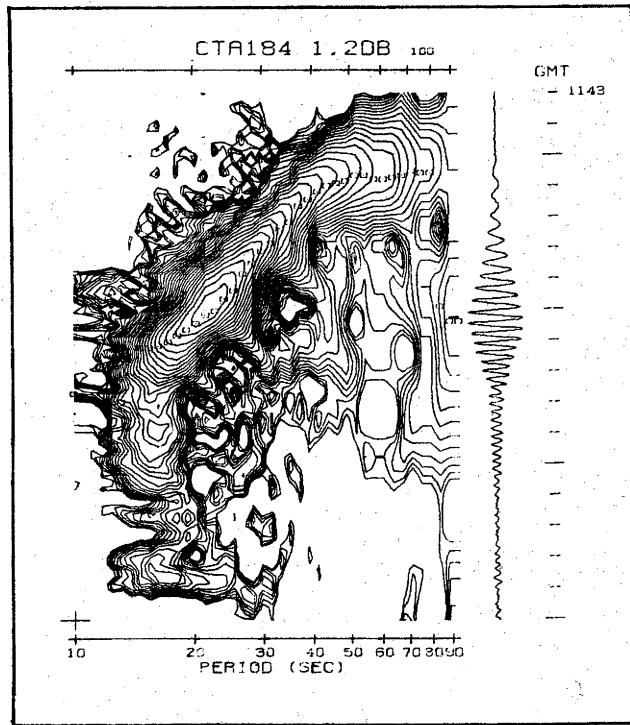
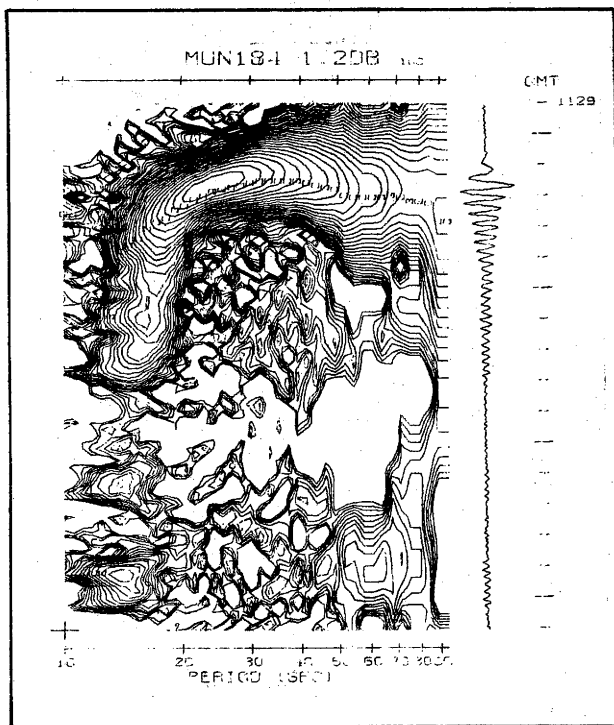
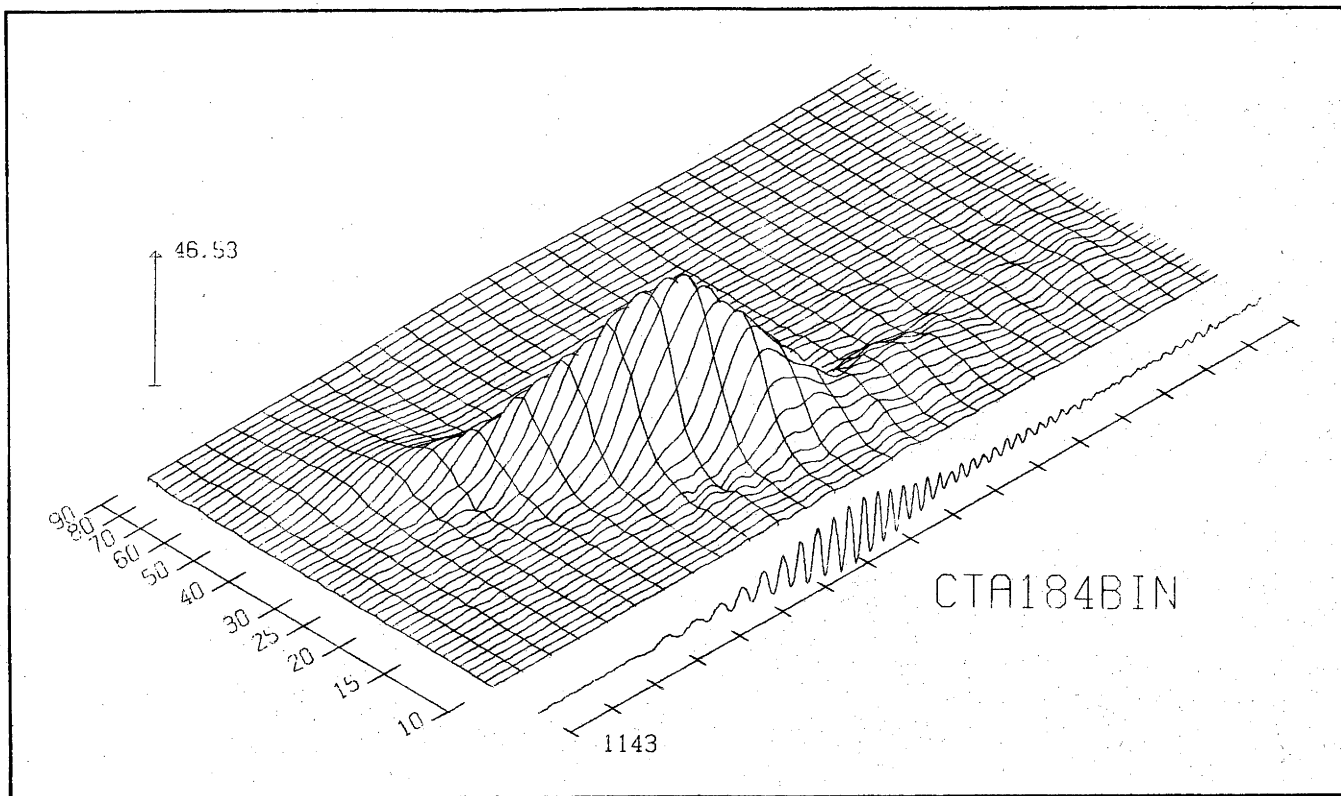
Papers by the author published prior to undertaking the investigations described in this thesis

PUBLICATIONS - JOHN H. GONCZ

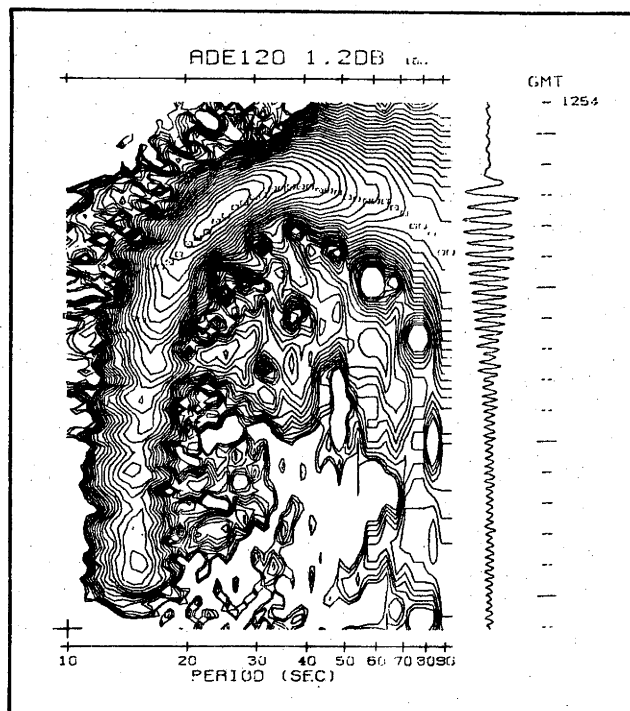
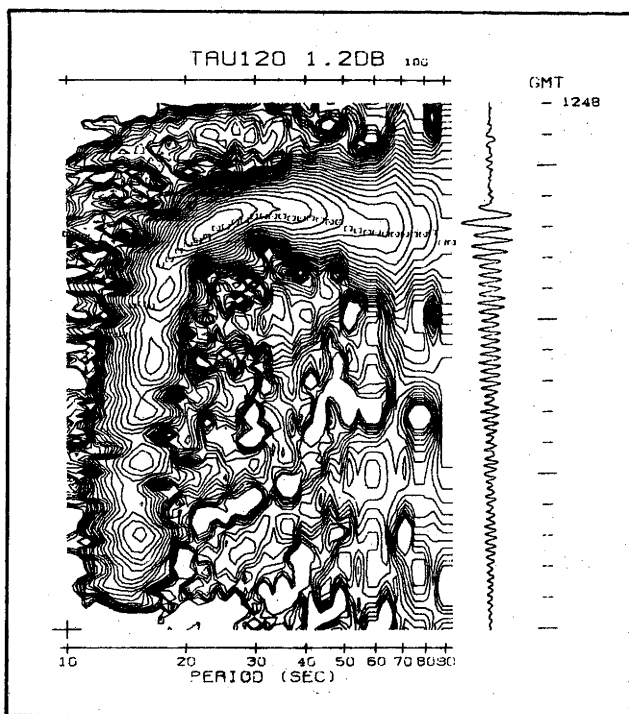
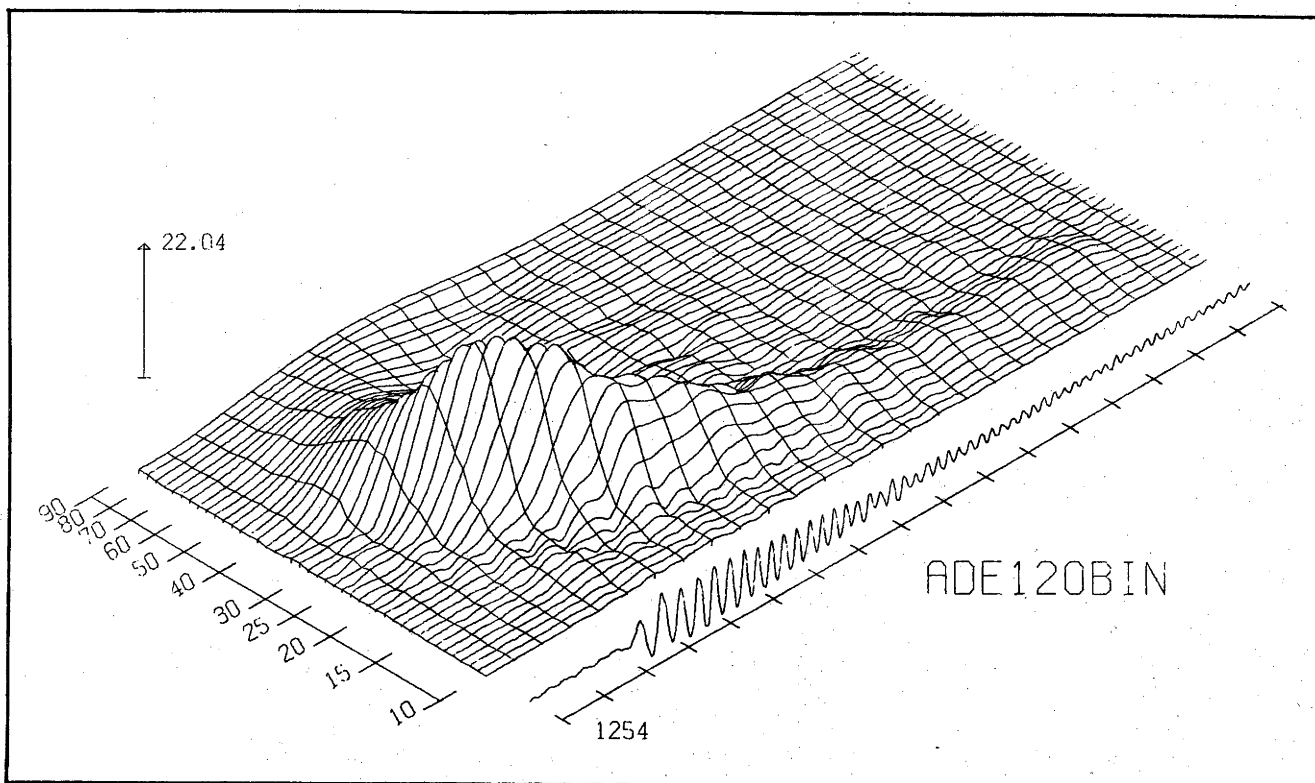
- 1961 Goncz, J.H. and Newell, P.B. - Geometry and impurity effects on low pressure breakdown in helium. Twenty-first conference on physical electronics, M.I.T.
- 1962 Edgerton, H.E. and Goncz, J.H. - "Strobes", in The Encyclopedia of Electronics, Reinhold Publishing Corporation, New York, C. Susskind, editor; 799-801.
- 1963 Edgerton, H.E., Goncz, J.H. and Jameson, P.W. - Xenon flash lamp limits of operation. Proceedings of sixth international conference on high speed photography, J.G.A. de Graaf and P. Tezelar, editors, H.O. Tjeek Willink and N.V. Zeen, Haarlem, 143-151.
- 1965 Goncz, J.H. - Resistivity of xenon plasma. J. Appl. Phys. 36: 742-743.
- 1965 Goncz, J.H. - Double pulsing boosts flashtube performance. Microwaves, 34-37, April.
- 1966 Goncz, J.H. - New developments in electronic flashtubes. ISA Transactions 5: 28-36.
- 1966 Goncz, J.H. and Newell, P.B. - Spectra of pulsed and continuous xenon discharges. J. Opt. Soc. Am. 56: 87-92.
- 1967 Goncz, J.H. and Mitchell, W.J. Jr. - Output spectra of krypton and xenon filled flashtubes. IEE Journal of Quantum Electronics, QE-3: 330-331.
- 1967 Goncz, J.H. - Programming round robins - World Tennis, Nov.
- 1972 Goncz, J.H. and Rose, C.W. - Energy exchange within the crop canopy of Townsville Style (*Stylosanthes Humilis* H.B.K.) Agric. Meteorol., 9: 405-419.
- 1972 Rose, C.W., Begg, J.E., Byrne, G.F., Goncz, J.H. and Torrsell, B.W.R. - Energy exchanges between a pasture and the atmosphere under steady and non-steady state conditions. Agric. Meteorol., 9: 385-403.
- 1972 Rose, C.W., Begg, J.E., Byrne, G.F., Torrsell, B.W.R. and Goncz, J.H. - A simulation model of growth-field environment relationships for Townsville Stylo (*Stylosanthes Humilis* H.B.K.) pasture. Agric. Meteorol., 10: 161-183.

APPENDIX D

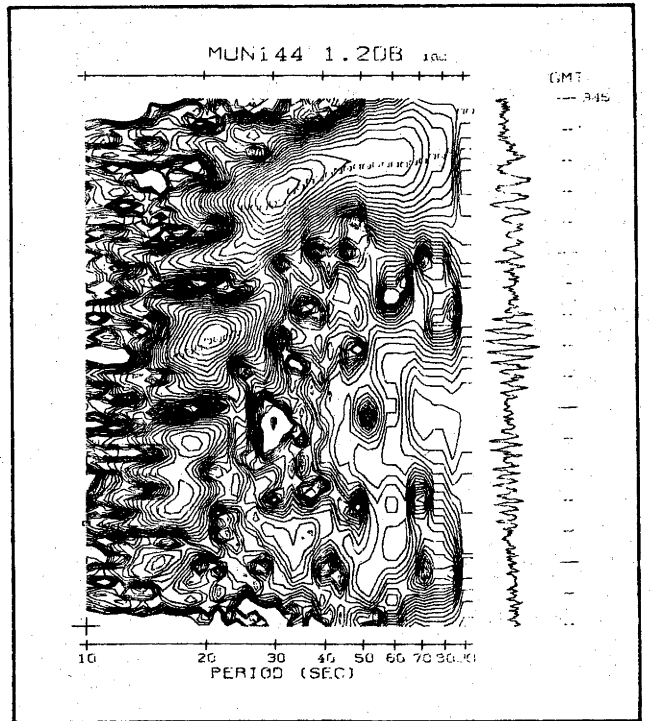
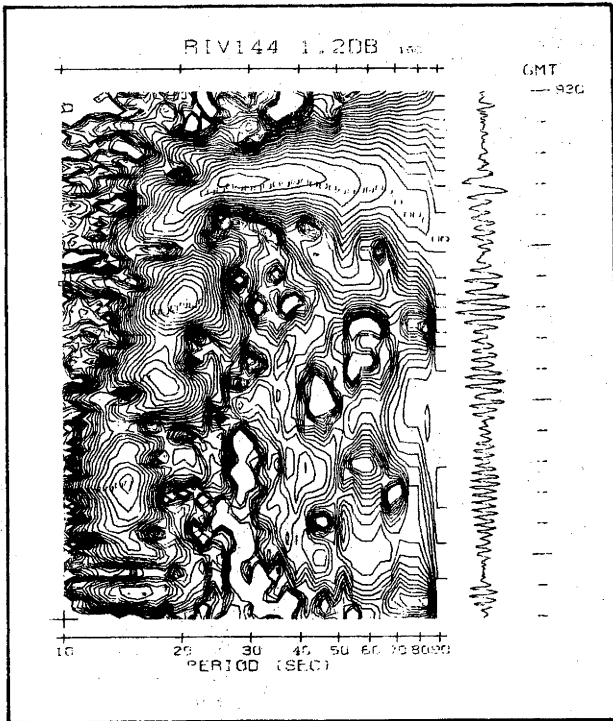
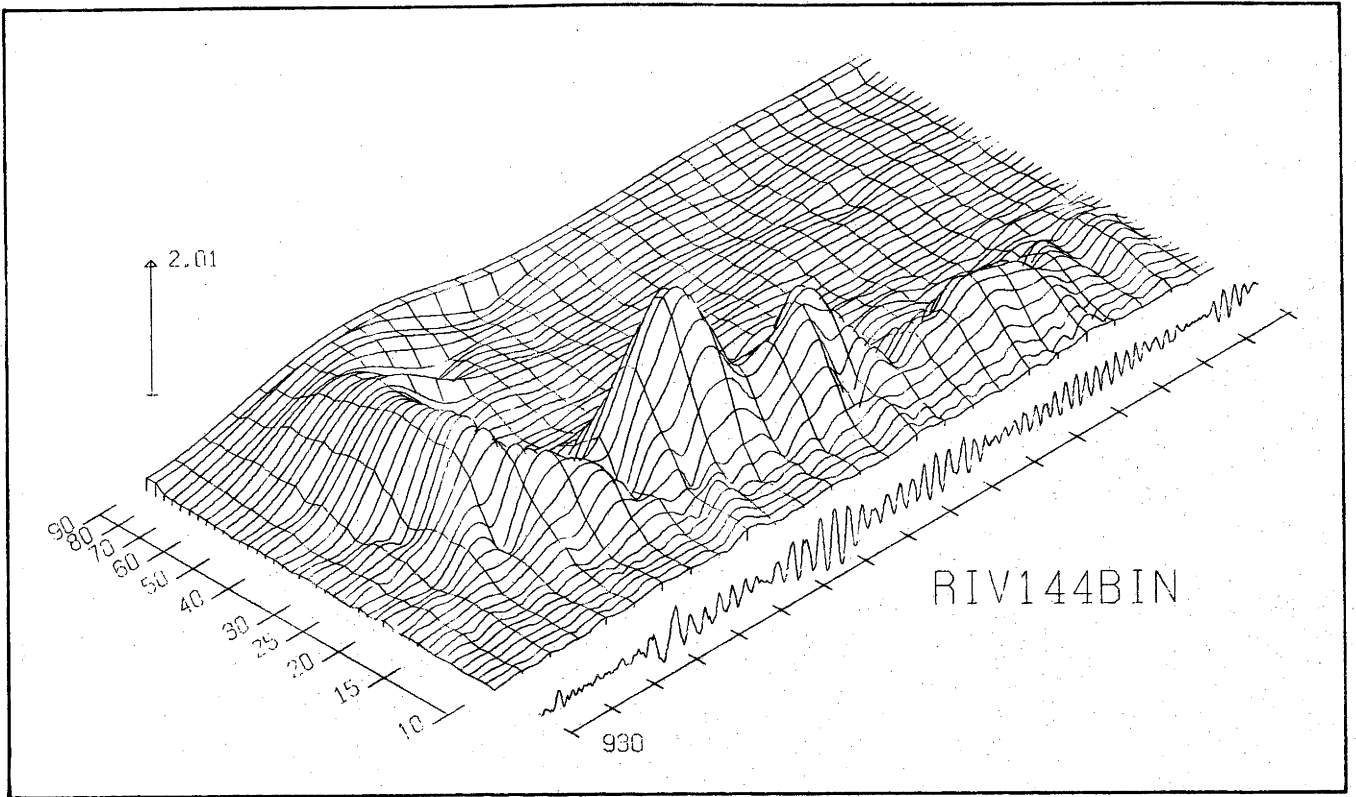
Examples of seismic signals and data presentation methods



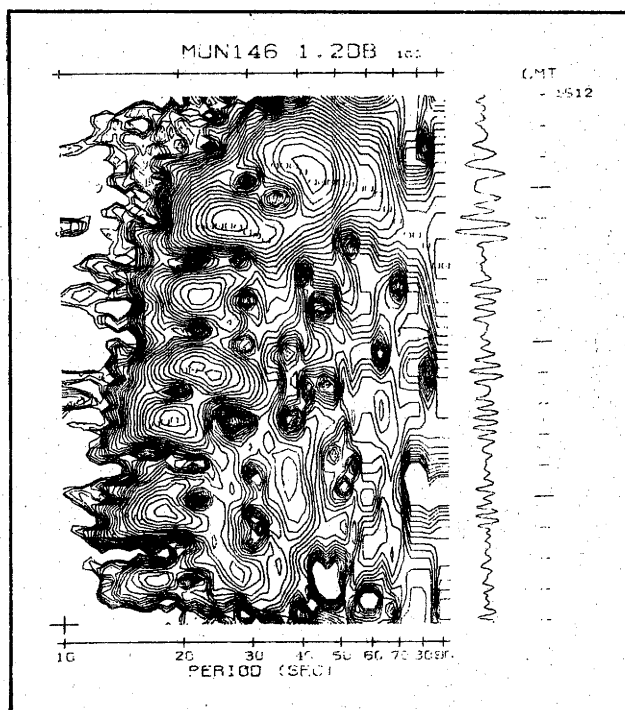
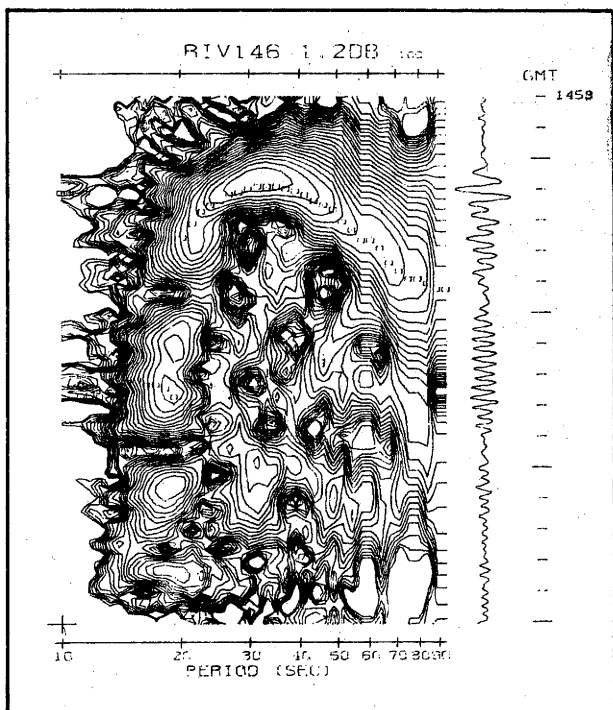
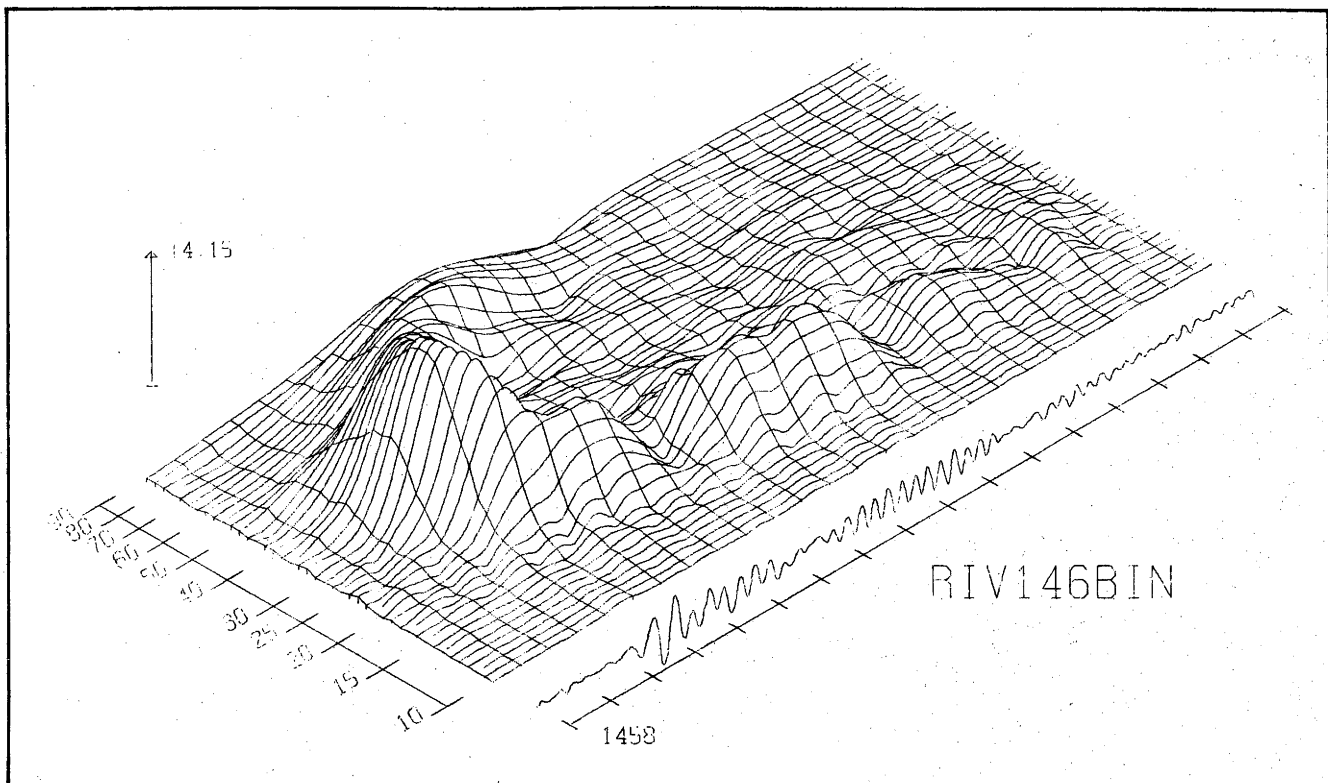
Group arrival time



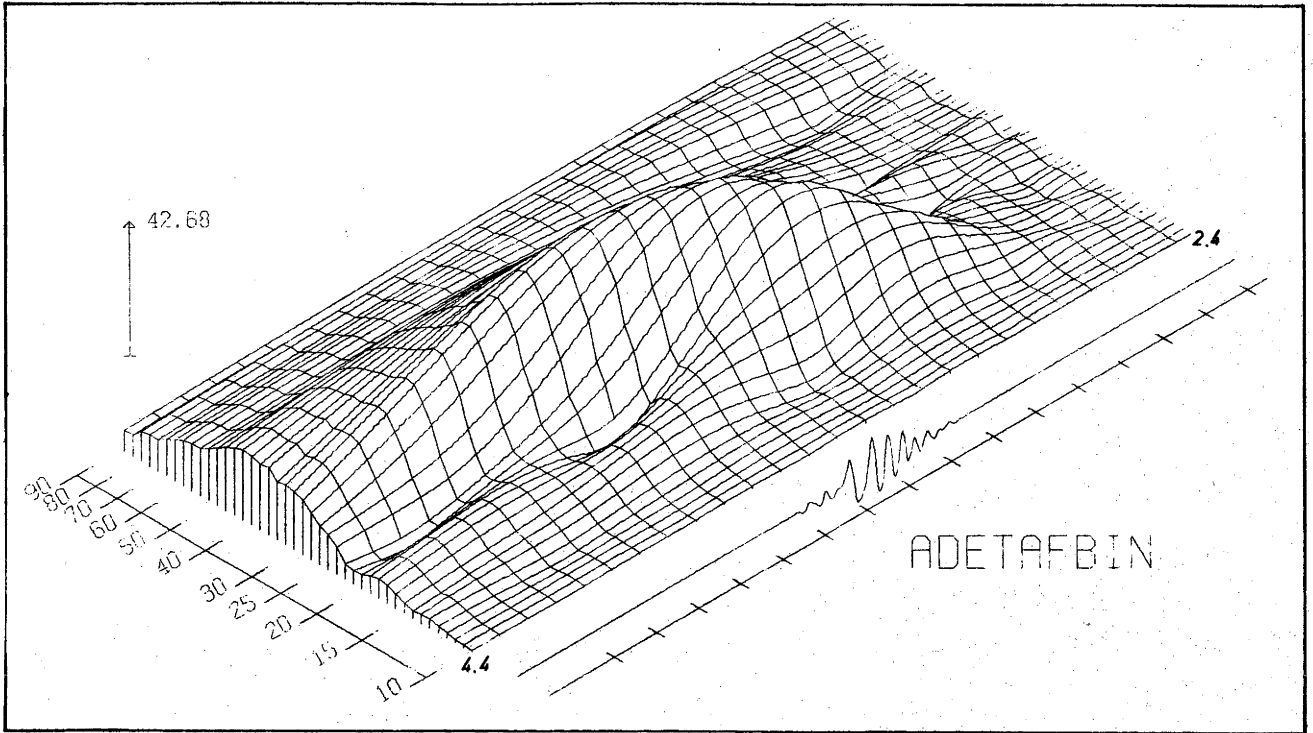
Group arrival time



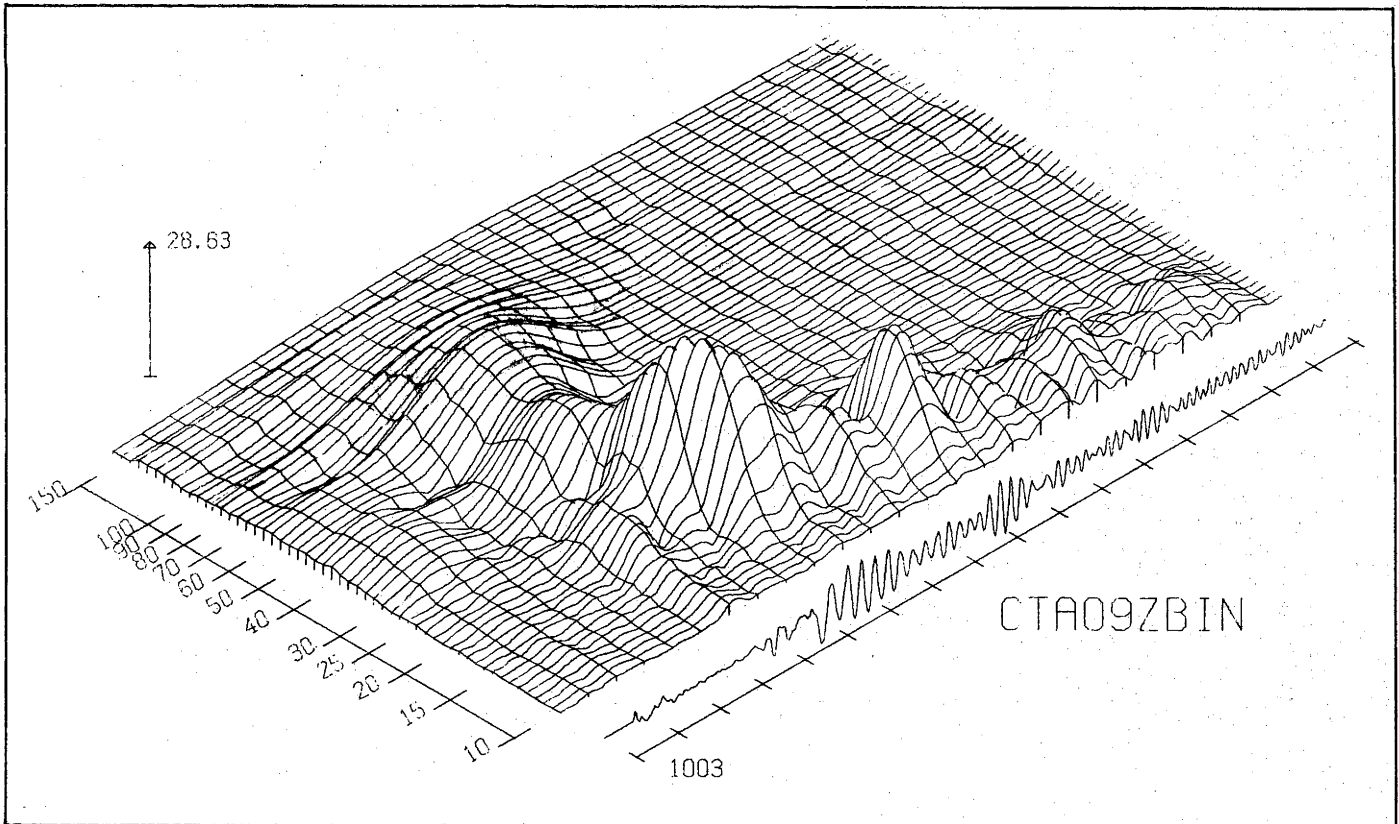
Group arrival time



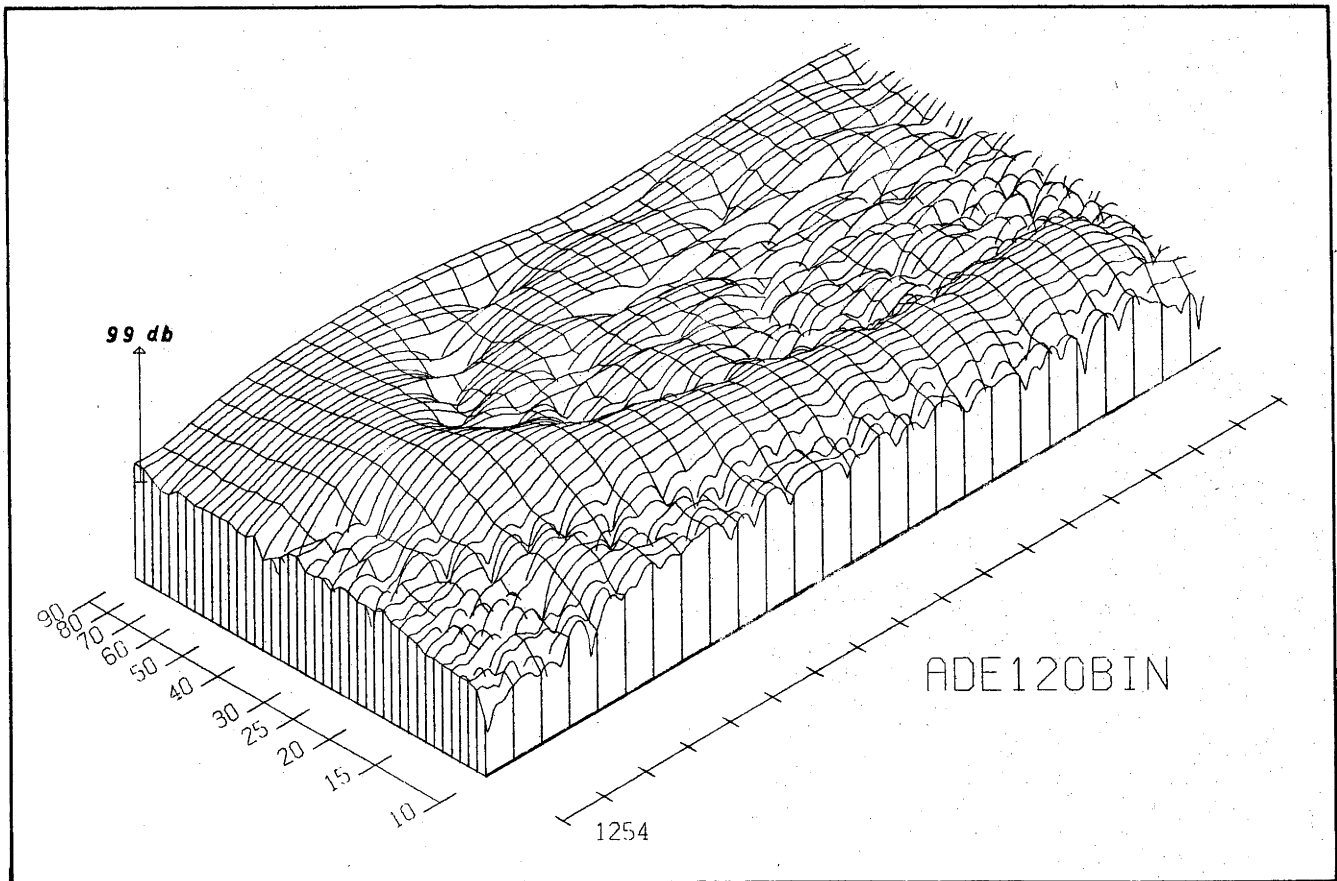
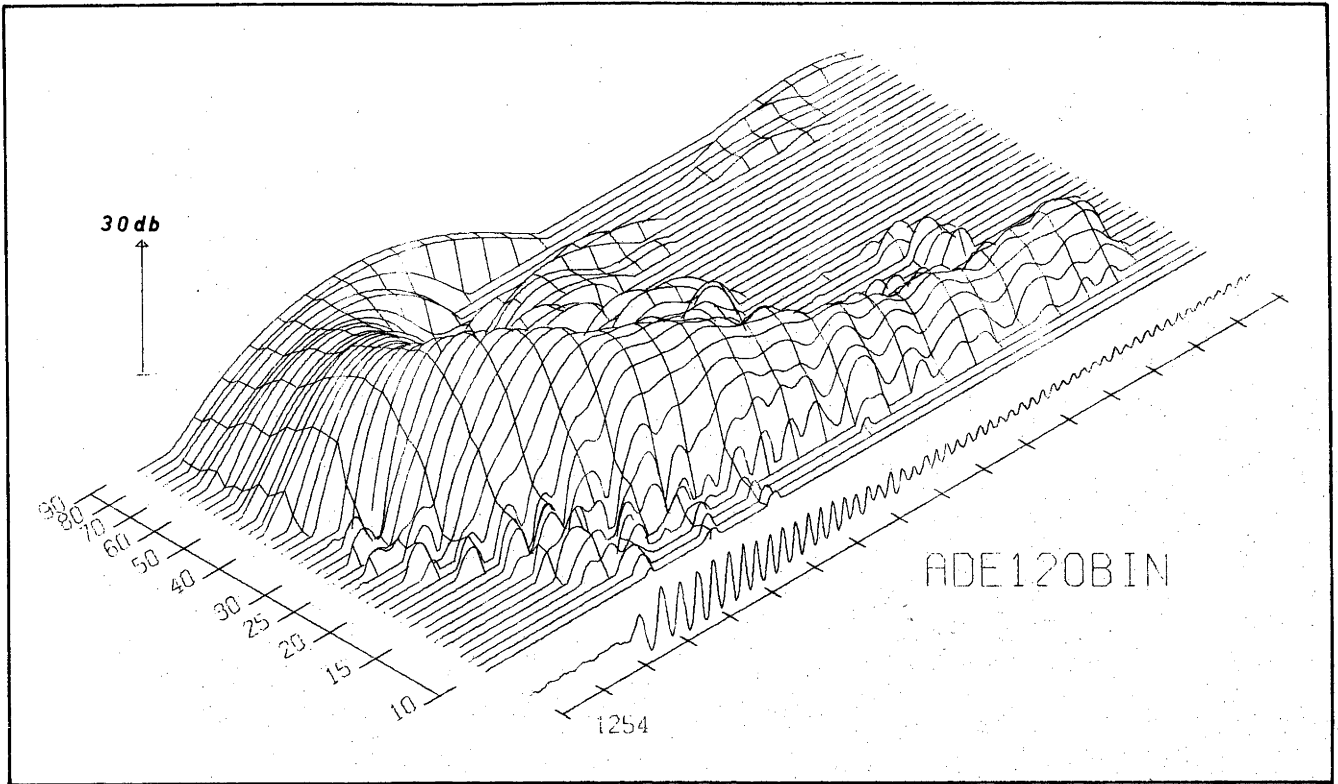
Group arrival time



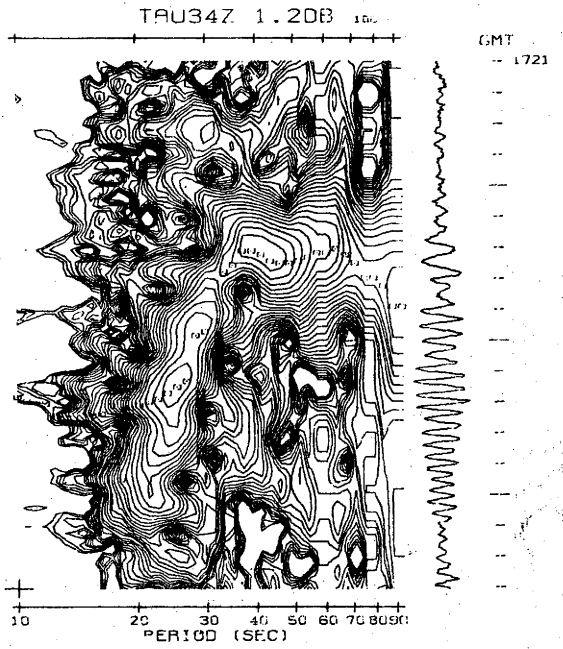
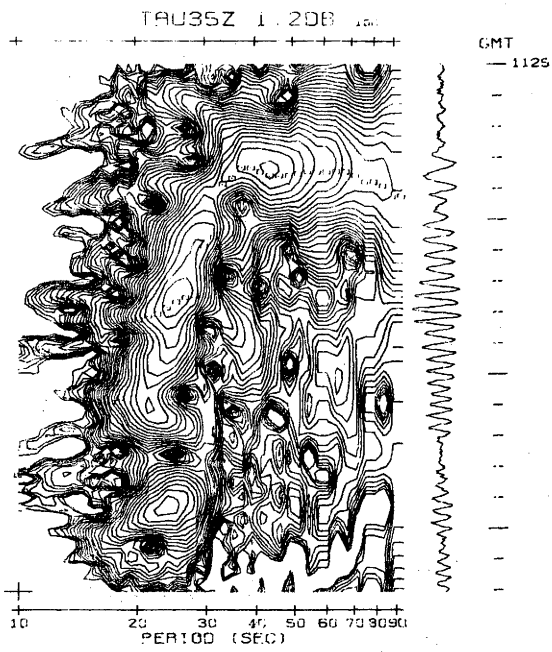
Group velocity



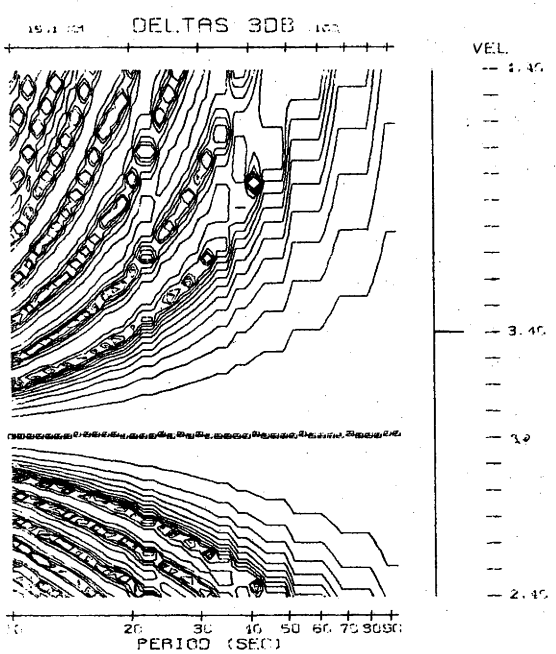
Group arrival time (180 sec)



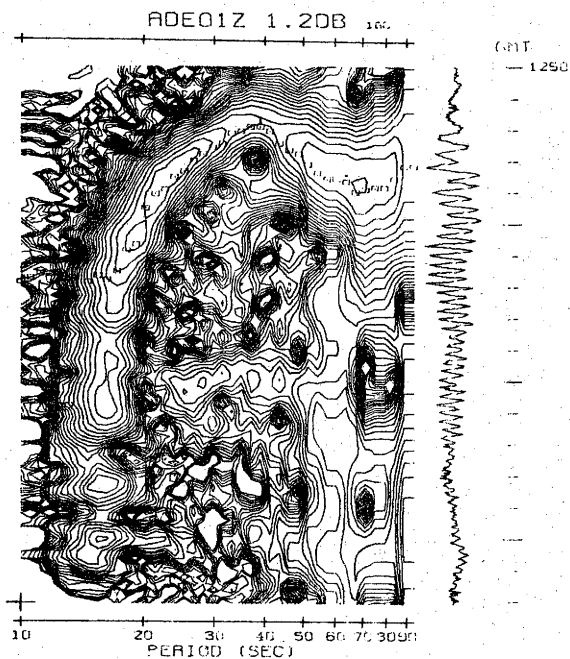
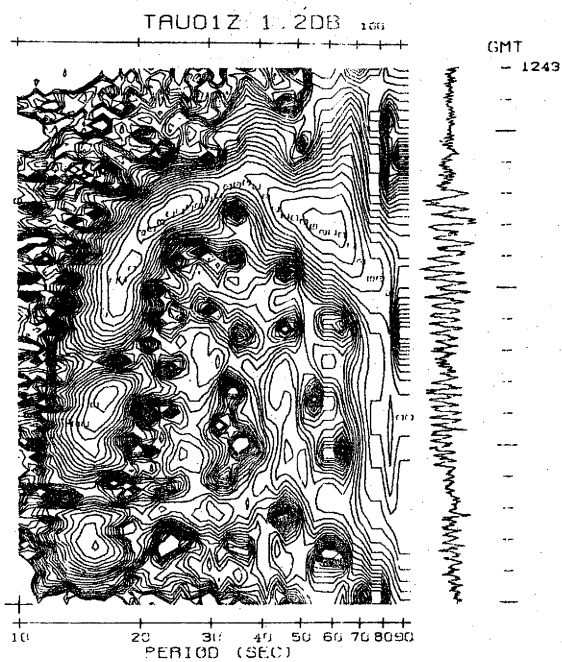
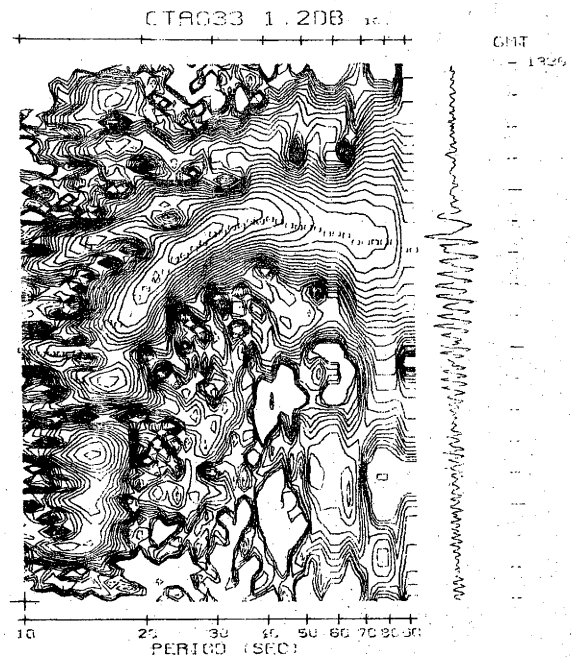
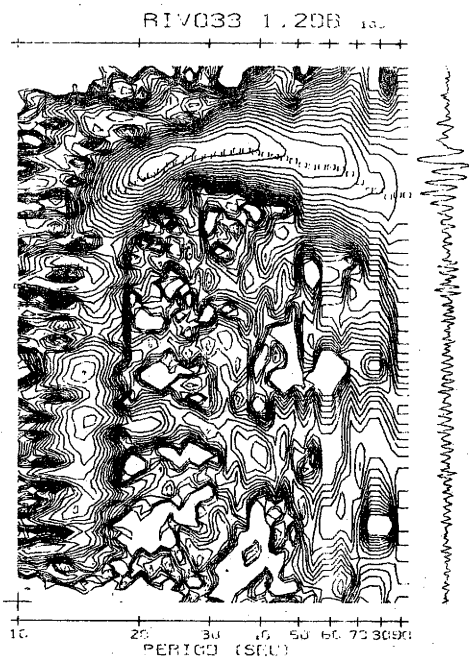
Signal amplitude in decibels



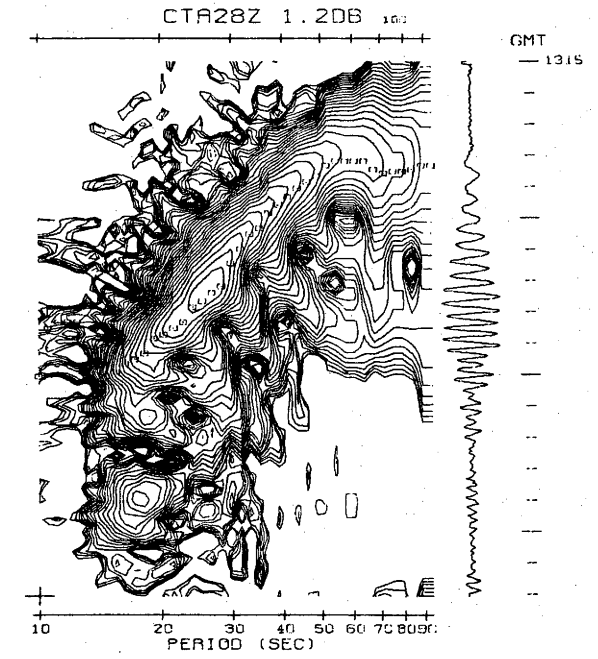
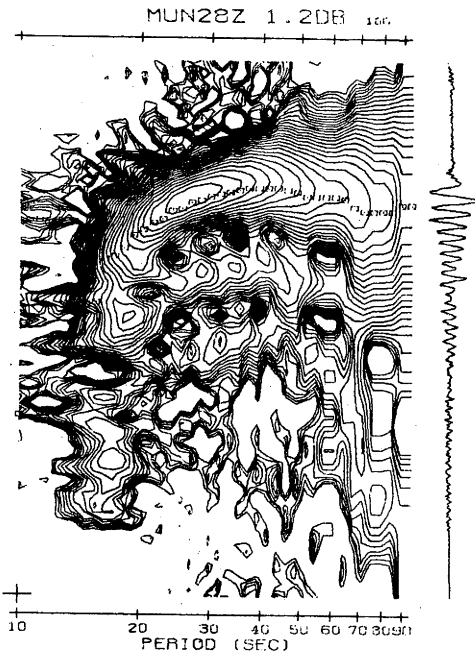
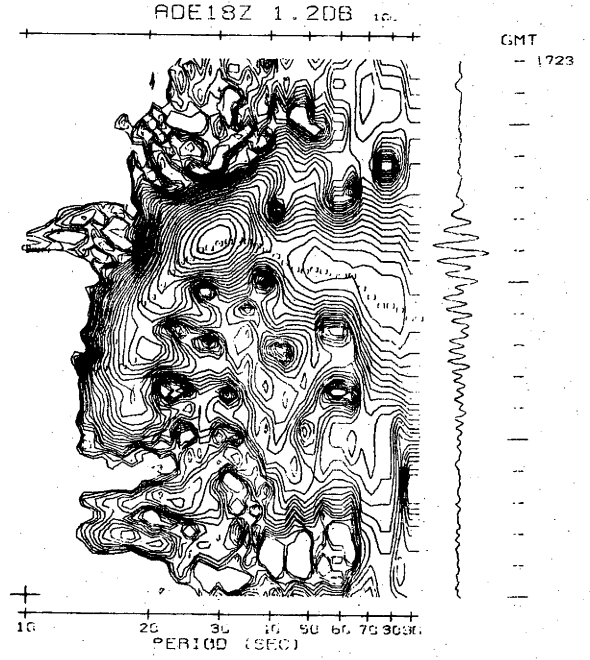
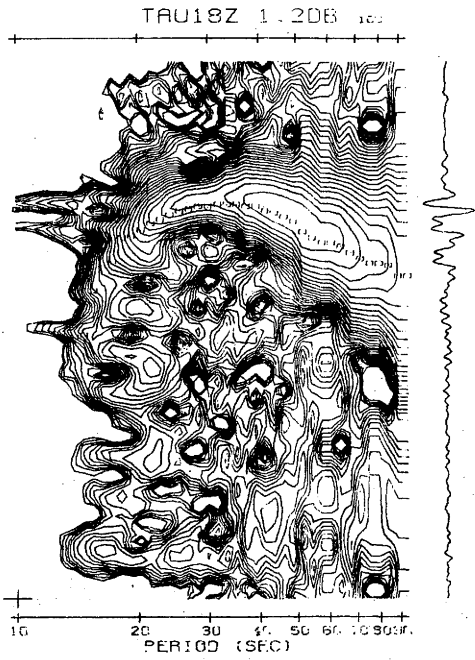
Group arrival time



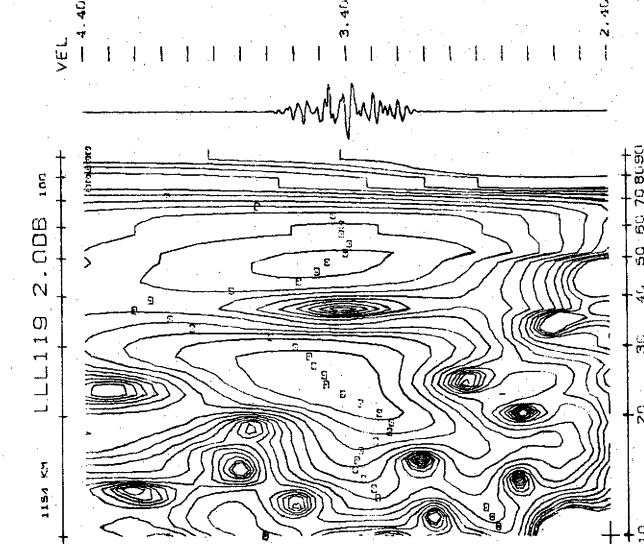
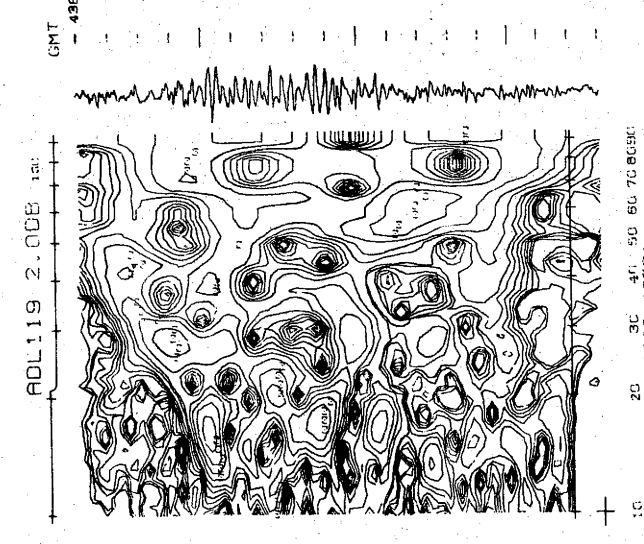
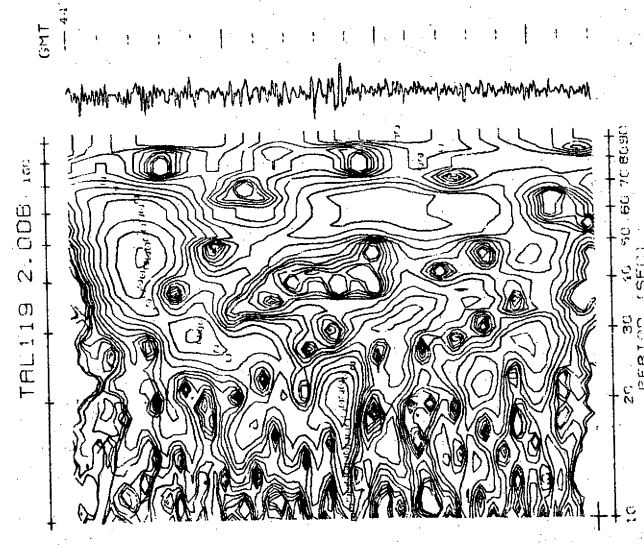
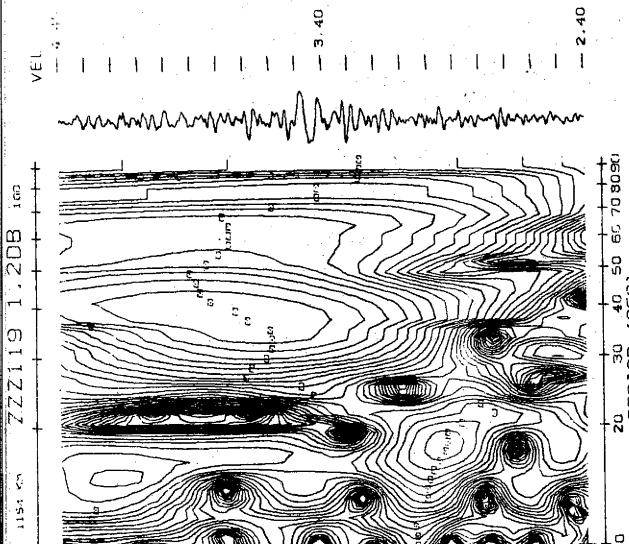
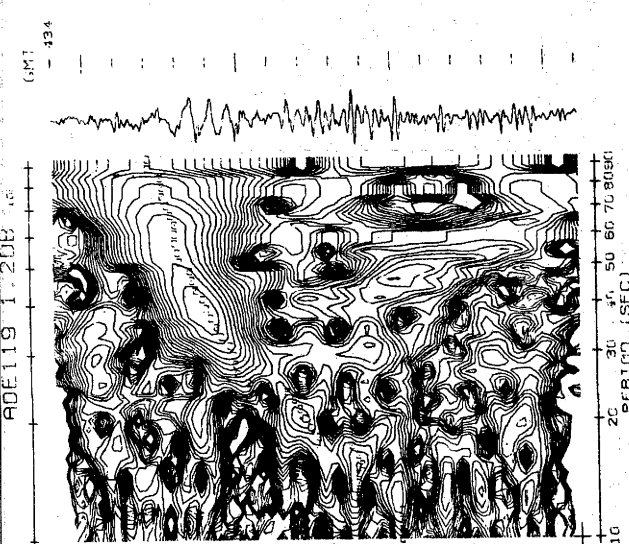
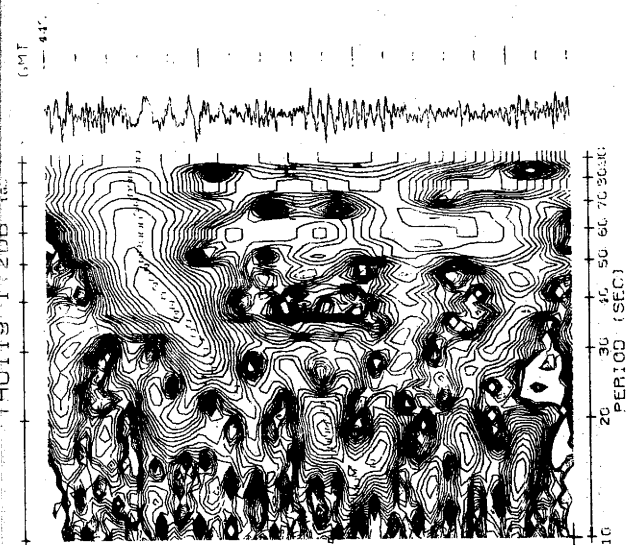
Program test

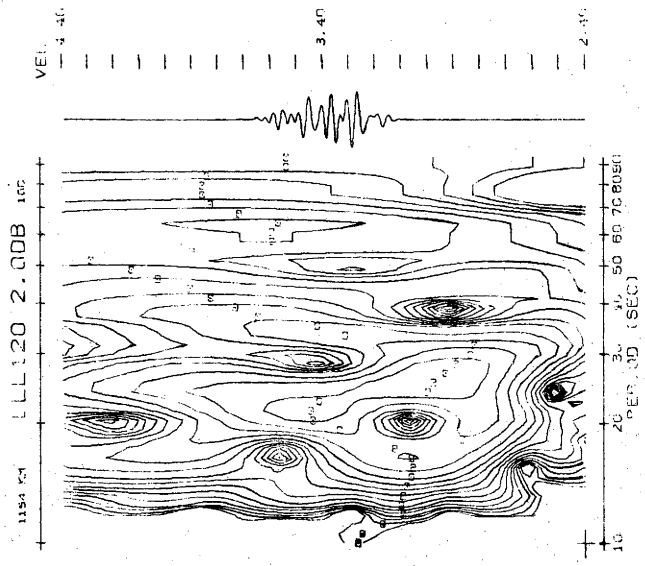
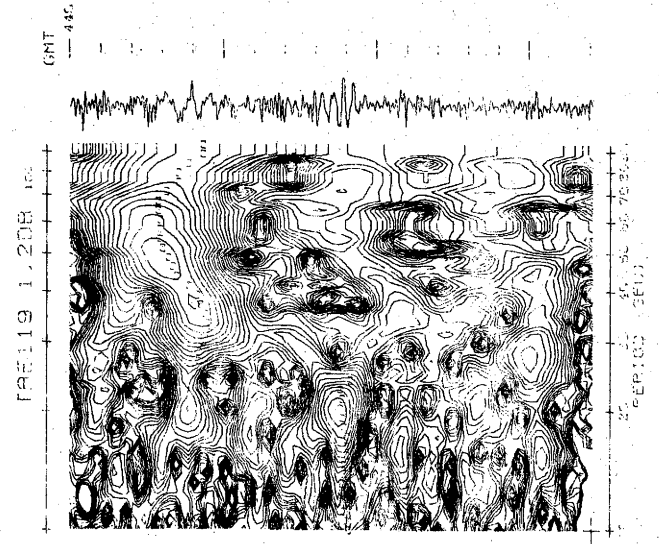
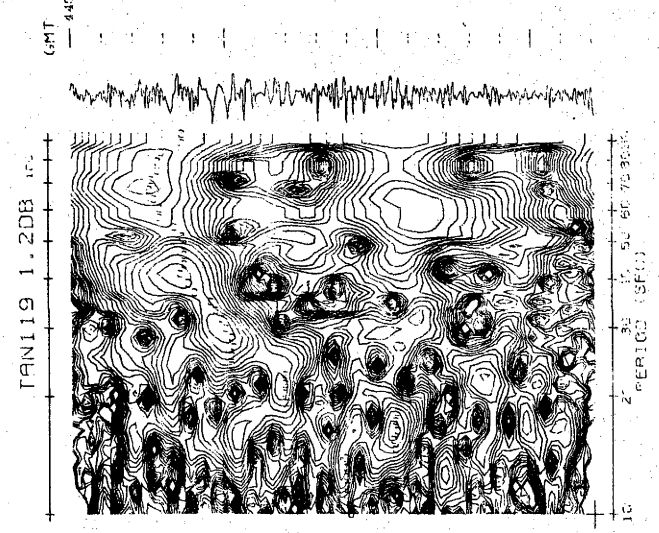
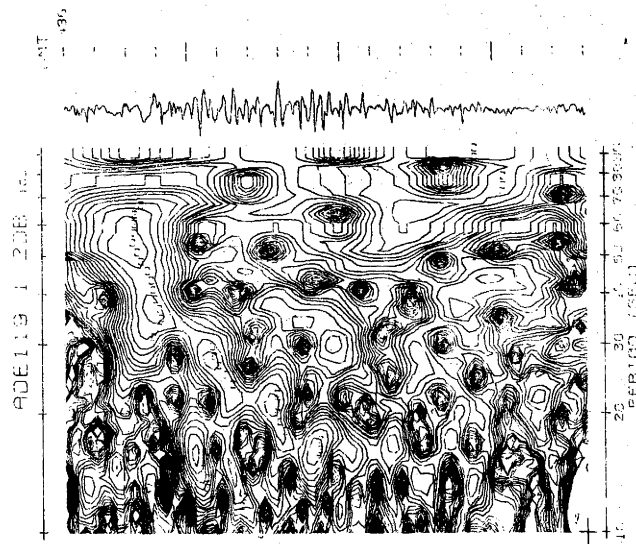
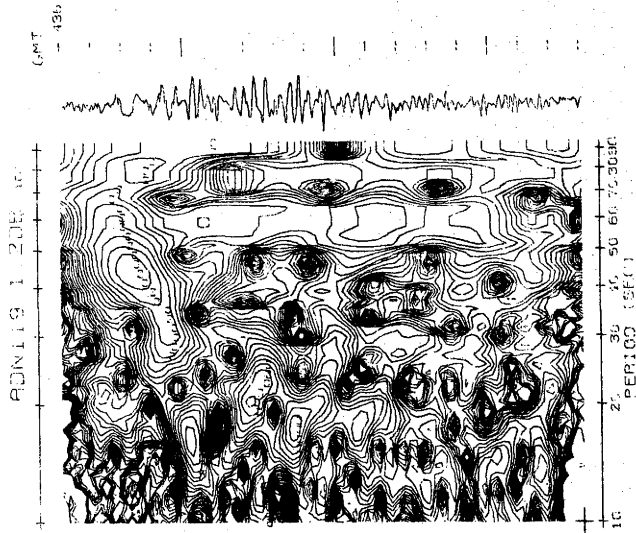


Group arrival time

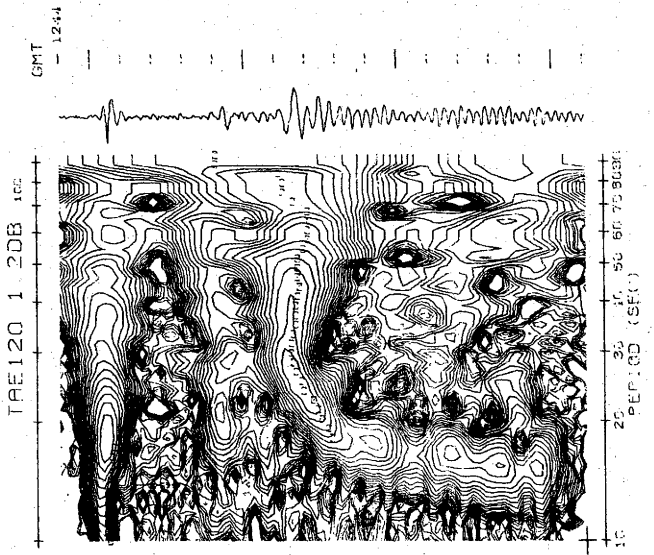
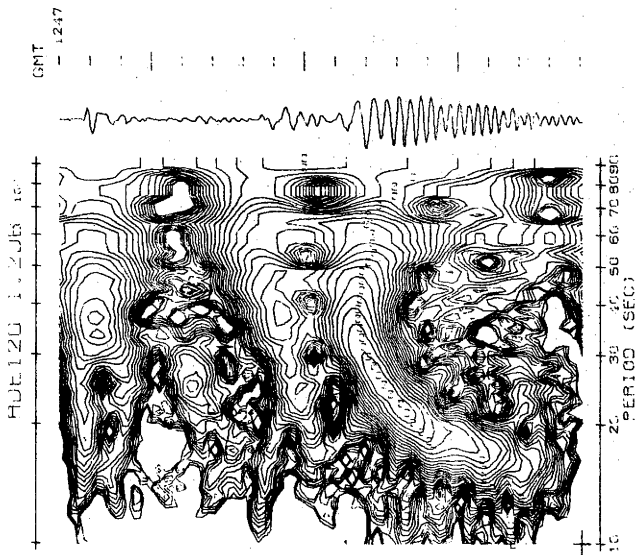
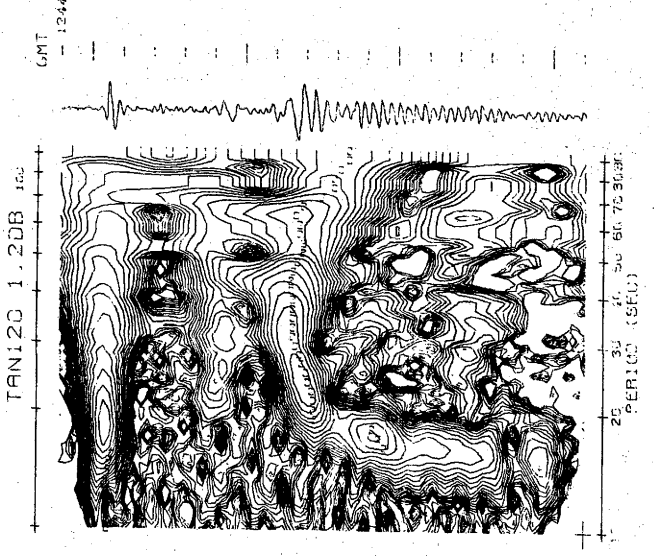
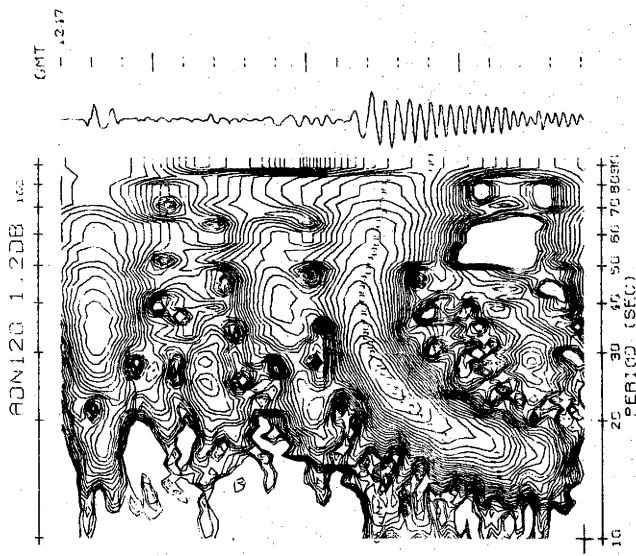
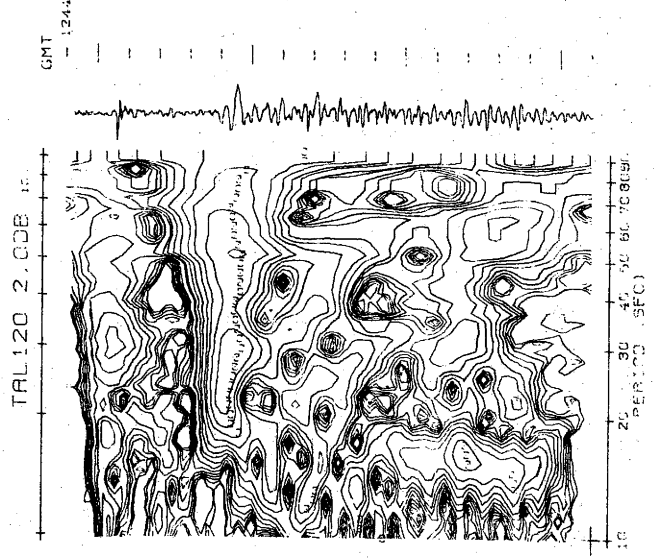
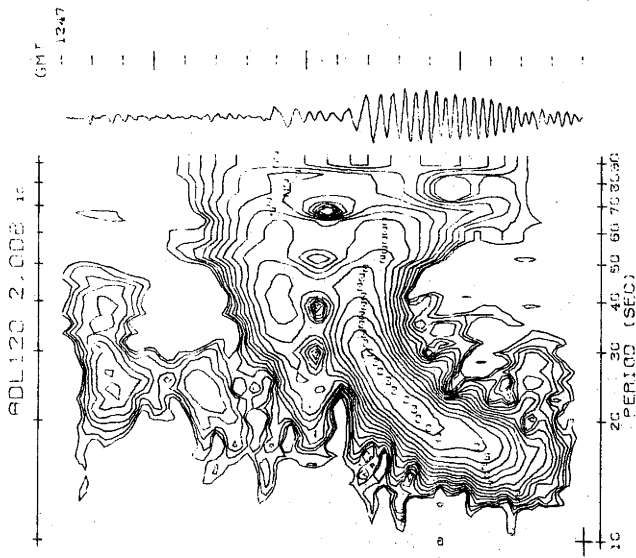


Group arrival time





Love wave study



I see water under

REFERENCES

- Aki, K. (1968). - Seismological evidence for the existence of soft thin layers in the upper mantle under Japan. *J. Geophys. Res.* 73, 585-594.
- Alexander, S.S. (1963). - Surface wave propagation in the western United States. Ph.D. Thesis, Calif. Inst. of Technology, Pasadena, California, 242 pp.
- Alexander, S.S. and R.W. Sherburne (1973). - Meeting of the International Association of Seismology and Physics of the Earth's Interior, Lima, Peru. (Abstract).
- Anderson, D.L. (1964). - Universal dispersion tables. 1. Love waves across oceans and continents on a spherical Earth. *Bull. Seism. Soc. Am.* 54, 681-726.
- Anderson, D.L. (1967). - Latest information from seismic observations, in: *The Earth's Mantle*, T.F. Gaskell, editor, pp.355-420, Academic Press, London and New York, 509 pp.
- Andersson, R.S., M.H. Worthington and J.R. Cleary (1972). - Density modelling by Monte Carlo Inversion - I. Methodology. *Geophys. J.R. astro. Soc.* 29, 433-444.
- Archambeau, C.B., J.C. Bradford, P.W. Broome, W.C. Deane, E.A. Flinn and R.L. Sax (1965). - Data processing techniques for the detection and interpretation of teleseismic signals. *Proc. IEEE* 53, 1860-1884.
- Archambeau, C.B., E.A. Flinn and D.B. Lambert (1966). - Detection, analysis and interpretation of teleseismic signals. 1. Compressional phases from the Salmon event. *J. Geophys. Res.* 71, 3483-3501.
- Backus, G.E. and J.F. Gilbert (1967). - Numerical applications of a formalism for geophysical inverse problems. *Geophys. J.R. astro. Soc.* 13, 247-276.
- Backus, G. and F. Gilbert (1968). - The resolving power of gross earth data. *Geophys. J.R. astro. Soc.* 16, 169-205.
- Backus, G. and F. Gilbert (1970). - Uniqueness in the inversion of inaccurate gross Earth data. *Phil. Trans. R. Soc. Series A.* 266, 123-192.
- Beck, A.E. (1956). - The measurement of the flow of heat through the crust of the Earth and through rocks. Ph.D. Thesis, The Australian National University.
- Bendat, J.S. and A.G. Piersol (1971). - *Random Data: Analysis and Measurement Procedure*. Wiley-Interscience, New York, 318 pp.

- Ben-Menahem, A. (1965). - Observed attenuation and Q values of seismic surface waves in the upper mantle. *J. Geophys. Res.* 70, 4641-4651.
- Biot, M.A. (1957). - General theorem concerning equivalence of group velocity and energy transport. *Phys. Rev.* 105, 1129-1137.
- Biswas, N.N. and L. Knopoff (1970). - Exact Earth flattening calculation for Love waves. *Bull. Seism. Soc. Am.* 60, 1123-1137.
- Bloch, S. (1969). - Surface wave dispersion in southern Africa. Ph.D. Thesis, University of Witwatersrand.
- Bloch, S. and A.L. Hales (1968). - New techniques for the determination of surface wave phase velocities. *Bull. Seism. Soc. Am.* 58, 1021-1034.
- Bloch, S., A.L. Hales and M. Landisman (1969). - Velocities in the crust and upper mantle of southern Africa from multi-mode surface wave dispersion. *Bull. Seism. Soc. Am.* 59, 1599-1629.
- Bolt, B.A. and M. Niazi (1964). - Dispersion of Rayleigh waves across Australia. *Geophys. J.R. astro. Soc.* 9, 21-35.
- Bolt, B.A., H.A. Doyle and D.J. Sutton (1958). - Seismic observations from the 1956 atomic explosion in Australia. *Geophys. J.R. astro. Soc.* 1, 135-145.
- Boore, D.M. (1969). - Effect of higher mode contamination on measured Love wave phase velocities. *J. Geophys. Res.* 74, 6612-6616.
- Bostrom, R.C. (1971). - Westward displacement of the lithosphere. *Nature* 234, 536-538.
- Brune, J.N. (1969). - Surface waves and crustal structure. In: P.J. Hart (editor), *The Earth's Crust and Upper Mantle*, American Geophysical Union, Washington, D.C., pp.230-242.
- Brune, J. and J. Dorman (1963). - Seismic waves and Earth structure in the Canadian Shield. *Bull. Seism. Soc. Am.* 53, 167-209.
- Brune, J.N., J.E. Nafe and J.E. Oliver (1960). - A simplified method for the analysis and synthesis of dispersed wave trains. *J. Geophys. Res.* 65, 287-304.
- Brune, J.N., J.E. Nafe and L.E. Alsop (1961). - The polar phase shift of surface waves on a sphere. *Bull. Seism. Soc. Am.* 51, 247-257.
- Capon, J. (1970). - Analysis of Rayleigh-wave multipath propagation at LASA. *Bull. Seism. Soc. Am.* 60, 1701-1731.
- Capon, J. (1971). - Comparison of Love- and Rayleigh-wave multipath propagation at LASA. *Bull. Seism. Soc. Am.* 61, 1327-1344.
- Capon, J. and J.F. Evernden (1971). - Detection of interfering Rayleigh waves at LASA. *Bull. Seism. Soc. Am.* 61, 807-849.

- Cara, M. (1973). - Filtering of dispersed wavetrains. *Geophys. J.R. astro. Soc.* 33, 65-80.
- Clark, S.P. and A.E. Ringwood (1964). - Density distribution and constitution of the mantle. *Rev. of Geophys.* 2, 35-88.
- Cleary, J. (1967). - P times to Australian stations from nuclear explosions. *Bull. Seism. Soc. Am.* 57, 773-781.
- Cleary, J. (1973). - Australian crustal structure. *Tectonophysics* 20, 241-248.
- Cleary, J.R. and H.A. Doyle (1962). - Application of a seismograph network and electronic computer in near earthquake studies. *Bull. Seism. Soc. Am.* 52, 673-682.
- Cleary, J. and A.L. Hales (1966). - An analysis of the travel times of P waves to North American stations, in the distance range 32° to 100°. *Bull. Seism. Soc. Am.* 56, 467-489.
- Cleary, J.R., D.W. Simpson and K.J. Muirhead (1972). - Variations in Australian upper mantle structure, from observations of the CANNIKAN explosion. *Nature* 236, 111-112.
- Cooley, J.W. and J.W. Tukey (1965). - An algorithm for the machine calculation of complex Fourier series. *Math. Comp.* 19, 297-301.
- David, Sir T.W.E., ed. W.R. Browne (1950). - *The Geology of the Commonwealth of Australia*, Edward Arnold and Co., London.
- Denham, D., D.W. Simpson, P.J. Gregson and D.J. Sutton (1972). - Travel times and amplitudes from explosions in Northern Australia. *Geophys. J.R. astro. Soc.* 28, 225-235.
- Der, Z., R. Massé and M. Landisman (1970). - Effects of observational errors on the resolution of surface waves at intermediate distances. *J. Geophys. Res.* 75, 3399-3409.
- Deutsch, R. (1969). - *Systems Analysis Techniques*, Prentice Hall, Inc., Englewood Cliffs, N.J., 472 pp.
- Dorman, J. (1962). - Period equation for waves of Rayleigh type on a layered, liquid-solid half space. *Bull. Seism. Soc. Am.* 52, 389-397.
- ³Dorman, J. and M. Ewing (1962). - Numerical inversion of seismic surface wave dispersion data and crust-mantle structure in the New York-Pennsylvania area. *J. Geophys. Res.* 67, 5227-5241.
- Doyle, H.A. and A.L. Hales (1967). - An analysis of the travel times of S waves to North American stations, in the distance range 28° to 82°. *Bull. Seism. Soc. Am.* 57, 761-771.
- Doyle, H.A. and I.B. Everingham (1964). - Seismic velocities and crustal structure in southern Australia. *J. geol. Soc. Aust.* 11, 141-150.

- Doyle, H.A., I.B. Everingham and T.K. Hogan (1959). Seismic recordings of large explosions in south-eastern Australia. *Aust. J. Phys.* 12, 222-230.
- Doyle, H.A., R. Underwood and E.J. Polak (1966). - Seismic velocities from explosions off the central coast of New South Wales. *J. geol. Soc. Aust.* 13, 355-372.
- Drake, L.A. (1972). - Love and Rayleigh waves in nonhorizontally layered media. *Bull. Seism. Soc. Am.* 62, 1241-1258.
- Dunkin, J.W. (1965). - Computation of modal solutions in layered elastic media at high frequencies. *Bull. Seism. Soc. Am.* 55, 335-358.
- Dziewonski, A.M. (1970a). - Correlation properties of free period partial derivatives and their relation to the resolution of gross Earth data. *Bull. Seism. Soc. Am.* 60, 741-768.
- *Dziewonski, A.M. (1970b). - On regional differences in dispersion of mantle Rayleigh waves. *Geophys. J.R. astro. Soc.* 22, 289-325.
- Dziewonski, A.M. (1971). - Upper mantle models from 'pure path' dispersion data. *J. Geophys. Res.* 76, 2587-2601.
- Dziewonski, A.M. and A.L. Hales (1972). - Numerical analysis of dispersed seismic waves. In: *Methods of Computational Physics*, Vol. II, Academic Press, Inc., New York and London, 39-85.
- Dziewonski, A. and M. Landisman (1970). - Great circle Rayleigh and Love wave dispersion from 100 to 900 seconds. *Geophys. J.R. astro. Soc.* 19, 37-91.
- Dziewonski, A., S. Bloch and M. Landisman (1969). - A technique for the analysis of transient seismic signals. *Bull. Seism. Soc. Am.* 59, 427-444.
- Dziewonski, A., J. Mills and S. Bloch (1972). - Residual dispersion measurement - a new method of surface wave analysis. *Bull. Seism. Soc. Am.* 62, 129-139.
- Evernden, J.F. (1953). - Direction of approach of Rayleigh waves and related problems (part I). *Bull. Seism. Soc. Am.* 43, 335-374.
- Evernden, J.F. (1954). - Direction of approach of Rayleigh waves and related problems (part II). *Bull. Seism. Soc. Am.* 44, 159-184.
- Ewing, M. and F. Press (1954). - Mantle Rayleigh waves from the KAMCHATKA earthquake of Nov. 4, 1952. *Bull. Seism. Soc. Am.* 44, 471-480.
- Ewing, W.M., W.S. Jardetzky and F. Press (1957). - *Elastic Waves in Layered Media*, McGraw-Hill Book Co. Inc., 380 pp.
- Goodspeed, M.J. and J.V. Savage (1968). - An analogue-to-digital converter for chart records. *J. Phys. E: Sci. Instrum.* 1, 451-455.

*The first page of this article lists '1970' as the year of publication. The year should read '1971'. Cf. item 31500, Bibliog. of Seismology, Vol.7, No.1, 1971, January-June.

- Green, R.W. and A.L. Hales (1968). - The travel times of P waves to 30° in the central United States and upper mantle structure. *Bull. Seism. Soc. Am.* 58, 267-289.
- Gupta, H.K. and T. Santó (1973). Worldwide investigation of mantle Rayleigh-wave group velocities. *Bull. Seism. Soc. Am.* 63, 271-281.
- Haddon, R.A.W. and K.E. Bullen (1969). - An Earth model incorporating free Earth oscillation data. *Phys. Earth. Planet. Int.* 2, 35-49.
- Hales, A.L. and S. Bloch (1969). - Upper mantle structure: are the low velocity channels thin? *Nature*, 221, 930-933.
- Hales, A.L. and H.A. Doyle (1967) - P and S travel time anomalies and their interpretation. *Geophys. J.R. astro. Soc.* 13, 403-415.
- Harkrider, D.G. (1970). - Surface waves in multilayered elastic media. II. Higher mode spectra and spectral ratios from point sources in plane layered Earth models. *Bull. Seism. Soc. Am.* 60, 1937-1987.
- Haskell, N.A. (1953). - The dispersion of surface waves on multilayered media. *Bull. Seism. Soc. Am.* 43, 17-34.
- Herrmann, R.B. (1973). - Some aspects of band-pass filtering of surface waves. *Bull. Seism. Soc. Amer.* 63, 663-671.
- Howard, L.E. and J.H. Sass (1964). - Terrestrial heat flow in Australia. *J. Geophys. Res.* 69, 1617-1626.
- Howell, B.F. Jr. (1966). - Simple digitizer for paper seismograms. *Bull. Seism. Soc. Am.* 56, 605-608.
- Inston, H.H., P.D. Marshall and C. Blamey (1971). - Optimization of filter bandwidth in spectral analysis of wavetrains. *Geophys. J.R. astro. Soc.* 23, 243-250.
- James, D.E. (1971a). - Anomalous Love wave phase velocities. *J. Geophys. Res.* 76, 2077-2083.
- James, D.E. (1971b). - Andean crustal and upper mantle structure. *J. Geophys. Res.* 76, 3246-3271.
- James, D.E. and A.L. Linde (1971). - A source of major error in the digital analysis of WSSN seismograms. *Bull. Seism. Soc. Am.* 61, 723-728.
- Johnson, C.E. (1972). - Regionalized Earth models from linear programming methods, M.Sc. Thesis, Massachusetts Inst. of Technology, Cambridge, Mass.
- Kanamori, H. (1970). - Velocity and Q of mantle waves. *Phys. Earth. Planet. Int.* 2, 259-275.
- Kanamori, H. and K. Abe (1968). - Deep structure of island arcs as revealed by surface waves. *Bull. Earthquake Res. Inst.* 46, 1001-1025.

- Keilis-Borok, V.I. and T.B. Yanovskaya (1967). - Inverse problems of seismology (structural review). *Geophys. J.R. astro. Soc.* 13, 223-234.
- Knopoff, L. (1972). - Observation and inversion of surface-wave dispersion. In: A.R. Ritsema (editor), *The Upper Mantle. Tectonophysics* 13(1-4), 497-519.
- Knopoff, L. and F.A. Schwab (1968). - Apparent initial phase of a source of Rayleigh waves. *J. Geophys. Res.* 73, 755-760.
- Knopoff, L., S. Mueller and W.L. Pilant (1966). - Structure of the crust and upper mantle in the Alps from the phase velocity of Rayleigh waves. *Bull. Seism. Soc. Am.* 56, 1009-1044.
- Landisman, M., A. Dziewonski and Y. Satô (1969). - Recent improvements in the analysis of surface wave observations. *Geophys. J.R. astro. Soc.* 17, 369-403.
- Lee, Y.W. (1960). - *Statistical Theory of Communication*, John Wiley and Sons, Inc., New York, 341 pp.
- Levshin, A.L., V.F. Pisarenko and G.A. Pogrebinsky (1972). - On a frequency-time analysis of oscillations. *Annales de Géophysique*, tome 28, 211-218.
- Liebermann, R.C. (1973). - Elasticity of the olivine-spinel and olivine-8 phase transformations and the 400-kilometer discontinuity of the mantle. *J. Geophys. Res.* 78, 7015-7017.
- Massé, R.P. (1973). - Shear velocity distribution beneath the Canadian Shield. *J. Geophys. Res.* 78, 6943-6950.
- McCowan, D.W. (1966). - Finite Fourier transform theory and its application to the computation of convolutions, correlations and spectra. Technical memorandum no. 8-66, Earth Sciences Division, Teledyne Industries, Inc., Alexandria, Virginia.
- McElhinny, M.W. and B.J.J. Embleton (1974). - Australian Palaeomagnetism and the Phanerozoic Plate tectonics of eastern Gondwanaland. *Tectonophysics* (in the press).
- McEvelly, T.V. (1964). - Central U.S. crust-upper mantle structure from Love and Rayleigh wave phase velocity inversion. *Bull. Seism. Soc. Am.* 54, 1997-2015.
- Morris, G.B., A.W. Raitt and G.G. Shor, Jr. (1969). - Velocity anisotropy and delay-time maps of the mantle near Hawaii. *J. Geophys. Res.* 74, 4300-4316.
- Oversby, B. (1971). - Palaeozoic plate tectonics in the South Tasman Geosyncline. *Nature Physical Science* 234, 45-47 and 60.
- Parker, R.L. (1970). - The inverse problem of electrical conductivity in the mantle. *Geophys. J.R. astro. Soc.* 22, 121-138.
- Pilant, W.L. and L. Knopoff (1964). - Observations of multiple seismic events. *Bull. Seism. Soc. Am.* 54, 19-39.

- Pilant, W.L. and L. Knopoff (1970). - Inversion of phase and group slowness dispersion. *J. Geophys. Res.* 75, 2135-2136.
- Press, F. (1956). - Determination of crustal structure from phase velocity of Rayleigh waves, part 1: Southern California. *Bull. Geol. Soc. Am.* 67, 1647-1658.
- Ringwood, A.E. (1962a). - A model for the upper mantle. *J. Geophys. Res.* 67, 857-867.
- Ringwood, A.E. (1962b). - A model for the upper mantle, 2. *J. Geophys. Res.* 67, 4473-4477.
- Rosenbaum, J.H. (1964). - A note on the computation of Rayleigh wave dispersion curves for layered elastic media. *Bull. Seism. Soc. Am.* 54, 1013-1019.
- Sass, J.H., S.P. Clark and J.C. Jaeger (1967). - Heat flow in the Snowy Mountains of Australia. *J. Geophys. Res.* 72, 2635-2647.
- Simpson, D.W. (1973). - P wave velocity structure of the upper mantle in the Australia region. Ph.D. Thesis, The Australian National University, Canberra.
- Satô, Y. (1955). - Analysis of dispersed surface waves by means of Fourier transform I. *Bull. Earthquake Res. Inst.* 33, 33-47.
- Satô, Y. (1956). - Analysis of dispersed surface waves by means of Fourier transform. II. Synthesis of movement near the origin. *Bull. Earthquake Res. Inst.* 34, 9-18.
- Satô, Y. (1956). - Analysis of dispersed surface waves by means of Fourier transform. III. Analysis of practical seismogram of South Atlantic earthquake. *Bull. Earthquake Res. Inst.* 34, 131-138.
- Stacey, Frank (1969). - *Physics of the Earth*, John Wiley & Sons, Inc., New York, London, Sydney, Toronto, 324 pp.
- Sutton, D.J. and R.E. White (1966). - A study of P travel-times from some Australian earthquakes. *Austral. J. Phys.* 19, 157-166.
- Takeuchi, H. and K. Sudo (1968). - Partial derivatives of free oscillation period with respect to physical parameter changes within the Earth. *J. Geophys. Res.* 73, 3801-3806.
- Takeuchi, H., J. Dorman and M. Saito (1964). - Partial derivatives of surface wave phase velocity with respect to physical parameter changes within the Earth. *J. Geophys. Res.* 69, 3429-3441.
- Takeuchi, H., Y. Hamano and Y. Hasegawa (1968). - Rayleigh- and Love-wave discrepancy and the existence of magma pools in the upper mantle. *J. Geophys. Res.* 73, 3349-3350.
- Thatcher, W. and J.N. Brune (1969). - Higher mode interference and observed anomalous apparent Love wave phase velocities. *J. Geophys. Res.* 74, 6603-6611.

- Thatcher, W. and J.N. Brune (1973). - Surface waves and crustal structure in the Gulf of California region. *Bull. Seism. Soc. Am.* 63, 1689-1698.
- Thomas, L. (1969). - Rayleigh wave dispersion in Australia. *Bull. Seism. Soc. Am.* 59, 167-182.
- Toksöz, M.N. and D.L. Anderson (1966). - Phase velocities of long period surface waves and structure of the upper mantle. I. Great-circle Love and Rayleigh wave data. *J. Geophys. Res.* 71, 1649-1658.
- Toksöz, M.N. and A. Ben-Menahem (1963). - Velocities of mantle Love and Rayleigh waves over multiple paths. *Bull. Seism. Soc. Am.* 53, 741-764.
- Toksöz, M.N., M.A. Chinnery and D.L. Anderson (1967). - Inhomogeneities in the Earth's mantle. *Geophys. J.R. astro. Soc.* 13, 31-59.
- Verma, R.K. (1960). - Elasticity of some high density crystals. *J. Geophys. Res.* 65, 757-766.
- Wang, C. (1972). - A simple Earth model. *J. Geophys. Res.* 77, 4318-4329.
- White, R.E. (1971). - P-wave velocities in the upper mantle beneath the Australian shield from earthquake data. *Geophys. J.R. astro. Soc.* 24, 109-118.
- Wickens, A.J. and F. Kollar (1967). - A wide range seismogram digitizer. *Bull. Seism. Soc. Am.* 57, 91-98.
- Wiggins, R.A. (1969). - Monte Carlo inversion of body-wave observations. *J. Geophys. Res.* 74, 3171-3181.
- Wiggins, R.A. (1972). - The general inverse problem: Implication of surface waves and free oscillations for Earth structure. *Rev. of Geophys. and Space Phys.* 10, 251-285.
- Worthington, M.H. (1973). - The inversion of seismic data using Monte Carlo and linear programming techniques. Ph.D. Thesis, The Australian National University.
- Worthington, M.H., J.R. Cleary and R.S. Anderssen (1972). - Density modelling by Monte Carlo inversion - II. Comparison of recent Earth models. *Geophys. J.R. astro. Soc.* 29, 445-457.